Characterization of the Self-Assembly of Pyrene-Labelled Macromolecules in Water

by

Howard Chun-Kui Siu

A thesis
presented to the University of Waterloo
in fulfillment of the
thesis requirement for the degree of
Doctor of Philosophy
in
Chemistry

Waterloo, Ontario, Canada, 2010

Author's Declaration

I hereby declare that I am the sole author of this thesis. This is a true copy of the thesis, including any required final revisions, as accepted by my examiners.

I understand that my thesis may be made electronically available to the public.

Abstract

The self-assembly of several pyrene-labelled amphiphilic macromolecules in water was characterized by fluorescence. Information on their self-assembly was obtained by monitoring the level of pyrene aggregation in solution. A measure of the level of association was obtained by determining the fraction of aggregated pyrene of the labelled macromolecules from the global analysis of their monomer and excimer fluorescence decays. Global analysis limits the degrees of freedom of the analysis thus reducing the error on the parameters retrieved from the analysis. Extensive developments in the global analysis of the pyrene monomer and excimer decays enabled the first characterization of the molar absorbance coefficient of the pyrene aggregates formed by aqueous solutions of pyrene-labelled poly(*N*,*N*-dimethylacrylamide) (PyPDMA) and poly(ethylene oxide) (PyPEO). The molar absorbance coefficients of the pyrene aggregates determined for PyPDMA and PyPEO were both found to be broader and red-shifted compared to that of unaggregated pyrene. These results agree with observations found in the scientific literature made by using absorption and excitation fluorescence measurements. Attempts to determine the molar absorbance coefficient of pyrene-labelled hydrophobically-modified alkali-swellable emulsion (PyHASE) polymers were unsuccessful. The inability to characterize the pyrene aggregates of PyHASE was attributed to the greater complexity of the PyHASE polymer compared to PyPDMA and PyPEO. For these simpler pyrene-labelled polymers, a protocol has been established which uses the global analysis of the pyrene monomer and excimer decays to determine quantitatively the level of association of pyrene-labelled polymers as well as the molar absorbance coefficient of their aggregates.

Changes in the level of aggregation of pyrene-labelled lipids (PLLs) having head groups bearing an alcohol (PSOH) or imido diacetic acid (PSIDA) embedded in 1-palmitoyl-2-oleyl-3-*sn*-phosphatidylcholines (POPC) or distearylphosphatidylcholine (DSPC) liposomes were probed by

fluorescence. Distribution of the PLLs in the fluid POPC membrane was found to be homogeneous while the PLLs phase-separated into amorphous channels created in the DSPC membranes. Multivalent cations Cu^{2+} and La^{3+} were found to bind to PSIDA, hindering diffusional encounters between unaggregated PSIDA but leaving the PLL aggregates intact. Using the fluorescence quenching ability of Cu^{2+}, the viscosity of the amorphous channels of the DSPC membrane was determined to be about six times greater than that of the more fluid POPC membrane.

Simultaneous rheological and fluorescence measurements were achieved by interfacing a rheometer with time-resolved and steady-state fluorometers using fiber-optic cables. This joint set up enabled the simultaneous rheological and fluorescence measurements of PyHASE solutions having concentrations ranging from 0.5 w/w% to 5 w/w%. The level of association of the PyHASE solutions was tracked using fluorescence at shear rates of 0, 0.1 and 100 s^{-1}. Despite the presence of shear thinning leading to viscosity drops of up to four orders of magnitude, no change in the fluorescence and hence the level of association was observed. The lack of change in level of association implied that the mechanism of shear thinning is due to a switching from inter- to intramolecular association rather than a drop in the level of association. This information will prove useful for future models attempting to predict the rheological behaviour of sheared associative polymers.

Acknowledgements

I would like to thank, first and foremost, my mother Rosanna Siu for her never faltering belief in me. Another guiding figure that I would like to thank, as well, is my supervisor Professor Jean Duhamel for giving me this invaluable opportunity in addition to lending his guidance and support throughout my graduate studies. I would also like to thank the members of my committee, Jamie Forrest, Thorsten Dieckmann, and especially Mario Gauthier for their advice and helpful discussions regarding my work.

There are also several others that I am grateful to for their support starting off with the University of Waterloo and GWC^2 for accepting me into their program. Also I would like to thank DOW Chemical for supplying my polymer samples, NSERC for funding, the secretarial staff of the Chemistry department for their aid in those troublesome administrative matters, and my lab colleagues who made working in the lab an enjoyable experience.

Finally, I would like to thank my wife Vivian for all of her love, support, and especially her patience while I completed my graduate studies.

Dedication

To my wife Vivian for always standing with me and to my father of whom I am quite certain I will see again.

Table of Contents

Author's Declaration ii
Abstract iii
Acknowledgements v
Dedication vi
Table of Contents vii
List of Figures x
List of Tables xiv
List of Schemes xvi
List of Abbreviations xviii
Chapter 1 Literature Review 1
1.1 Introduction 1
1.2 Amphiphilic Molecules 2
1.2.1 Self-Assembly 2
1.3 Micelles and Vesicles 3
1.3.1 Liposomes as Drug Delivery Agents 4
1.3.2 Organization in Bilayer Membranes 6
1.4 Hydrophobically-Modified Water-Soluble Polymers 7
1.5 Pyrene as a Label 12
1.5.1 Pyrene Species Classification 16
1.6 Fluorescence Instrumentation 20
1.7 Goal of the Thesis 23
Chapter 2 Nanodomain Formation in Lipid Membranes Probed by Time-Resolved Fluorescence 28
2.1 Overview 28
2.2 Introduction 29
2.3 Experimental 33
2.4 Results 39
2.5 Discussion 49
2.6 Conclusions 58
Chapter 3 Molar Absorption Coefficient of Pyrene Aggregates in Water 59
3.1 Overview 59
3.2 Introduction 60

3.3 Theory 62
3.4 Experimental 70
3.5 Results 73
3.6 Discussion 86
3.7 Conclusions 95
Chapter 4 Determination of the Level of Association of a Poly(Ethylene Oxide) Singly End-Labelled with Pyrene using a Model Free Global Analysis 97
4.1 Overview 97
4.2 Introduction 97
4.3 Theory 100
4.3.1 Birks Scheme[31,32] 102
4.3.2 Fluorescence Blob Model (FBM)[16,36] 103
4.3.3 Model Free Analysis[38] 106
4.3.4 Free Pyrene Monomer 107
4.3.5 Ground-State Aggregation 108
4.3.6 Brief Summary of the Models 109
4.3.7 Determination of Pyrene Fractions 109
4.4 Experimental 111
4.5 Results 115
4.6 Discussion 130
4.7 Conclusions 135
Chapter 5 Determination of the Level of Association of Hydrophobically-Modified Alkali-Swellable Emulsion Polymers Randomly Labelled with Pyrene 137
5.1 Overview 137
5.2 Introduction 137
5.3 Results and Discussion 141
5.4 Conclusions 147
Chapter 6 Simultaneous Probing of Hydrophobic Interactions of an Associative Thickener under Sheared Conditions Using Fluorescence 148
6.1 Overview 148
6.2 Introduction 149
6.3 Experimental 152

6.4 Results and Discussion 160
6.5 Conclusions 174
Chapter 7 Summary 177
Appendix 183
Chapter 2 Supporting Information 183
Chapter 3 Supporting Information 201
Chapter 4 Supporting Information 217
Chapter 5 Supporting Information 237
Chapter 6 Supporting Information 240
References 250
Chapter 1 250
Chapter 2 254
Chapter 3 256
Chapter 4 260
Chapter 5 263
Chapter 6 264
Chapter 7 267

List of Figures

Figure 1.1: Chemical structure of a typical HASE polymer where R represents the hydrophobic pendant. 10

Figure 1.2: Chemical structure of a 1-pyrenyl unit. 13

Figure 1.3: Fluorescence emission spectra of pyrene solutions in cyclohexane having concentrations of 2 μM (▬) and 20 mM (—), λ_{ex} = 336 nm. 14

Figure 1.4: Absorption spectra normalized at the 0-0 peak of 2500 g/mol poly(ethylene oxide) labelled at one end with pyrene which is aggregated in water (—) and unaggregated in tetrahydrofuran (▬)..... 17

Figure 1.5: Shift observed in the fluorescence excitation spectra of the monomer and excimer taken at 375 nm (▬) and 510 nm (—), respectively, for aqueous solutions of pyrene-labelled poly(*N*,*N*-dimethylacrylamide) having 645 μM of pyrene per gram of polymer. 18

Figure 1.6: Excimer fluorescence decays excited at 344 nm and obtained at 510 nm for a 2500 g/mol poly(ethylene oxide) labelled at one end with pyrene which is aggregated in water (◆) and unaggregated in acetonitrile (□). 19

Figure 1.7: Excited pyrene species that a) exist as isolated monomeric pyrenes, b) form excimers via diffusive encounters between an excited pyrene and a GS pyrenes, and c) exist as aggregated pyrenes. 19

Figure 1.8: Schematic of a steady-state spectrofluorometer (Reprinted from Joseph R. Lakowicz Principles of Fluorescence Spectroscopy; Plenum Press: New York, 1983, Figure 2.1, pp.21)..... 20

Figure 1.9: Schematic diagram of a single photon counter. 22

Figure 1.10: A simulated bi-exponential decay fitted with a a) bi-exponential and b) mono-exponential function. 24

Figure 2.1**:** Structures of PSIDA and PSOH. 32

Figure 2.2**:** Fluorescence emission spectra normalized at 376 nm of POPC solutions containing 1 mol% of PSOH (·····) or PSIDA (—), and DSPC solutions containing 1 mol% PSOH (▪▪▪▪) or PSIDA (▬) in 0.02 M MOPS, 0.1 M NaCl, pH 7.4 buffer solution. λ_{ex} = 344 nm. 40

Figure 2.3**:** Monomer (◆) and excimer (□) time-resolved fluorescence decays for 1:99 mixtures of a) PSOH:POPC, b) PSOH:DSPC, c) PSIDA:POPC, and d) PSIDA:DSPC in MOPS buffer solution. λ_{ex} = 344 nm; λ_{em} (monomer) = 376 nm, λ_{ex} (excimer) = 510 nm. 41

Figure 2.4**:** I_E/I_M values for 1:99 mixtures of a) PSOH:POPC, b) PSOH:DSPC, c) PSIDA:POPC, and d) PSIDA:DSPC in MOPS buffer with (◆) Cu^{2+}, (□) Ca^{2+} and (●) La^{3+} 46

Figure 2.5**:** Fluorescence fractions f_{agg} (▲), f_{diff} (◇), and f_{free} (□), for a) 1% PSIDA/POPC with La^{3+}, b) 1% PSIDA/DSPC with La^{3+}. The error bars associated with each data point are smaller than the symbols. 49

Figure 3.1: Pyrene monomer (solid thin line) and excimer (thick lines) fluorescence excitation spectra of PyPDMA263 (**– – –**), PyPDMA479 (**— — —**), and PyPDMA645 (**————**). 75

Figure 3.3: I_E/I_M and P_A values of a) PyPDMA263, b) PyPDMA479, and c) PyPDMA645 with increasing optical densities. 77

Figure 3.4: Fluorescence fractions f_M^f (●,■,◆) and molar fraction f_M (○,□,◇) obtained for 4.8 g/L PyPDMA263 (circles), 15 g/L PyPDMA479 in water (squares) and 0.09 g/L PyPDMA645 in water (diamonds). 83

Figure 3.5: Molar absorption coefficient of the pyrene monomer ($\varepsilon_M(\lambda)$, ——) and pyrene aggregates ($\varepsilon_{E0}(\lambda)$) for PyPDMA263 with a concentration of 4.8 g/L (△), PyPDMA479 with a concentration of 0.01 g/L (□), 0.08 g/L (◇), and 1.8 g/L (▲), and PyPDMA645 with a concentration of 0.09 g/L (■) and 2.2 g/L (◆). 84

Figure 3.6: Plot of f_{agg} versus P_A value. 89

Figure 3.7: Plot of f_M^f (■) and 1 – f_M^f (□), as a function of excitation slit width for a solution of 4.8 g/L of PyPDMA263 in water. 90

Figure 3.8: Plot of $\langle n \rangle [Poly]/[Py_{diff}]$ versus $[Py_{agg}]/[Py_{diff}]$ for all Py-PDMA samples. 92

Figure 4.1**:** The fluorescence blob model applied to describe the excimer formation kinetics for a polymer randomly labelled with pyrene. 104

Figure 4.2: Diffusional quenching according to the Birks' scheme for pyrene in cyclohexane (◆), DMF (■), and acetonitrile (▲), and 1-pyrenemethanol in acetonitrile (△) 119

Figure 4.3: Diffusional quenching according to the model free approach for pyrene in cyclohexane (◆), DMF (■), and acetonitrile (▲), and 1-pyrenemethanol in acetonitrile (△) calculated using a) Equation 8 and b) Equation 9. 122

Figure 4.4: Fluorescence contribution to the monomer and excimer by the aggregated pyrene fraction for PyPEO in acetonitrile (◆), and water (■) 124

Figure 4.5: Viscosity uncorrected (hollow) and corrected (filled) excimer formation rate constants for PyPEO in acetonitrile (◆, ◇), and water (■, □). 125

Figure 4.6: Actual (filled) and fluorescence (hollow) fractions of aggregated pyrenes for aqueous solutions of PyPEO having concentrations of a) 5, b) 10 and c) 13 mM. 128
Figure 4.7: Molar absorbance coefficients of unassociated PyPEO in water (×) and pyrene aggregates determined for PyPEO solutions in water of 5 (△), 10 (◇), and 13 (□) mM. 129
Figure 4.8: Averaged molar absorbance coefficients of pyrenes that are aggregated, $<\varepsilon_{E0}>$, determined for PyPEO (◆) and PyPDMA (■) in water. 129
Figure 5.1: Fluorescence fractions of aggregated (hollow) and unaggregated (filled) pyrenes for PyHASE12 (■,□) and PyHASE65 (▲,△) in 0.01 M Na_2CO_3, pH 9 solution. 142
Figure 5.2: Molar fraction of aggregated pyrenes for PyHASE12 (■), PyHASE35 (◆), and PyHASE65 (△) in 0.01 M Na_2CO_3, pH 9 solution using $\varepsilon_M = \varepsilon_M^{PyPEO}$. 144
Figure 5.3: Absorption spectra normalized at the 0-0 transition peak for a) PyHASE12 (▪▪▪), PyHASE 65 (▬▬), and 2 mM PyPEO (—) solutions; b) PyPDMA solutions having pyrene contents of 6 (—), 263 (▪▪▪), 479 (▬ ▬ ▬) , and 645 (▬▬) mM pyrene/g polymer. ... 144
Figure 5.4: Excimer fluorescence decays of a solution of PyHASE65 (◆) and PyPDMA (□) having a pyrene content of 645 μM/g, λ_{ex} = 332 nm. 145
Figure 6.1: Joint rheometer/fluorometer setup with A) parallel plate and B) bob and cup (Couette flow) geometries. 158
Figure 6.2: Fibre optic set up inside the sample chambers of the single photon counter (left) and the steady-state flurometer (right). 159
Figure 6.3: Fibre optic configuration at the rheometer site for the parallel plate (left) and the Couette flow (right) geometries. 159
Figure 6.4: The light shielding poly(vinyl chloride) box encasing the rheometer (left) and the rheometer inside the box (right). 160
Figure 6.5: Shear thinning profiles of 2 (◇) and 5 (●) w/w% PyHASE65 in 0.01 M Na_2CO_3, pH 9 aqueous solution using the parallel plate geometry. 161
Figure 6.6: Shear thinning profiles of 0.5 (□) and 1 (▲) w/w% PyHASE65 in 0.01 M Na_2CO_3, pH 9 aqueous solution using the bob and cup geometry. 162
Figure 6.7: Overlapped fluorescence emission spectra normalized at 375 nm of 5 w/w% PyHASE65 solution in 0.01 M Na_2CO_3, pH 9 aqueous solutions acquired with steady-shear rates of 0 (—), 0.1 (—), and 100 (…) s^{-1} and also in a triangular cuvette (▬). 163
Figure 6.8: a) I_E/I_M ratio and b) f_{agg} of 0.5 (□), 1 (▲), 2 (◇), 3 (■), 4 (△), and 5 (●) w/w% PyHASE65 solutions as a function of the measured shear viscosity 164

Figure 6.9: Overlapped fluorescence decays of the monomer (left) and excimer (right) of 5 w/w% PyHASE65 solution in 0.01 M Na_2CO_3, pH 9 aqueous solution acquired at steady-shear rates of 0 (◇), 0.1 (□), and 100 (△) s^{-1}. 165

Figure 6.10: Shear thinning profiles of 3 w/w% PyHASE65 in 0.01 M Na_2CO_3, pH 9 aqueous solution with 0 (■), 0.5 (◇), 1 (□), and 2 (△) w/w% 480 nm diameter polystyrene latex particles. 170

Figure 6.11: I_E/I_M ratio of 3 w/w% PyHASE65solution in the presence of 0 (■), 0.5 (◇), 1 (□), and 2 (△) w/w% 480 nm diameter polystyrene latex particles as a function of the measured shear viscosity. 171

Figure 6.12: Fluorescence intensity at 375 nm of 3 w/w% PyHASE65 sheared at a rate of 100 s^{-1} withdrawing the shear after 60 s at resolutions of a) 1; b) 10; c) 100; d) 999 points per second. 175

List of Tables

Table 1.1: Expected aggregate structure formed as a function of the critical packing parameter $\phi = \frac{v}{a_0 l_c}$ (reproduced from Myers, D. *Surfactant Science and Technology, 2nd Ed.*; VCH: New York, 1992, p. 166).[3] 4

Table 2.1**:** Averaged parameters obtained from global FBM analyses for solutions of POPC and DSPC with 1 mol% PLL. The reported errors are the standard deviation of the parameters obtained by fitting the experimental decays acquired with either no cations or with Ca^{2+} cations. 43

Table 3.1: Symbols used for the molar absorption coefficients and radiative rate constants of the various pyrene species. 68

Table 3.2: Pyrene contents (μ_{Py}), weight averaged molecular weights (M_W), P_A values in water, and names of the PyPDMA samples. 71

Table 3.3: Averaged FBM parameters obtained for excitation wavelengths ranging from 325 to 350 nm for various pyrene labellings and optical densities of PyPDMA and using $k_2 = 3.4 \times 10^8$ s^{-1}. 82

Table 3.4: Molar absorption coefficient of unassociated pyrenes, ε_M, for PyPDMA. 85

Table 3.5: Averaged absorption coefficient of the pyrene aggregates, ε_{E0}, for PyPDMA. 86

Table 3.6: Fractions of the various pyrene species present in the six PyPDMA solutions studied. 87

Table 4.1: Fluorescence lifetimes obtained for solutions of pyrene and pyrene derivatives studied in various solvents. 113

Table 4.2**:** Parameters retrieved from Birks' scheme analysis of pyrene in cyclohexane from current study and previously obtained by Birks. 117

Table 4.3: Averaged parameters retrieved from Birks' scheme analysis of pyrene in cyclohexane, DMF, and acetonitrile and 1-pyrenemethanol in acetonitrile and DMF (obtained from Ingratta and Duhamel) 120

Table 4.4**:** Averaged parameters retrieved from model free analysis of pyrene in cyclohexane, DMF, and acetonitrile and 1-pyrenemethanol in acetonitrile. 121

Table 4.5: Averaged extinction coefficient of the pyrene aggregates ε_{E0} for PyPEO in water. 130

Table 5.1: Notation used for the molar absorbance coefficients, fluorescence fractions and molar fractions of the pyrene species. 141

Table 6.1: Pyrene fluorescence fractions of PyHASE65 in 0.01 M Na_2CO_3, pH 9 aqueous solutions obtained by the FBM global analysis of the monomer and excimer decays with τ_{E0} and τ_{ES} fixed. Note: samples marked with * were analyzed using decays obtained for solutions in a triangular cell. 167

Table 6.2: Pyrene fluorescence fractions of 3 w/w% PyHASE65 solutions with 480 nm polystyrene latex particles obtained by global FBM analysis of the monomer and excimer decays with τ_{E0} = 62 ns and τ_{ES} = 3.5 ns. 171

Table 6.3: Fitted parameters using a sum of exponentials for the fluorescence monomer (top) and excimer (bottom) decays for 3 w/w% solutions of PyHASE65 in the bulk using an untreated triangular cell, adsorbed onto a piranha treated (hydrophilic), and 1,1,1,3,3,3-hexamethyldisilizane (hydrophobic) treated surface of fused silica. 173

List of Schemes

Scheme 1.1: Vesicle (closed) and extended plane (open) conformations taken by bilayer membranes formed by double-chained lipids. 5

Scheme 1.2: Formation of an extended network by a telechelic HMWSP. 8

Scheme 1.3: a) Fluorescence quenching of an excited chromophore (C*) by a quencher (Q) attached onto a polymer confirming b) the encounter of the two molecular segments where the labels are attached. 13

Scheme 1.4: Birks' scheme describing excimer formation of pyrene modified to include excitation of GS pyrene aggregates. 15

Scheme 2.1: Modified Birks' scheme illustrating the possible pathways leading to excimer formation. 32

Scheme 2.2**:** Representation of the distribution of PLLs (black circles) in POPC (left) and DSPC (right) matrices with amorphous (white circles) and crystalline (gray circles) domains divided into fluorescence blobs (ovals). 52

Scheme 2.3**:** Representation of the change in the distribution of PSOH (left) and PSIDA (right) in a POPC matrix where the head groups of the PLLs and POPC are black and white, respectively. 53

Scheme 2.4**:** Representation of the two competing quenching processes experienced by an excited PSIDA with a bound Cu^{2+}. Excimer formation by diffusive encounter with another PSIDA is possible when Cu^{2+} is not bound to the other lipid (left) and impossible if both bear a Cu^{2+} ion (right). 57

Scheme 3.1: Kinetic scheme depicting the relationship between the pyrene species Py_{diff} = Py*, Py_{k2} = (Py* Py), and the excimer *E0** = (Py Py)*. Diffusion-controlled encounters between pyrene monomers to yield the species Py^{*}_{k2} occur with a "time-dependent rate constant" $f(t)$ given in Equation 3.9. Rapid rearrangement of the pyrenes with the rate constant k_2 results in the formation of the pyrene excimers *E0**. Poorly stacked pyrenes yield long-lived dimers *EL** = (Py Py)*. 63

Scheme 4.1: The Birks' scheme 101

Scheme 4.2: The fluorescence blob model (FBM) 104

Scheme 5.1: Birks' scheme modified to include direct excitation of GS pyrene aggregates. 138

Scheme 5.2: Birks' scheme modified to include the aggregated pyrene intermediate Py_{k2}^{*} and GS pyrene aggregates. 146
Scheme 6.1: Proposed effect of an external shearing force on the equilibrium between associated and unassociated hydrophobic pendants of an HMWSP network in the presence of latex particles. 169

List of Abbreviations

$\langle n \rangle$	average number of pyrenes per blob
AT	associative thickener
DMF	*N*,*N*-dimethylformamide
DSPC	distearylphosphatidylcholine
ε_{E0}	molar absorbance coefficient of the pyrene species *E0*
ε_{M}	molar absorbance coefficient of unaggregated pyrenes
EL	poorly-stacked long-lived pyrene dimers
E0	well-stacked pyrene dimers
ES	short-lived pyrene aggregates
f_{agg}	molar fraction of aggregated pyrenes in solution
FBM	fluorescence blob model
f_{diff}	molar fraction of pyrenes forming excimer via diffusion in solution
f_{free}	molar fraction of isolated pyrenes in solution
f_{agg}^{f}	fluorescence contribution of the fraction of aggregated pyrenes
f_{diff}^{f}	fluorescence contribution of the fraction of pyrenes forming excimer via diffusion
f_{free}^{f}	fluorescence contribution of the fraction of isolated pyrenes
GS	ground-state
GSPD	ground-state pyrene dimer
HASE	hydrophobically-modified alkali-swellable emulsion
HEUR	hydrophobically-modified ethoxylated urethane
HMDS	hexamethyldisilizane
HMHEC	hydrophobically-modified hydroxyethylcellulose
HMWSP	hydrophobically-modified water-soluble polymer
I_E/I_M	ratio of the excimer to monomer intensities
k_{blob}	rate constant for excimer formation within a blob between an excited and ground-state pyrene

$k_{ex}[blob]$	rate constant of pyrene exchange between blobs times the blob concentration
MF	model free
N_{agg}	average number of hydrophobic pendants per aggregate
P_A	peak-to-valley ratio of the pyrene absorption at the 0-0 transition and its adjacent trough
PDMA	poly(*N*,*N*-dimethylacrylamide)
PEO	poly(ethylene oxide)
PLL	pyrene-labelled lipid
POPC	1-palmitoyl-2-oleyl-3-*sn*-phosphatidylcholine
PSIDA	*N*-[8-(1-octadecyl-2-(9-(1-pyrenyl)-nonyl)-*rac*-glyceroyl)-3,6-dioxaoctyl]iminodiacetic acid
PSOH	8-[1-octadecyl-2-(9-(1-pyrenyl)nonyl)-*rac*-glyceroyl]-3,6-dioxaoctan-1-ol
Py	pyrene
Py_{agg}	aggregated pyrenes
Py_{diff}	pyrenes forming excimer via diffusion
Py_{free}	isolated pyrenes
PyHASE	pyrene-labelled hydrophobically-modified alkali-swellable emulsion
PyHMWSP	pyrene-labelled hydrophobically-modified water-soluble polymer
Py_{k2}	loosely aggregated pyrenes absorbing and fluorescing as a monomer
PyPDMA	pyrene-labelled poly(*N*,*N*-dimethylacrylamide)
PyPEO	pyrene-labelled poly(ethylene oxide)
THF	tetrahydrofuran

Chapter 1
Literature Review

1.1 Introduction

The phase separation of hydrophobic molecules in water is a well known phenomenon. By its very definition, hydrophobic literally means *water fearing*. Rather than being miscible with water, hydrophobic molecules preferentially coagulate with themselves to minimize the amount of exposed surface to the water. One needs only to visualize the example of a mixture of water and oil quickly separating to form discreet layers composed of solely water or oil. The driving force causing this separation of hydrophobic species from water can be explained from thermodynamic principles using the concept of the change in Gibbs' free energy associated with mixing ΔG_M whose expression is given in Equation 1.1.

$$\Delta G_M = \Delta H_M - T\Delta S_M \tag{1.1}$$

In Equation 1.1, T is the temperature and ΔH_M and ΔS_M are defined as the changes in enthalpy and entropy with mixing, respectively. In order for a substance to spontaneously mix with water, ΔG_M must be negative. At first glance, the mixing of any species into water would be entropically favourable since the mixing leads to a more disordered state. This view however is obviously incorrect since hydrophobic molecules do not spontaneously mix with water. Energetically, the interaction between a hydrophobic molecule and water is favourable ($\Delta H_M < 0$). However, the overall entropy of the system decreases greatly ($\Delta S_M < 0$) when mixing a hydrophobe in water making the process unfavourable.[1] This can be reasoned by picturing the hydration of the hydrophobic molecule in water requiring the collective orientation of several water molecules. While the disorder of the

hydrophobe increases, the order of the water supporting the hydrophobe in actuality leads to a more ordered state overall. As hydrophobic molecules do not interact much with the water molecules from an energy point of view, the entropy dominates thus making the phase separation an entropy driven process.

1.2 Amphiphilic Molecules

Amphiphilic molecules are species which contain both *water fearing* and *water loving* components, that is hydrophobic and hydrophilic parts. One major class of amphiphiles is the surfactant. Surfactants are molecules composed of a hydrophilic head group connected to a hydrophobic tail or tails. Surfactants are soluble in water as their hydrophilic components support the hydrophobic components in solution. Surfactants, or surface active agents, are capable of locating themselves at the water/air interface.[2,3] At these interfaces, the hydrophilic component interacts with the water phase while the hydrophobic component interacts with non-water phase.

1.2.1 Self-Assembly

In addition to interactions at water interfaces, amphiphilic molecules have been known to self-assemble into specific arrangements in solution. This phenomenon is well documented and has been a topic of great interest. In aqueous solution, amphiphilic molecules associate to minimize the exposure of the hydrophobic components to the water phase forming hydrophobic microdomains which are stabilized in solution by the hydrophilic components.[1–4] Depending on the architecture of the amphiphilic molecules, the self-assembly can adopt a variety of shapes ranging from micelles to mono- and bilayer membranes to extended networks. These self-assembled structures can be used for a broad range of applications from hydrophobic drug encapsulation and delivery[5–9] to rheological modification of aqueous solutions.[10,11] Two examples of self-assembly that this thesis will discuss in detail are the organization of double-chained lipids into bilayer

membranes forming vesicles and the network formation of hydrophobically-modified water-soluble polymers (HMWSPs).

1.3 Micelles and Vesicles

As mentioned in the previous section, the structure that an amphiphile may self-assemble into depends on the chemical structure of the amphiphile. For amphiphilic surfactants, the critical packing parameter ϕ determines the self-assembled structure the surfactants will adopt in water.[2,3] The expression for the parameter ϕ is given in Equation 1.2 where v is the volume of the hydrophobic component, a_0 is the optimum head group area, and l_c is the maximum extended length that the hydrophobic tail can take.

$$\phi = \frac{v}{a_0 l_c} \tag{1.2}$$

The value of ϕ dictates the expected structure in which the surfactants will self-assemble. For ϕ values < 0.33, surfactants in water are expected to form closed spherical or ellipsoidal micellar structures. Closed micellar structures consist of a core comprised of the hydrophobic tails surrounded by a corona of the hydrophilic head groups. It is believed that the environment of the hydrophobic core of surfactant micelles is comparable to that of a liquid hydrocarbon medium. This medium is capable of solubilizing other hydrophobic materials. The formation of surfactant micelles in water has been monitored using surface tension, turbidity or light scattering measurements.

Many double-chain surfactants including a variety of lipids, consisting of a polar head group and two flexible hydrophobic chains, self-associate into bilayer structures.[2,3] The bilayer membranes with a ϕ value ≈ 1.0 adopt an extended "open" planar conformation while those having a ϕ value between 0.5 and 1.0 form discreet "closed" vesicles. The closed vesicle and open extended planar

conformations are shown in Scheme 1.1. Since the individual lipids are relatively insoluble in water thus discouraging exchange of lipids from the vesicle to the aqueous phase, the vesicles formed by double-chained lipids are generally stable. A summary of the aggregated structures with their associated ϕ values are listed in Table 1.1.

Table 1.1: Expected aggregate structure formed as a function of the critical packing parameter $\phi = \frac{v}{a_0 l_c}$ (reproduced from Myers, D. *Surfactant Science and Technology, 2nd Ed.*; VCH: New York, 1992, p. 166).[3]

$\phi = \frac{v}{a_0 l_c}$	General Surfactant Type	Expected Aggregate Structure
< 0.33	Simple surfactants with single chains and relatively large head groups.	Spherical or ellipsoidal micelles
0.33 – 0.5	Simple surfactants with relatively small head groups or ionics in the presence of large amounts of electrolytes.	Relatively large cylindrical or rod-shaped micelles
0.33 – 1.0	Double-chain surfactants with large head groups and flexible chains	Vesicles and flexible bilayer structures
1.0	Double-chain surfactants with small head group or rigid, immobile chains	Planar extended bilayers

1.3.1 Liposomes as Drug Delivery Agents

As is the case of the hydrophobic core of micelles, hydrophobic materials present in solution can be incorporated into the hydrophobic domains formed by a bilayer membrane. Since there are many drugs that are hydrophobic and hence difficult to administer to patients, the encapsulation of hydrophobic drugs into discreet, stable, lipid vesicles provides a drug administration option for

patients. Vesicles composed of either polymeric[5] or lipid[6,7] units have been investigated in order to optimize their *in vivo* stability and rate of drug delivery. The optimized vesicles were then used *in vivo* to investigate their efficiency at antitumor therapy having been loaded with antitumor drugs such as doxorubicin. In one particular study, lymphoma and colon carcinoma tumours treated with sterically stabilized liposome drug carriers were found to contain over 10 times the concentration of anti-tumour drugs compared to treatments using free drugs in addition to a marked decrease in uptake of the drugs by the liver and spleen.[7] In a similar study, treatment of C-26 colon carcinoma tumours in mice using sterically stabilized liposomes containing doxorubicin was found to arrest tumour growth, whereas treatments using equivalent doses of the drug in free form have been found to be ineffective.[9]

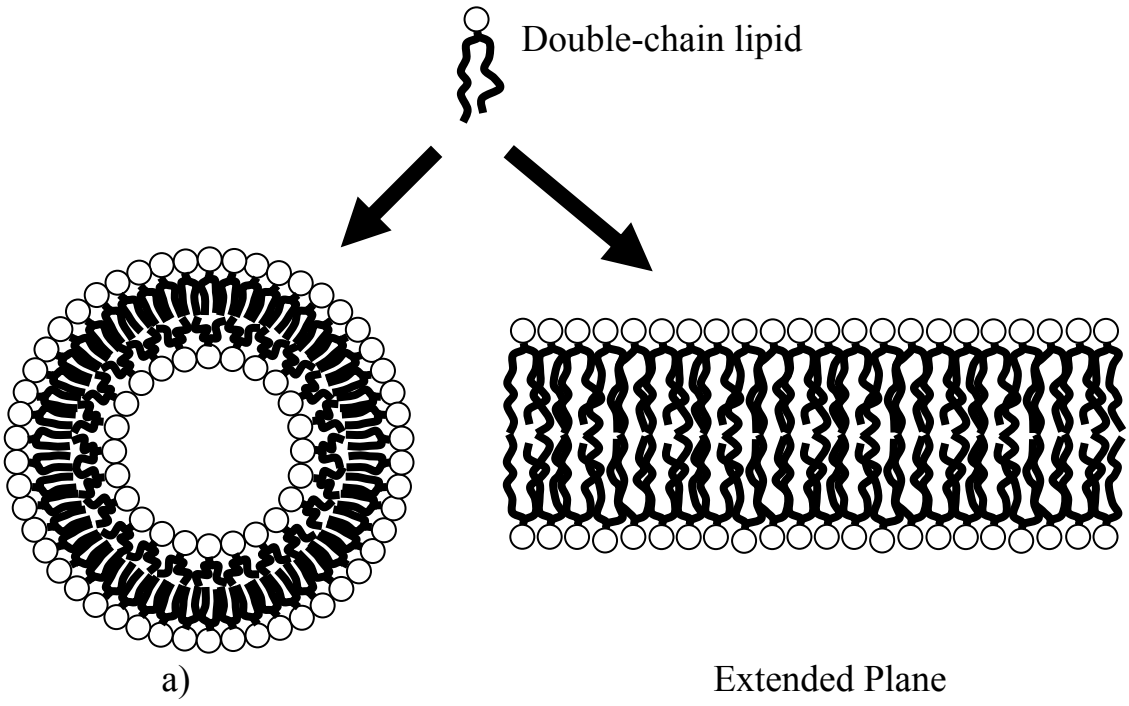

Scheme 1.1: Vesicle (closed) and extended plane (open) conformations taken by bilayer membranes formed by double-chained lipids.

1.3.2 Organization in Bilayer Membranes

In bilayer membranes composed of more than one type of double-chained lipid, the lipids may organize into heterogeneous regions on the membrane surface. Organization of the heterogeneous regions can also be influenced by external conditions such as temperature and surface pressure.[12–14] Another particularly interesting external factor is the selective binding of external ligands to sites on the surface of the membrane causing a reorganization of the lipids. [15–19] This observation has led to the design of specifically modified head groups capable of binding to specific ligands. The modified lipids rearrange themselves in the membrane upon binding of a specific ligand.

Cell membrane receptors are typically transmembrane proteins embedded in a heterogeneous region of the cell membrane. These play a critical role in the process of cell signalling which is the ability of a cell to respond to extracellular signalling molecules or ligands. One example of organized regions incorporating proteins that play a role in cell signalling are lipid rafts which are heterogeneous domains containing saturated lipids such as sphingolipids, cholesterol, and membrane proteins.[21–24] The term "raft" refers to the ordered nature of a tightly-packed, heterogeneous region of lipids, cholesterol, and proteins in a bilayer membrane. The laterally fluid nature of the rafts brought on by the mixture of lipids and cholesterol facilitates the mobility of the membrane proteins within the confines of the raft. This ordered domain floats within the disordered lipid membrane which has drawn analogies to an actual raft on a body of water. In mixtures of sphingolipids and phospholipids, rafts spontaneously self-assemble with sphingolipids phase separating from the phospholipids. These rafts self-assemble in the cell membrane and are thought to play a major role in cell functions such as membrane trafficking and binding with external ligands for cell signalling purposes. The binding of an external ligand to a cell membrane as a form of signalling is one method in which cells can interact with their environment such as immuno-responses to foreign species and also communicate with other cells such as the synaptic signalling with neurotransmitters.[20]

Capitalizing on the idea inspired by cellular systems, several groups have designed synthetic lipids possessing polar head groups capable of binding to external ligands to induce reorganization of lipids. Functionalization of the binding head group of the lipids or the embedding of specific proteins or polypeptides in the membrane enables a specificity of ligand that will bind to the membrane. Ligands that have been successfully bound to the functionalized vesicles include multivalent ions,[17,18,25–27] viruses,[28] and proteins.[29–31] Changes in the vesicle organization induced by binding of a ligand can occur at sub-ppb levels. The reorganization of the lipids in a vesicle by the binding of a ligand can be monitored by observing changes in the gel-to-liquid transition temperature of the membrane using differential scanning calorimetry[18] or the topography of the membrane surface imaged using atomic force[26,27,31] or transmission electron microscopy.[17,25] In addition, the functionalized lipids may be tailored to include chromophores or other optically active species capable of changing their fluorescent[25–27] or colorimetric[28–30] properties upon binding of a ligand. Having the advantage of high sensitivity to low concentrations of ligands, high selectivity of the ligands that can be detected, and the variety of methods to signal binding of the ligands to the lipids head, these functionalized lipid vesicles have great appeal and potential for the development of biosensors.

1.4 Hydrophobically-Modified Water-Soluble Polymers

HMWSPs are water-soluble polymers covalently labelled with a small number of hydrophobic pendants. Upon solvation in aqueous solution, the hydrophobic pendants aggregate together. Above the polymer overlap concentration, some polymer molecules form intermolecular bridges between different hydrophobic aggregates resulting in the formation of an extended network (Scheme 1.2). Numerous architectures can be selected to design HMWSPs, although telechelic structures, such as hydrophobically-modified ethoxylated urethane (HEUR) polymers, and comb-branched structures, such as hydrophobically-modified hydroxyethylcellulose (HMHEC) and alkali-swellable emulsion (HASE) polymers, are common.[32] Regardless of the specific structure, potential HMWSPs require a

hydrophobic functionality of two or greater in order to facilitate network formation. This physically cross-linked network is held together by the hydrophobic aggregates which can be easily disrupted by application of a shear force. At high levels of shear, the network will usually deteriorate as the polymer molecules acting as intermolecular bridges holding the hydrophobic aggregates together rearrange themselves to favour more intramolecular associations.[10,11,32–36] The disruption of the network caused by shear is reversible as the extended network quickly reforms once the shear is removed. The presence of the network greatly increases the macroscopic viscosity of the solution while the application of shear causes a great reduction in viscosity as the network is disrupted, a phenomenon called shear thinning.

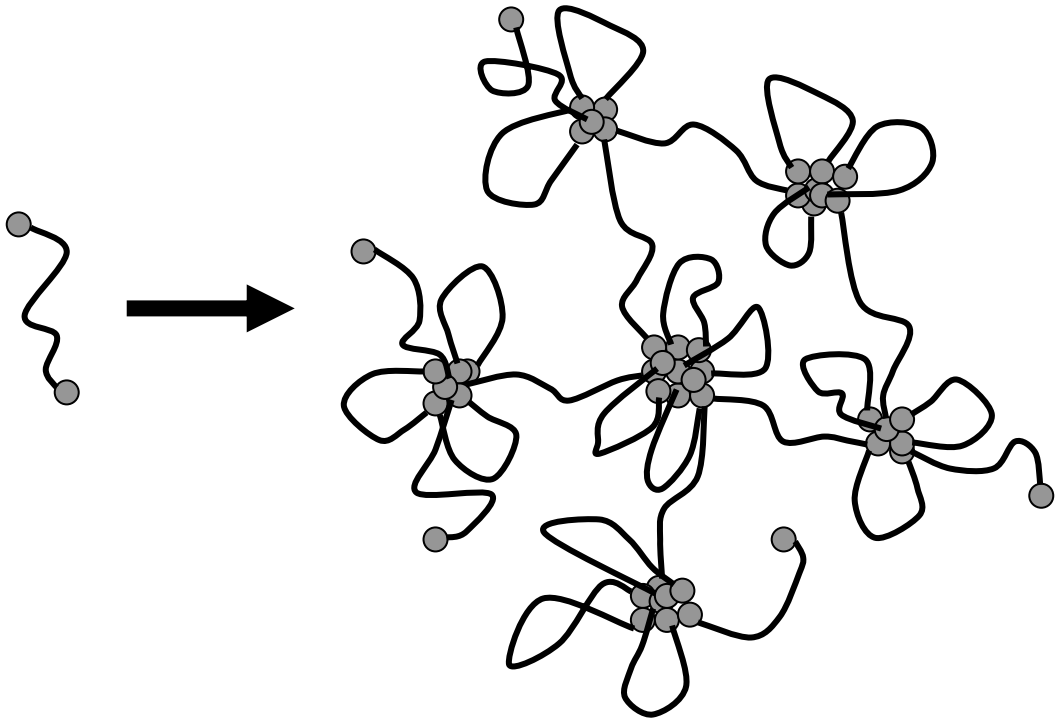

Scheme 1.2: Formation of an extended network by a telechelic HMWSP.

The peculiar viscoelastic properties of HMWSP solutions have led to the use of HMWSPs as rheological modifiers for latex based paints and coatings. The class of HMWSPs which enhance the viscosity of paint and coating formulations have been termed associative thickeners (ATs).[10,11,32] The formation of an AT network at rest increases the paint viscosity. As shear is applied to the paint via a paint brush or roller, the AT network is disrupted, reducing the solution viscosity and facilitating uptake of paint onto the brush or roller. Since the network quickly reforms, the viscosity of the paint on the brush recovers sufficiently to prevent dripping prior to application. During application, the drop in viscosity facilitates the transfer of paint from the brush to the surface. Afterwards, the increase in viscosity as the network reverts to its original state prevents sagging or running of the paint. In addition to viscosity modification, the distribution of hydrophobic domains throughout the solution can also interact with other hydrophobic particles found in the solution such as latex particles, stabilizing them in solution by anchoring the hydrophobes onto the latex surface and spreading its water-soluble chain into the solution. This has led to the application of ATs as stabilizers for colloidal suspensions. Three AT families have become mainstays of the paints and coatings industry: hydrophobically-modified cellulose derivatives such as HMHEC, HEUR, and HASE polymers.[11]

Cellulose derivatives have the advantage of low manufacturing costs and a readily available and renewable supply of base polymeric materials, that is cellulose. Hydrophobically-modified cellulose ethers display thickening and shear thinning behaviours but exhibit relatively poor rheological performance for paint applications as well as high water sensitivity. Telechelic HEUR polymers consist of essentially a poly(ethylene oxide) (PEO) backbone terminated at both ends by a hydrophobic pendant. HEUR polymers have the advantage of possessing superior rheological properties and lower water sensitivity compared to HMHEC polymers. In addition, depending on the synthesis protocol used, narrow molecular weight HEUR polymers can be produced having well defined rheological characteristics making them ideal model ATs.[37,38] One major disadvantage of

HEUR polymers is their high cost of manufacturing, especially for those having narrow molecular weight distributions. The chemical structure of a HASE polymer, a terpolymer of methacrylic acid, ethyl acrylate and a hydrophobic macromonomer, is given in Figure 1.1. The macromonomer is typically an α-methylstyrene attached via a urethane linker to a PEO chain end-terminated by the hydrophobic pendant.

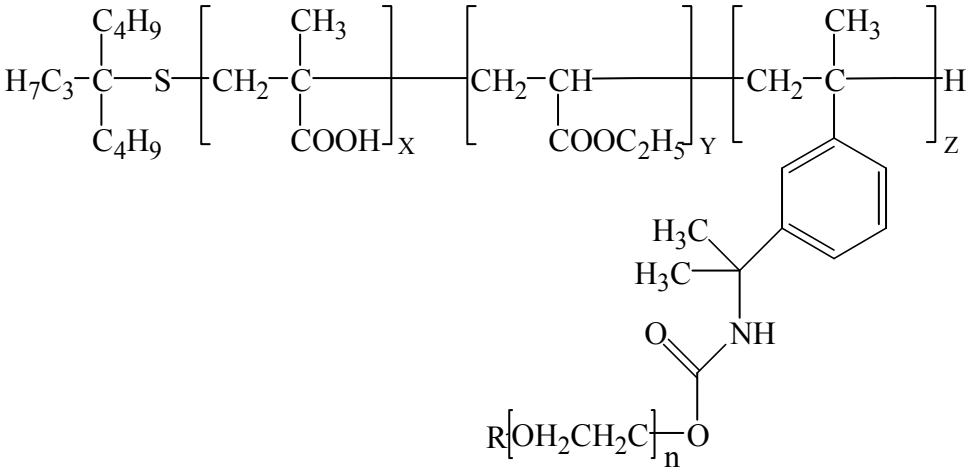

Figure 1.1: Chemical structure of a typical HASE polymer where R represents the hydrophobic pendant.

In highly alkaline media, the majority of the methacrylic acid monomers of HASE assume their ionized form. The overall negative charge of the polymer backbone results in the expansion of the polymer coil due to electrostatic repulsion of the individual charges of the ionized monomers. Thus, the polymer experiences competing effects since the high local concentration of hydrophobic pendants drives the polymer coil to self-associate into a collapsed conformation whereas the charged nature of the backbone forces the polymer chain to expand. As such, the rheological behaviours of a HASE polymer can be controlled by modifying different aspects of the composition such as the molar

ratios of the monomers, the length of the PEO chain, and the choice of hydrophobe. Astute modification of the composition of the HASE polymers can result in rheological properties that are comparable to that of HEUR polymers, while having production costs even lower than that of HMHEC. Having comparable rheological performance and lower costs compared to HEUR polymers, HASE polymers have become the AT of choice for interior architectural coatings. However, HEUR polymers still remain superior to HASE polymers in terms of resistance to harsh environmental conditions and are therefore the AT of choice for exterior architectural coatings.[11]

Due to their important commercial applications, network formation of HMWSPs in aqueous solution has been modelled by many different groups in order to gain a better understanding of their behaviour.[33,38–45] Typically, the models center on a transient cross-linked network with polymer chains continually detaching and reattaching themselves to cross-link points. Based on the models presented by the different groups, four important parameters can be defined which describe the network formed by HMWSPs. The average number of hydrophobic pendants per aggregate, N_{agg}, and the level of association quantifying the fraction of hydrophobic pendants that are aggregated, f_{agg}, together describes the hydrophobic junctions binding the network. Coupled with the average number of intermolecular "bridging" associations connecting the hydrophobic aggregates, these three parameters describe the static network formed by HMWSPs. The migration of a single chain inside the network, an indicator of the solution's viscosity, requires the coordinated detachment and reattachment of its hydrophobic pendants from the aggregates in a process termed "sticky reptation".[39,40] As the detachment of the hydrophobe is critical to the rate of movement inside the network, the residence time of a hydrophobic pendant inside an aggregate, τ_{res}, describes the dynamics associated with the disruption and formation of the network.

1.5 Pyrene as a Label

Characterization of the self-assembly of amphiphilic molecules, be they small lipids or large HMWSPs, can be carried out by labelling the amphiphilic molecules with chromophores and quenchers.[46–49] The fluorescence quenching of the chromophore by the quencher indicates that the two labels and hence the segments of the molecules where the chromophore and quenchers are attached have come into close contact mimicking the self-assembling process (Scheme 1.3). An ideal chromophore label is the 1-pyrenyl derivative whose structure is given in Figure 1.2. Pyrene absorbs and emits strongly due to its high molar absorbance coefficient in the near UV region and high quantum yield.[50] The pyrene monomer fluorescence is characterized by several sharp peaks at wavelengths between 370 and 420 nm. The presence of sharp peaks in the fluorescence emission spectrum indicates the presence of discreet vibration levels in the pyrene monomer ground-state. An example of the fluorescence emission spectrum of pyrene is given in Figure 1.3.

In addition to the fluorescence of the pyrene monomer in the blue wavelength region, an excited pyrene has the ability to complex with a ground-state pyrene to form an excimer. The excimer fluoresces in the green wavelength region with a broad structureless emission centered at 460 to 480 nm. In aqueous solution, pyrene excimers may also be generated by the direct excitation of ground-state (GS) pyrene aggregates. The different possible photophysical pathways undergone by an excited pyrene are shown in the modified Birks' scheme given in Scheme 1.4.[50] By forming an excimer, pyrene can act as both the chromophore when it is in the excited state and the quencher when it is in the GS. A relative indicator of the degree of association of the pyrene labels of macromolecules can be obtained by measuring the ratio of the fluorescence intensities of the excimer I_E, integrated from 500 to 530 nm, to the monomer I_M, integrated from 372 to 378 nm. The intensity ratio I_E/I_M is proportional to the rate constant of excimer formation k_1, and also the local pyrene concentration, $[Py]_{loc}$.[51] Thus changes observed in I_E/I_M for a given pyrene-labelled polymer indicate a change in the

local pyrene concentration, i.e. I_E/I_M may be used to gauge the relative proximity of the pyrenes to each other. Since $[Py]_{loc}$ is larger for a coiled chain than for an extended chain, the I_E/I_M ratio has been referred to as the coiling index.[46]

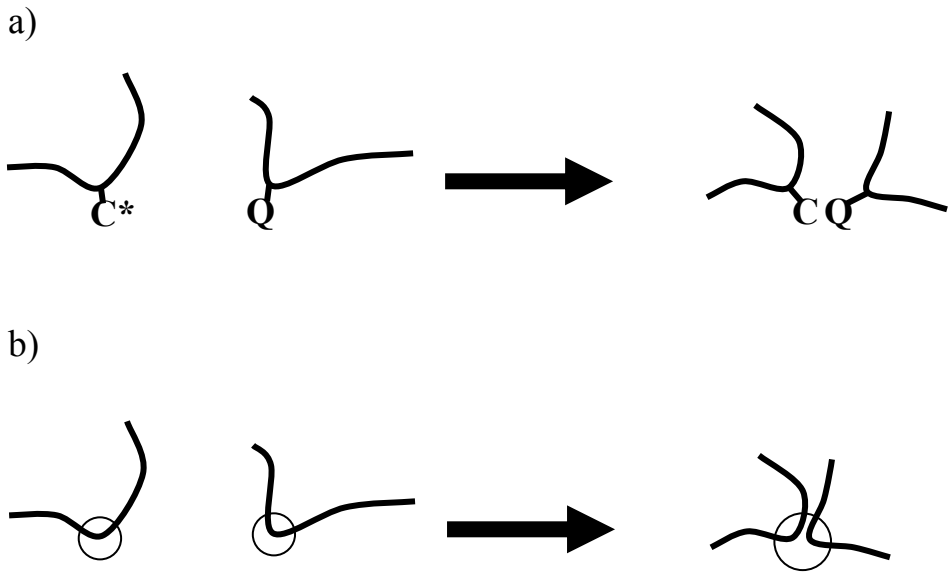

Scheme 1.3: a) Fluorescence quenching of an excited chromophore (C*) by a quencher (Q) attached onto a polymer confirming b) the encounter of the two molecular segments where the labels are attached.

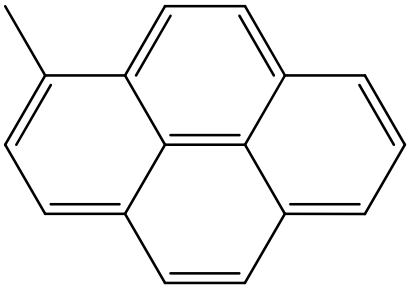

Figure 1.2: Chemical structure of a 1-pyrenyl unit.

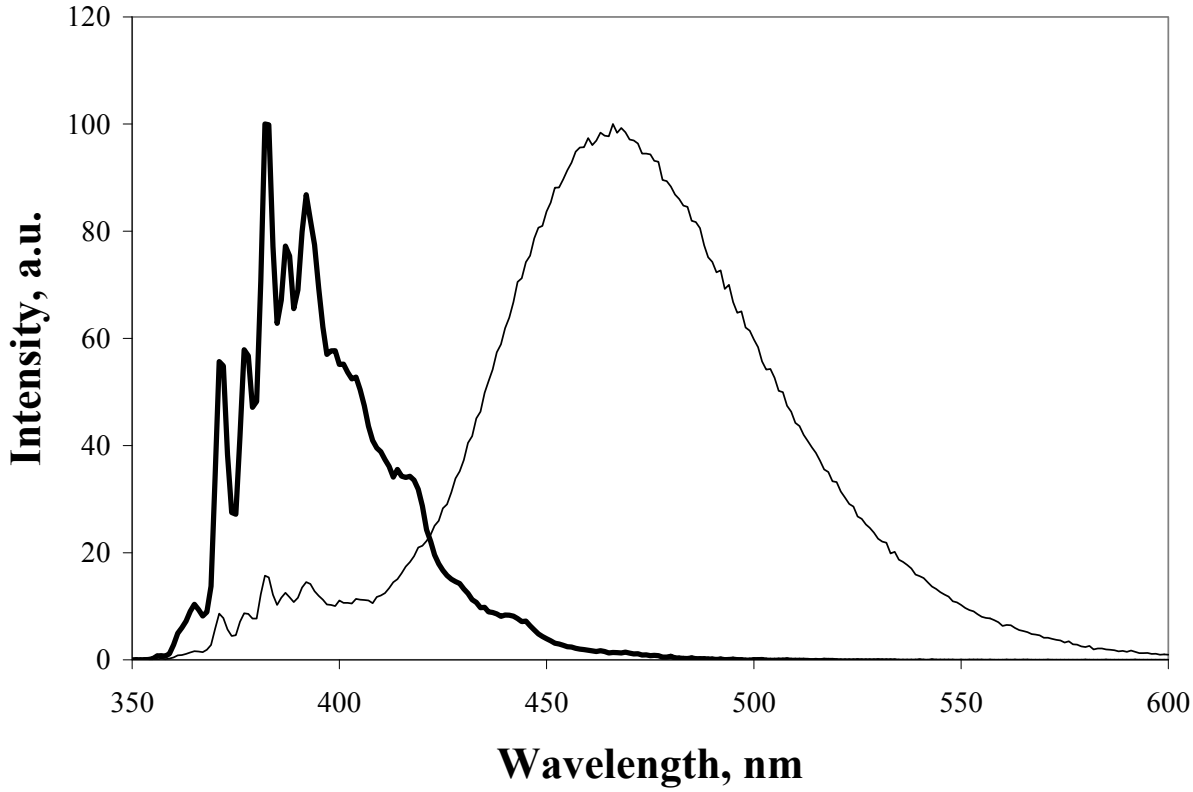

Figure 1.3: Fluorescence emission spectra of pyrene solutions in cyclohexane having concentrations of 2 μM (▬) and 20 mM (—), λ_{ex} = 336 nm.

The labelling of polymers with pyrene to characterize their behaviour in solution by fluorescence has become a common procedure. In fact, Francoise Winnik stated in her 1993 review on pyrene aggregates that pyrene is "*by far the most frequently used dye in fluorescence studies of labeled polymers*".[47] Pyrene labelling has been effective in monitoring polymer backbone[44] and side-chain dynamics[52] in organic solvents, temperature induced coil-to-globule transitions for polymers,[53–55] and the strength of hydrophobic associations for HMWSPs in aqueous solutions.[47,48]

Expressions for the rate constant of excimer formation k_1 may vary depending on the local distribution of pyrenes near an excited pyrene. Pyrenes covalently attached onto polymers and separated by a

specific chain length form excimer with a time-independent rate constant, k_1.[50,56] This rate constant can be easily determined by analyzing the time-resolved fluorescence decay of the pyrene monomer. However, in polymers randomly labelled with pyrene, the distribution of distances spanning every pyrene pair yields a distribution of rate constants k_1. This causes k_1 to become time-dependent as pyrene pairs separated by a short chain segment form excimer more quickly than those separated by a larger chain segment. In such a situation, a fluorescence blob model (FBM) which partitions the polymer coil into discreet volumes referred to as blobs has been successfully applied to model the rate of excimer formation of polymers randomly labelled with pyrene in solution.[57]

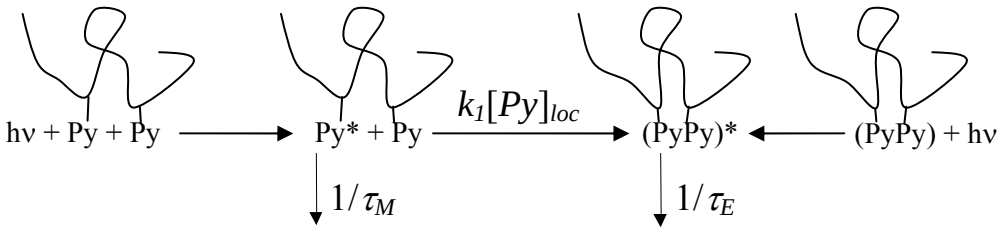

Scheme 1.4: Birks' scheme describing excimer formation of pyrene modified to include excitation of GS pyrene aggregates.

The two pathways leading to the formation of pyrene excimer are the direct excitation of GS pyrene aggregates and the diffusional encounters of an excited pyrene monomer with a GS pyrene. As both excimer species possess spectrally similar features, it is difficult to distinguish between the two species from the fluorescence emission spectrum alone. Several methods have been used in the past to differentiate between excimers formed by the direct excitation of GS pyrene aggregates and diffusional encounters between an excited pyrene and a GS pyrene. These methods include the examination of the peak-to-valley ratio, P_A, of the 0-0 transition peak and its adjacent trough in its

absorbance spectrum (Figure 1.4),[47] the degree of red-shifting in the excimer excitation spectrum relative to that of the monomer (Figure 1.5),[47] and the relative weight of the rise time in the excimer fluorescence decay (Figure 1.6).[58] The broadening of the absorption spectrum and the red-shift of the excimer excitation spectrum both indicate that the absorbance of the pyrene aggregates is broader and red-shifted compared to that of the monomeric pyrenes. While the existence of a difference between the two absorption spectra is well known, the molar absorbance coefficient of the pyrene aggregates has never been quantified due to the inability of isolating the contribution from the aggregated pyrene species to the absorbance. The formation of excimer via diffusive encounters between pyrenes is delayed relative to the initial excitation. This is exhibited in the excimer fluorescence decay as a rise time. Those excimers formed by the direct excitation of pyrene aggregates form excimer quasi-instantaneously and therefore the fluorescence decay does not exhibit a rise time. The relative contributions of the excimers formed either by diffusional encounters or pre-associated aggregates to the excimer fluorescence decay is dependent on the populations of the two types of excimers present in solution and their associated molar absorbance coefficients.

1.5.1 Pyrene Species Classification

The excited pyrenes present in solution can be classified into three separate species within the timeframe of an excited pyrene lifetime: isolated monomeric pyrenes that fluoresce with their natural lifetime, Py^*_{free}, monomeric pyrenes that diffuse to form excimers with GS pyrenes, Py^*_{diff}, and aggregated pyrenes that form excimers quasi-instantaneously, Py^*_{agg}.[59,60] The three pyrene species are illustrated in Figure 1.7. Pyrene species Py^*_{free} and Py^*_{diff} contribute to the monomer fluorescence while Py^*_{diff} and Py^*_{agg} contribute to the excimer fluorescence. The fractions of the contribution of

Py^*_{free}, Py^*_{diff}, and Py^*_{agg} to the fluorescence signal (f^f_{free}, f^f_{diff}, and f^f_{agg}, respectively) are dependent on their concentrations as well as their molar absorbance coefficient.

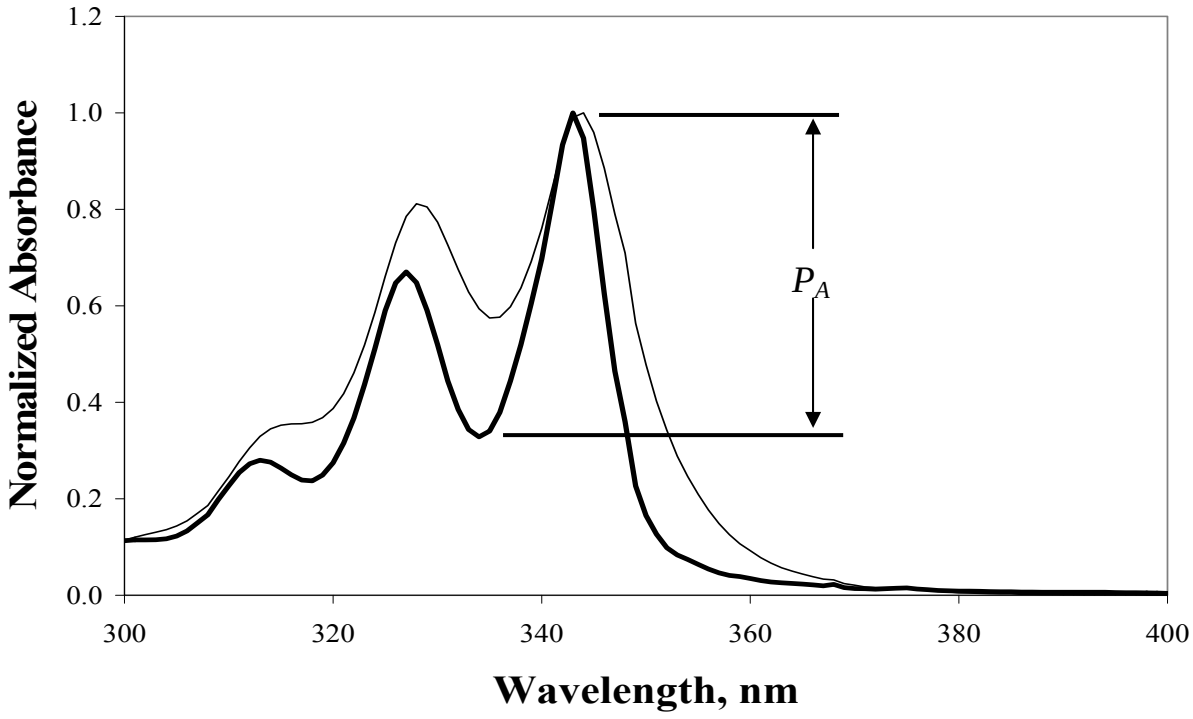

Figure 1.4: Absorption spectra normalized at the 0-0 peak of 2500 g/mol poly(ethylene oxide) labelled at one end with pyrene which is aggregated in water (—) and unaggregated in tetrahydrofuran (▬).

These fluorescence fractions can be obtained from the global analysis of the monomer and excimer decays and have been used previously as a measure of the level of association of pyrene. For instance, the fractions f^f_{free}, f^f_{diff}, and f^f_{agg} have been determined for aqueous solutions of pyrene-labelled HASE (PyHASE) polymers mixed with the anionic surfactant sodium dodecyl sulfate (SDS).[60] As SDS was added to the solution, the surfactant "melted" the hydrophobic association of

the pyrenes, which was marked by a decrease in f_{agg}^{f}. A drop in the fluorescence fraction f_{agg}^{f} implies that the level of pyrene aggregation f_{agg} also decreases with SDS concentration above its critical micelle concentration.

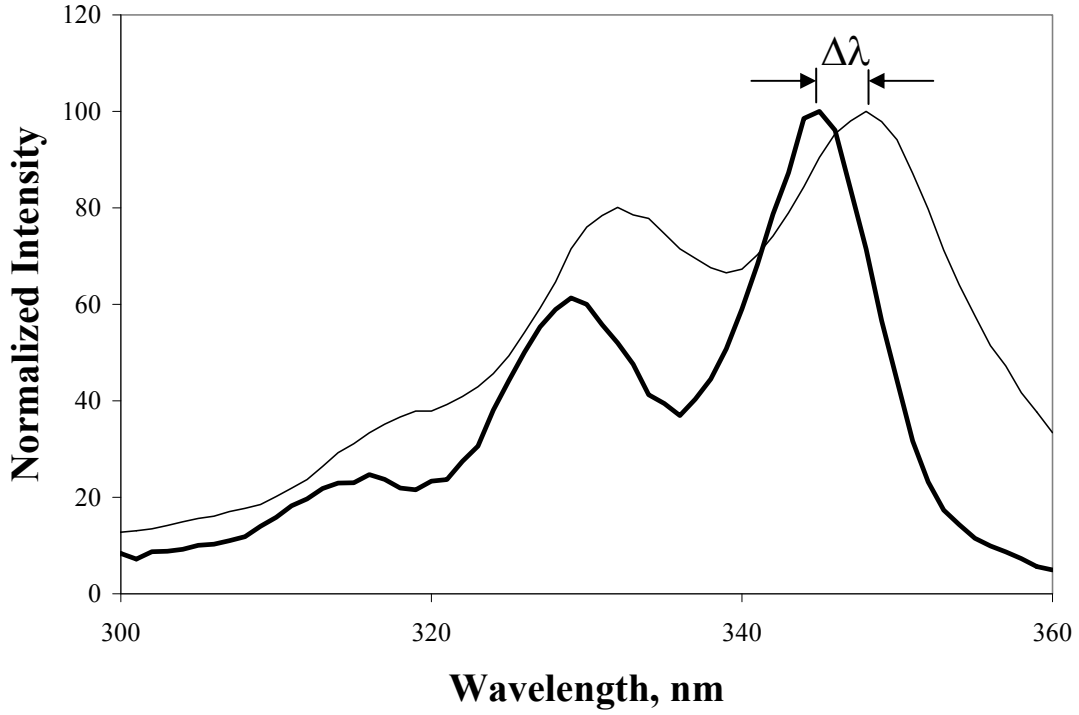

Figure 1.5: Shift observed in the fluorescence excitation spectra of the monomer and excimer taken at 375 nm (**—**) and 510 nm (—), respectively, for aqueous solutions of pyrene-labelled poly(*N*,*N*-dimethylacrylamide) having 645 μM of pyrene per gram of polymer.

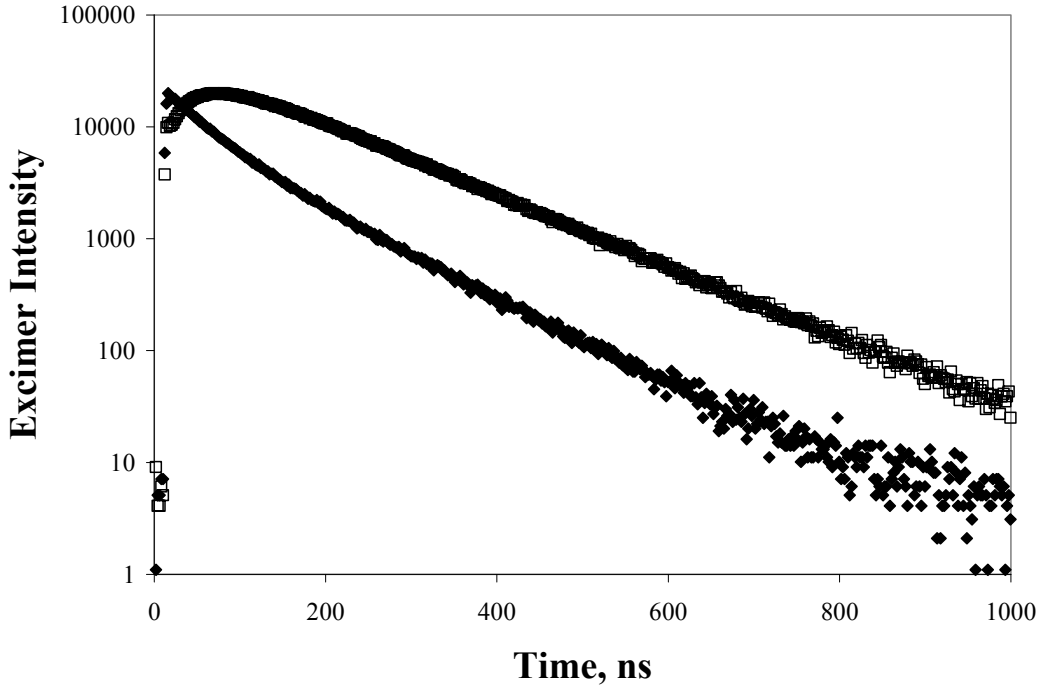

Figure 1.6: Excimer fluorescence decays excited at 344 nm and obtained at 510 nm for a 2500 g/mol poly(ethylene oxide) labelled at one end with pyrene which is aggregated in water (◆) and unaggregated in acetonitrile (□).

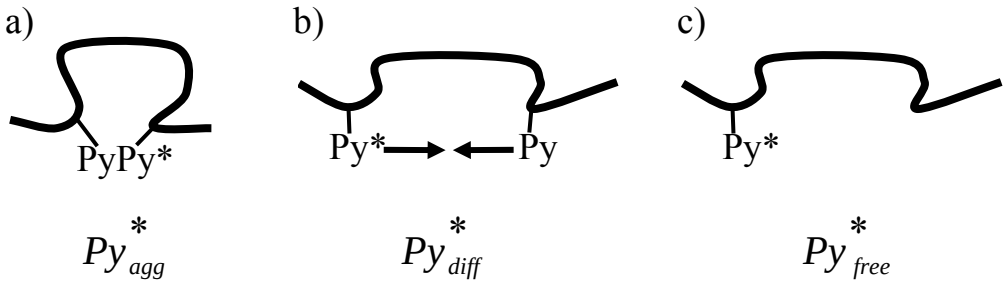

Figure 1.7: Excited pyrene species that a) exist as isolated monomeric pyrenes, b) form excimers via diffusive encounters between an excited pyrene and a GS pyrenes, and c) exist as aggregated pyrenes.

1.6 Fluorescence Instrumentation

Steady-State Fluorescence Measurements: A schematic of the steady-state spectrofluorometer used to acquire the fluorescence spectra is shown in Figure 1.8. The light source used was a 75 watt xenon arc lamp capable of supplying polychromatic light at UV wavelengths as low as 250 nm to near-infrared wavelengths of 800 nm at high intensities.[61] Both excitation and emission wavelength were selected with a monochromator containing a diffraction grating. The motorized movements of the diffraction gratings inside the monochromators were controlled by a computer. The fluorescence emission was detected with a photomultiplier tube that converts the intensity of the fluorescence signal into a corresponding electrical current which was then recorded by the computer. The fluorescence spectra acquired on the computer were saved as text files of fluorescence intensity versus wavelength.

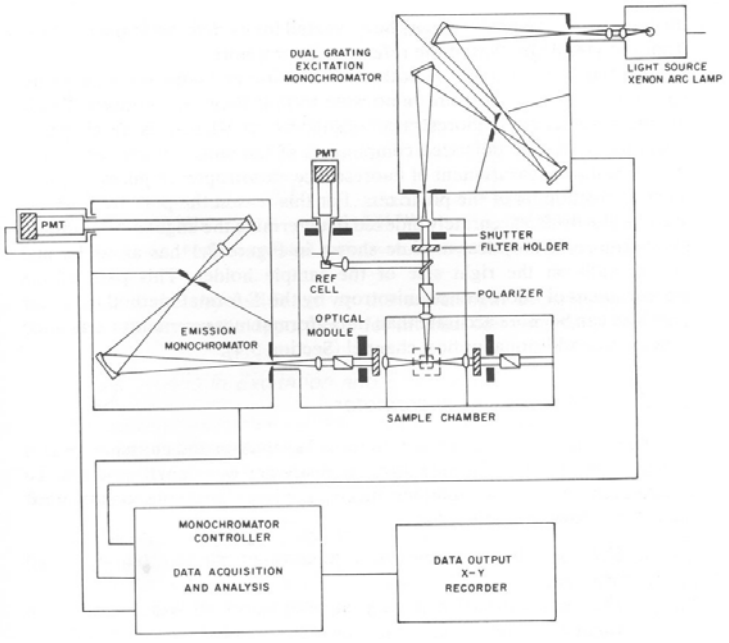

Figure 1.8: Schematic of a steady-state spectrofluorometer (Reprinted from Joseph R. Lakowicz Principles of Fluorescence Spectroscopy; Plenum Press: New York, 1983, Figure 2.1, pp.21).[61]

Emission spectra were acquired by setting the excitation wavelength at a constant value while scanning the emission wavelength. Acquisition of excitation spectra is carried out by setting the emission wavelength to a constant value while scanning the excitation wavelength. Although the steady-state spectrofluorometer was capable of correcting for lamp intensity fluctuations, reference standards can also be used. However, no corrections to the fluorescence spectra presented in this thesis were performed save for simple baseline subtractions.

Time-Resolved Fluorescence Measurements: The pyrene monomer and excimer fluorescence decays were acquired using the single photon counting technique. The schematic of a single photon counter given in Figure 1.9 is similar to that of the spectrofluorometer with the difference being the additional complexity of the electronics used. The light source of the single photon counter was a solid-state LED capable of emitting nanosecond pulses of 344 nm UV light at frequencies of up to 1 MHz. With each lamp pulse, the time-to-amplitude converter triggered a voltage ramp whose voltage increased linearly with time. The voltage ramp was terminated by an exit pulse from the emission detector filtered by the discriminator. The voltage value of the terminated ramp, corresponded to a channel number in the multichannel analyzer and one count was added to the channel. The start/stop cycle was repeated numerous times to generate a statistical profile representing the fluorescence decay of the sample with a minimum of 10,000 counts acquired at the maximum to ensure a good signal-to-noise ratio. To avoid skewing of the acquired decay, the intensity of the signal was adjusted so that one exit pulse out of 50 lamp pulses (2% of the signal) was being detected.[61] The fluorescence decays were saved in the form of count number versus channel as text files on the computer with the time per channel conversion factor recorded.

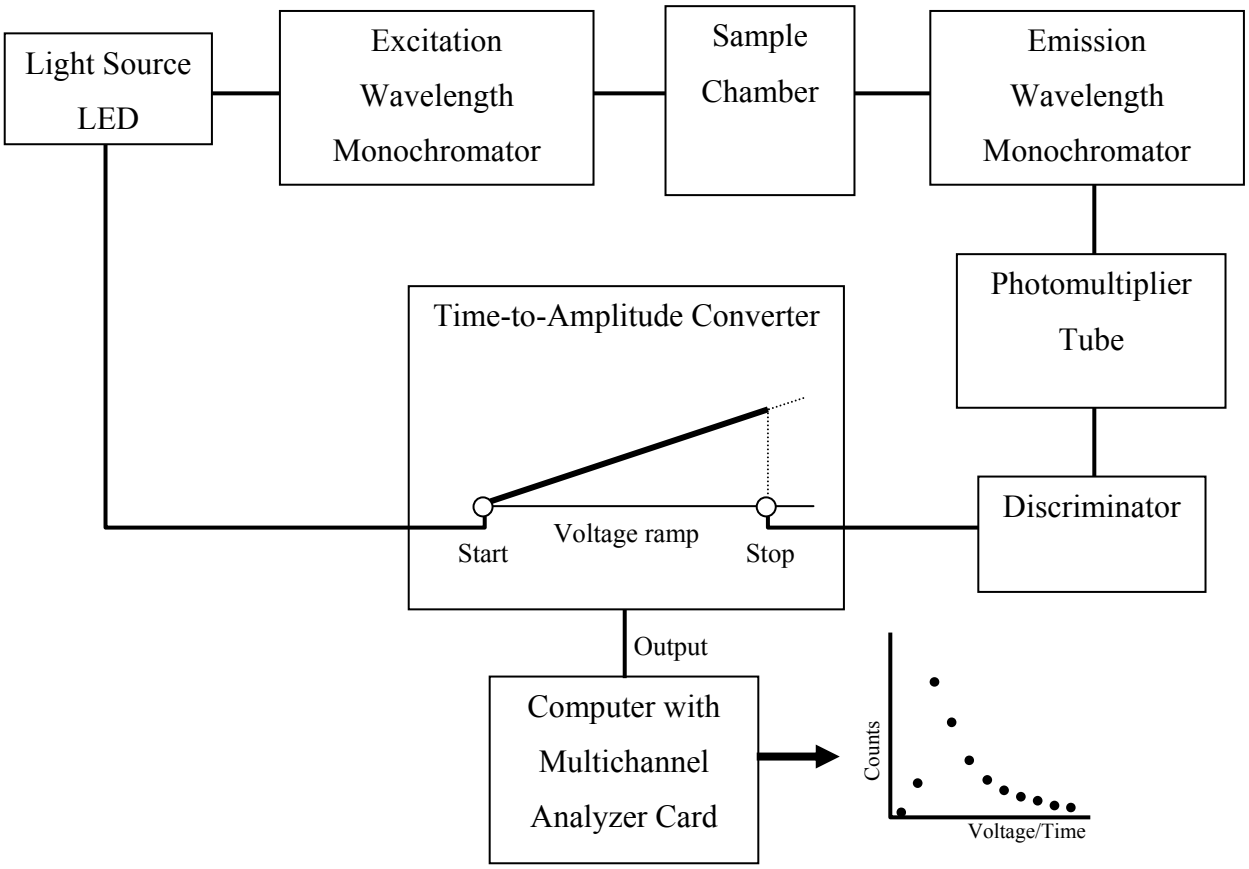

Figure 1.9: Schematic diagram of a single photon counter.

In addition to the fluorescence decay of the sample, the lamp function was also acquired. This enabled the deconvolution of the acquired decay in order to obtain the true fluorescence decay of the sample. Analysis of the decays involved fitting them with a given mathematical function. The "goodness" of the fit was characterized by comparing the theoretical decay, calculated from the fitted function, with the data points of the experimentally acquired decay. The "goodness" of the fit was quantified by using a χ^2 function

$$\chi^2 = \sum_{i=1}^{N} \frac{(R(i) - R_c(i))^2}{R(i)} \qquad (1.3)$$

where, for a decay having N channels, $R(i)$ and $R_c(i)$ are the measured and calculated decay values at channel i, respectively. Based on the expression of Equation 1.3, the optimal value for χ^2 should theoretically be zero although in practice, Poisson noise in the decays leads to a minimum χ^2 value of 1.0. A fit is considered poor when it yields a χ^2 value greater than 1.2. In Figure 1.10, a simulated decay having two lifetimes was fit with both a mono- and bi-exponential function. Fitting the decay with a bi-exponential function yielded a good fit having a χ^2 value of 0.95 while the mono-exponential fit yielded a poor χ^2 value of 1.7. Another indicator of a good fit is the normalized residual which is given by $[R(i) - R_c(i)] / \sqrt{R_c(i)}$. A good fit yields residuals that are randomly distributed around zero such as for the bi-exponential fit in Figure 1.10a. The existence of a pattern in the residuals such as for the mono-exponential fit in Figure 1.10b indicates a poor fit.

1.7 Goal of the Thesis

The overall purpose of this thesis is to characterize the self-assembly of amphiphilic molecules, be they pyrene-labelled lipids self-assembling inside a lipid bilayer or pyrene-labelled polymer self-assembling in aqueous solution. Since hydrophobic aggregation is the primary driving force leading to the formation of the structures, the labelling of a hydrophobic chromophore such as pyrene onto the self-assembling molecules enables one to monitor the behaviour of these pyrene aggregates by fluorescence. Although pyrene is considered to be an ideal chromophore label due to its ability to form pyrene aggregates that can be probed at a different wavelength in the fluorescence spectrum, the differences in absorbance properties between unaggregated and aggregated pyrene

species complicate the determination of the contributions of the different pyrene species by fluorescence. This thesis addresses these concerns by developing a protocol for determining the molar absorbance coefficient of the pyrene aggregates for two pyrene-labelled polymers.

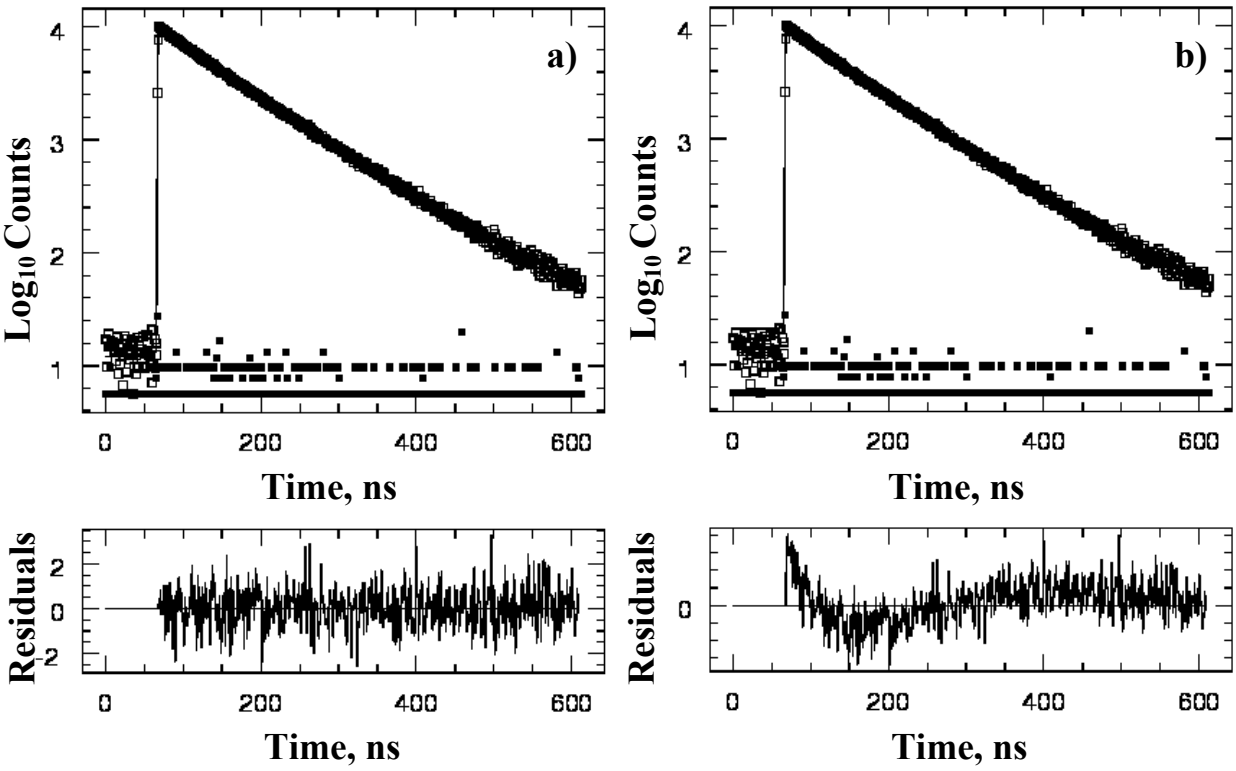

Figure 1.10: A simulated bi-exponential decay fitted with a a) bi-exponential and b) mono-exponential function.

In Chapter 2, lipid vesicles containing a small fraction of functionalized lipids labelled with pyrene were studied by fluorescence to determine the organization of the functionalized lipids in the membrane and how the organization changes with the introduction of divalent ions capable of binding to the functionalized lipid head groups. In particular, attention to changes for fluorescence fractions

f_{free}^{f}, f_{diff}^{f}, and f_{agg}^{f} was given as greater phase separation increases the fractions f_{diff}^{f} and f_{agg}^{f} that describe excimer formation at the expense of the fraction attributed to isolated pyrene lipids, f_{free}^{f}. In addition, the fluidity of the two types of phospholipids vesicles the fluid 1-palmitoyl-2-oleyl-3-*sn*-phosphatidylcholines (POPC) and the gel-like distearylphosphatidylcholine (DSPC), was characterized by fluorescence.[62]

The hydrophobic pendants of the HMWSPs can be substituted with pyrene, which is sufficiently hydrophobic to induce network formation in water.[34,63] As with typical HMWSPs, the hydrophobic pyrene pendants of pyrene-labelled HMWSPs (PyHMWSPs) aggregate to form networks at sufficiently high polymer concentrations. These PyHMWSP solutions possess rheological properties similar to that of their alkyl-modified analogues.[59] The unassociated pyrene pendants in solution fluoresce as monomers while the hydrophobic pyrene aggregates are expected to fluoresce as excimers. Thus, direct fluorescence measurements of the hydrophobic aggregates can be performed to differentiate between aggregated versus unaggregated pyrenes. These experiments yield f_{agg}, the fraction of aggregated pyrene pendants, a parameter that has been often poorly characterized.

Previously, the hydrophobic association of PyHMWSP has been studied with qualitative indicators such as the P_A and I_E/I_M ratios, the magnitude of the shift observed between the monomer and excimer fluorescence excitation spectra, and the existence of a rise time in the excimer fluorescence decay.[34,45,46,64] More recently, the fluorescence fractions were used to gain information on the aggregation of pyrene for PyHASE in aqueous solution.[59,60] In order to fully characterize the parameter f_{agg} for PyHMWSPs by fluorescence, information on the absorbance properties of the pyrene aggregates must also be known. Chapter 3 focuses on the development of a protocol which is used to determine f_{agg} for pyrene-labelled poly(*N*,*N*–dimethylacrylamide) (PyPDMA) and the molar absorbance coefficient of the pyrene aggregates of PyPDMA in water. The results from Chapter 3 have been published in the *Journal of Physical Chemistry B*.[65]

This protocol was then applied to determined the molar absorbance coefficient of the pyrene aggregates found in a sample of pyrene-labelled poly(ethylene oxide) (PyPEO) in Chapter 4. Hydrophobically terminated PEO chains are the key component of two families of commercial HMWSPs: hydrophobically-modified ethoxylated urethane (HEUR) and hydrophobically-modified alkali-swellable emulsion (HASE) polymers. In order to characterize the kinetics of excimer formation by diffusion for PyPEO, a model free approach[64] was developed to analyze the fluorescence decays and determine the fractions of the different pyrene species in solution. Chapter 5 describes the attempts to use the protocol established in Chapters 3 and 4 to determine the level of association of PyHASE quantitatively. Although the application of the protocol did not yield satisfactory values of f_{agg} for PyHASE, the various attempts and modifications made to the model have been documented in this chapter.

In Chapter 6, a PyHASE polymer was studied by fluorescence as the PyHASE solution was sheared. Under static conditions, the associations of the pyrene pendants for HMWSPs are allowed to reach equilibrium. Upon the application of shear deformation to the solution, the strain caused by the shear force leads to the disruption of the network. The status of the hydrophobic aggregates as shear is applied to the solution, whether the network experiences an increase in dangling ends or merely a switching from intermolecular bridges to intramolecular associations, has been conjectured but has never been decisively determined.[32–36] Monitoring the fluorescence fractions obtained from the monomer and excimer decays of the pyrene labels of PyHASE was expected to give information on the effect that shear has on the hydrophobic aggregates holding the network together. If dangling ends were created by the application of shear, the fluorescence fraction of pyrenes that are aggregated f_{agg}^{f} would be expected to decrease. To accomplish this experiment, the development of a remote sensing unit capable of acquiring fluorescence measurements at the rheometer site was required. This joint fluorometer/rheometer unit, based on the remote set up designed by Richey et al.,[34] is comprised of a

fluorometer where the fluorescence signal is transmitted via fiber optic cables to and from the rheometer where the sample is sheared. In the previously designed setup, only steady-state fluorescence experiments could be performed whereas the setup designed in this thesis allowed both steady-state and time-resolved fluorescence measurements to be performed.

With this thesis, it is hoped that information obtained from the experiments characterizing the self-assembly of two amphiphilic molecules, pyrene-labelled lipids and pyrene-labelled HMWSPs, will yield valuable insight on the self-assembly of their non-pyrene labelled analogues. Furthermore, it is hoped that the experiments on the absorbance properties of the pyrene aggregates will lead to a standard protocol where the level of association parameter f_{agg} may be obtained for any PyHMWSP. This would be an important achievement since it is an important parameter in modelling the rheological behaviour of HMWSPs in solution.

Chapter 2
Nanodomain Formation in Lipid Membranes Probed by Time-Resolved Fluorescence

2.1 Overview

Time-resolved fluorescence measurements on liposomes prepared with 1 mol% of pyrene-labelled lipids (PLLs) with a head group bearing either an alcohol (PSOH) or an imido diacetic acid (PSIDA) and 99 mol% of 1-palmitoyl-2-oleyl-3-*sn*-phosphatidylcholines (POPC) or 99 mol% of distearylphosphatidylcholine (DSPC) were performed to investigate how lipids phase separate within the membrane bilayer. Global analysis of the fluorescence decays with the fluorescence blob model (FBM) led to the conclusion that the PLLs were homogeneously distributed on the surface of POPC vesicles while the PLLs phase-separated in the DSPC vesicles. The analysis yielded the fraction of aggregated pyrenes, f_{agg}. The large f_{agg} values found for PSIDA suggest that the imido diacetic acid head group of PSIDA induces self-aggregation and phase separation in both membranes. The addition of external cations such as Cu^{2+} and La^{3+} was shown to hinder diffusional encounters between PSIDAs. The cations seem to target preferentially unassociated PSIDAs rather than aggregated PSIDA clusters. Accounting for the quenching of pyrene by Cu^{2+} enables one to use PSIDA to probe the microviscosity of the lipid membrane. Using this effect, the environment of PSIDA in the DSPC membrane was found to be about 6 times more viscous than in the POPC membrane. This difference is attributed to the difference in viscosity of the fluid POPC membrane and the gel-like DSPC membranes.

2.2 Introduction

Membrane structure and phase composition are critical to the function of integral and associated proteins and, consequently, to the health of cells.[1] Diabetes[2] and Alzheimer's[3] are among the many diseases linked to the physical parameters of the cell membrane, such as stiffness, fluidity, and lipid composition. Microscale heterogeneity of the membrane due to the phase separation of lipids with similar or complementary interactions into domains plays a significant role in the function of cellular processes.[4] Membrane microdomains, sometimes referred to as rafts, are molecular assemblies composed of lipids and proteins that are considered to be the platform for signaling events, endocytotic processes, and protein activity.[5] These structures are believed to vary in size and lifetimes, consisting of just a handful of molecules to near micron scale superassemblies.[6] Changes in intermolecular interaction through electrostatics, packing order, and hydrogen bonding altered through ligand complexation may be a trigger for the assembly and disassembly of raft-like structures. Although much has been learned on phase separation at the microscale from model systems,[6,7] our understanding of assemblies that form in the sub-micron regime trails far behind.

Phase separation in lipid membranes can be induced through a variety of interactions, the most common of which is due to differences in phase transition temperature of the lipid components. For example, gel phase lipids will spontaneously separate from a membrane containing fluid phase lipids due to the energetics involved with packing order.[8] The phase separation can also be induced by the recognition, or binding, of metal ions to charged lipid headgroups that results in the increase in phase transition temperature of one lipid component, or through bridging interactions of multivalent ions with multiple lipids.[9] It is also possible to use molecular shape to create complementary packing order to facilitate the assembly of ordered domains, such as with cholesterol-sphingomyelin liquid ordered phases.[10]

A variety of lipids with unique structure and functionality for ligand binding have been synthesized and used in studies of membrane organization directed by host-guest interactions.[11–14] Optical probes were attached on the tails of these synthetic lipids as reporters of local aggregation. Assemblies of metal chelating lipids in a phosphatidylcholine lipid membrane have been found to reorganize in response to metal binding due to a switch in electrostatics of the lipid headgroup.[15,16] Fluorescence spectroscopy[17] and atomic force microscopy[18] have been used to characterize the state-to-state changes in lipid assembly prior to and after metal ion exposure. Such dynamics in molecular assembly driven by the simplest of host-guest interactions demonstrate the temporal influence of ligand binding on membrane structure.

Further understanding of how lipid structure, chemistry, and ligand binding induces membrane organization at the level of molecular clusters would provide much needed insight and routes towards control over molecular assembly in lipid membranes. Herein, we report on the development of a model system and analytical tools that allow us to probe the assembly of functionalized lipids and the reorganization of membrane structures upon metal ion binding using fluorescence spectral and lifetime measurements. The membrane system uses pyrene-labeled lipids (PLLs) to probe local membrane viscosity and heterogeneity by monitoring ground state and excited state monomers and dimers. The effects of metal ion binding were evaluated by using an imino diacetic acid-functionalized lipid called PSIDA as the metal chelator and incorporating the lipid into phosphatidylcholine lipid matrices. PSIDA exhibits high affinity for multivalent metal ions, such as Cu^{2+}, Cr^{3+}, and Fe^{3+},[17] while its carboxylate and amino functionality can promote intermolecular hydrogen bond interactions. Previously, it was found through steady-state fluorescence studies that PSIDA strongly aggregates in the gel phase matrix of DSPC (distearoylphosphatidylcholine). However, upon Cu^{2+} binding the PSIDA lipids disperse into the DSPC matrix as a consequence of electrostatic repulsion of cationic metal-chelated headgroups. This process was proven to be

reversible with the removal of Cu^{2+} ions allowing the reformation of these phase-separated domains. A more subtle effect also occurs in fluid phase POPC (1-palmitoyl-2-oleoyl-sn-glycero-3-phosphocholine) membranes. While the gross changes in molecular aggregation have been evaluated, details of the factors that influence changes in lipid local environment and molecular assembly/disassembly with metal ion binding remain largely unexplored.

The formation and fate of isolated PLLs and aggregated lipids can be readily followed using pyrene fluorescence. As seen in a modified Birks' scheme given in Scheme 2.1,[19] unassociated pyrenes (Py), called monomers, may either fluoresce in the blue region of the visible spectrum or form an excimer (E*) via a diffusive encounter with a ground-state pyrene. Direct excitation of pre-associated ground-state (GS) pyrene aggregates (PyPy) results also in the formation of excimers whose fluorescence spectrum overlaps that of excimers formed via diffusive encounter between an excited and a ground-state pyrene. The spectral overlap between the two excimer species makes it quite difficult to assign how each species contributes to the excimer emission. Differentiation between excimers generated by the direct excitation of pre-formed aggregates versus the diffusive encounter between a ground-state and excited pyrene can be achieved through the examination of the time-resolved fluorescence decay of the excimer.[20,21] The analysis applied to describe quantitatively the various processes at play requires using a model that handles both excimer forming processes concurrently. This can be achieved by applying the Fluorescence Blob Model (FBM)[22] to describe the diffusive encounters between PLLs randomly distributed in the lipid membrane and fitting the monomer and excimer fluorescence decays globally so that any contribution to the excimer not handled by the FBM is directly attributed to these excimers formed by direct excitation of GS pyrene aggregates. This procedure has been applied successfully to numerous pyrene-labelled polymers in aqueous solution to determine the molar fraction of aggregated pyrenes, f_{agg}.[23]

$$Py^{*} + Py + h\nu \longrightarrow Py^{*} + Py \longrightarrow E^{*} \longleftarrow PyPy + h\nu$$

$$\downarrow \frac{1}{\tau_M} \qquad\qquad \downarrow \frac{1}{\tau_E}$$

Scheme 2.1: Modified Birks' scheme illustrating the possible pathways leading to excimer formation.[19]

This study characterizes the organization of PLLs on the surface of a vesicle membrane by determining f_{agg} using a combination of steady-state and time-resolved fluorescence and applying the procedure described above. In addition to PSIDA, we also employed PSOH (8-[1-octadecyl-2-(9-(1-pyrene)nonyl)-*rac*-glyceroyl]-3,6-dioxaoctan-1-ol) as a control with its similar structure but non-metal chelating headgroup (Figure 2.1). We assessed the distribution of PSOH in vesicles composed of both fluid phase (POPC) and gel phase (DSPC) to quantitatively determine f_{agg} for PSOH. The mobility of PSOH in both matrices was characterized and compared. The ability of PSIDA to self-assemble in the POPC and DSPC membranes was then compared and the results used to evaluate the roles of intermolecular interactions, molecular level heterogeneity of the membrane, and metal ion binding on lipid aggregation.

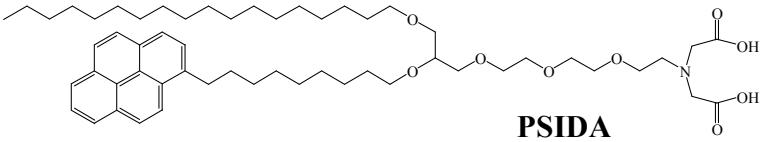

PSIDA

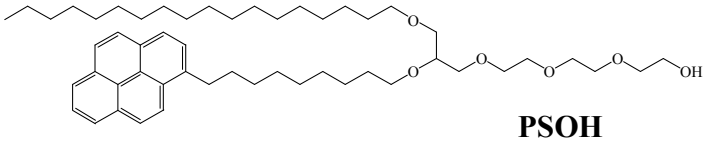

PSOH

Figure 2.1**:** Structures of PSIDA and PSOH.

2.3 Experimental

Lipids and liposomes: Syntheses of PSIDA and PSOH are described elsewhere.[24] POPC and DSPC were purchased from Avanti Polar Lipids (Alabaster, AL). All organic solvents were obtained from Fisher Scientific. Aqueous solutions were prepared from deionized water obtained through a Barnstead Type D4700 NANOpure Analytical Deionization System with ORGANICfree cartridge registering an 18.0 MΩ-cm resistance.

The liposomes were prepared by dissolving the equivalent of 0.1 or 1 mol% of PSIDA or PSOH in a DSPC or POPC chloroform solution yielding a total lipid concentration of ca. 1.5 mM. The lipid solutions containing 0.1 mol% PLL were used uniquely for the purpose of determining the lifetime of the pyrene monomer τ_M. The solution was evaporated to a thin film on the walls of a glass centrifuge tube using a rotary evaporator. Residual solvent was removed from the film by further drying overnight under high vacuum. The film was then hydrated in either 3.0 mL of MOPS buffer solution (0.02 M 4-morpholino-propanesulfonic acid, 0.1 M NaCl, in deionized water, pH 7.4) or deionized water at 65 ^oC with vortex stirring, producing a total lipid concentration of 3.5 mM. The suspended film was then deaerated by bubbling with N_2 for several minutes, followed by sonication with a 3 mm probe tip using 25W power and maintaining an atmosphere of N_2. Sonication was performed in 4 minute cycles with 1 minute resting between each cycle for a total of 20 minutes, intermittently cooling the solution in an ice bath. The translucent solution was centrifuged for 20 minutes at 16,000 g to remove large bilayer aggregates. The supernatant was then filtered through a 0.2 micron filter. Solutions for fluorescence measurements were diluted with additional MOPS buffer to a baseline corrected optical density value of 0.1 at 344 nm.

Steady-State Fluorescence: The steady–state fluorescence spectra were obtained using a Photon Technology International LS–100 steady–state fluorometer equipped with either a pulsed xenon flash lamp or an Ushio UXL-75Xe xenon arc lamp and a PTI 814 photomultiplier detection system. The

emission spectra were acquired by exciting the samples at 344 nm. The fluorescence intensities were calculated by integrating the intensities from 372 to 378 nm for the pyrene monomer, I_M, and from 500 to 530 nm for the pyrene excimer, I_E. All solutions were aerated.

Time-Resolved Fluorescence Decays: The fluorescence decay profiles were acquired with an IBH Ltd. time-resolved fluorometer equipped with either a 5000F coaxial nanosecond flash lamp filled with H_2 gas or an IBH 340 nm NanoLED. All solutions were excited at 344 nm. The emission wavelength was set at 374 and 510 nm for the pyrene monomer and excimer decays, respectively. To reduce the noise stemming from stray scattered light, cutoff filters of 370 and 495 nm were used to acquire the monomer and excimer decays, respectively. All samples were aerated. All decays were collected over 1,024 channels with a minimum of 40,000 and 15,000 counts taken at the maximum of the monomer and excimer decays, respectively, to ensure a high signal–to–noise ratio. Deoxygenated solutions of PPO [2,5–diphenyloxazole] in cyclohexane (τ = 1.42 ns) and BBOT [2,5–bis(5–tert–butyl–2–benzoxazolyl)thiophene] in ethanol (τ = 1.47 ns) were used as references for the monomer and excimer decays, respectively. The MIMIC method[25] was applied to the fluorescence decays of the reference compounds to determine the instrument response function of the fluorometer at the excitation and emission wavelengths where the monomer (λ_{ex} = 344 nm, λ_{em} = 376 nm) and the excimer (λ_{ex} = 344 nm, λ_{em} = 510 nm) decays were acquired. All measured decays were deconvoluted from the instrument response function and fitted to the desired function using a least–squares optimization routine. The resulting fits were characterized as "good" when the χ^2 parameter was smaller than 1.3 and the residuals and the autocorrelation function of the residuals were randomly distributed around zero.

Analysis of the Fluorescence Decays: All monomer and excimer decays were first fitted with a sum of exponentials whose expression is given in Equation 2.1.

$$I_X(t) = \sum_{i=1}^{i=N} a_{Xi} \exp(-t/\tau_{Xi}) \qquad (2.1)$$

In Equation 2.1, the symbol *X* represents either the monomer *M* or the excimer *E*, and the index *N* is the number of exponentials used in the fit. *N* values ranged from 2 to 4.

The FBM equation used to fit the monomer fluorescence decays is given in Equation 2.2. It was derived using the mathematical treatment proposed by Tachiya[26]

$$[Py^*]_{(t)} = [Py^*_{diff}]\exp\left[-\left(A_2 + \frac{1}{\tau_M}\right)t - A_3\left(1-\exp\left(-A_4\, t\right)\right)\right] + [Py^*_{free}]\exp\left(-t/\tau_M\right) \qquad (2.2)$$

where $[Py^*_{diff}]$ and $[Py^*_{free}]$ are the concentrations of the excited pyrenes that form excimer via diffusional encounters with other pyrenes and excited isolated pyrenes that do not form excimer, respectively. The parameters A_2, A_3, and A_4 used in Equation 2.2 are functions of the parameters k_{blob}, $\langle n \rangle$, and $k_{ex}[blob]$ which are the rate constant of quenching by a ground-state pyrene in a blob, the average number of pyrenes per blob, and the rate constant of pyrene exchange between blobs, respectively. The expressions of A_2, A_3, and A_4 as a function of k_{blob}, $\langle n \rangle$, and $k_{ex}[blob]$ are given in Equation 2.3. Equation 2.2 and 2.3 are equivalent to those derived by Tachiya to study the exchange of quenchers between surfactant micelles.[27]

$$A_2 = < n > \frac{k_{blob} k_{ex}[blob]}{k_{blob} + k_{ex}[blob]} \qquad A_3 = < n > \frac{k_{blob}^2}{\left(k_{blob} + k_{ex}[blob]\right)^2}$$

$$A_4 = k_{blob} + k_{ex}[blob] \tag{2.3}$$

In Equation 2.2, τ_M represents the lifetime of the unquenched pyrene monomer. τ_M was determined by fitting the monomer fluorescence decays of vesicle solutions containing 0.1 mol% PSOH and 99.9 mol% of POPC and DSPC with Equation 2.1. The longest decay time retrieved in the analysis was attributed to τ_M which was found to equal 115 and 185 ns for PSOH in POPC and DSPC, respectively. As usually done when the medium where excimer formation takes place restricts the number of possible geometries available for the proper stacking of two pyrene moieties, several excimer species needed to be considered.[20,21,23,28] Proper stacking of two pyrene molecules results in the formation of an excimer *E0**, while improper stacking of two pyrenes results in the formation of excited pyrene dimers which are either shorter- (*ES**) or longer- (*EL**) lived than *E0**. The lifetimes of *ES**, *E0**, and *EL** are referred to as τ_{ES}, τ_{E0}, and τ_{EL}, respectively. The three species *ES*, *E0*, and *EL* exist in the ground-state but *E0** can also be produced by the diffusive encounter between an excited monomer and a ground-state monomer. Whereas the existence of the species *E0** and *EL** was necessary to properly fit the excimer fluorescence decays acquired with PSOH, no contribution from the *ES** species could be detected. Assumption of the existence of all three species, *ES**, *E0**, and *EL**, was required to fit the excimer fluorescence decays acquired with PSIDA. The concentrations of these species were incorporated in Equation 2.4 used to fit the excimer fluorescence decays.[23]

$$[E^*] = -[Py^*_{diff}]_{(t=0)}\, e^{-A_3} \sum_{i=0}^{\infty} \frac{A_3^{\,i}}{i!} \frac{A_2 + i\,A_4}{\frac{1}{\tau_M} - \frac{1}{\tau_{E0}} + A_2 + i\,A_4} \exp\left(-\left(\frac{1}{\tau_M} + A_2 + i\,A_4 \right) t \right)$$

$$+ \left([E0^*]_{(t=0)} + [Py^*_{diff}]_{(t=0)}\, e^{-A_3} \sum_{i=0}^{\infty} \frac{A_3^{\,i}}{i!} \frac{A_2 + i\,A_4}{\frac{1}{\tau_M} - \frac{1}{\tau_{E0}} + A_2 + i\,A_4} \right) e^{-t/\tau_{E0}}$$

$$+ [ES^*]_{(t=0)}\, e^{-t/\tau_{ES}} + [EL^*]_{(t=0)}\, e^{-t/\tau_{EL}} \tag{2.4}$$

The fractions f_{diff}, f_{free}, f_{ES}, f_{EL}, and f_{E0}, representing the pyrene species Py^*_{diff}, Py^*_{free}, *ES**, *EL**, and *E0**, respectively, were obtained from fitting the monomer and excimer fluorescence decays with Equation 2.2 and 2.4, respectively. These fractions are defined in Equations 2.5 to 2.9. The fraction representing all species of aggregated pyrenes is estimated with Equation 2.10.

$$f_{diff} = \frac{[Py^*_{diff}]_{(t=0)}}{[Py^*_{diff}]_{(t=0)} + [Py^*_{free}]_{(t=0)} + [ES^*]_{(t=0)} + [EL^*]_{(t=0)} + [E0^*]_{(t=0)}} \tag{2.5}$$

$$f_{free} = \frac{[Py^*_{free}]_{(t=0)}}{[Py^*_{diff}]_{(t=0)} + [Py^*_{free}]_{(t=0)} + [ES^*]_{(t=0)} + [EL^*]_{(t=0)} + [E0^*]_{(t=0)}} \tag{2.6}$$

$$f_{ES} = \frac{[ES^*]_{(t=0)}}{[Py^*_{diff}]_{(t=0)} + [Py^*_{free}]_{(t=0)} + [ES^*]_{(t=0)} + [EL^*]_{(t=0)} + [E0^*]_{(t=0)}} \tag{2.7}$$

$$f_{EL} = \frac{[EL^*]_{(t=0)}}{[Py^*_{diff}]_{(t=0)} + [Py^*_{free}]_{(t=0)(t=0)} + [ES^*]_{(t=0)} + [EL^*]_{(t=0)} + [E0^*]_{(t=0)}} \tag{2.8}$$

$$f_{E0} = \frac{[E0^*]_{(t=0)}}{[Py^*_{diff}]_{(t=0)} + [Py^*_{free}]_{(t=0)(t=0)} + [ES^*]_{(t=0)} + [EL^*]_{(t=0)} + [E0^*]_{(t=0)}} \tag{2.9}$$

$$f_{agg} = f_{E0} + f_{EL} + f_{ES} \qquad (2.10)$$

The method used to obtain the pyrene fractions given in Equations 2.5 – 2.10 has been described in greater detail previously.[21]

In the analysis of the excimer fluorescence decays obtained with PSOH, $[ES^*]_{(t=0)}$ in Equation 2.4 is set equal to zero. To improve the accuracy of the parameters retrieved from the analysis of the pyrene monomer and excimer decays with Equations 2.2 and 2.4, respectively, the analysis of the monomer and excimer decays was performed globally.

Optimization of the parameters used in Equations 2.1, 2.2, and 2.4 to fit the fluorescence decays was performed with the Marquardt-Levenberg algorithm.[29] A background correction was applied to fit the fluorescence decays. As done in earlier publications, a light scattering correction was also applied to account for those pyrene pairs which are in close contact and form excimer on a time-scale which is too fast to be detected accurately by our instrument.

Error Analysis: The error on the parameters retrieved from the global analysis of the monomer and excimer fluorescence decays was estimated by using the following method. The parameters obtained from the fits (see Table SI.2.2) were used to generate 10 simulated monomer and excimer fluorescence decay pairs having different Poisson noise patterns. These 10 simulated decays were globally analyzed yielding a set of 10 parameters whose average (m) and standard deviation (σ) were determined. The ratio σ/m took values of 0.10 or less except for the occasional fluorescence fraction having a value of less than 0.10 where σ/m was larger, but always smaller than 0.20. Errors on the averaged values of a parameter obtained over a range of divalent ion concentrations were determined by taking the standard deviation of those values. The σ/m ratios obtained from a set of parameters retrieved from the fit of different experimental decays were always larger than those obtained by the

global analysis of a set of 10 simulated decays, thus demonstrating the reliability of the analysis program.

Based on the above, the errors reported on the parameters obtained from the global analysis of one experimentally acquired monomer and excimer decay pair are the standard deviations of the parameters obtained by fitting a set of 10 simulated decay pairs. However, when parameters obtained from the analysis of different experimentally acquired fluorescence decays were averaged, the reported error is the standard deviation of these experimentally determined parameters since this error is larger than that generated by the analysis program.

2.4 Results

Fluorescence spectra and decays of the pyrene-labeled lipids: The steady-state fluorescence spectra of the lipid bilayers containing 1 mol% of the pyrene-labelled lipids (PLLs) were acquired in two lipid matrices made of the fluid POPC or gel-like DSPC.[30] The fluorescence spectra obtained with the four lipid combinations are shown in Figure 2.2 after having been normalized at the 376 nm peak. The intensity of the excimer peak observed around 480 nm in Figure 2.2 provides an estimate of the efficiency of a given lipid composition at promoting encounters between PLLs. Rapid inspection of Figure 2.2 indicates that for a given PLL, excimer formation is not promoted in the fluid POPC matrix but is facilitated in the more rigid DSPC matrix.[30] This is contrary to what would be expected as the higher viscosity medium should hinder excimer formation by diffusion. This effect can be rationalized by considering the local pyrene concentration. Since these experiments were conducted with the same PLL content of 1 mol%, the enhanced excimer formation observed with DSPC vesicles suggests that these vesicles promote the formation of pyrene-rich regions.

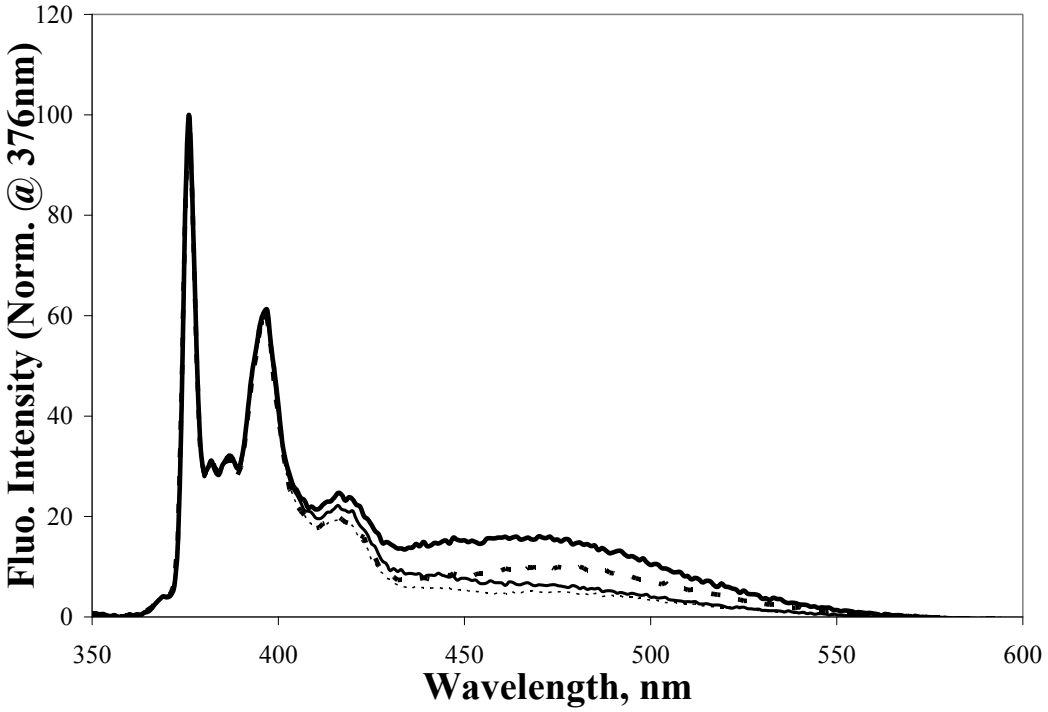

Figure 2.2**:** Fluorescence emission spectra normalized at 376 nm of POPC solutions containing 1 mol% of PSOH (·····) or PSIDA (—), and DSPC solutions containing 1 mol% PSOH (▪▪▪▪) or PSIDA (▬) in 0.02 M MOPS, 0.1 M NaCl, pH 7.4 buffer solution. λ_{ex} = 344 nm.

This suggestion was corroborated by conducting time-resolved fluorescence measurements. Figure 2.3 shows the monomer and excimer decays of the four solutions. The fluorescence decays were fitted with a sum of exponentials according to Equation 2.1. The decay times and associated pre-exponential factors retrieved from the fits have been listed in Table SI.2.1 of Supporting Information. The excimer decays shown in Figure 2.3 display great differences in their features. Excimer decays acquired with PSOH exhibit a significant rise time. However, the excimer generated by PSIDA, while still having a rise time, exhibits also a fast decay at the early times characterized by a lifetime of

approximately 3 ns. This fast decay reflects the presence of a short-lived species that has been documented previously where a pyrene-labelled macromolecule was found to generate significant amounts of ground-state pyrene aggregates.[28] This observation suggests that PSIDA induces strong interactions between the pyrene labels although the presence of a rise time indicates that excimer formation by diffusion still occurs.

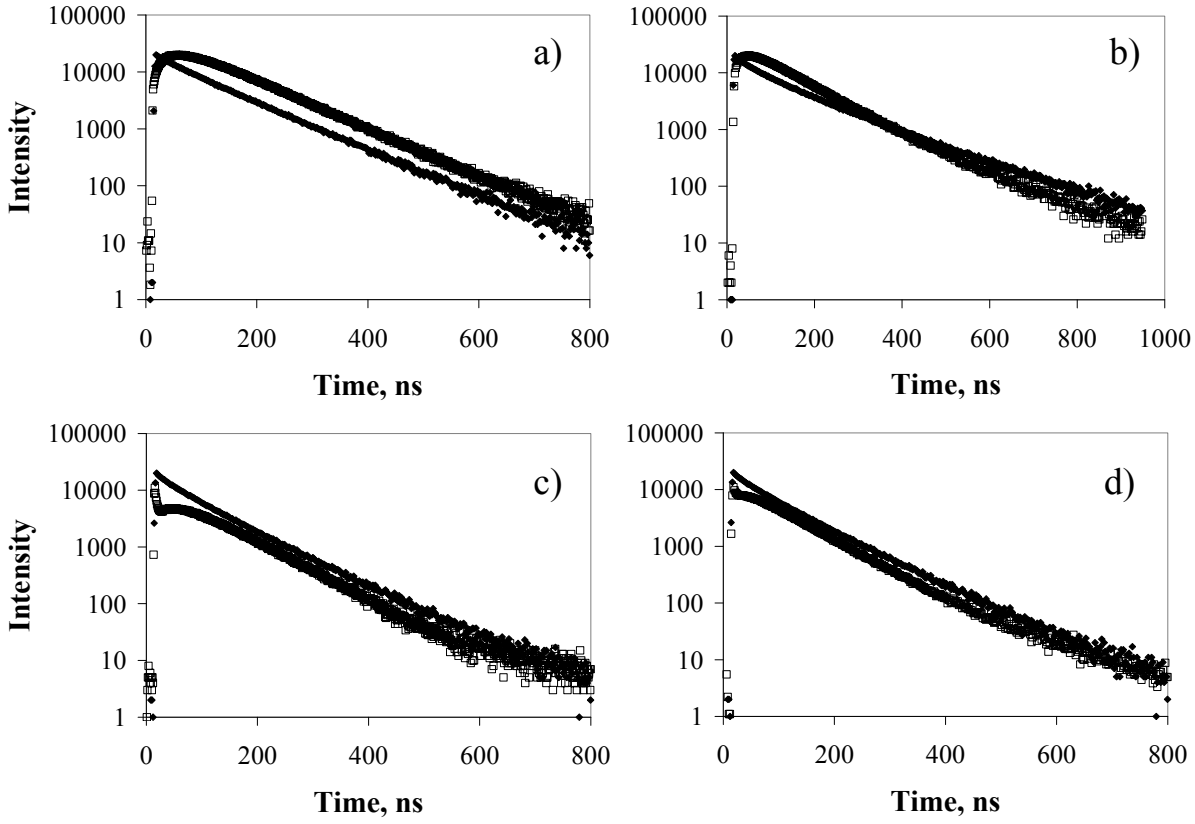

Figure 2.3**:** Monomer (◆) and excimer (□) time-resolved fluorescence decays for 1:99 mixtures of a) PSOH:POPC, b) PSOH:DSPC, c) PSIDA:POPC, and d) PSIDA:DSPC in MOPS buffer solution. λ_{ex} = 344 nm; λ_{em} (monomer) = 376 nm, λ_{ex} (excimer) = 510 nm.

To gain a greater in-depth understanding of the information given by time-resolved fluorescence, the monomer and excimer fluorescence decays were also analyzed globally using the Fluorescence Blob Model (FBM) to describe excimer formation via diffusion. The FBM is an analytical tool used to describe pyrene excimer formation by diffusion occurring in media that hinder the homogeneous distribution of the pyrene label.[22] Although the FBM has been mostly used to study polymers randomly labelled with pyrene in solution, the viscous vesicle membrane can be viewed as the conceptual equivalent of a rigid polymer backbone that hinders the homogeneous redistribution of the pyrene pendants inside the polymer coil. Following this analogy and according to the FBM assumptions, a blob for the vesicles represents a domain of the membrane that can be probed by a PLL while pyrene is excited. The parameters obtained from fitting the decays with Equation 2.2 for the monomer and Equation 2.4 for the excimer are listed in Table SI.2.2 of Supporting Information. An example of the global fit of the monomer and excimer decays is given in Figure SI.2.1 of Supporting Information. The addition of Ca^{2+} to solutions containing either PSOH or PSIDA induced no noticeable change in the fluorescence decays of the lipid solutions even at concentrations as high as 10 mM. Since the monomer and excimer decays without ions and with Ca^{2+} ions were identical within experimental error, the FBM parameters obtained by fitting these decays were averaged and taken as the baseline values to describe the behaviour of the PLLs in the absence of ion. The averaged values have been listed in Table 2.1.

In the analysis, the lifetime of the pyrene monomer, τ_M, was obtained from solutions containing 0.1 mol% of PSIDA or PSOH in DSPC or POPC in the absence of any metal ions. The small mole fraction of PLL used to prepare the liposomes ensures that very little excimer is being formed and that the fluorescence decays of the pyrene monomer exhibit a strong contribution from isolated pyrene monomers that emit with the longest decay time τ_{M3} with more than 50% of the overall pre-exponential weight (see a_{M3} values in Table SI.2.1e). Based on the PSOH results where the long

decay time τ_{M3} was obtained with the largest pre-exponential factor and thus greater accuracy, the lifetime τ_M taken to equal τ_{M3} was determined to equal 115 and 185 ns for PSOH in POPC and DSPC, respectively. The longer lifetime found for the excited pyrene monomer in the DSPC vesicles likely reflects the larger microviscosity in the region of the DSPC membranes where pyrene resides which reduces diffusional quenching by molecularly dissolved oxygen. It should be noted that the monomer decays acquired for POPC and DSPC vesicles containing 0.1 mol% PSIDA exhibit increased quenching compared to those acquired for POPC and DSPC vesicles containing 0.1 mol% PSOH. Indeed, for DSPC vesicles containing 0.1 mol% PSIDA, the long decay time taken as τ_M is actually approximately 10 ns smaller than that obtained for the DSPC vesicles containing 0.1 mol% PSOH. This result suggests that the excited pyrenes undergo diffusional quenching likely due to a larger local pyrene concentration brought on by stronger interactions between the PSIDA head groups.

Table 2.1**:** Averaged parameters obtained from global FBM analyses for solutions of POPC and DSPC with 1 mol% PLL. The reported errors are the standard deviation of the parameters obtained by fitting the experimental decays acquired with either no cations or with Ca^{2+} cations.

System	$k_{ex}[blob]$ $\times 10^7\ s^{-1}$	k_{blob} $\times 10^7\ s^{-1}$	$<n>$	f_{agg}	f_{diff}	f_{free}	$k_{blob} \times <n>$ $\times 10^7\ s^{-1}$
PSOH/POPC	1.3 ± 0.3	1.5 ± 0.2	0.54 ± 0.09	0.02 ± 0.01	0.55 ± 0.05	0.43 ± 0.05	0.76 ± 0.06
PSOH/DSPC	0.8 ± 0.1	2.0 ± 0.2	0.77 ± 0.02	0.09 ± 0.01	0.68 ± 0.01	0.23 ± 0.01	1.55 ± 0.08
PSIDA/POPC	1.5 ± 0.2	2.7 ± 0.3	0.54 ± 0.04	0.37 ± 0.06	0.49 ± 0.05	0.13 ± 0.03	1.44 ± 0.12
PSIDA/DSPC	0.5 ± 0.1	1.7 ± 0.2	1.40 ± 0.05	0.55 ± 0.02	0.41 ± 0.02	0.04 ± 0.00	2.35 ± 0.17

The parameters listed in Table 2.1 can be used to describe how the POPC and DSPC membranes affect the behaviour of PSOH and PSIDA. In particular, the product $k_{blob}\times\langle n\rangle$ has been found to be proportional to first, the pyrene concentration felt locally by the excited pyrene and second, the inverse of the viscosity.[31–33] In other words, $k_{blob}\times\langle n\rangle$ should depend on the membrane microviscosity and the local pyrene concentration $[Py]_{loc}$. The membrane microviscosity being larger in the gel-like DSPC bilayer,[30] it is thus significant that $k_{blob}\times\langle n\rangle$ is always greater in the DSPC matrix. It suggests that $[Py]_{loc}$ is much larger in the DSPC matrix. In other words, DSPC appears to promote the aggregation of PLLs. The notion that the pyrenes are held closer to each other in the DSPC vesicles is further reinforced upon examination of the fractions obtained by the global analysis of the monomer and excimer decays. The overall fractions of isolated pyrene monomers, f_{free}, equals 0.43 ± 0.05, 0.23 ± 0.01, 0.13 ± 0.03, and 0.04 ± 0.00 for the 1:99 lipid mixtures of PSOH:POPC, PSOH:DSPC, PSIDA:POPC, and PSIDA:DSPC, respectively. The larger f_{free} values obtained with POPC indicate that the PLLs are better solvated in the POPC membranes which can accommodate a larger number of non-aggregated PLLs than the DSPC membrane. It was also found that switching the lipid matrix from POPC to DSPC resulted in an increase in the level of pyrene aggregation with f_{agg} increasing from 0.02 ± 0.01 to 0.09 ± 0.01 for PSOH and from 0.37 ± 0.06 to 0.55 ± 0.02 for PSIDA. This observation confirms that DSPC is much more efficient at inducing the formation of pyrene-rich domains than POPC and that this efficiency can be further enhanced by changing the PLL from PSOH to PSIDA.

PLLs fluorescence spectra and decays in the presence of Cu^{2+} and La^{3+} cations: The fluorescence spectra of the PLLs in POPC and DSPC were monitored as copper or lanthanum cations were added to the lipid solutions. In all instances, the presence of the cations did not have any effect on the fluorescence spectra of PSOH as was expected since the oligo(ethylene oxide) head of PSOH has been shown not to interact with these cations.[17] Assuming that La^{3+} binds to PSIDA as Cu^{2+} does, the

binding of either cation to PSIDA is expected to affect similarly the manner in which PSIDA arranges itself in the membrane which in turn should have an effect on the process of excimer formation. The efficiency of excimer formation is characterized by the I_E/I_M ratio obtained by taking the fluorescence intensity of the excimer (I_E), determined by integrating the fluorescence spectra from 500 to 530 nm, and dividing it by the fluorescence intensity of the monomer (I_M), determined by integrating the spectra from 372 to 378 nm. In Figure 2.4, the ratio I_E/I_M for all four lipid combinations determined from their fluorescence emission spectra are given as a function of added cation concentration. The I_E/I_M ratios obtained for PSOH remained constant with cation concentration regardless of the nature of the cation. Changes in the I_E/I_M ratio were observed solely when either La^{3+} or Cu^{2+} was added to the lipid solutions that contained PSIDA. As La^{3+} was added to the solutions containing PSIDA, I_E/I_M dropped from 0.057 to 0.038 for PSIDA/POPC and from 0.171 to 0.105 for PSIDA/DSPC. The addition of Cu^{2+} also caused a drop in I_E/I_M from 0.057 to 0.035 for PSIDA/POPC and from 0.171 to 0.071 for PSIDA/DSPC. However, the trends obtained upon addition of Cu^{2+} need to be interpreted carefully since Cu^{2+} is a known quencher of pyrene.[34]

As a matter of fact, in addition to a drop in I_E/I_M, a decrease in the overall intensity of the fluorescence spectra was observed when Cu^{2+} was added to POPC or DSPC solutions containing 1 mol% of PSIDA, confirming that pyrene quenching by copper is indeed occurring. However, since quenching of the pyrene monomer with Cu^{2+} should result in a decrease in I_M and a concomitant increase in the ratio I_E/I_M when pyrene aggregates are present in solution,[35] the decrease in I_E/I_M observed in Figure 2.4c and 2.4d suggests that both La^{3+} and Cu^{2+} induce a similar change in the way PSIDA arranges itself in the lipid membrane upon binding to these cations. To gain a more detailed understanding of the effects induced by the addition of cations to the lipid solutions, the pyrene monomer and excimer fluorescence decays were examined.

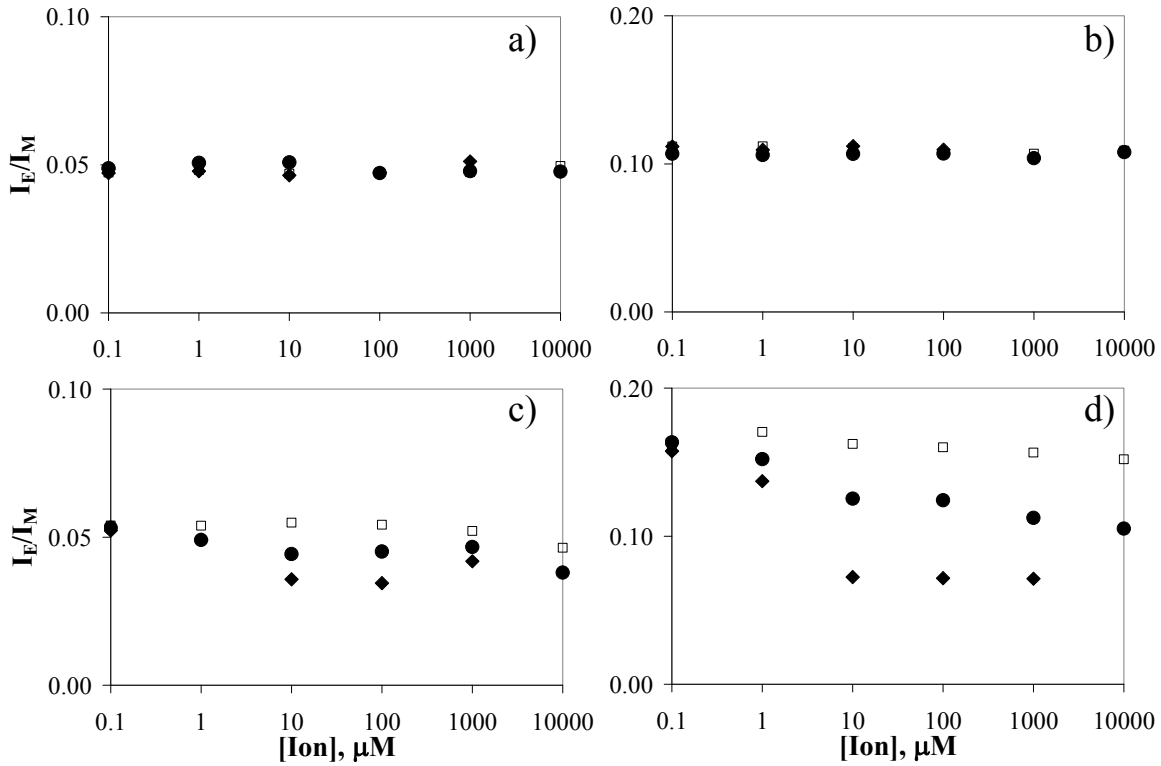

Figure 2.4**:** I_E/I_M values for 1:99 mixtures of a) PSOH:POPC, b) PSOH:DSPC, c) PSIDA:POPC, and d) PSIDA:DSPC in MOPS buffer with (◆) Cu^{2+}, (□) Ca^{2+} and (●) La^{3+}.

As for the steady-state emission spectra, the presence of Cu^{2+}, Ca^{2+}, and La^{3+} for PSOH and Ca^{2+} for PSIDA has no obvious effect on the fluorescence decays of the PLLs. According to the parameters listed in Table SI.2.1 retrieved from the fit of the fluorescene decays with a sum of exponentials, PSOH always yields a larger long decay time τ_{M3} than PSIDA. Indeed when the PLL is switched from PSOH to PSIDA, τ_{M3} is found to drop from 105 ns to 95 ns in POPC and from 165 ns to 150 ns in DSPC. The shorter τ_{M3} found with PSIDA results from the enhanced interactions induced by the imido diacetic acid heads that increase $[Py]_{loc}$ and favour more efficient diffusive encounters between pyrenes. However, upon the addition of La^{3+}, τ_{M3} for PSIDA in either the POPC or DSPC

membrane increases to values equal to or even slightly greater than those obtained for solutions containing 0.1 mol% of PSOH in their respective lipid matrices. This increase in τ_{M3} was also observed when Cu^{2+} was added to the solutions containing 1 mol% of PSIDA in DSPC, which is surprising since diffusional quenching by Cu^{2+} should reduce τ_{M3}, as seen for the solutions containing 1 mol% of PSIDA in POPC. These observations suggest that diffusional quenching plays a lesser role than expected when Cu^{2+} is added to the DSPC solutions with 1 mol% of PSIDA. This point will be addressed in more detail later in the Discussion section.

The global analysis of the monomer and excimer fluorescence decays with Equations 2.2 and 2.4 was generally successful but proved problematic for 1 mol% PSIDA solutions containing Cu^{2+} ions. Since Cu^{2+} ions are capable of quenching the excited pyrenes of PSIDA, the monomer and excimer fluorescence decays become uncoupled thus preventing their global analysis. Additionally, the quenching of pyrene by Cu^{2+} may also directly influence the FBM parameters obtained. For this reason, no global FBM analysis of solutions containing PSIDA with Cu^{2+} ions is reported herein. However, useful information was still retrieved from the monomer and excimer fluorescence decays of solutions of PSIDA with Cu^{2+} by fitting the decays separately with a sum of exponentials.

In general, La^{3+} was found to have little effect on the FBM parameters $\langle n \rangle$, $k_{ex}[blob]$, and k_{blob}. In DSPC, the parameters $\langle n \rangle$, k_{blob}, and $k_{ex}[blob]$ that describe the process of excimer formation by diffusion for PSIDA in the presence of La^{3+} remained constant within experimental error at values of 1.2 ± 0.1, 2.2 ± 0.4 $\times 10^7$ s^{-1}, and 0.8 ± 0.2 $\times 10^7$ s^{-1}, respectively. Similarly, constant $\langle n \rangle$, k_{blob}, and $k_{ex}[blob]$ values of 0.7 ± 0.1, 2.3 ± 0.4 $\times 10^7$ s^{-1}, and 1.4 ± 0.2 $\times 10^7$ s^{-1} were found when La^{3+} was added to vesicle solutions of 1:99 mixtures of PSIDA:POPC. This result indicates that addition of La^{3+} does not affect excimer formation by diffusive encounters of PSIDA in the lipid bilayer. Since the fluorescence spectra show substantial change upon addition of cations (Figure 2.4), and since

excimer formation by diffusion is unaffected by the presence of cations, the addition of cations to the vesicles must affect the contribution of the pyrene species present in solution.

To this end, the molar fractions of the pyrene species found in the vesicles were determined from the global analysis of the fluorescence decays and are listed in Table SI.2.3 in Supporting Information. They are also shown in Figure 2.5 as a function of La^{3+} concentration. Addition of La^{3+} leads to similar trends for the solutions containing 1 mol% of PSIDA in both POPC and DSPC with the isolated pyrene fraction, f_{free}, increasing at the expense of f_{diff}, the fraction that represents the pyrenes forming excimer diffusionally. The fraction of pyrenes that are aggregated, f_{agg}, remains constant for all lanthanum ion concentrations. Although the global FBM analysis cannot be trusted when Cu^{2+} is added to the PLL solutions, information on how addition of Cu^{2+} affects excimer formation can be retrieved from the parameters obtained by fitting the excimer decays with a sum of exponentials. According to the parameters listed in Table SI.2.1c, the addition of Cu^{2+} to the POPC solutions containing 1 mol% PSIDA results in a drop in the magnitude of the preexponential weight a_{E2} which is negative and describes the magnitude of the rise time that reflects diffusional encounters between PSIDAs. A drop in a_{E2} with increasing Cu^{2+} concentration indicates that the contribution to the excimer fluorescence decay of the aggregated pyrenes increases at the expense of the contribution of the pyrenes forming excimer by diffusion. For solutions of DSPC containing 1 mol% of PSIDA and Cu^{2+} concentrations greater than 1 μM, the excimer decays exhibit no rise time whatsoever indicating that the excited pyrenes forming excimer by diffusion contribute little to the excimer fluorescence decay. Since excimer formation by diffusion is due to isolated pyrenes and since the contribution disappears from the excimer decays, it implies that Cu^{2+} targets preferentially isolated PSIDA molecules. The modest decrease in the magnitude of a_{E2} for the DSPC and POPC solutions containing 1 mol% of PSIDA as La^{3+} is added is less marked than when Cu^{2+} is added to these solutions because La^{3+} does not quench the excited pyrene monomer. Nevertheless, the reduction in

a_{E2} is also a result of hindered excimer formation by diffusion resulting from the preferred targeting of isolated PSIDA molecules by La^{3+}.

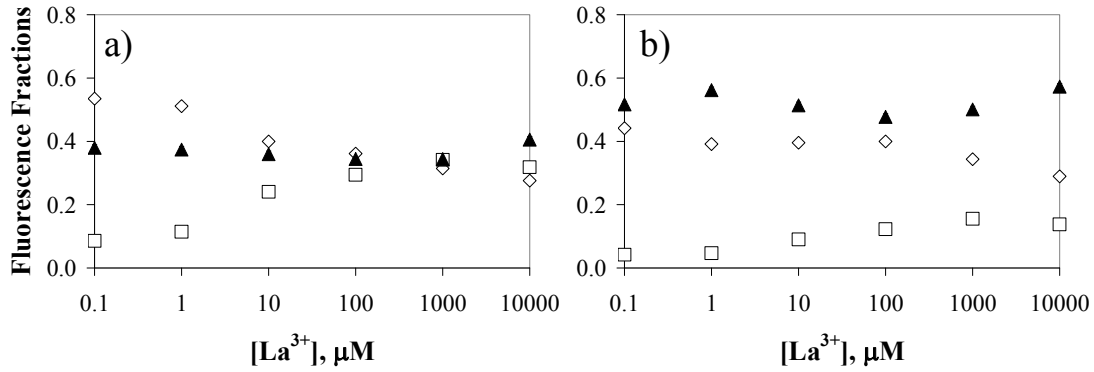

Figure 2.5**:** Fluorescence fractions f_{agg} (▲), f_{diff} (◇), and f_{free} (□), for a) 1% PSIDA/POPC with La^{3+}, b) 1% PSIDA/DSPC with La^{3+}. The error bars associated with each data point are smaller than the symbols.

2.5 Discussion

The information obtained by time-resolved fluorescence provides an understanding of the topography of the surface of the vesicles as well as how the functionalized lipids interact with one another. Since the PSOH head groups do not interact with the metal cations, a study of PSOH in the POPC and DSPC matrices allows one to highlight the differences between the two lipid bilayers with no interference from the cations present in solution.

Differences between the POPC and DSPC membranes: The first difference to be observed between the two lipid matrices was with the lifetime τ_M of pyrene in both matrices. A 50% increase in the long lifetime of the pyrene monomer was observed upon changing the bilayer from a POPC (τ_M = 115 ns)

to a DSPC (τ_M = 185 ns) membrane. This increase in lifetime for pyrene from a POPC to a DSPC membrane reflects a decrease in collisional quenching by molecular oxygen. The decreased rate of oxygen quenching is likely due to the more viscous environment probed by the PLL in the DSPC matrix.[30] Taking into consideration that some lipids in a DSPC membrane are incorporated into semi-crystalline microdomains,[36] in addition to being in a gel state at room temperature, it is likely that the surface of the vesicle can be viewed as an array of semi-crystalline domains separated by channels possessing greater amorphous, and hence fluid, character. Pyrene-labelled lipids (PLLs) dissolved in such a medium would more likely be excluded from the semi-crystalline regions and would reside predominantly in these amorphous channels.[37,38] This clustering of the PLLs in the DSPC membrane contrasts with the more homogeneous distribution of the PLLs in the fluid and amorphous POPC membrane.

The suggestion that the PLLs are excluded from certain areas of the DSPC membranes compared to their homogeneous distribution in the POPC vesicles is reflected by the increase in the local pyrene concentration described by the product $k_{blob}\times\langle n\rangle$ found in Table 2.1. As mentioned earlier, $k_{blob}\times\langle n\rangle$ is proportional to the inverse of the microviscosity, which happens to be larger in the DSPC membrane, and to $[Py]_{\mathrm{loc}}$. Although the larger microviscosity of DSPC membranes would be expected to lower $k_{blob}\times\langle n\rangle$, larger $k_{blob}\times\langle n\rangle$ values are obtained for the same overall PLL concentration (1 mol%) in DSPC indicating that the PLLs are closer to each other in the DSPC membranes. The phase separation of the membrane into PLL-rich domains might be a consequence of the semi-crystalline nature of the DSPC membrane where crystalline DSPC-rich domains exclude pyrene and therefore the PLLs, thus confining the PLLs to an area considerably smaller than the total surface area of the vesicle. This observation is internally consistent with the larger fractions f_{agg} and f_{diff} and the smaller fraction f_{free} found for the PLLs in the DSPC membrane implying that the PLLs are closer to each other.

Phase-separation of the PLLs from the DSPC membrane also affects exchange of the PLLs between blobs as switching from POPC to DSPC was found to effectively halve $k_{ex}[blob]$. Since a larger viscosity decreases k_{ex} and increases [*blob*], the product $k_{ex}[blob]$ should not be significantly affected by changes in viscosity. Indeed it has been found to be insensitive to changes in solution viscosity from 0.364 to 5.47 mPa·s in the case of excimer formation between pyrene pendants randomly attached onto a polymer.[33] The smaller $k_{ex}[blob]$ values found for DSPC suggests that exchange between blobs is hindered in the DSPC membrane and since this hindrance is unlikely to be due to the microviscosity of the medium experienced by PLL in DSPC, it must result from geometric constraints induced by the phase separation of the PLLs from the semicrystalline microdomains generated in the DSPC membrane. This hypothesis is depicted in Scheme 2.2 where the PLLs expelled from the semi-crystalline DSPC domains form PLL-rich fluid channels between DSPC-rich domains. In effect, this organization of the PLLs reduces the points of contact between blobs, thus hindering the exchange of PLLs between blobs. Since the microviscosity of the DSPC membranes is larger than that of the POPC membrane, the area travelled by a PLL while pyrene remains excited is smaller in the more viscous DSPC membrane, resulting in a smaller blob size in DSPC relative to POPC. However, the greater local pyrene concentration reflected by the large $k_{blob}\times\langle n\rangle$ values obtained for DSPC membranes indicates that while the pyrenes may not be able to travel as far, they encounter more pyrenes due to their closer proximity stemming from their location into PLL-rich domains. This is also supported by the larger I_E/I_M values obtained for solutions containing 1 mol% of PLL in DSPC versus POPC.

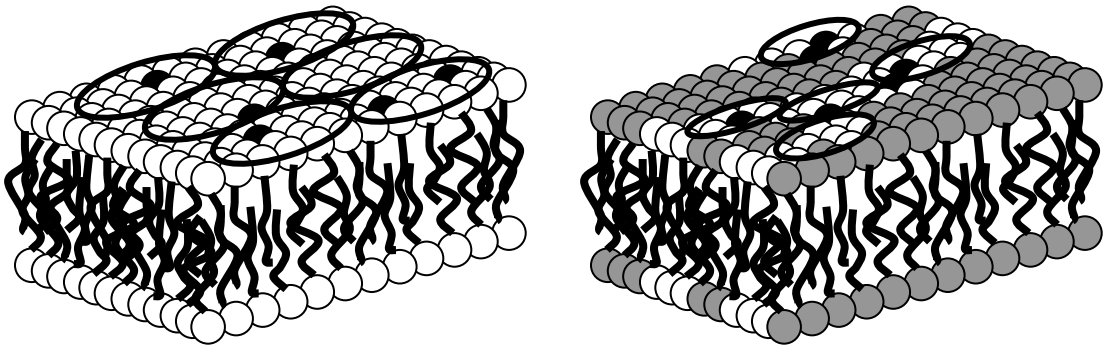

Scheme 2.2**:** Representation of the distribution of PLLs (black circles) in POPC (left) and DSPC (right) matrices with amorphous (white circles) and crystalline (gray circles) domains divided into fluorescence blobs (ovals).

Differences in the chemical nature of the head groups of PSOH and PSIDA were expected to affect the fluorescence of the pyrene labels in response to different interactions between the functionalized heads. This was indeed observed by the appearance of a short decay time in the excimer fluorescence decay of PSIDA indicating the presence of short-lived ground-state pyrene aggregates as has been reported previously.[28] Favourable interactions between the PSIDA heads induce the formation of pyrene aggregates where the pyrenes are held together in conformations that are not ideal for excimer formation. This clustering effect is quantified by the significant jump in the parameter f_{agg} which gives the fraction of aggregated PLLs as reflected by fluorescence as well as the drop in isolated PLLs given by f_{free}. In addition, the product $k_{blob}\times\langle n\rangle$ that can be viewed as a $[Py]_{loc}$-indicator is effectively doubled when the head groups of the PLL is changed from an oligo(ethylene oxide) (PSOH) to an imino diacetic acid (PSIDA). Clustering of PSIDA is not only observed in the DSPC membrane where PSIDA phase-separates from the semi-crystalline DSPC matrix into PSIDA-rich domains, but also in the POPC matrix. Despite the PLLs being able to distribute themselves throughout the POPC membrane, f_{free} in Table 2.1 drops from its original value of 0.43 ± 0.05 to 0.13

± 0.03 when the PLL is changed from PSOH to PSIDA, while f_{agg} increases from 0.02 ± 0.01 to 0.37 ± 0.06. Differences in the distribution of the PLLs in the POPC and DSPC membranes induced by the two heads are illustrated in Scheme 2.3. Even though PSIDA induces a greater amount of pyrene aggregation, the mobility of isolated PSIDA lipids appears to remain the same as reflected by $k_{ex}[blob]$ which takes similar values between PSOH and PSIDA. However, while the mobility of an individual PSIDA isolated in the POPC matrix is not affected, the same cannot be said for the PSIDA lipids held together into PSIDA aggregates by interactions between the imido diacetic acid head groups. Interactions between the PSIDA heads are expected to reduce the mobility of an individual PSIDA within the cluster. In addition, the entire cluster would also experience lower mobility being a collectively larger mass. Analysis of the fluorescence data obtained for the different lipid compositions led to the pictorial representation of the membranes depicted in Schemes 2.2 and 2.3.

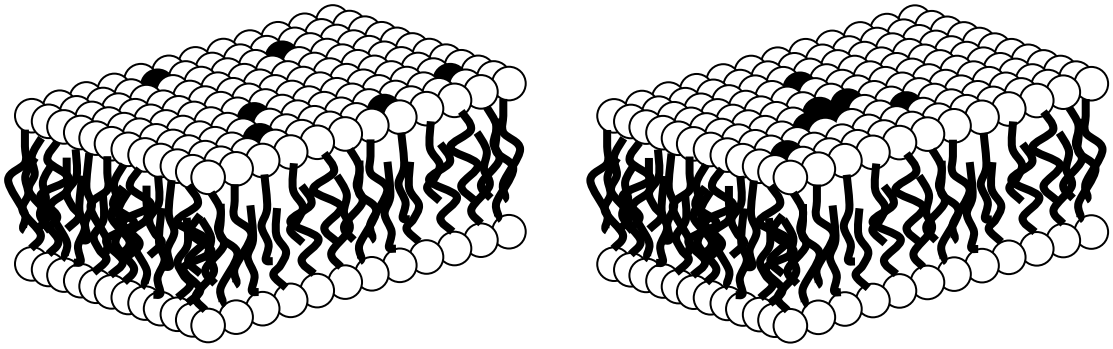

Scheme 2.3**:** Representation of the change in the distribution of PSOH (left) and PSIDA (right) in a POPC matrix where the head groups of the PLLs and POPC are black and white, respectively.

PLL response upon addition of cations: The effect that the addition of cations has on the nature of the membranes is now considered. It has been suggested that the drop in I_E/I_M seen in Figures 2.4c and

2.4d upon addition of Cu^{2+} and La^{3+} was due to the disruption of the PSIDA clusters following the binding of a specific ion to PSIDA.[16] Both La^{3+} and Cu^{2+} have been found to bind strongly to the imido diacetic acid head of PSIDA whereas binding of Ca^{2+} to PSIDA was considerably weaker.[17] The trends shown in Figure 2.4 support this conclusion.

The addition of La^{3+} to the DSPC solution containing 1 mol% of PSIDA led to an increase of the long decay time τ_{M3} (Table SI.2.1d) to values that approached the lifetime τ_M of PLLs in the DSPC membranes. This observation led to the conclusion that the addition of La^{3+} to the solution prevented excimer formation between PSIDA molecules, which were therefore capable of fluorescing with their natural lifetime τ_M in that particular medium. In effect, some PSIDA lipids became isolated from each other. However, the isolation of some PSIDA molecules did not reduce the level of pyrene aggregation as the fraction of aggregated pyrenes f_{agg} remained constant, while f_{free} increased at the expense of f_{diff} with increasing concentrations of La^{3+} ions. This trend suggests that the cations binding to lone PSIDA head groups have a greater impact than those that bind to an aggregated cluster. Since cations prefer to bind where the positive charge is smallest, binding of a first cation to a domain of aggregated PLLs inhibits the binding of additional cations. A similar example of this preferential binding is the neutralization of a polyacid by hydroxide anions. Within any particular short segment of the polyacid chain, abstraction of the first proton by a hydroxide ion is easy. The successive abstractions of protons within that segment however become increasingly difficult because the carboxylate ions generated from previous abstractions repel any incoming hydroxide ion.[39] The same effect enhances the binding of cations to the isolated PSIDA lipids which then repel each other. This process effectively isolates the PLLs thus increasing the population of "free" pyrenes not participating in the diffusional formation of excimers while leaving the aggregates intact. This proposal is also supported by the decrease in the I_E/I_M ratio shown in Figure 2.4c and 2.4d since this effect hinders the

formation of excimer by diffusion, thereby reducing the excimer intensity while increasing that of the monomer.

Cu^{2+} ions were expected to interact with PSIDA in a manner similar to La^{3+}, with the added benefit that their ability to quench pyrene would highlight the location of the bound ions. The concept that the PSIDA aggregates were not effectively dispersed upon binding to the ions was further reinforced as, both in the POPC and DSPC medium, the decreased presence of a rise time in the excimer fluorescence decays indicates that Cu^{2+} ions were preferentially quenching unassociated PSIDA. Diffusional quenching of an excited chromophore usually results in a decrease in the lifetime of the chromophore. While this was seen for the POPC solution containing 1 mol% PSIDA, this was not observed for the DSPC solution containing 1 mol% of PSIDA where the longest decay time τ_{M3} actually increased (Table SI.2.1d). The opposite effects found for PSIDA in POPC and DSPC suggest that competing effects are taking place when Cu^{2+} ions are being added. Addition of Cu^{2+} is expected to shorten τ_{M3} due to the diffusional quenching of pyrene by Cu^{2+}, but it can also induce an increase in τ_{M3} due to the isolation of PSIDA lipids resulting from electrostatic repulsion upon binding to the Cu^{2+} cation. Whereas the latter effect is believed to occur in both the POPC and DSPC membranes, the former effect is expected to be reduced in the more viscous DSPC matrix.

To explain the difference between the effect of Cu^{2+} ions on the PSIDA/DSPC and PSIDA/POPC mixtures, the differences between the two lipid matrices must be carefully examined. The POPC matrix, being more fluid than the DSPC matrix, enables the excited pyrene to diffuse to the surface of the bilayer membrane where it can encounter a Cu^{2+} ion resulting in quenching. The DSPC matrix, being more viscous than that of POPC, hinders the diffusion of pyrene to the surface within the time span of the excited pyrene lifetime. Thus, the electrostatic repulsion between PSIDA lipids brought on by the binding of Cu^{2+} to the PSIDA heads must be more important than diffusional quenching by Cu^{2+} in the DSPC matrix. The competition between the two effects resulting from the

binding of Cu^{2+} on the fluorescence of PSIDA is illustrated in Scheme 2.4. The decay time τ_{M3} can be used to derive Equation 2.11

$$\frac{1}{\tau_{M3}} = \frac{1}{\tau_M} + k_q + < k > \qquad (2.11)$$

where k_q represents the intramolecular rate constant for quenching of an excited PSIDA by Cu^{2+} and $<k>$ is the pseudo-unimolecular rate constant for excimer formation between isolated PLLs whose decay time equals τ_{M3}. At high La^{3+} concentrations, $<k>$ is negligible in solutions of both POPC and DSPC since τ_{M3} becomes approximately equal to τ_M. Thus, $<k>$ can be approximated to equal zero in this range of cation concentrations. This approximation for $<k>$ can be applied to the binding of Cu^{2+} to PSIDA since Cu^{2+} is expected to bind to PSIDA in a similar manner as La^{3+}. At high concentrations of Cu^{2+}, τ_{M3} for PSIDA approaches values of 77 ± 3 and 164 ± 1 ns in POPC and DSPC, respectively. Thus, the rate constant k_q was calculated to be 4.3 and 0.7 × 10^6 s^{-1} in POPC and DSPC, respectively. In turn, the mobility of the pyrenyl moiety of PSIDA in the bilayer is reflected by k_q. According to the k_q values, the pyrene label of PSIDA experiences a local microviscosity in the DSPC membrane that is k_q(POPC)/k_q(DSPC) = 5.4 times greater than that in the POPC membrane. This result suggests that the amorphous channels of DSPC where pyrene and hence the PLLs reside are 5.4 times more viscous than bulk POPC membranes.

The 5.4-fold apparent increase in viscosity probed by diffusional quenching of pyrene by Cu^{2+} in the amorphous channels of the semicrystalline DSPC membrane is smaller than the 16-fold viscosity increase observed from fluorescence anisotropy experiments conducted on 1,6-diphenyl-1,3,5-hexatriene (DPH) embedded in POPC and DSPC membranes.[30] However these different results are certainly a consequence of fundamental differences pertaining to both experiments. First fluorescence anisotropy and quenching experiments probe rotational and translational diffusion,

respectively. Whereas both types of experiments respond to changes in the local viscosity of the medium, their response can be expected to depend, in part, on the location of the probe within the lipid membrane, whether the probe is at the center or the surface of the membrane. This location is expected to be different for the pyrene label of the PLLs and DPH. Second, DPH has been found to partition itself randomly between the semicrystalline and amorphous domains of the DSPC membrane.[40] On the contrary, the PLLs are segregated in amorphous and certainly less viscous channels of the DSPC membrane. These inherent differences encountered in both types of experiments rationalize why the microviscosity of the DSPC membrane relative to that of POPC membranes probed by fluorescence quenching of PSIDA by Cu^{2+} appears to be somewhat smaller than that obtained by fluorescence anisotropy experiments.

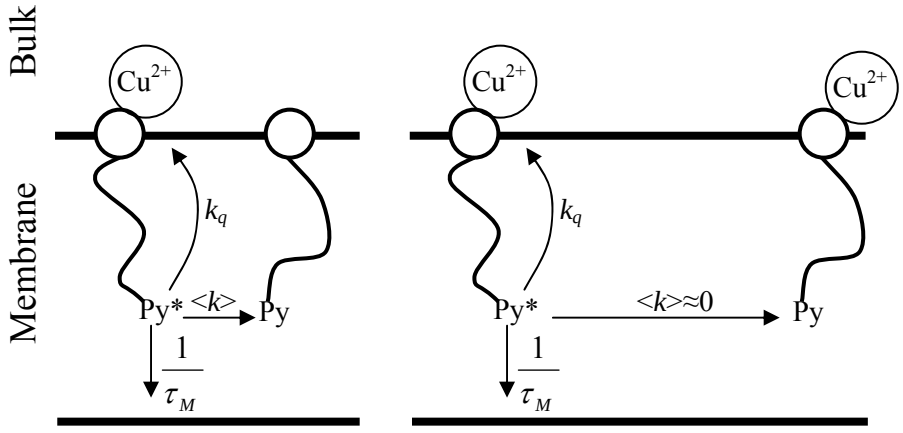

Scheme 2.4**:** Representation of the two competing quenching processes experienced by an excited PSIDA with a bound Cu^{2+}. Excimer formation by diffusive encounter with another PSIDA is possible when Cu^{2+} is not bound to the other lipid (left) and impossible if both bear a Cu^{2+} ion (right).

2.6 Conclusions

This study highlighted the differences in the organization of molecular components in fluid and gel phase matrices and how molecular structure and headgroup interaction can influence ligand binding and membrane organization at the molecular level. We found that the fluid POPC membrane provided a medium where the PLLs could distribute themselves relatively homogeneously as compared to the gel-like DSPC membrane, which forced the PLLs into amorphous channels excluding them from the DSPC semi-crystalline domains. Interestingly, in both fluid and gel phase matrices the interaction of iminodiacetic acid headgroups of PSIDA enabled the formation of clusters. While binding of cations to isolated PSIDA decreased diffusional collisions, the PSIDA clusters remained generally unaffected, suggesting that cation binding in these small molecular assemblies is not favorable. The results thus show that chemical recognition on membrane surfaces is affected by the local inhomogeneities induced both by larger scale phase separations and molecular level interactions.

The comparison of the decaytimes τ_{M3} obtained from the analysis of the monomer decays acquired with PSIDA when La^{3+} or Cu^{2+} were added to the solutions provided an estimate of the microviscosity of the POPC and DSPC membranes. Since the addition of 100 μmol.L^{-1} of La^{3+} was found to essentially prevent excimer formation by diffusion between isolated PLLs described by the longer decay time τ_{M3}, the smaller τ_{M3} values found with addition of Cu^{2+} were attributed to quenching of the excited pyrene monomer by Cu^{2+}. Equation 2.11 was used to estimate the intramolecular rate constant of pyrene quenching by Cu^{2+}, k_q, which was found to be 5.4 times smaller in the DSPC membrane than in the POPC membrane, reflecting the higher microviscosity experienced by the pyrene in the PSIDA-rich channels found in the DSPC membrane.

Chapter 3
Molar Absorption Coefficient of Pyrene Aggregates in Water

3.1 Overview

The molar absorption coefficient of pyrene aggregates, ε_{E0}, was determined for a series of pyrene labelled poly(*N*,*N*-dimethylacrylamide)s (PyPDMA) having different pyrene contents. Aqueous solutions of PyPDMA having pyrene contents ranging from 263 to 645 μmol of pyrene per gram of polymer were studied by UV-Vis absorbance and time-resolved fluorescence spectroscopy. The global analysis of the monomer and excimer fluorescence decays with the fluorescence blob model yielded the fractions of the overall absorption contributed by all the pyrene species present in solution. The combined knowledge of the fractions obtained from the global analysis of the time-resolved fluorescence decays, the total absorption of the PyPDMA solution obtained from UV-Vis spectroscopy, and the total pyrene concentration in the solution obtained from the known pyrene content of each PyPDMA sample led to the determination of the molar absorption coefficient of pyrene aggregates. Regardless of the pyrene content of the PyPDMA samples and hence the level of association of the pyrene pendants in solution, all PyPDMA samples yielded similar ε_{E0} values over the range of wavelengths studied, namely from 325 to 350 nm. The averaged ε_{E0} was found to be red shifted relative to unassociated pyrenes by 3 nm as well as having a value at the 0-0 peak of 21000 $M^{-1}.cm^{-1}$ reduced from 34700 $M^{-1}.cm^{-1}$ for unassociated pyrenes. The determination of ε_{E0} enabled the first determination of the absolute fraction of associated pyrenes for aqueous solutions of a series of pyrene-labeled water-soluble polymers. The procedure outlined in this study is applicable to any pyrene-labeled water-soluble polymer and provides a new means to study quantitatively the effect of the hydrophilic-to-lipophilic balance on the hydrophobic associations generated by hydrophobically

modified water-soluble polymers. As an application, the average number of pyrenes involved in a pyrene aggregate generated by PyPDMA in water is determined.

3.2 Introduction

The physical properties of many macromolecules result often from associations taking place between specific parts of the macromolecule. These associations can be due to π–π interactions between aromatic side-chains such as base pair stacking in DNA,[1] electrostatic forces between charged monomers as encountered in ionomers,[2] or van der Waals forces between hydrophobic residues as found in proteins.[3] The interactions between segments of the macromolecule can occur intra- or intermolecularly and are usually responsible for the specific properties displayed by a given macromolecule.[2-6] Among those interactions, the hydrophobic associations of hydrophobic pendants play a major role and are invoked to rationalize the hydrophobic collapse of a folding protein[7] or the peculiar viscoelastic properties of hydrophobically modified water soluble polymers (HMWSP).[4-6]

Over the years, numerous studies have contributed to establishing the reliability of fluorescence-based techniques to characterize the apolar nature of microdomains present in a macromolecule by monitoring the response of an intrinsic (tryptophan in proteins) or extrinsic (dansyl for proteins, ethidium bromide for DNA) chromophore.[8,9] A widely used fluorescence experiment employed to characterize the behavior of HMWSPs in aqueous solution consists of replacing the hydrophobes of a HMWSP with the hydrophobic chromophore pyrene to yield a pyrene-labeled HMWSP (PyHMWSP).[10,11] In aqueous solution, the association of the hydrophobic pyrenes results in the formation of pyrene aggregates whose presence can be established by a variety of spectroscopic techniques.[10,11] For instance, UV-Vis absorption measurements yield broader absorption spectra when pyrene aggregates are present and the broadness of the absorption spectra can be characterized from their peak-to-valley ratio or P_A value. The excitation fluorescence spectrum of the pyrene excimer is red-shifted by a few nanometers compared to that of the pyrene monomer. The rise time typically

observed in the excimer fluorescence decays of pyrene-labeled polymers in organic solvents is notoriously reduced or even absent for PyHMWSPs in aqueous solution since direct excitation of a pyrene aggregate results in the quasi-instantaneous formation of an excimer.

The properties associated with the photophysics of pyrene aggregates have been thoroughly reviewed and have contributed to making pyrene *by far the most frequently used dye in fluorescence studies of labelled polymers*.[10] In all instances, these experiments are conducted to describe the associative strength of PyHMWSPs in water. Yet despite sustained scientific interest in characterizing the behavior of PyHMWSPs in aqueous solutions,[10,11] it is rather striking that quantitative information about the associative strength of PyHMWSPs, namely the fraction of aggregated pyrenes (f_{agg}), is invariably absent in almost all literature pertaining to the study of PyHMWSPs! This situation is mostly due to the fact that the molar absorption coefficient of a pyrene aggregate has yet to be determined.

By combining the use of a new powerful Light Emitting Diode (LED) whose emission is centered at 333 nm where pyrene absorbs, improved modeling of the encounters of pyrene labels randomly attached onto a chain related to the Fluorescence Blob Model (FBM),[12] and the global analysis of monomer and excimer fluorescence decays acquired with incremental 1 nm excitation steps, the molar absorption coefficient of the pyrene aggregates generated in aqueous solution by a series of pyrene-labeled poly(*N*,*N*-dimethylacrylamide) samples (PyPDMAs) was determined from 325 to 350 nm. This study enables the first quantitative determination of f_{agg} for a series of PyHMWSPs. It offers one of the very few means currently available for scientists to characterize quantitatively the effect that the hydrophilic-to-lipophilic balance has on the associations between the pyrene pendants of PyHMWSPs.

3.3 Theory

In organic solvents where pyrene is soluble, excimer formation between pyrenes randomly attached onto a polymer can usually be described by assuming the presence of four pyrene species in solution.[12] These pyrene species are isolated pyrenes that do not form excimer (Py_{free}) and hence fluoresce in the monomer wavelength region with a lifetime τ_M, pyrenes forming excimer via diffusion (Py_{diff}), well-stacked pre-associated pyrenes (*E0*) that yield excimers that emit with a lifetime τ_{E0}, and poorly stacked pre-associated pyrenes (*EL*) that generate long-lived excimers with a longer lifetime τ_{EL}. However, in some situations where the local pyrene concentration is large such as in polymers having a high pyrene content or in pyrene aggregates, an additional pyrene species is found. This additional species, Py_{k2}, represents those pyrene monomers that are improperly stacked and are held within close proximity to one another by either hydrophobic forces in aqueous media or the subsequent incorporation of pyrene-labelled monomers into the polymer.[13,14] These pyrenes form excimer by first undergoing a fast rearrangement process in order to adopt the proper conformation for excimer formation. The reaction pathways undergone by the pyrene species leading to excimer formation are depicted in Scheme 3.1. The rapid rearrangement of the pyrene aggregates is assumed to yield the excimer type *E0**. The exact nature of pyrene aggregates being not well-established, particularly with respect to the number of pyrene moieties involved in the species yielding an *E0** or *EL**-type emission, the *E0* and *EL* species refer to individual pyrene molecules which happen to be incorporated inside a pyrene aggregate, and as such, emit as an excimer.

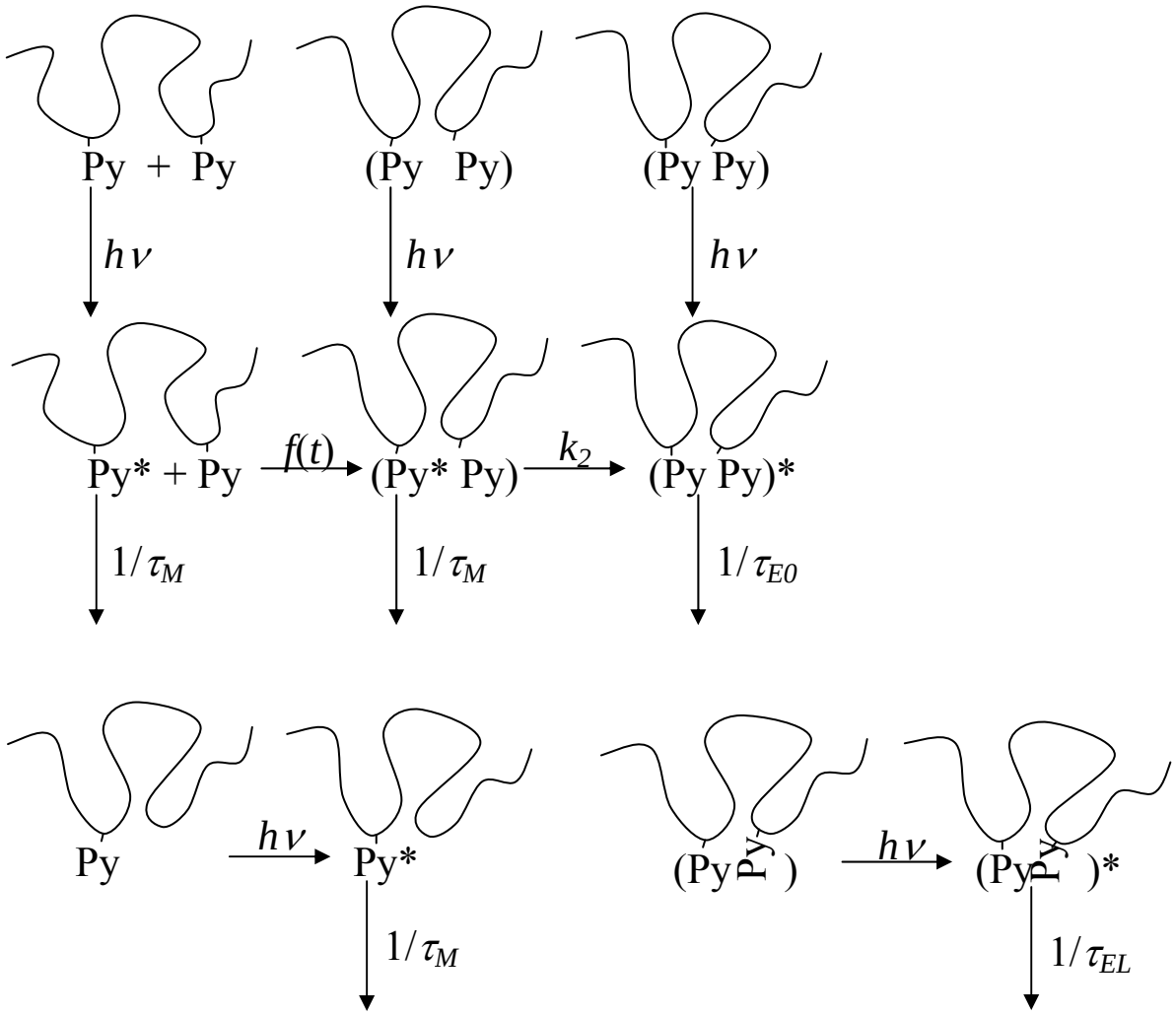

Scheme 3.1: Kinetic scheme depicting the relationship between the pyrene species Py_{diff} = Py*, Py_{k2} = (Py* Py), and the excimer *E0** = (Py Py)*. Diffusion-controlled encounters between pyrene monomers to yield the species Py^{*}_{k2} occur with a "time-dependent rate constant" *f*(*t*) given in Equation 3.9. Rapid rearrangement of the pyrenes with the rate constant k_2 results in the formation of the pyrene excimers *E0**. Poorly stacked pyrenes yield long-lived dimers *EL** = (Py Py)*.

In Scheme 3.1, encounters between pyrene pendants by diffusion are described by the time dependent function $f(t)$ which results from the distribution of rate constants for diffusion controlled encounters between pyrenes randomly distributed along a polymer.[15] Nearby pyrenes encounter quickly whereas pyrenes that are farther apart encounter more slowly. The equations that describe the time dependent profiles of the excited state of all the pyrene species are obtained by solving the following set of differential equations:

$$\frac{d\left[Py^*_{diff}\right]}{dt} = -f(t) - \frac{1}{\tau_M}\left[Py^*_{diff}\right] \tag{3.1}$$

$$\frac{d\left[Py^*_{free}\right]}{dt} = -\frac{1}{\tau_M}\left[Py^*_{free}\right] \tag{3.2}$$

$$\frac{d\left[Py^*_{k2}\right]}{dt} = f(t) - \left(k_2 + \frac{1}{\tau_M}\right)\left[Py^*_{k2}\right] \tag{3.3}$$

$$\frac{d[E0^*]}{dt} = k_2\left[Py^*_{k2}\right] - \frac{1}{\tau_{E0}}[E0^*] \tag{3.4}$$

$$\frac{d[EL^*]}{dt} = -\frac{1}{\tau_{El}}[EL^*] \tag{3.5}$$

These differential equations are straightforward to resolve if the function $f(t)$ is known. An expression for $f(t)$ can be obtained by observing that the Fluorescence Blob Model (FBM) can be applied to describe the time dependent form of $[Py^*_{diff}]$.[14-16] According to the FBM, an excited pyrene can probe within its lifetime a restricted volume called a *blob*. Associated with this volume are the three parameters k_{blob}, $k_e[blob]$, and $\langle n \rangle$ which are the rate constant for the encounter between one

excited pyrene and one ground-state (GS) pyrene species inside the same blob, the product of the rate constant describing how GS pyrene species exchange between blobs times the *blob* concentration inside the polymer coil, and the average number of GS pyrene species per blob, respectively.[17] In the case where the pyrene pendants are not associated, the GS pyrene species represent the GS pyrene monomers. If pyrene aggregates are present, the GS pyrene species are comprised of both GS pyrene aggregates and GS pyrene monomers. According to the FBM, $[Py^{*}_{diff}](t)$ is given by Equation 3.6:

$$\left[Py^{*}_{diff}\right](t) = \left[Py^{*}_{diff}\right]_0 \exp\left[-\left(A_2 + \frac{1}{\tau_M}\right)t - A_3\left(1-\exp\left(-A_4 t\right)\right)\right] \tag{3.6}$$

where the parameters A_2, A_3, and A_4 are functions of k_{blob}, $k_e[blob]$, and $<n>$ whose expressions are given in Equation 3.7:

$$A_2 = < n > \frac{k_{blob}k_e[blob]}{k_{blob} + k_e[blob]} \qquad A_3 = < n > \frac{{k_{blob}}^2}{\left(k_{blob} + k_e[blob]\right)^2} \quad A_4 = k_{blob} + k_e[blob] \tag{3.7}$$

Equation 3.6 enables one to rewrite Equation 3.1 into Equation 3.8 to solve for $f(t)$ whose expression is given in Equation 3.9.

$$f(t) = \frac{1}{\tau_M}\left[Py^{*}_{diff}\right](t) - \frac{d\left[Py^{*}_{diff}\right]}{dt} \tag{3.8}$$

$$f(t) = [Py^{*}_{diff}]_o e^{-A_3} \sum_{i=0}^{\infty} \frac{A_3^i}{i!}(A_2 + iA_4) \times \exp\left(-\left(A_2 + iA_4 + \frac{1}{\tau_M}\right)t\right) \tag{3.9}$$

$f(t)$ can be used for the integration of Equations 3.3 and 3.4. The integration of Equations 3.2 and 3.5 is trivial. Following this procedure, the time profile of all the pyrene species found in the monomer and excimer decays can be determined and their expressions are given in Supporting Information (SI) as Equations SI.3.1-3.5. After weighing the contribution of each species with their absorption coefficient and radiative rate constant, Equations 3.10 and 3.11 are obtained that describe the experimentally obtained fluorescence decays of the pyrene monomer and excimer, respectively.

$$I_M(t) = \alpha_M \left[\varepsilon_M k_{rad}^M [Py_{diff}] \exp\left(-\left(A_2 + \frac{1}{\tau_M} \right) t - A_3 \left(1 - \exp(-A_4 t)\right) \right) \right.$$

$$+ \left(\varepsilon_M k_{rad}^M [Py_{k2}] + \varepsilon_M k_{rad}^M [Py_{diff}] e^{-A_3} \sum_{i=0}^{\infty} \frac{A_3^i}{i!} \frac{A_2 + iA_4}{A_2 + iA_4 - k_2} \right) \exp\left(-\left(k_2 + \frac{1}{\tau_M} \right) t \right)$$

$$- \varepsilon_M k_{rad}^M [Py_{diff}] e^{-A_3} \sum_{i=0}^{\infty} \frac{A_3^i}{i!} \frac{A_2 + iA_4}{A_2 + iA_4 - k_2} \exp\left(-\left(A_2 + iA_4 + \frac{1}{\tau_M} \right) t \right)$$

$$\left. + \varepsilon_M k_{rad}^M [Py_{free}] \exp\left(-\frac{t}{\tau_M} \right) \right] \qquad (3.10)$$

$$I_E(t) = \alpha_E \left[k_2 \left(\left(\varepsilon_M k_{rad}^{E0} [Py_{k2}] + \varepsilon_M k_{rad}^{E0} [Py_{diff}] e^{-A_3} \sum_{i=0}^{\infty} \frac{A_3^i}{i!} \frac{A_2 + iA_4}{A_2 + iA_4 - k_2} \right) \right.\right.$$

$$\left.\left. \times \frac{\exp\left(-\frac{t}{\tau_{E0}} \right) - \exp\left(-\left(k_2 + \frac{1}{\tau_M} \right) t \right)}{k_2 + \frac{1}{\tau_M} - \frac{1}{\tau_{E0}}} + \right.\right.$$

$$\varepsilon_M k_{rad}^{E0}[Py_{diff}]e^{-A_3}\sum_{i=0}^{\infty}\frac{A_3^i}{i!}\frac{A_2+iA_4}{A_2+iA_4-k_2}\frac{\exp\left(-\left(A_2+iA_4+\frac{1}{\tau_M}\right)t\right)-\exp\left(-\frac{t}{\tau_{E0}}\right)}{A_2+iA_4+\frac{1}{\tau_M}-\frac{1}{\tau_{E0}}}\Bigg)$$

$$+\ \varepsilon_{E0}k_{rad}^{E0}[E0]\times\exp\left(-\frac{t}{\tau_{E0}}\right)+\varepsilon_{EL}k_{rad}^{EL}[EL]\times\exp\left(-\frac{t}{\tau_{EL}}\right)\Bigg] \qquad (3.11)$$

The coefficients α_M and α_E are scaling constants which depend on several factors which include the geometry and the response of the photomultiplier tube of the time-resolved fluorometer, the total optical density of the sample and the amount of light absorbed within the cell. The molar absorption coefficients ε_M, ε_{E0}, and ε_{EL} together with the radiative rate constants k_{rad}^{M}, k_{rad}^{E0}, and k_{rad}^{EL} are attributed to the pyrene species listed in Table 3.1. Fitting the decays with Equations 3.10 and 3.11 yields the relative weight of the pre-exponential factors. The concentrations appearing in Equations 3.10 and 3.11 are those of the ground-state pyrene species in solution and not those concentrations representing the pyrene species excited at time t = 0 such as in Equation 3.6 or Equations SI.3.1 – 3.5 in SI.

Having six unknowns made of three molar absorption coefficients and three radiative rate constants in addition to the presently unknown concentrations of all pyrene species yields an unsolvable set of equations. Thus one assumption needed to be made. The preformed pyrene aggregates *E0* and *EL* were assumed to have a same molar absorption coefficient, namely $\varepsilon_{E0} = \varepsilon_{EL}$. This in turn implied that the radiative rate constant k_{rad}^{EL} was equal to k_{rad}^{E0}, since the radiative rate constant of a chromophore is determined from its absorption coefficient.[18] Fitting the monomer and excimer decays with Equations 3.10 and 3.11 yields the relative pre-exponential contributions, which, after taking into account the assumptions made earlier, can be rearranged into the fractions listed in

Equations 3.12 – 3.16. The superscript f indicates that these fractions are obtained from the fluorescence decays and describe the contributions to the fluorescence decays of all pyrene species present in solution.

Table 3.1: Symbols used for the molar absorption coefficients and radiative rate constants of the various pyrene species.

Pyrene species	Molar absorption coefficient	Radiative rate constants in the monomer/excimer decay
Py_{diff}	ε_M	$k_{rad}^{M} / k_{rad}^{E0}$
Py_{free}	ε_M	k_{rad}^{M} /n.a.
Py_{k2}	ε_M	$k_{rad}^{M} / k_{rad}^{E0}$
$E0$	ε_{E0}	n.a./ k_{rad}^{E0}
EL	ε_{EL}	n.a./ k_{rad}^{EL}

$$f_{free}^{f} = \frac{\varepsilon_M [Py_{free}]_0}{\varepsilon_M [Py_{diff}]_0 + \varepsilon_M [Py_{free}]_0 + \varepsilon_M [Py_{k2}]_0 + \varepsilon_{E0}[E0]_0 + \varepsilon_{E0}[EL]_0} \tag{3.12}$$

$$f_{diff}^{f} = \frac{\varepsilon_M [Py_{diff}]_0}{\varepsilon_M [Py_{diff}]_0 + \varepsilon_M [Py_{free}]_0 + \varepsilon_M [Py_{k2}]_0 + \varepsilon_{E0}[E0]_0 + \varepsilon_{E0}[EL]_0} \tag{3.13}$$

$$f_{k2}^{f} = \frac{\varepsilon_M [Py_{k2}]_0}{\varepsilon_M [Py_{diff}]_0 + \varepsilon_M [Py_{free}]_0 + \varepsilon_M [Py_{k2}]_0 + \varepsilon_{E0}[E0]_0 + \varepsilon_{E0}[EL]_0} \tag{3.14}$$

$$f_{E0}^{f} = \frac{\varepsilon_{E0}[E0]_0}{\varepsilon_M[Py_{diff}]_0 + \varepsilon_M[Py_{free}]_0 + \varepsilon_M[Py_{k2}]_0 + \varepsilon_{E0}[E0]_0 + \varepsilon_{E0}[EL]_0} \quad (3.15)$$

$$f_{EL}^{f} = \frac{\varepsilon_{E0}[EL]_0}{\varepsilon_M[Py_{diff}]_0 + \varepsilon_M[Py_{free}]_0 + \varepsilon_M[Py_{k2}]_0 + \varepsilon_{E0}[E0]_0 + \varepsilon_{E0}[EL]_0} \quad (3.16)$$

Equations 3.12 – 3.16 define a set of four independent equations (since $f_{diff}^{f} + f_{free}^{f} + f_{k2}^{f} + f_{E0}^{f} + f_{EL}^{f} = 1$) where f_{diff}^{f}, f_{free}^{f}, f_{k2}^{f}, f_{E0}^{f}, and f_{EL}^{f} are known experimentally and $[Py_{diff}]$, $[Py_{free}]$, $[Py_{k2}]$, $[E0]$, $[EL]$, and ε_{E0} are the six unknowns. The absorption coefficient of the pyrene monomer, ε_M, can be estimated with a model compound. Two additional equations are obtained by considering the absorption of the solution (*Abs*) given in Equation 3.17 where *L* is the irradiation path length and the conservation of pyrenes in Equation 3.18.

$$Abs = \left(\varepsilon_M[Py_{diff}] + \varepsilon_M[Py_{free}] + \varepsilon_M[Py_{k2}] + \varepsilon_{E0}[E0] + \varepsilon_{E0}[EL]\right)L \quad (3.17)$$

$$[Py]_T = [Py_{diff}] + [Py_{free}] + [Py_{k2}] + [E0] + [EL] \quad (3.18)$$

Equations 3.12 – 3.18 constitute a set of six independent equations which can be solved as follows to determine the six unknowns. The absorption of the solution can be determined with a spectrophotometer. The molar absorption coefficient of the pyrene monomer, ε_M, can be determined with a model compound so that the concentrations $[Py_{free}]_0$, $[Py_{diff}]_0$, and $[Py_{k2}]_0$ can be calculated from the knowledge of the fractions f_{free}^{f}, f_{diff}^{f}, and f_{k2}^{f} as $f_{free}^{f} Abs/\varepsilon_M$, $f_{diff}^{f} Abs/\varepsilon_M$, and $f_{k2}^{f} Abs/\varepsilon_M$, respectively. Since the overall pyrene concentration $[Py]_T$ is known, Equation 3.18 can be rearranged to yield Equation 3.19 where the right-hand side of the equation is a now known quantity. The sum $[E0]_0 + [EL]_0$ in Equation 3.19 equals $\left(f_{E0}^{f} + f_{EL}^{f}\right)Abs/\varepsilon_{E0}$, itself equal to the

known quantity $[Py]_T - [Py_{free}]_0 - [Py_{diff}]_0 - [Py_{k2}]_0$. Since f_{E0}^f, f_{EL}^f, and *Abs* are known experimentally, ε_{E0} can be determined. The concentrations, $[E0]_0$ and $[EL]_0$ can then be calculated as $f_{E0}^f Abs/\varepsilon_{E0}$ and $f_{EL}^f Abs/\varepsilon_{E0}$, respectively.

$$[E0]_0 + [EL]_0 = [Py_T] - [Py_{free}]_0 - [Py_{diff}]_0 - [Py_{k2}]_0 \qquad (3.19)$$

3.4 Experimental

Chemicals: 1-Pyrenemethanol was purchased from Aldrich. It was purified by 3 crystallizations in ethanol (Caledon, HPLC grade). Distilled in glass *N*,*N*-dimethylformamide (DMF) was purchased from Caledon. The synthesis of the pyrene-labeled poly(*N*,*N*-dimethylacrylamide) (PyPDMA) has been described in detail in an earlier publication.[19] The weight-average molecular weight (M_w) and pyrene content (μ_{Py}) of the PyPDMAs used in this study are listed in Table 3.2. Milli-Q Millipore filtered water (18 MΩ) was used for all aqueous solutions.

Pyrene concentration: The pyrene concentration of an aqueous PyPDMA solution was determined by two methods giving equivalent results. In the first method, a known amount of a PyPDMA aqueous solution was freeze-dried on a Labconco Freezone 6 freeze drier. The mass of freeze-dried PyPDMA was recorded and the pyrene concentration in the aqueous solution was determined from the pyrene content of the PyPDMA sample given in Table 3.2. The second method involved mixing a drop of concentrated PyPDMA aqueous solution with DMF, and further diluting the mixture with known amounts of DMF until an OD ~ 1.0 was obtained. The water contribution to the final solution could be neglected and the pyrene concentration in DMF could be determined from the molar absorption coefficient of 1-pyrenemethanol in DMF (ε_{PyMeOH} = 38,900 $M^{-1}.cm^{-1}$ in DMF). The pyrene concentration in the original PyPDMA aqueous solution was back-calculated from the known dilution

factors. DMF was used because it solubilizes both the PDMA backbone and the pyrene label so that the absorption spectrum of PyPDMA in DMF is not distorted by the presence of ground-state pyrene aggregates.

Table 3.2: Pyrene contents (μ_{Py}), weight averaged molecular weights (M_W), P_A values in water, and names of the PyPDMA samples.

Name	Pyrene Content (μ_{Py}) μmol/g	M_W kg/mol	P_A*
PyPDMA6	6	85	2.49 ± 0.03
PyPDMA263	263	165	1.65 ± 0.02
PyPDMA479	479	123	1.56 ± 0.02
PyPDMA645	645	105	1.41 ± 0.01

* The P_A value was obtained by taking the ratio of the absorption corresponding to the most intense band (around 344 nm) to that of the adjacent trough (around 334 nm).

UV-Vis Absorbance Measurements: Peak-to-valley (P_A) ratios shown in Figure 3.3 were determined from the UV-Vis absorbance spectra acquired with a Hewlett Packard 8452A diode array spectrophotometer with a 2 nm resolution. The P_A ratios were obtained by taking the ratio of the absorption corresponding to the most intense band (around 344 nm) to that of the adjacent trough (around 334 nm). A Beckman DU640 spectrophotometer was used for all other absorbance measurements due to its higher 0.5 nm wavelength resolution. To ensure linearity in the response of the spectrophotometer absorbance, cells with path lengths of 10, 1, and 0.1 mm were used to keep the absorbance signals between 0.05 and 2.

Steady-State Fluorescence: The steady-state emission spectra were acquired on a Photon Technology International LS-100 steady-state fluorometer with an Ushio UXL-75Xe xenon arc lamp and PTI 814 photomultiplier detection system. For PyPDMA samples having optical densities above 2, fluorescence measurements were performed with a front face geometry using a Hellma triangular cell in order to minimize the inner filter effect during fluorescence measurements. For all other PyPDMA samples, measurements were performed in a 1 cm square fluorescence cell using the right angle geometry. The fluorescence spectra of all PyPDMA aqueous solutions were acquired under aerated conditions. The emission spectra were acquired by exciting the samples at 344 nm. The I_E/I_M ratios were determined by integrating the fluorescence intensity of the pyrene monomer from 372 to 378 nm and that of the excimer from 500 to 530 nm to yield I_M and I_E, respectively. The excitation spectra were acquired with the emission wavelength set at 375 nm for the monomer and 510 nm for the excimer.

Time-Resolved Fluorescence: The fluorescence decays were obtained with a time-correlated single photon counter manufactured by IBH Ltd. using a NanoLED having a maximum intensity at 333 nm. The full width of the instrument response function at ½ and $1/100^{th}$ of the maximum intensity equaled 0.9 and 2.6 ns, respectively. The emission wavelength was set at 375 and 510 nm for the pyrene monomer and excimer decays, respectively, while the excitation spectral bandwidth was set to a value as low as 1 nm and as high as 32 nm depending on the type of experiment being conducted. The detector was an IBH model TBX-04 photon detector module. To reduce potential stray scattered light, cutoff filters at 370 and 495 nm were used to acquire the monomer and excimer decays, respectively. For PyPDMA samples with optical densities larger than 2, the front face geometry was used to acquire the fluorescence decays. For all other PyPDMA samples, the decays were acquired with the right angle geometry. All fluorescence decays were acquired on aerated samples. All decays were collected over 1,024 channels with a minimum of 10,000 counts taken at the maximum of the

monomer and excimer decays to ensure a high signal to noise ratio and were fitted globally to Equations 3.10 and 3.11. A scattering latex solution was used to obtain the instrument response function of the IBH fluorometer for the monomer and excimer decays. Within experimental error, no difference could be detected in the parameters retrieved from the analysis of the fluorescence decays, whether the fluorescence decays were acquired using a scattering solution or reference solutions such as PPO [2,5-diphenyloxazole] in cyclohexanol (τ = 1.42 ns) and BBOT [2,5-bis(tert-butyl-2-benzoxazolyl)thiopene] in ethanol (τ =1.47 ns) for the monomer and excimer decays, respectively (see Table SI.3.1 in Supporting Information (SI)). All measured decays were deconvoluted from the instrument response function and fitted to the desired function using a least squares analysis.[20] A scattering and background correction was applied to all fluorescence decay analyses.[21] The parameters in Equations 3.10 and 3.11 were optimized with the Marquardt-Levenberg algorithm.[22] The resulting fits were described as "good" when the global χ^2 was smaller than 1.3 and the residuals and the autocorrelation function of the residuals were randomly distributed around zero.

3.5 Results

In order to determine the absorption coefficient of a pyrene aggregate in water, pyrene aggregates must first be generated. Since pyrene is inherently insoluble in water, pyrene aggregates can only be generated in water by attaching pyrene moieties onto a water-soluble molecule which enables the solubilization of a sufficient amount of pyrene in water to yield pyrene aggregates. To this end, a series of pyrene-labeled poly(*N*,*N*-dimethylacrylamide)s (PyPDMA) were used. The weight-average molecular weight, M_w, and pyrene content, μ_{Py}, of the PyPDMA samples are listed in Table 3.2. When dissolved in water, the pyrene pendants of the PyPDMA samples tend to associate into pyrene aggregates which are stabilized in solution by the water-soluble PDMA chains. The pyrene

aggregates produced in the aqueous PyPDMA solutions could then be studied by absorption and fluorescence.

Some common methods which are found in the literature[10,11] to gauge the level of association of pyrene pendants attached onto a water-soluble polymer include measuring the peak-to-valley (P_A) ratio of the 0-0 transition of the pyrene absorbance spectrum with its adjacent trough as well as the relative red shift of the 0-0 transition of the excimer to the monomer fluorescence excitation spectra. Both of these methods rely on the fact that the molar absorption coefficient profile of the associated pyrenes is broader and red-shifted relative to the unassociated pyrenes. The monomer and excimer excitation spectra of three PyPDMA samples were acquired and normalized at their maximum value. They are shown in Figure 3.1. Regardless of the pyrene content of the PyPDMA samples, all excitation spectra of the pyrene monomer overlap, showing a maximum at 345 nm. This is expected since the pyrene monomers exhibit the same spectral features regardless of pyrene content. On the other hand, all excimer fluorescence excitation spectra of the PyPDMA samples exhibit a maximum that is red-shifted with respect to the maximum of the monomer excitation spectra by 1 nm for PyPDMA263 and 3 nm for the higher pyrene content polymers. In addition, the red edge of the excimer peak shifts to higher wavelengths with increasing pyrene content. These shifts are a clear indication that all PyPDMA samples in water contain pyrene aggregates and the trends in the shifts confirm that the PyPDMA samples having a larger pyrene content generate more pyrene aggregates. As shown in Scheme 3.1, a pyrene excimer is formed by either the diffusional encounter between an excited pyrene and a ground-state pyrene followed by their rapid rearrangement to yield the conformation expected to form an *E0** excimer, or direct excitation of a pre-formed pyrene aggregate. As μ_{Py} increases, the equilibrium between free and aggregated pyrenes promotes aggregation and the excitation spectrum of the excimer broadens and shifts to larger wavelengths.

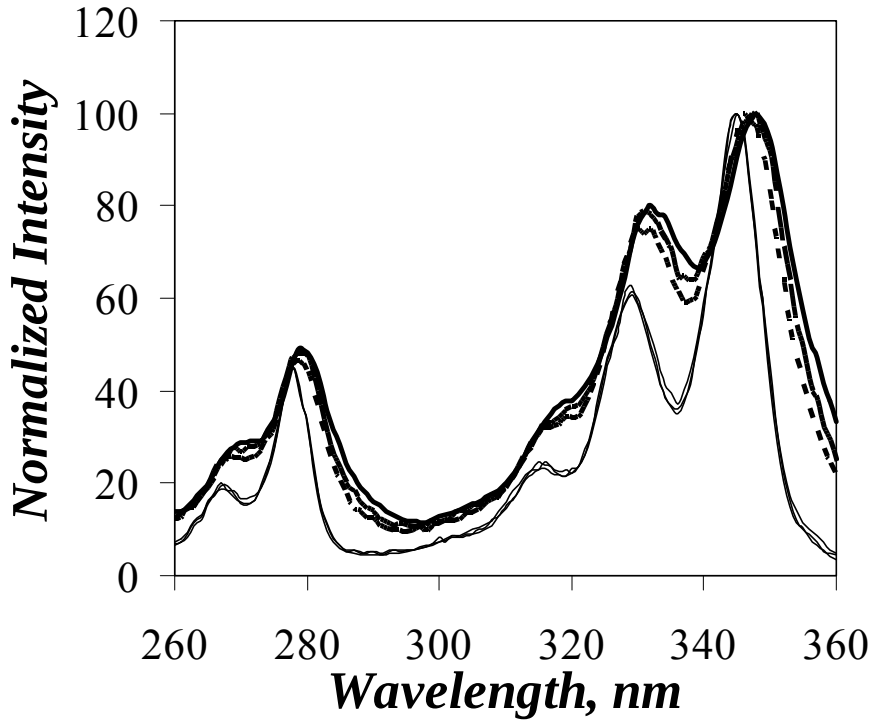

Figure 3.1: Pyrene monomer (solid thin line) and excimer (thick lines) fluorescence excitation spectra of PyPDMA263 (- - -), PyPDMA479 (— — —), and PyPDMA645 (————).

Although the equilibrium between free and aggregated pyrenes is shifted toward aggregation upon increasing μ_{Py}, increasing the concentration of a given PyPDMA sample results in no change in the features of the absorption spectrum, even though the absorbance increases over three orders of magnitude in Figure 3.2. This lack of change was observed for PyPDMA263, PyPDMA479, and PyPDMA645. Although the features of the absorption spectra did not change with increasing polymer concentration, the absorption peak broadened with increasing μ_{Py}, with a P_A value dropping from 1.65 ± 0.02 for PyPDMA263 to 1.41 ± 0.01 for PyPDMA645 (Table 3.2). The observations made with the

absorption spectra in Figure 3.2 suggest that excimer formation increases intramolecularly when μ_{Py} increases, but does not increase intermolecularly over the range of polymer concentrations studied.

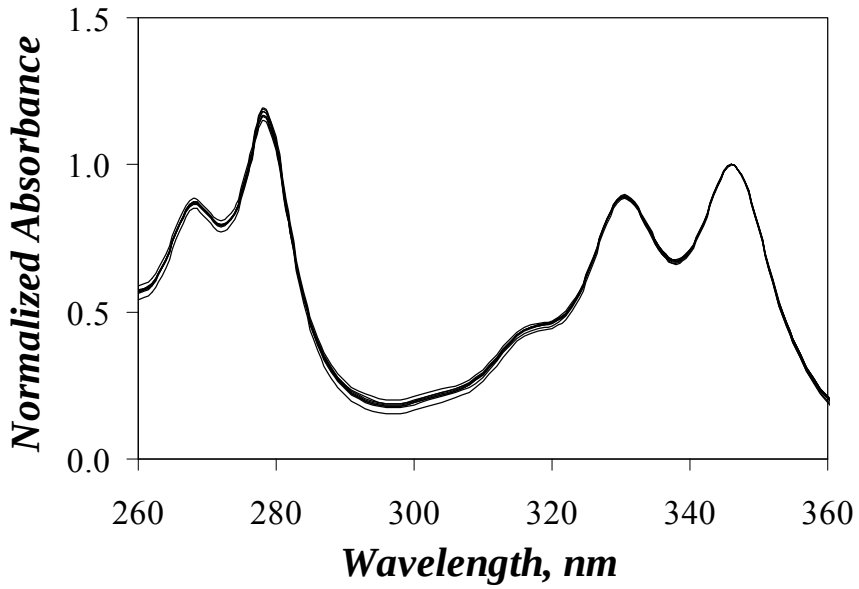

Figure 3.2: Spectra of the normalized absorbance of PyPDMA645 with optical densities of 0.05, 0.13, 0.39, 0.86, 1.7, 4.8, 9.5, 15, 33, and 57. The spectra were normalized at 346 nm.

This fact is further confirmed by monitoring the ratio of the fluorescence intensity of the excimer, I_E, over that of the monomer, I_M, as a function of polymer concentration shown in Figure 3.3. For all PyPDMA samples, the I_E/I_M ratio increased by about 50% when the polymer concentration of the solution was increased by three orders of magnitude, or for pyrene concentrations ranging from 2×10^{-6} M to 2×10^{-3} M. For concentrations of molecular pyrene above 10^{-4} M, the I_E/I_M ratio is expected to increase linearly with pyrene concentration.[23] Obviously, the data shown in Figure 3.3 for the PyPDMA samples exhibit a much smaller increase in the I_E/I_M ratio with polymer concentration

than expected. This was observed over a 1000-fold increase in polymer concentration, further substantiating the notion that excimer formation for these polymers in water occurs predominantly intramolecularly.

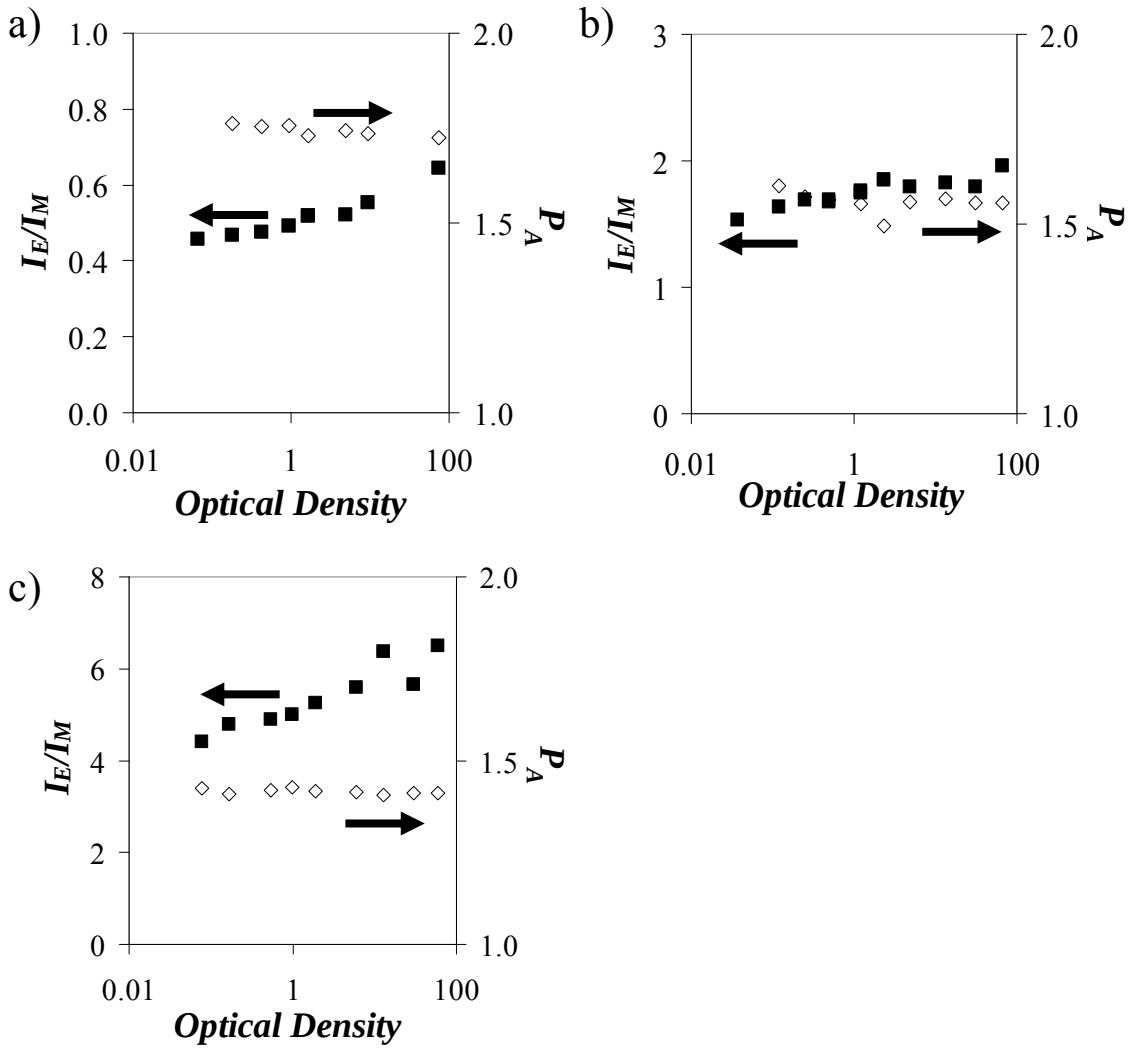

Figure 3.3: I_E/I_M and P_A values of a) PyPDMA263, b) PyPDMA479, and c) PyPDMA645 with increasing optical densities.

Further evidence that aggregated pyrenes were present was obtained by fitting the excimer fluorescence decays with a sum of three exponentials. A sample excimer decay is shown in Figure SI.3.1. All excimer fluorescence decays exhibited a reduced risetime similar to the one shown in Figure SI.3.1. A reduced risetime can be readily inferred from the ratio the sum of the negative pre-exponential factors over the sum of the positive pre-exponential factors, i.e. the A_{E-}/A_{E+} ratio. The fluorescence decays acquired with an excitation wavelength of 344 nm yielded an A_{E-}/A_{E+} ratio equal to –0.13, –0.19, and –0.21 for PyPDMA645, PyPDMA479, and PyPDMA263, respectively. In the absence of ground-state pyrene aggregates or dimers, the A_{E-}/A_{E+} ratio would equal –1.0, but more positive values such as those found for all PyPDMAs are expected in the presence of pyrene aggregates. This observation further confirms the results obtained from the fluorescence excitation spectra (Figure 3.1) and the absorption spectra (Figure 3.2 and the P_A values in Table 3.2).

In general, the association of two molecules, A and B, is characterized by a constant K = [AB]/([A]×[B]) describing the equilibrium A + B ↔ AB. In turn, K is determined by monitoring a change in a given colligative property φ for one of the molecules of interest, say A, as it binds to increasing amounts of molecule B. Working with A alone yields φ_A. When all A molecules are complexed with B in the presence of a large excess of B, φ_{AB} can be determined. For any A and B mixture, the colligative property φ of the mixture depends on φ_A, φ_{AB}, and the concentrations of A and the complex AB, so that [A] and [AB] can be determined, which yields [B] as $[B] = [B]_T - [AB]$. By preparing a series of A and B mixtures of different composition, the concentrations [A], [B], and [AB] can be measured from the colligative property φ and the equilibrium constant K is calculated. This procedure is used routinely to determine the equilibrium constant between molecules undergoing any type of molecular association. A well-known example deals with the complexation of rhodamine 6G into rhodamine dimers upon increasing the rhodamine concentration using the solution absorption as

φ.[24] The data shown in Figure 3.2 demonstrate how inadequate this procedure is to determine the equilibrium constant for the association of the pyrene monomers of the PyPDMA samples into pyrene aggregates. Increasing the concentration of the associating species (pyrene) results in no change in absorption, the colligative property of choice when dealing with aromatic molecules. This, the complexity of the kinetics of excimer formation between pyrenes located in a polymeric aggregate, and the multitude of pyrene species present in solution (Py_{diff}, Py_{free}, Py_{k2}, *E0*, and *EL*) explain why the photophysical properties of pyrene aggregates have never been quantified in terms of their molar absorption coefficient.

As illustrated in Figure 3.2, absorption spectra alone can not yield the concentration of pyrene aggregates in solution because the colligative property of a pyrene aggregate related to absorption, i.e. its molar absorption coefficient ε_{E0}, can not be determined by increasing the concentration of pyrene. An obvious second colligative property that could be used to characterize the association between pyrene monomers is the quantum yield of the different pyrene species. Unfortunately, steady-state fluorescence does not allow one to distinguish whether the fluorescence of the excimer arises from the diffusional encounter between an excited pyrene and a ground-state pyrene which occurs over time, or the direct excitation of an aggregate of ground-state pyrenes which occurs instantaneously. Furthermore the efficiency achieved by the instantaneous formation of excimer by the direct excitation of a *E0* or *EL* pyrene aggregate is mitigated by a suspected lower quantum yield of these directly excited pyrene species due to self-quenching.[25-28]

A thorough appreciation of the list of hurdles encountered above leads to the obvious conclusion that characterizing the association of the pyrene pendants of a PyHMWSP in water is a daunting task. Yet research carried out in this laboratory has led to many improvements in the analysis of the fluorescence decays of PyHMWSPs in aqueous solution which together enable the first determination of the absorption coefficient of a pyrene aggregate. The first improvement was

mathematical by realizing that diffusional encounters between the pyrene pendants of a polymer randomly labeled with pyrene can be accounted for by a Fluorescence Blob Model (FBM).[12] This led to the derivation of an expression for the function $f(t)$ given in Equation 3.9 which is used as a pivot to analyze globally the monomer and excimer decays.[14,15] The second improvement was analytical. By noting that the differential equations describing the process of excimer formation by diffusion in the monomer and excimer decays were coupled, several analysis packages were developed in this laboratory over the years to fit the monomer and excimer decays globally and improve the accuracy of all the parameters used to describe the process of excimer formation.[15,29] The third and last improvement was instrumental. As will be shown in this report, the advent of powerful and cheap LED light sources having a very high repetition rate to acquire time-resolved fluorescence decays enabled the acquisition of time-resolved fluorescence decays within a reasonable time where the spectral bandwidth of the excitation wavelength was narrowed down to 1 nm.

Equipped with these powerful mathematical, analytical, and experimental tools, we set out to acquire the monomer and excimer fluorescence decays for aqueous solutions of the PyPDMA263, PyPDMA479, and PyPDMA645 samples with different polymer concentrations using a 1 nm slit width for the excitation wavelength, and excitation wavelengths ranging from 325 to 350 nm. For a given pyrene content, polymer concentration, and excitation wavelength, the monomer and excimer fluorescence decays were fitted globally with Equations 3.10 and 3.11, respectively.

Since the rate of rearrangement, k_2, occurs on a much shorter time scale than the rate of diffusion, it is poorly resolved in the monomer and excimer decays, and needs to be fixed in the analysis. To determine its value accurately, the monomer and excimer fluorescence decays were acquired in duplicate using broader slit width and with a time per channel of 2.04 or 0.12 ns/ch for the monomer and 1.02 or 0.12 ns/ch for the excimer. The decays acquired with a 0.12 ns/ch time per channel focused on the initial times of the monomer and excimer decays which were more sensitive to

the k_2 value. Fitting globally the four fluorescence decays with Equations 3.10 and 3.11 enabled the determination of k_2 with improved accuracy. This procedure was applied to several PyPDMA solutions and resulted in the k_2 values which, within experimental error, remained constant and equal to $3.4 \pm 0.3 \times 10^8$ s^{-1}. Thus, all decays reported in this study were analyzed with a k_2 value fixed to 3.4×10^8 s^{-1}.

The parameters retrieved from the global analysis of the monomer and excimer fluorescence decays with Equations 3.10 and 3.11 were tabulated and are listed in Tables SI.3.2 – 3.7 in Supporting Information (SI). The fits were good yielding χ^2 that never exceeded 1.30. An example of the quality of fit of the fluorescence decays is shown in Figure SI.3.1 for a 0.09 g/L solution of PyPDMA645 excited at 334 nm. Within experimental error, the parameters k_{blob}, $k_{ex}[blob]$, $\langle n \rangle$, τ_{E0}, and τ_{EL} remained constant with wavelength for any given PyPDMA solution and their averaged values are summarized in Table 3.3. The constancy of these parameters with wavelength is expected since those constants describe either bimolecular processes occurring between an excited pyrene and a ground-state pyrene (k_{blob}, $k_{ex}[blob]$, $\langle n \rangle$) or unimolecular relaxation processes occurring for a given pyrene species (τ_{E0}, τ_{EL}). However, for a given PyPDMA solution, $\langle n \rangle$ depends on the local concentration of ground-state pyrene species, whereas τ_{E0} and τ_{EL} do not depend on the PyPDMA concentration. The results in Table 3.3 substantiate that claim with $\langle n \rangle$ depending strongly on pyrene content and τ_{E0} and τ_{EL} remaining constant with pyrene content and equal to 44 ± 4 and 81 ± 6 ns, respectively. These parameters do not depend on the concentration of excited species in solution and as a result, are wavelength and concentration independent.

Although the FBM parameters do not depend on the excitation wavelength, the fractions of the fluorescence contributed by the pyrene monomers and excimers do as shown in Figure 3.4 for the pyrene monomer. The fraction $f_M^f = f_{diff}^f + f_{k2}^f + f_{free}^f$ shows a distinct minimum and maximum

around 334 and 343 nm, respectively, as does the absorption coefficient of the pyrene monomer in Figure 3.5. The pronounced undulations observed for f_M^f in Figure 3.4 reflect differences in the absorption coefficients of the pyrene monomer (ε_M) and aggregate (ε_{E0}) which depend on wavelength.

Table 3.3: Averaged FBM parameters obtained for excitation wavelengths ranging from 325 to 350 nm for various pyrene labellings and optical densities of PyPDMA and using $k_2 = 3.4 \times 10^8$ s^{-1}.

Pyrene Content μmol/g	OD	[*PyPDMA*] g/L	<*n*>	$k_{blob}\times10^7$ s^{-1}	$k_{ex}[blob] \times10^7$ s^{-1}	τ_{E0} ns	τ_{EL} ns
645	1	0.09	1.7 ± 0.1	1.7 ± 0.2	0.6 ± 0.1	43.1 ± 3.1	79.7 ± 3.6
	30	2.2	1.6 ± 0.1	1.7 ± 0.2	0.5 ± 0.1	44.6 ± 1.9	79.7 ± 2.5
479	0.1	0.01	1.2 ± 0.1	1.6 ± 0.2	0.6 ± 0.1	38.9 ± 2.8	74.9 ± 3.0
	0.7	0.08	1.1 ± 0.0	1.6 ± 0.2	0.6 ± 0.1	45.4 ± 7.2	80.8 ± 4.4
	15	1.8	1.1 ± 0.0	1.5 ± 0.3	0.6 ± 0.1	43.0 ± 2.3	79.2 ± 3.0
263	30	4.8	0.8 ± 0.0	1.4 ± 0.2	0.5 ± 0.1	42.9 ± 2.6	88.6 ± 7.5

As outlined in the theoretical section, $\varepsilon_M(\lambda)$ must be known to determine $\varepsilon_{E0}(\lambda)$. $\varepsilon_M(\lambda)$ was obtained with a PyPDMA sample containing 6 μmol pyrene per gram of polymer, PyPDMA6. PyPDMA6 was found to yield virtually no excimer emission in water as verified from the visual inspection of its fluorescence spectrum. The absorbance spectrum of a known concentration of PyPDMA6 in water was acquired. It yielded $\varepsilon_M(\lambda)$ as a function of wavelength between 325 and 350 nm. The $\varepsilon_M(\lambda)$ values obtained are listed in Table 3.4. It must be noted that the P_A value of

PyPDMA6 equals 2.5 which is smaller than 3.0, the P_A value expected for a pyrene labeled polymer in organic solvents where no aggregation between pyrenes takes place.[10] Although a low P_A value might indicate residual pyrene aggregation, it can also be induced by interactions between pyrene and the PDMA backbone. This latter explanation is certainly the case here, since the P_A value of another pyrene-labeled water-soluble polymer, namely a poly(ethylene oxide) labeled at one end with pyrene (Py-PEO), yields a P_A value of 2.8 in water, also smaller than 3.0, despite showing no excimer formation in its fluorescence spectrum.[30]

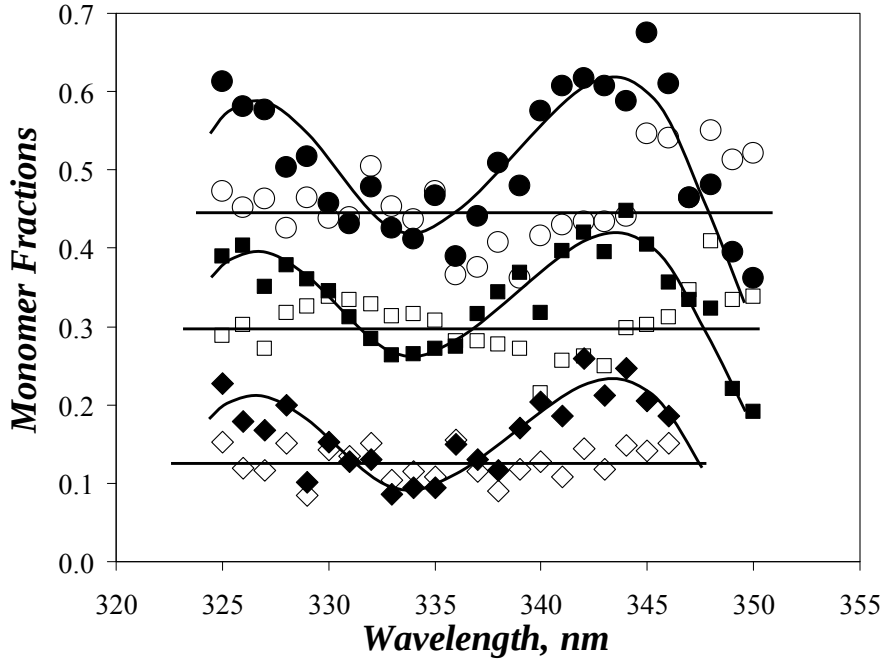

Figure 3.4: Fluorescence fractions f_M^f (●,■,◆) and molar fraction f_M (○,□,◇) obtained for 4.8 g/L PyPDMA263 (circles), 15 g/L PyPDMA479 in water (squares) and 0.09 g/L PyPDMA645 in water (diamonds).

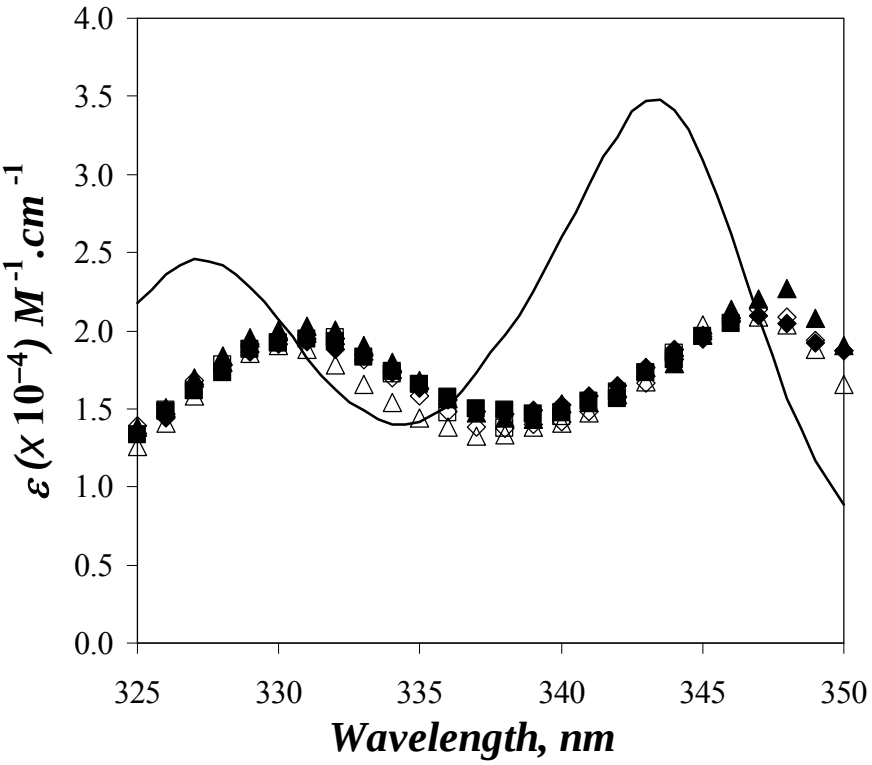

Figure 3.5: Molar absorption coefficient of the pyrene monomer ($\varepsilon_M(\lambda)$, ——) and pyrene aggregates ($\varepsilon_{E0}(\lambda)$) for PyPDMA263 with a concentration of 4.8 g/L (△), PyPDMA479 with a concentration of 0.01 g/L (□), 0.08 g/L (◇), and 1.8 g/L (▲), and PyPDMA645 with a concentration of 0.09 g/L (■) and 2.2 g/L (◆).

The concentrations of the various pyrene species and the $\varepsilon_{E0}(\lambda)$ values were determined using Equations 3.12 – 3.19 as discussed in the Theory section for different concentrations of PyPDMA263, PyPDMA479, and PyPDMA645. Within experimental error, the fraction representing the molar concentration of unassociated pyrenes (f_M) remains constant with wavelength (Figure 3.4), as the pronounced undulations observed for f_M^f are strongly dampened with f_M. The $\varepsilon_{E0}(\lambda)$ values recovered

for each PyPDMA sample were plotted as a function of wavelength in Figure 3.5. They overlap regardless of pyrene content or polymer concentration. The good agreement observed with this set of six $\varepsilon_{E0}(\lambda)$ values obtained with three different polymers for six different polymer concentrations suggests that the procedure outlined in this study is robust and yields reliable molar absorption coefficients for the pyrene aggregates in water. The $\varepsilon_{E0}(\lambda)$ values were averaged at each wavelength for all data points and their averaged values are listed in Table 3.5. The P_A value of the pyrene aggregates of PyPDMA was found to equal 1.5 ± 0.1, much lower than the value of 2.5 found for isolated pyrene pendants. Finally, the fractions of all pyrene species present in solution could be determined quantitatively. They are listed in Table 3.6.

Table 3.4: Molar absorption coefficient of unassociated pyrenes, ε_M, for PyPDMA.

Wavelength nm	$<\varepsilon_M>$ $L \cdot mol^{-1} \cdot cm^{-1}$	Wavelength nm	$<\varepsilon_M>$ $L \cdot mol^{-1} \cdot cm^{-1}$
325	21800	338	19700
326	23600	339	22500
327	24600	340	26000
328	24200	341	29300
329	22700	342	32400
330	20700	343	34700
331	18200	344	34100
332	16200	345	30900
333	14800	346	26200
334	14000	347	20900
335	14200	348	15700
336	15200	349	11700
337	17300	350	8800

Table 3.5: Averaged absorption coefficient of the pyrene aggregates, ε_{E0}, for PyPDMA.

Wavelength nm	$<\varepsilon_{E0}>$ $L \cdot mol^{-1} \cdot cm^{-1}$	$\pm <\varepsilon_{E0}>$ $L \cdot mol^{-1} \cdot cm^{-1}$	Wavelength nm	$<\varepsilon_{E0}>$ $L \cdot mol^{-1} \cdot cm^{-1}$	$\pm <\varepsilon_{E0}>$ $L \cdot mol^{-1} \cdot cm^{-1}$
325	13400	500	338	14100	600
326	14700	400	339	14300	400
327	16500	500	340	14700	500
328	17800	300	341	15300	500
329	18900	400	342	16000	300
330	19300	400	343	17200	500
331	19500	500	344	18400	400
332	19100	700	345	19700	400
333	18100	900	346	20900	400
334	17100	900	347	21300	500
335	16000	1000	348	21100	1100
336	15100	700	349	19500	900
337	14300	800	350	17005	1200

3.6 Discussion

The plot in Figure 3.5 was built through the global analysis of 136 monomer and 136 excimer fluorescence decays. The monomer and excimer decays were fitted according to Equations 3.10 and 3.11, respectively, which were derived according to the model depicted in Scheme 3.1. Although not discussed in the text, two models other than the one depicted in Scheme 3.1 were also tried. First, it was assumed that Py_{k2}^{*} was formed not by diffusion but by direct excitation only, and that diffusive encounters between pyrene monomers would yield the excimer *E0**. Analysis of the 136 monomer and excimer decays yielded trends where the molar fraction of the pyrene monomers in the solution,

f_M, would vary greatly with wavelength, much more than the f_M trend shown in Figure 3.4. Since a molar fraction is wavelength independent, this model was rejected. The second model that was explored assumed that both *E0** and *EL** were generated sequentially, first by forming the species Py^*_{k2} by the diffusive encounters between two pyrene monomers followed by a rapid rearrangement with a rate constant k_2 to yield either *E0** or *EL**. In this case, analysis of the 136 fluorescence decays yielded molar fractions f_M that remained constant with wavelength, but the spread in the $\varepsilon_{E0}(\lambda)$ values was larger than in Figure 3.5, particularly so at the higher wavelengths close to 350 nm. Consequently, this model was disregarded in favor of the one depicted in Scheme 3.1.

Table 3.6: Fractions of the various pyrene species present in the six PyPDMA solutions studied.

Pyrene Content μmol/g	OD	[PyPDMA] g/L	f_{diff}	f_{free}	f_{k2}	f_{E0}	f_{EL}
645	1	0.09	0.07 ± 0.01	0.00 ± 0.00	0.05 ± 0.01	0.53 ± 0.08	0.34 ± 0.07
	30	2.2	0.06 ± 0.01	0.00 ± 0.00	0.06 ± 0.02	0.53 ± 0.06	0.34 ± 0.04
479	0.1	0.01	0.18 ± 0.03	0.02 ± 0.00	0.11 ± 0.02	0.32 ± 0.08	0.36 ± 0.07
	0.7	0.08	0.18 ± 0.02	0.02 ± 0.00	0.13 ± 0.03	0.43 ± 0.06	0.24 ± 0.05
	15	1.8	0.17 ± 0.02	0.01 ± 0.00	0.12 ± 0.03	0.41 ± 0.06	0.28 ± 0.06
263	30	4.8	0.25 ± 0.02	0.06 ± 0.01	0.12 ± 0.02	0.40 ± 0.06	0.17 ± 0.04

Although Py_{k2} behaves spectroscopically as a monomer, this species represents pyrenes which are associated, and as such, must be included in the calculation of $f_{agg} = f_{k2} + f_{E0} + f_{EL}$. It is unfortunate that f_{agg} is not equal to $f_E = 1 - f_M = f_{E0} + f_{EL}$. Whereas f_E can be obtained from a simple absorption measurement, f_{k2} can only be obtained through the acquisition of a monomer and excimer fluorescence decay followed by their global analysis with Equations 3.10 and 3.11, respectively. It is important to point out that according to the present study, absolute f_{agg} values can only be obtained via a combination of absorption and time-resolved fluorescence measurements following the procedure outlined in the Theory section.

Since the molar fractions of the individual pyrene species present in solution could be determined, the molar fraction of the aggregated pyrenes, $f_{agg} = f_{k2} + f_{E0} + f_{EL}$, was plotted as a function of the P_A value in Figure 3.6. As the P_A value increases, the absorption spectrum exhibits sharper features indicating stronger contribution from the pyrene monomer. Consequently, f_{agg} decreases with increasing P_A value.

All time-resolved fluorescence experiments conducted in this study used an excitation bandwidth of 1 nm which reduced the signal strongly, as can be seen from the noise level in Figure SI.3.1. In the laboratory, fluorescence lifetime experiments are usually conducted with broader excitation bandwidth to enhance the fluorescence signal. The monomer and excimer fluorescence decays of PyPDMA263 with a concentration of 4.8 g/L were acquired as a function of the excitation bandwidth with the excitation wavelength fixed at 340 nm. For each excitation bandwidth, the monomer and excimer decays were fitted globally and the fraction f_M^f was determined. f_M^f and 1 – f_M^f are plotted as a function of excitation bandwidth in Figure 3.7. Within experimental error, f_M^f and 1 – f_M^f remain constant with excitation bandwidth indicating that these fractions do not seem to be strongly affected by the width of the excitation slits, when the excitation wavelength is fixed at 340

nm. The trends shown in Figure 3.7 confirm that within experimental error, widening the slits to increase the fluorescence signal does not affect the values of the fractions shown in Equations 3.12 – 3.16 and obtained through the global analysis of the monomer and excimer decays with Equations 3.10 and 3.11, and in turn does not affect the values of the molar fractions of the pyrene species present in solution. This is an important piece of information from an experimentalist point of view, since the acquisition of fluorescence decays with 1 nm excitation slit width cuts down the fluorescence signal substantially and would make it rather inconvenient to obtain f_{agg} on a routine basis.

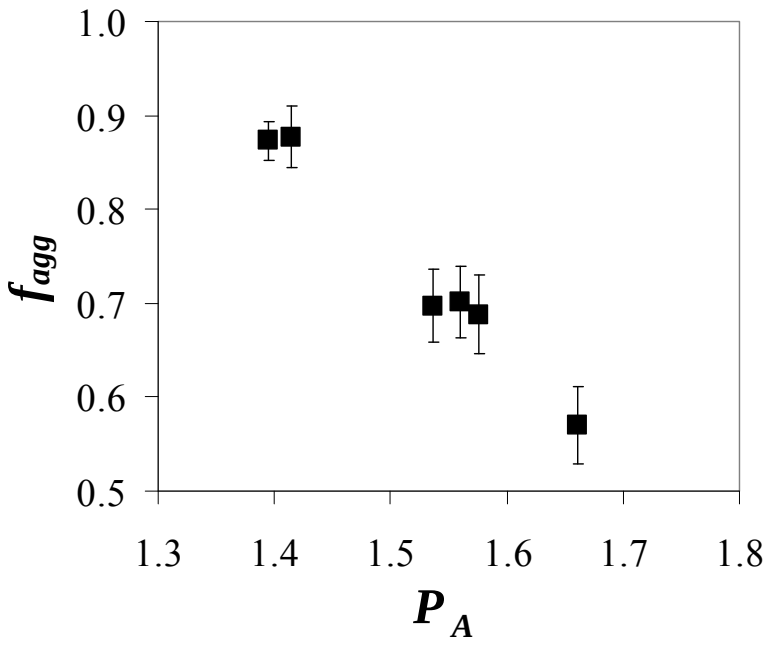

Figure 3.6: Plot of f_{agg} versus P_A value.

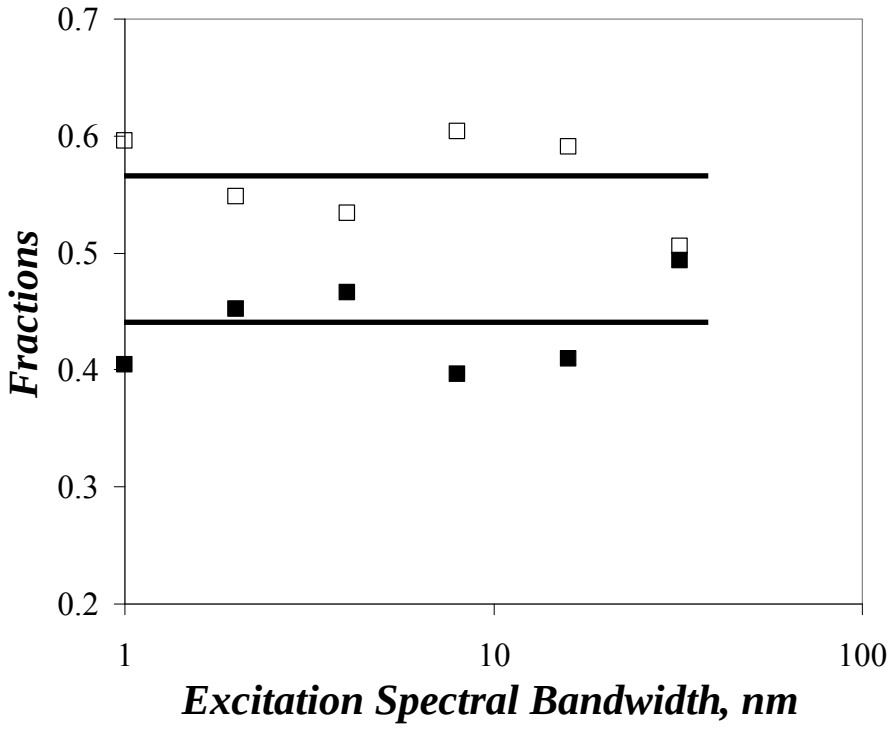

Figure 3.7: Plot of f_M^f (■) and 1 – f_M^f (□), as a function of excitation slit width for a solution of 4.8 g/L of PyPDMA263 in water.

The FBM yields the average number of ground-state pyrene species present inside a *blob* given by <*n*> in Table 3.3. The ground-state pyrene species in solution are the isolated and aggregated pyrenes whose concentration is given by [Py_{diff}] and [Py_{agg}]/N_{agg}, respectively, where N_{agg} represents the average number of pyrenes constituting a pyrene aggregate. The overlap of the molar absorption coefficients obtained for the six polymer solutions in Figure 3.5 suggests that the nature of the ground-state pyrene aggregates is not affected by the pyrene content or polymer concentration. As a result, N_{agg} can be assumed to remain constant for the three PyPDMA samples. Based on the above, Equation 3.20 can be derived.

$$< n >= \frac{[Py_{diff}] + [Py_{agg}] / N_{agg}}{[blob]} \qquad (3.20)$$

By definition, a *blob* is the volume probed by an excited pyrene during its lifetime, V_{blob}. Since pyrene is being attached to the same PDMA backbone for all PyPDMA samples, V_{blob} is expected to be the same for all polymer samples. Thus [*blob*] must be proportional to the polymer concentration according to a proportionality factor *c* such that [*blob*] = *c*×[*Poly*]. Based on the above, Equation 3.20 can be rewritten into Equation 3.21.

$$\frac{< n > \times [Poly]}{[Py_{diff}]} = \frac{1}{c} + \frac{1}{c \times N_{agg}} \frac{[Py_{agg}]}{[Py_{diff}]} \qquad (3.21)$$

Following Equation 3.21, the quantity <*n*>×[*Poly*]/[Py_{diff}] was plotted as a function of [Py_{agg}]/[Py_{diff}] in Figure 3.8 with [Py_{agg}] = [Py_{k2}] + [*E0*] + [*EL*]. A straight line was obtained and the ratio of the intercept by the slope yielded an N_{agg} value equal to 3.1 ± 1.6.

The N_{agg} value of 3.1 is small when compared to the N_{agg} value of 20 ± 2 found for the polymeric aggregates generated by poly(ethylene oxide) chains terminated at one end with a pyrene moiety (Py-PEO).[30] However these results are consistent with the notion that hydrophobic aggregates generated by hydrophobes attached onto a polymer are usually smaller, the shorter the linker connecting the hydrophobe to the polymer backbone is.[31] Three atoms separate the pyrene hydrophobe from the PDMA backbone in the PyPDMA samples. This is a rather short linker which results in a small N_{agg} value, in part, due to steric hindrance from the backbone which prevents two pyrene pendants from coming in close contact. In the case of Py-PEO, the pyrene moiety is attached at one end of the chain, resulting in less steric hindrance and a larger N_{agg} value.

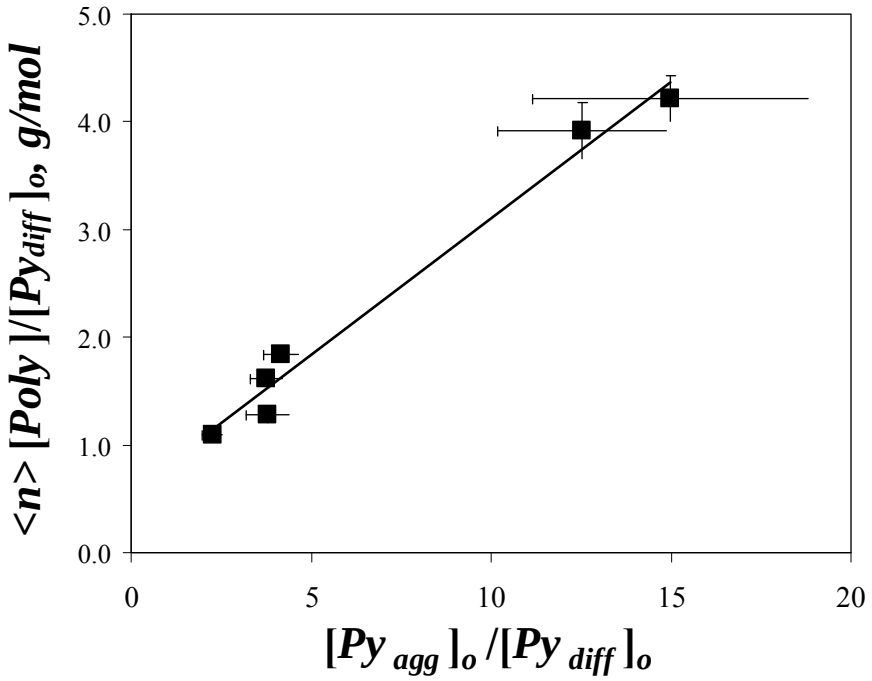

Figure 3.8: Plot of $<n>[Poly]/[Py_{diff}]$ versus $[Py_{agg}]/[Py_{diff}]$ for all Py-PDMA samples.

Relationship with earlier works: The existence of ground-state pyrene dimers (GSPD) like those found for the PyPDMA samples has been demonstrated qualitatively for numerous pyrene-labeled macromolecules by applying the procedures outlined in Winnik's authoritative review[10] such as monitoring a shift in the excitation spectra (Figure 3.1), a broadening of the absorption spectra (Figure 3.2), and the absence of a risetime in the excimer decays (Figure SI.3.1). However much fewer studies have reported the quantitative analysis of the fluorescence data obtained with pyrene-labeled polymers exhibiting GSPD. To date, most of the analytical work dealing with GSPD has been conducted with well-defined pyrene-labeled macromolecules in organic solvents. For instance, numerous studies of pyrene end-labeled oligomethylene chains 2 to 32 methylene units in length have demonstrated that pyrene derivatives substituted in the 1-position induce the formation of two well-defined types of

excimer,[32-37] and depending on the oligomethylene length, GSPD.[35-37] GSPD have also been characterized quantitatively for a short monodispersed (M_n = 10,600 g.mol^{-1}, PDI = 1.09) polystyrene chain labelled at both ends with pyrene via an amide linker.[38] In cyclohexane, hydrogen-bonding through the amide bonds induced the formation of GSPD. GSPD were also described quantitatively during the coil-to-globule collapse of a short monodispersed (M_n = 3,300 g.mol^{-1}, PDI = 1.05) poly(ethylene oxide) chain in toluene.[39] As the temperature was lowered below the θ–temperature of PEO in toluene, the rise-time in the excimer decay disappeared. More recently, the FBM has been applied to analyze the fluorescence decays of poly(*N*,*N*-dimethylacrylamide)[40,41] and polystyrene[42] randomly labeled with pyrene as the polymers underwent a coil-to-globule transition in methanol and cyclohexane, respectively. The increased local pyrene concentration that resulted from the coil-to-globule transition yielded GSPD.

Although quite informative, it is noticeable that all the above studies were conducted in organic solvents where pyrene is soluble to a much larger extent than in water. In organic solvents, the pyrene dimers and excimers are more likely to adopt the conformations predicted by theoretical simulations.[43-45] The situation is quite different in water however where pyrene is usually considered insoluble, its solubility having been reported to equal 0.3 μM[46] and 0.7 μM.[47] In water, the driving force for pyrene association is expected to depend not on the gain in energy obtained by holding two pyrene moieties 0.35 nm apart, but rather on the gain in energy afforded by an aggregate of several pyrenes to minimize the hydrophobic surface of individual pyrenes exposed to the polar water. Furthermore, the pyrene aggregates generated by PyHMWSP such as those formed with PyPDMA in the present study or PyPEO[30] must also accommodate the bulky polymer chain to which pyrene is covalently attached. Consequently, the well defined graphite-type, slipped parallel, or crossed conformations predicted theoretically[44,45] and observed experimentally for some well-characterized

pyrene-labeled macromolecules in organic solvents[32-37] might not be the optimal conformations found for pyrene aggregates in water.

As argued in the Introduction, the complexity of the photophysical processes encountered in aqueous solutions of PyHMWSP has resulted in a rather small number of studies where the fluorescence data obtained with PyHMWSP were analyzed quantitatively. In 1989, Char et al. used an enhanced capture radius to account for the enhanced associative ability displayed by pyrenes attached at the ends of a series of short monodispersed PEOs.[48] Using a water-soluble iodide quencher, Duhamel et al. were able to analyze quantitatively the Stern-Volmer plots of a short PEO chain labelled at both ends with pyrene to yield a measure of the fraction of aggregated pyrenes, $f_{agg}^{f} = f_{k2}^{f} + f_{E0}^{f} + f_{EL}^{f}$ where f_{k2}^{f}, f_{E0}^{f}, and f_{EL}^{f} have been defined in Equations 3.14 – 3.15.[49] This analysis relied on the fact that quenching of an excited pyrene monomer by an iodide ion would affect the fraction of excimer formed diffusionally but not the fraction of those excimers generated from the direct excitation of a pyrene aggregate. Procedures aiming at determining f_{agg}^{f} from the analysis of the pyrene monomer and excimer fluorescence decays acquired with Py–HMWSP were introduced later. These procedures can be classified according to whether they are based on the analysis of the fluorescence decays with sums of exponentials[50-52] or the FBM.[16,19,28,29,53] Sums of exponentials are usually well-suited when the kinetics of excimer formation are simple enough that they result in two exponentials to fit the fluorescence decays. Such decays are also well-handled by the FBM, as well as the more complex decays shown in Figure SI.3.1.

Regardless of whether the analysis of the fluorescence data is based on an enhanced capture radius,[48] differences in quenching mechanism,[49] sum of exponentials,[32-39,50-52] or FBM[16,19,28,29,40-42,53] fitting of fluorescence decays, all these analyses provide only relative information about the level of pyrene association since they have been conducted without knowing the molar absorption coefficient

of a GSPD. Thanks to the knowledge of the molar extinction coefficient of the GSPD generated by PyPDMA solutions, the present study stands out from earlier work[16,19,28,29,40-42,48-53] in that it yields for the first time the absolute f_{agg} values of a series of PyHMWSPs in aqueous solution.

3.7 Conclusions

This study represents the first example in the literature where the absorption coefficient of pyrene aggregates in water has been determined. The pyrene aggregates in water were generated by preparing aqueous solutions of PyPDMA. The hydrophobic pyrene pendants associated in water forming pyrene aggregates, whose presence was evidenced from the shift observed between the monomer and excimer fluorescence excitation spectra (Figure 3.1), the broadening of the absorption spectra (Figure 3.2 and Table 3.2), and although not discussed in this report, a much reduced risetime in the excimer fluorescence decays (see Figure SI.3.1). The absorption coefficient of the pyrene aggregates was determined in a somewhat unorthodox manner by combining results obtained by absorption and time-resolved fluorescence measurements. Taking advantage of the increased power afforded by new LEDs, fluorescence decays could be acquired by exciting the PyPDMA solutions at a given wavelength with a 1 nm bandwidth, enabling the monitoring of fluctuations in the monomer and excimer fluorescence decays due to variations in the absorption coefficients of both species. This effect was exploited by analyzing the monomer and excimer fluorescence decays globally and retrieving the contributions to the fluorescence decays given in Equations 3.12 – 16 due to the pyrene monomer and aggregates. Since these contributions were weighed by the absorption coefficients of the pyrene monomer and aggregates, knowledge of the absorption coefficient of the pyrene monomer enabled the determination of the molar fractions of all pyrene species in solution as well as the absorption coefficient of the pyrene aggregates. By repeating this operation at each wavelength, ε_{E0} could be determined at each wavelength yielding the profiles given in Figure 3.5. Altogether, six PyPDMA samples were prepared with three polymers and at six different concentrations. In most

cases, the fluorescence decays were acquired by changing the excitation wavelength 1 nm at the time over 25 nm from 325 to 350 nm. A total of 136 monomer and excimer decays were acquired and analyzed globally with Equations 3.10 and 3.11. The set of 136 $\varepsilon_{E0}(\lambda)$ values converged on a single master curve regardless of polymer composition or solution concentration, suggesting that this master curve represents the true absorption coefficient of the pyrene aggregates generated by PyPDMA in water.

Chapter 4
Determination of the Level of Association of a Poly(Ethylene Oxide) Singly End-Labelled with Pyrene using a Model Free Global Analysis

4.1 Overview

The monomer and excimer fluorescence decays of a PyPEO polymer in water were fitted to a model free global analysis scheme to determine the fraction of pyrenes that were aggregated in solution f_{agg} and also the molar absorbance coefficient of the pyrene aggregates, ε_{E0}. Prior to being applied to PyPEO, the model free (MF) analysis was first tested by fitting the monomer and excimer decays of pyrene in cyclohexane, *N*,*N*-dimethylformamide, and acetonitrile as well as 1-pyrenemethanol in acetonitrile. The diffusional rate constant of excimer formation $< k_1 >=< \tau^{-1} > -\frac{1}{\tau_M}$ determined for the solutions retrieved from the MF fits of the monomer and excimer decays was found to compare exactly to the k_1 parameter obtained by the Birks scheme. This result led to the conclusion that both analyses yield similar information on the diffusional encounters of molecular pyrene in solution. Thus, the MF analysis was confirmed to describe effectively the kinetics of excimer formation by diffusion. The global analysis using MF analysis to account for the pyrenes forming excimer via diffusion was applied to the monomer and excimer decays of PyPEO solutions to obtain the level of association f_{agg}. In addition to determining f_{agg} values, the molar absorbance coefficient of the PyPEO aggregates ε_{E0} for a range of wavelengths from 325 to 347 nm was also obtained.

4.2 Introduction

Associative polymers (APs) are hydrophobically-modified water-soluble polymers (HMWSPs) consisting of a hydrophilic backbone modified with a small amount of hydrophobic

pendants.[1] Upon solvation in aqueous media, HMWSPs self-assemble as their hydrophobic pendants reorganize themselves to reduce their exposure to water. Depending on the architecture of the HMWSPs, the self-assembled structures may take the form of extended reversible networks. HMWSPs forming extended networks are particularly interesting since such reversible networks can induce a great increase in the overall viscosity of the solution even at modest concentrations (1 – 2 wt%). As such, HMWSPs are used commercially as rheology modifiers to enhance the performance of numerous industrial products, especially in the paints and coatings industry.[2–4]

Several groups have attempted to model the interesting viscoelastic properties of the networks formed by self-associating HMWSPs.[5–14] One particular model assumes that the polymeric network consists of HMWSPs whose hydrophobic pendants or "stickers" hold onto other stickers to create the network.[5,6] Movement of one macromolecule in this network requires the coordinated detachment and reattachment of the stickers, a phenomenon called *sticky reptation*.[6] This model describes the network with four parameters which are the average number of hydrophobic pendants per aggregate N_{agg}, the level of association or fraction of hydrophobic pendants that are aggregated f_{agg}, the ratio of inter- to intra-molecular associations made by the hydrophobes, and finally the residence time of a hydrophobic pendant in an aggregate τ_{res}. Despite its importance, f_{agg} is rarely accounted for or is taken to equal 1.0 in most models implying that all hydrophobes are aggregated.[7,13] Hence little effort has been made to characterize f_{agg} experimentally.

One procedure that yields f_{agg} consists in replacing the hydrophobic pendants of a HMWSP with the hydrophobic chromophore pyrene to yield a pyrene-labelled HMWSP (PyHMWSP). The ability of pyrene to form excimers that fluoresce at a different wavelength from the pyrene monomer has made it an ideal choice to study polymer chain dynamics,[15,16] coil-to-globule transitions,[16,17] and the level of association (f_{agg}).[15,16,18,19] Lifetime decay measurements of the monomer and excimer of PyHMWSPs have been used to yield the fractions of aggregated and unaggregated pyrenes weighed

by the molar absorbance coefficient and radiative rate constant of the respective pyrene species. PyHMWSPs which were studied in such a manner include pyrene-labelled hydrophobically-modified alkali-swellable emulsion copolymer (PyHASE)[20,21] and poly(*N*,*N*-dimethylacrylamide) (PyPDMA).[22] The weighed fraction representing the pyrene aggregates is referred to as f_{agg}^{f} where the superscript "*f*" indicates that f_{agg}^{f} is determined from the analysis of the fluorescence decays. f_{agg}^{f} depends also on the efficiency of a pyrene aggregate to absorb an excitation photon and emit an emission photon. In other words, f_{agg}^{f} depends not only on f_{agg}, but also on the molar absorbance coefficient of the pyrene aggregates ε_{E0} and their radiative rate constant k_{rad}^{E0}. Unfortunately, values for ε_{E0} and k_{rad}^{E0} are not widely available in the scientific literature. A recent breakthrough in the analysis of the pyrene monomer and excimer fluorescence decays has enabled the quantitative determination of f_{agg} of PyPDMA solutions by relating f_{agg}^{f} obtained by time-resolved fluorescence measurements to the concentrations of the pyrene species in solution, their extinction coefficients, and the solution absorbance.[23]

The purpose of this study is to adapt the general procedure used for the determination of f_{agg} for PyPDMA to short α-telechelic pyrene-labelled poly(ethylene oxide) chains (PyPEO). Hydrophobically end-capped poly(ethylene oxide) chains are key components of the hydrophobic pendants of two commercial HMWSPs, namely the hydrophobically-modified ethoxylated urethane (HEUR) and HASE polymers.[2,3] Thus, establishing a robust procedure that enables the experimental determination of the level of association of PyPEO may provide useful insight into the aggregation of pyrene-labelled analogues of the HASE and HEUR polymers. However, the determination of f_{agg} for PyPEO in water requires first being able to handle mathematically the kinetics describing the diffusive encounters between PyPEO chains. As it turns out, this is not a straightforward task even in organic solvents such as acetonitrile that dissolve and yield homogeneous PyPEO solutions. Indeed, it has

been observed that excimer formation of polystyrene chains labelled at one end with pyrene in toluene deviates from the Birks' scheme traditionally used to model such kinetics, with the rate constant of diffusional excimer formation becoming time-dependent.[24] Based on these earlier studies, the Birks' scheme is not expected to describe the kinetics of diffusional excimer formation for PyPEO solutions. The fluorescence blob model (FBM) used to determine f_{agg} for solutions of PyPDMA assumes that random labelling of the polymer chain generates pyrene-rich and pyrene-poor regions inside the polymer coil. The pyrenes distribute themselves among these regions according to a Poisson distribution. Obviously PyPEO with its unique pyrene covalently attached at the end of a PEO chain is not randomly labelled with pyrene and hence the FBM does not apply. This study investigates the possibility of using a "model free" approach to describe the kinetics of excimer formation by diffusion for PyPEO solutions in water and organic solvents. The results presented herein suggest that the model free approach combines the ability to handle quantitatively the complex kinetics of excimer formation together with the possibility of retrieving f_{agg}.

4.3 Theory

Within the time span during which a pyrene remains excited, the excited pyrene pendants of a HMWSP in solution can be classified into three general populations, depending on whether they behave as isolated pyrenes which do not interact with other pyrenes, Py^*_{free}, pyrenes that interact with other pyrenes via diffusional encounters, Py^*_{diff}, and preassociated pyrenes, Py^*_{agg}.[16,21] The Py^*_{free} species contributes solely to the monomer fluorescence and fluoresces with the natural lifetime of pyrene, τ_M. Py^*_{agg} can be divided further into three subgroups, depending on whether they form long-lived excited pyrene dimers *EL** with a lifetime τ_{EL} greater than 70 ns, short-lived excited pyrene dimers *ES** with a lifetime $\tau_{ES} \approx 3.5$ ns,[25–27] and well-stacked pyrene dimers *E0** that are also formed

by the diffusional encounters of an excited pyrene with a ground-state (GS) pyrene, which emit with a lifetime τ_{E0} in the 40 – 70 ns range. While *E0** is present in any system that forms excimer, the presence of *EL** and *ES** depends on the type of pyrene-labelled polymer studied. Py^{*}_{diff} forms the excimer population *E0** after the diffusional encounter of Py^{*}_{diff} with a GS pyrene species. The rate of encounter depends on the distribution of the GS pyrene species in solution.

For molecular pyrene dissolved in organic solvents, the pyrenes are homogeneously distributed throughout the solution and the rate of diffusional encounter can be characterized by a single rate constant. The scheme developed by Birks has been very effective at characterizing quantitatively the kinetics of excimer formation depicted in Scheme 4.1 for molecularly dissolved pyrene, as well as for monodispersed pyrene-labelled telechelic polymers.[28–32] For polymers randomly-labelled with pyrene, a distribution of rate constants is required to describe the diffusional encounters between pyrenes which greatly complicates the quantitative analysis of the fluorescence decays acquired with these polymers.[33–35] More recently, a fluorescence blob model (FBM), where a blob is defined as the volume probed by an excited fluorophore, has been successfully applied to describe the process of excimer formation of several polymers randomly labelled with pyrene with a set of three parameters. The mathematical basis for the Birks' scheme, FBM, and model free analyses will now be discussed in detail.

$$Py + Py + h\nu \longrightarrow \underset{\downarrow \frac{1}{\tau_M}}{Py^{*}} + Py \underset{k_{-1}}{\overset{k_1[Py]}{\rightleftharpoons}} \underset{\downarrow \frac{1}{\tau_{E0}}}{E0^{*}}$$

Scheme 4.1: The Birks' scheme

4.3.1 Birks Scheme[31,32]

Excimer formation between molecularly dissolved aromatic molecules in solution is described in Scheme 4.1 which was introduced by J.B. Birks[32] and is referred to as the Birks' scheme. According to the Birks' scheme, an excited pyrene monomer having a lifetime τ_M forms excimers via diffusional encounters with a GS pyrene with a rate constant k_1. Pyrene excimers can either fluoresce with a lifetime τ_{E0} or dissociate back into an excited pyrene monomer and a GS pyrene with a rate constant k_{-1}. Since the quenching of the pyrene monomer by other pyrenes is linked to the formation of pyrene excimers and excimer dissociation leads directly to the formation of monomers, the kinetics describing the behaviour of the monomer and excimer are coupled. The mathematical expressions describing the time-dependent concentration of the excited pyrene monomer and excimer are given in Equations 4.1 and 4.2.

$$[Py^*_{diff}] = \frac{[Py^*_{diff}]_{(t=0)}}{\tau_2^{-1} - \tau_1^{-1}}\left(\left(\tau_2^{-1} - X\right)\exp\left(-\frac{t}{\tau_1}\right) + \left(X - \tau_1^{-1}\right)\exp\left(-\frac{t}{\tau_2}\right)\right) \tag{4.1}$$

$$[E0^*] = \frac{k_1[Py][Py^*_{diff}]_{(t=0)}}{\tau_2^{-1} - \tau_1^{-1}}\left(\exp\left(-\frac{t}{\tau_1}\right) - \exp\left(-\frac{t}{\tau_2}\right)\right) \tag{4.2}$$

The observed decay times τ_1 and τ_2 are defined as

$$\tau_{1,2}^{-1} = \frac{1}{2}\left(X + Y \mp \left\{(Y - X)^2 + 4k_{-1}k_1[Py]\right\}^{1/2}\right) \tag{4.3}$$

where the parameters X and Y are defined in Equations 4.4 and 4.5, respectively.

$$X = \frac{1}{\tau_M} + k_1[Py] \tag{4.4}$$

$$Y = \frac{1}{\tau_{E0}} + k_{-1} \tag{4.5}$$

The Birks' scheme is applicable when excimer formation can be described by a single time-independent rate constant. Excimer formation by molecularly dissolved pyrene[31] and α,ω-pyrene labelled telechelic polymers[28] in organic solvents are examples where the kinetics of excimer formation are well described by the Birks' scheme.

4.3.2 Fluorescence Blob Model (FBM)[16,36]

The fluorescence blob model (FBM) described in Scheme 4.2 has been derived to handle conditions where the excimer formation results from by a distribution of rate constants. This model assumes that an excited pyrene monomer can probe a finite volume within its lifetime, τ_M. Thus, the coil of a polymer randomly labelled with pyrene can be divided into blobs where the pyrenes distribute themselves according to a Poisson distribution with an average number of pyrene per blob, $<n>$. An excited pyrene monomer can be diffusionally quenched by a GS pyrene within the blob with a rate constant k_{blob} and GS pyrenes can be exchanged between blobs with a rate constant $k_{ex}[blob]$. The FBM applied to a pyrene-labelled polymer is shown in Figure 4.1. Diffusional encounters between excited and ground-state pyrenes result in the formation of the *E0** excimer species which fluoresces with a lifetime τ_{E0}.

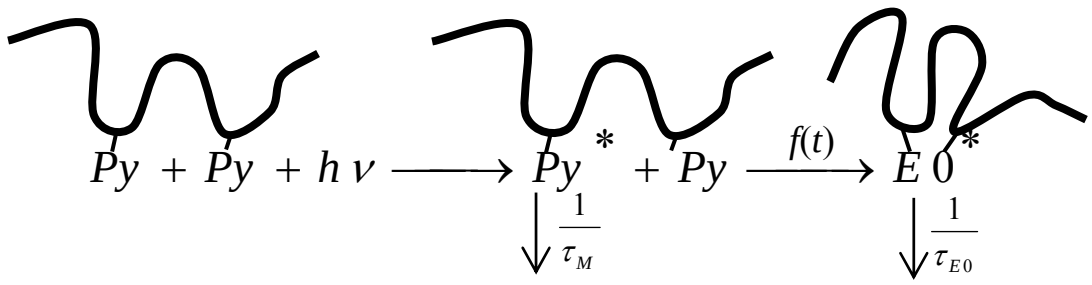

Scheme 4.2: The fluorescence blob model (FBM)

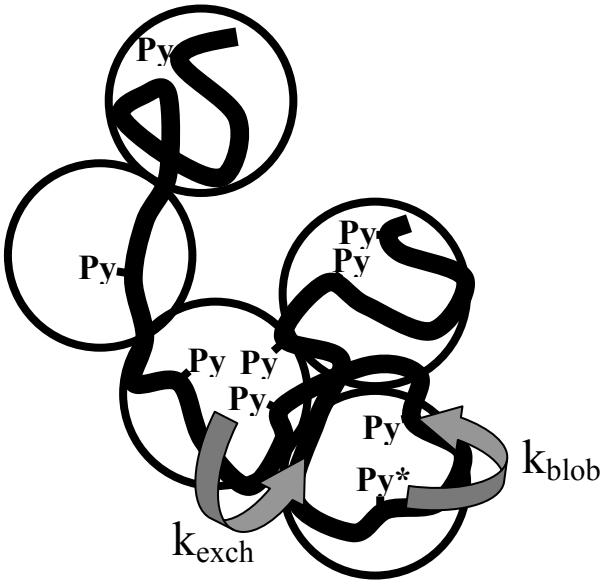

Figure 4.1**:** The fluorescence blob model applied to describe the excimer formation kinetics for a polymer randomly labelled with pyrene.

There are two major differences between the FBM and the Birks' scheme. The first one is that excimer dissociation is assumed to be minimal when dealing with the FBM so that $k_{-1} \approx 0$. This

assumption is appropriate for pyrene solutions at temperatures below 45 °C.[37] The second difference is that excimer is formed by a distribution of rate constants resulting in a time-dependent rate constant for excimer formation given by $f(t)$ in Scheme 4.2. The kinetics of excimer formation depicted in Scheme 4.2 can be described by the differential Equations 4.6 and 4.7.

$$\frac{d[Py^*_{diff}]}{dt} = \frac{1}{\tau_M}[Py^*_{diff}] - f(t) \tag{4.6}$$

$$\frac{d[E0^*]}{dt} = \frac{1}{\tau_{E0}}[E0^*] + f(t) \tag{4.7}$$

Since $[Py^*_{diff}]_{(t)}$ is known mathematically and is given in Equation 4.8, $f(t)$ can be determined from Equation 4.6 and used to integrate Equation 4.7 resulting in the expression of $[E0^*]_{(t)}$ given in Equation 4.9.

$$[Py^*_{diff}]_{(t)} = [Py^*_{diff}]_{(t=0)} \exp\left[-\left(A_2 + \frac{1}{\tau_M} \right) t - A_3 \left(1 - \exp\left(-A_4 t \right) \right) \right] \tag{4.8}$$

$$[E0^*]_{(t)} = -[Py^*_{diff}]_{(t=0)} e^{-A_3} \sum_{i=0}^{\infty} \frac{A_3{}^i}{i!} \frac{A_2 + i A_4}{\frac{1}{\tau_M} - \frac{1}{\tau_{E0}} + A_2 + i A_4} \exp\left(-\left(\frac{1}{\tau_M} + A_2 + i A_4 \right) t \right)$$

$$+ [Py^*_{diff}]_{(t=0)} e^{-A_3} \sum_{i=0}^{\infty} \frac{A_3{}^i}{i!} \frac{A_2 + i A_4}{\frac{1}{\tau_M} - \frac{1}{\tau_{E0}} + A_2 + i A_4} e^{-t/\tau_{E0}} \tag{4.9}$$

The parameters A_2, A_3, and A_4 depend on the rate constants k_{blob} and $k_{ex}[blob]$, as well as $<n>$.

$$A_2 = < n > \frac{k_{blob} k_{ex}[blob]}{k_{blob} + k_{ex}[blob]} \qquad A_3 = < n > \frac{k_{blob}^2}{\left(k_{blob} + k_{ex}[blob]\right)^2}$$

$$A_4 = k_{blob} + k_{ex}[blob] \tag{4.10}$$

4.3.3 Model Free Analysis[38]

Contrary to the derivation done in the FBM section, the model-free (MF) analysis takes a phenomenological approach by making no assumptions about the process of excimer formation so that $f(t)$ in Scheme 4.2 is not defined by set parameters. The MF analysis acknowledges that the monomer decay can always be fitted by a sum of exponentials as shown in Equation 4.11. Equation 4.11 can be used to find an expression for $f(t)$ in Scheme 4.2 which is then applied to investigate the differential Equation 4.7 yielding Equation 4.12 representing the time-dependent profile of the excimer decay.

$$[Py^*_{diff}]_{(t)} = [Py^*_{diff}]_{(t=0)} \sum_{i=1}^{n} a_i \exp\left(-\frac{t}{\tau_i}\right) \tag{4.11}$$

$$\begin{aligned}[E0^*]_{(t)} = &-[Py^*_{diff}]_{(t=0)} \sum_{i=1}^{n} a_i \frac{\frac{1}{\tau_i} - \frac{1}{\tau_M}}{\frac{1}{\tau_i} - \frac{1}{\tau_{E0}}} \exp\left(-\frac{t}{\tau_i}\right) \\ &+[Py^*_{diff}]_{(t=0)} \sum_{i=1}^{n} a_i \frac{\frac{1}{\tau_i} - \frac{1}{\tau_M}}{\frac{1}{\tau_i} - \frac{1}{\tau_{E0}}} \exp\left(-\frac{t}{\tau_{E0}}\right)\end{aligned} \tag{4.12}$$

The pre-exponential factors a_i are such that $\sum_{i=1}^{n} a_i$ equals unity. It is important to note that the same decay times τ_i are found in the expressions describing the monomer and excimer fluorescence decays. The parameters a_i and τ_i can be used to calculate the average rate constant of excimer formation $\langle k_1 \rangle$ using Equation 4.13 or 4.14. Equations 4.13 and 4.14 use either the number-average decay rate, $\langle \tau^{-1} \rangle$,[39] or the number-average decay time, $\langle \tau \rangle$,[33] respectively.

$$\langle k_1 \rangle = \sum_{i=1}^{n} a_i \frac{1}{\tau_i} - \frac{1}{\tau_M} = \langle \tau^{-1} \rangle - \frac{1}{\tau_M} \tag{4.13}$$

$$\langle k_1 \rangle = \frac{1}{\sum_{i=1}^{n} a_i \tau_1} - \frac{1}{\tau_M} = \frac{1}{\langle \tau \rangle} - \frac{1}{\tau_M} \tag{4.14}$$

$\langle k_1 \rangle$ is a pseudounimolecular rate constant that includes the local pyrene concentration $[Py]_{loc}$. For homogeneous solutions, $[Py]_{loc} = [Py]$.

4.3.4 Free Pyrene Monomer

The pyrene pendants of polymers randomly labelled with pyrene in organic solvents distribute themselves in an inhomogeneous manner, creating pyrene-rich and pyrene-poor domains within the polymer coil. This partitioning of the pyrenes leads to the isolation of some of the pyrene pendants which are incapable of diffusionally encountering other pyrenes within the lifetime of an excited pyrene. These pyrenes are represented as the species Py^*_{free} whose contribution to the monomer is given in Equation 4.15

$$[M^*]_{(t)} = [Py^*_{diff}]_{(t)} + [Py^*_{free}]_{(t=0)} \exp\left(-\frac{t}{\tau_M}\right) \tag{4.15}$$

where the expression for $[Py^*_{diff}]_{(t)}$ is described by Equations 4.1, 4.8, or 4.11 for the Birks' scheme, FBM, or MF analysis, respectively.

4.3.5 Ground-State Aggregation

The overwhelming majority of reports investigating pyrene excimer formation in organic solvents find that excimer formation is the result of a diffusive encounter between an excited pyrene and a GS pyrene. This process results in Equations 4.2, 4.9, and 4.12 for the excimer decays described by the Birks' scheme, FBM, and MF analyses, respectively. However, pyrene excimer formation is also often applied to probe restricted spaces at the molecular level where the pyrenes aggregate. In this case, direct excitation of pre-formed ground-state pyrene aggregates needs to be accounted for by Equations 4.2, 4.9, and 4.12. Excited pyrene aggregates have been found to fluoresce either as pyrene excimers *E0**, shorter-lived excimer *ES** with a lifetime τ_{ES}, or longer-lived excimer *EL** with a lifetime τ_{EL}. Assuming a potential contribution to the fluorescence excimer decay from pyrene species *ES**, *E0**, and *EL** the equations describing the excimer populations becomes Equation 4.16

$$\begin{aligned}[E^*]_{(t)} &= [E0^*]_{(t)} + [E0^*]_{(t=0)} \exp\left(-\frac{t}{\tau_{E0}}\right) \\ &+ [ES^*]_{(t=0)} \exp\left(-\frac{t}{\tau_{ES}}\right) + [EL^*]_{(t=0)} \exp\left(-\frac{t}{\tau_{EL}}\right)\end{aligned} \tag{4.16}$$

4.3.6 Brief Summary of the Models

The Birks' scheme has been effective in characterizing the kinetics of excimer formation by diffusion for homogeneous solutions of small aromatic molecules[31,40] and monodispersed polymers labelled at both ends.[28–30] On the other hand, the fluorescence blob model (FBM) has been effective in characterizing the kinetics of diffusional excimer formation for randomly labelled polymers. Finally, the model free analysis has been shown to handle the kinetics of excimer formation for polymers randomly labelled with pyrene by taking a phenomenological approach that does not make any specific assumptions on the process of excimer formation.[38]

4.3.7 Determination of Pyrene Fractions

The pyrene pendants of a pyrene labelled polymer in solution can be present as one of the five following species: ES, $E0$, EL, Py_{diff}, and Py_{free}. The contributions of the pyrene species found from the analysis of the monomer and excimer fluorescence decays, also referred to as the fluorescence fractions,[21] are related to the concentrations of the pyrene species and their associated molar absorbance coefficients as described in Equations 4.17 – 4.21.

$$f_{diff}^{f} = \frac{\varepsilon_M [Py_{diff}^{*}]_{(t=0)}}{\varepsilon_M [Py_{diff}^{*}]_{(t=0)} + \varepsilon_M [Py_{free}^{*}]_{(t=0)} + \varepsilon_{E0} [E0^{*}]_{(t=0)} + \varepsilon_{ES} [ES^{*}]_{(t=0)} + \varepsilon_{ES} [EL^{*}]_{(t=0)}} \quad (4.17)$$

$$f_{free}^{f} = \frac{\varepsilon_M [Py_{free}^{*}]_{(t=0)}}{\varepsilon_M [Py_{diff}^{*}]_{(t=0)} + \varepsilon_M [Py_{free}^{*}]_{(t=0)} + \varepsilon_{E0} [E0^{*}]_{(t=0)} + \varepsilon_{ES} [ES^{*}]_{(t=0)} + \varepsilon_{ES} [EL^{*}]_{(t=0)}} \quad (4.18)$$

$$f_{E0}^{f} = \frac{\varepsilon_{E0} [E0^{*}]_{(t=0)}}{\varepsilon_M [Py_{diff}^{*}]_{(t=0)} + \varepsilon_M [Py_{free}^{*}]_{(t=0)} + \varepsilon_{E0} [E0^{*}]_{(t=0)} + \varepsilon_{ES} [ES^{*}]_{(t=0)} + \varepsilon_{ES} [EL^{*}]_{(t=0)}} \quad (4.19)$$

$$f_{ES}^{f} = \frac{\varepsilon_{ES} [ES^{*}]_{(t=0)}}{\varepsilon_M [Py_{diff}^{*}]_{(t=0)} + \varepsilon_M [Py_{free}^{*}]_{(t=0)} + \varepsilon_{E0} [E0^{*}]_{(t=0)} + \varepsilon_{ES} [ES^{*}]_{(t=0)} + \varepsilon_{ES} [EL^{*}]_{(t=0)}} \quad (4.20)$$

$$f_{EL}^{f} = \frac{\varepsilon_{EL}[EL^{*}]_{(t=0)}}{\varepsilon_{M}[Py_{diff}^{*}]_{(t=0)} + \varepsilon_{M}[Py_{free}^{*}]_{(t=0)} + \varepsilon_{E0}[E0^{*}]_{(t=0)} + \varepsilon_{ES}[ES^{*}]_{(t=0)} + \varepsilon_{ES}[EL^{*}]_{(t=0)}} \quad (4.21)$$

In Equations 4.17 – 4.21, the molar absorbance coefficient of the three aggregated species ε_{EL}, ε_{ES}, and ε_{E0} are approximated to be equal. Knowing the fluorescence fractions and values of ε_{E0} and ε_{M} enables one to calculate the fractions of the pyrene species in solution given in Equations 4.22 – 4.26.[23]

$$f_{diff} = \frac{[Py_{diff}]_{(t=0)}}{[Py_{diff}]_{(t=0)} + [Py_{free}]_{(t=0)} + [E0]_{(t=0)} + [ES]_{(t=0)} + [EL]_{(t=0)}} \quad (4.22)$$

$$f_{free} = \frac{[Py_{free}]_{(t=0)}}{[Py_{diff}]_{(t=0)} + [Py_{free}]_{(t=0)} + [E0]_{(t=0)} + [ES]_{(t=0)} + [EL]_{(t=0)}} \quad (4.23)$$

$$f_{E0} = \frac{[E0]_{(t=0)}}{[Py_{diff}]_{(t=0)} + [Py_{free}]_{(t=0)} + [E0]_{(t=0)} + [ES]_{(t=0)} + [EL]_{(t=0)}} \quad (4.24)$$

$$f_{ES} = \frac{[ES]_{(t=0)}}{[Py_{diff}]_{(t=0)} + [Py_{free}]_{(t=0)} + [E0]_{(t=0)} + [ES]_{(t=0)} + [EL]_{(t=0)}} \quad (4.25)$$

$$f_{EL} = \frac{[EL]_{(t=0)}}{[Py_{diff}]_{(t=0)} + [Py_{free}]_{(t=0)} + [E0]_{(t=0)} + [ES]_{(t=0)} + [EL]_{(t=0)}} \quad (4.26)$$

The fraction of pyrenes that are aggregated in solution, f_{agg}, is equal to the sum of all fractions representing aggregated pyrenes, namely $f_{E0} + f_{ES} + f_{EL}$.

4.4 Experimental

Materials: The organic solvents hexanes (HPLC, Caledon), cyclohexane (distilled, EM Science), N,N-dimethylformamide (distilled in glass, Caledon), tetrahydrofuran (distilled in glass, Caledon), diethyl ether (GR ACS, EMD), methanol (HPLC, Caledon), and acetonitrile-190 (HPLC, Caledon) were used as received. All aqueous solutions were prepared with Milli-Q water with a resistivity of over 18 MΩ•cm. Pyrene (98%, Aldrich) and 1-pyrenemethanol (98%, Aldrich) used in this study were both purified by three recrystallizations in methanol.

Poly(ethylene oxide) labelled at one end by pyrene (PyPEO): PyPEO was synthesized by DOW Chemical (Union Carbide division) following a procedure which has been described elsewhere.[2,3] PyPEO was purified as followed. PyPEO solutions in THF were precipitated three times with hexanes. The PyPEO precipitate was dissolved in water and it was washed three times against diethyl ether. PyPEO was then dissolved in methanol at room temperature and allowed to cool in the refrigerator to 5 ^{o}C. The precipitated PyPEO was filtered and this step was repeated five times. The molecular weight of PyPEO was determined to be 2500 g/mol by UV-Vis absorption end-group analysis using the molar absorbance coefficient of 1-pyrenemethanol in tetrahydrofuran (ε = 42,700 $M^{-1}cm^{-1}$). The polydispersity index of PyPEO was determined to be 1.3 by gel permeation chromatography using a DRI detector.

UV-Vis Measurements: A Beckman DU640 spectrophotometer was used for all absorbance measurements. All absorbance spectra were obtained with a spectral bandwidth resolution of 1 nm. To ensure linearity in the response of the spectrophotometer, cells with path lengths of 10, 1, and 0.1 mm were used to keep the absorbance signals between 0.05 and 2. The molar absorption coefficient of the unassociated PyPEO in water was obtained by using a 2.5 μM solution of PyPEO in water sufficiently dilute to ensure that the little contribution to the absorbance by pyrene aggregates was negligible.

Steady-State Fluorescence Measurements: Steady-state fluorescence spectra of pyrene were obtained using a Photon Technology International LS-100 steady-state fluorometer having a continuous Ushio UXL-75Xe xenon arc lamp and a PTI 814 photomultiplier detection system. The emission spectra were acquired by exciting the samples at 338 nm for pyrene solutions or 344 nm for 1-pyrenemethanol or PyPEO solutions. At pyrene concentrations above 50 μM, the spectra were acquired using the front-face geometry. The spectra acquired for concentrations of pyrene equal to or lower than 50 μM used a right-angle geometry. All pyrene and pyrene derivative solutions in organic solvents were bubbled under a gentle flow of N_2 gas for 40 minutes to remove molecularly dissolved oxygen. All aqueous solutions were left aerated.

Time-Resolved Fluorescence Measurements: Fluorescence decays were acquired with an IBH Ltd. time-resolved fluorometer equipped with an IBH 340 nm NanoLED. All solutions were excited at 344 nm. The emission wavelength was set at 375 and 510 nm for the pyrene monomer and excimer decays, respectively. To reduce the noise stemming from stray scattered light, cutoff filters of 370 and 495 nm were used to acquire the monomer and excimer decays, respectively. Samples in organic solvents were degassed under a gentle flow of high purity nitrogen having a maximum impurity content of 4.8 ppm for 40 minutes to remove molecularly dissolved oxygen. All aqueous samples were left aerated. All decays were collected over 1,024 channels with a minimum of 10,000 counts taken at the maximum of the monomer and excimer decays, respectively, to ensure a high signal–to–noise ratio. A light scattering suspension was used to obtain the profile of the lamp response. All measured decays were deconvoluted from the lamp profile and fitted to the desired function using a least–square analysis.[41] The resulting fits were characterized as "good" when the χ^2 parameter was smaller than 1.3 and the residuals and the autocorrelation function of the residuals were randomly distributed around 0. The monomer natural lifetime τ_M of pyrene or 1-pyrenemethanol in the various organic solvents was determined by fitting the monomer decay of a 2 μM solution to a

monoexponential function and taking the lifetime obtained through the fit as the value for τ_M. The parameters obtained from the fits of the 2 μM solutions are given in Table 4.1. For pyrene, τ_M was determined to be 422, 285, and 322 ns in cyclohexane, DMF, and acetonitrile, respectively. In acetonitrile, τ_M for 1-pyrenemethanol equaled 255 ns. The unquenched monomer lifetime, τ_M, of PyPEO in acetonitrile and water was found to equal 279 and 155 ns, respectively. This was accomplished by fitting the monomer decay of a 2 μM PyPEO aqueous solution to a biexponential function and taking the strongly contributing (95%) long decay time as τ_M. The origin of the short decay time of PyPEO in solution might be a result of residual interactions taking place between pyrene and the PEO backbone.

Table 4.1: Fluorescence lifetimes obtained for solutions of pyrene and pyrene derivatives studied in various solvents.

Fluorophore	Solvent	τ_1 ns	τ_2 ns	a_1	a_2	χ^2
Pyrene	cyclohexane	422		1.00		1.03
	DMF	285		1.00		1.25
	acetonitrile	322		1.00		1.13
1-Pyrenemethanol	acetonitrile	255		1.00		1.09
PyPEO	acetonitrile	279	60	0.96	0.04	1.00
	water	155	51	0.95	0.05	0.94

Analysis of the monomer and excimer fluorescence decays: The majority of equations dealing with the kinetics of pyrene excimer formation take the form of sums of exponentials as is the case for a Birks

scheme analysis (Equations 4.1 and 4.2) or MF analysis (Equations 4.11 and 4.12). Even the FBM Equations 4.8 and 4.9 are in effect sums of exponentials. Rapid comparison of the equations describing the monomer and fluorescence decays in each scenario (Birks scheme, FBM, or MF analysis) illustrates that the decay times describing excimer formation by diffusion are found in both equations, a consequence of the decay of the pyrene monomer being coupled to the formation of the pyrene excimer. The conservation of the decay times found in the equations describing the monomer and excimer fluorescence decays constitutes the cornerstone of any analysis dealing with the kinetics of excimer formation by diffusion.

The first procedure that was used to analyze the monomer and excimer fluorescence decays was performed by fitting the monomer decay and the excimer decay separately to a sum of exponentials and estimating how close the decay times retrieved from the analysis were from each other.[28,31] Of course, this procedure was highly subjective since there is a high level of uncertainty for decay times retrieved from a sum of exponentials when the associated pre-exponential factor is small. Consequently, validation of the models used to fit the decays consisted of estimating whether deviations from the expected behavior were due to uncertainties associated with the analysis procedure. When validation of the model was established, the pre-exponential factors and decay times were used to determine the parameters describing the kinetics of excimer formation, such as the rate constants of formation (k_1) and dissociation (k_{-1}).

Analysis of the monomer and excimer fluorescence decays was greatly improved upon introduction of global analysis whereby the monomer and excimer fluorescence decays were analyzed globally and the decay times common to both monomer and excimer equations were kept the same.[16,20,38] Global analysis eliminated questions about the possible implications of retrieving different decay times between the monomer and excimer decays, since the decay times were set to be the same in the global analysis. Unfortunately, this major improvement did not take into account the

pre-exponential factors which were optimized independently. Analysis of the kinetic parameters associated with excimer formation is based on the value of the pre-exponential factors. Consequently, validation of a given model implies that the kinetic parameters must be compatible with all pre-exponential factors and decay times retrieved from the analysis. This is not always the case. Discussions to determine the reason for the discrepancy are usually centered about the inherent coupling that exists between the decay times and the pre-exponential factors that is in effect severed when the pre-exponential factors are optimized independently during a typical global analysis.

To eliminate any possible discussion revolving about the equivalence existing between the decay times and pre-exponential factors on the one hand and the kinetic parameters on the other hand, all monomer and fluorescence decays presented in this thesis have been analyzed globally by optimizing the kinetic parameters directly instead of the decay times and pre-exponential factors. This represents a major departure from what is typically done and improves the accuracy of the kinetic parameters.

4.5 Results

The study on solutions of pyrene in cyclohexane by Birks was performed at pyrene concentrations $\geq$ 4 mM.[32] The choice of concentrations made by Birks was likely due to the excimer fluorescence which was sufficiently strong to enable the acquisition of the excimer decay within a reasonable time. The global analysis developed in this study improves the accuracy of the parameters retrieved from the decay analysis, thus allowing one to investigate the kinetics of excimer formation at concentrations below 1 mM. In the present study, the kinetics of excimer formation for pyrene derivative concentrations ranging from 2 μM to 10 mM were examined. At pyrene derivative concentrations below 0.2 mM, the excimer fluorescence intensity was negligible compared to the monomer intensity as is shown in Figure SI. 4.1 of Supporting Information. It should therefore be

kept in mind that the results obtained from the global analysis of dilute pyrene solutions (< 0.2 mM) are retrieved from excimer decays acquired from weakly emitting solutions.

The monomer and excimer fluorescence decays were acquired for solutions of pyrene in cyclohexane having concentrations ranging from 2 μM to 10 mM. The unquenched lifetime of pyrene τ_M in cyclohexane was determined to be 422 ns (Table 4.1). The τ_M value of 422 ns differs from that of 450 ns obtained by Birks[31] but is close to the τ_M value of 430 ns obtained by Hara and Ware.[42] Differences in τ_M values might be the result of differences in the solvent purity or degassing techniques. The relatively good agreement found between the τ_M value obtained by Hara and Ware and us (2% difference) suggests that our sample preparation is satisfactory. The decays were analyzed globally according to the Birks' scheme using Equations 4.1 and 4.2 to fit the monomer and excimer decays, respectively, setting $[Py^*_{free}]_{(t=0)}$, $[ES^*]_{(t=0)}$, and $[E0^*]_{(t=0)}$ equal to zero in the analysis. However, the fits using Equations 4.1 and 4.2 yielded increasingly poor fits at pyrene concentrations below 1 mM. According to Equation 4.2, the pre-exponential factors of the excimer decay are equal and opposite if no GS pyrene dimer is present ($[E0^*]_{(t=0)} = 0$). However, when their contributions were set free during analysis, the fits improved but values for τ_{E0} and k_{-1} grew increasingly unreasonable: $k_1[Py]$ became non-linear with monomer concentration, and the values for a_{E1} diverged from a_{E2} as the pyrene concentration decreased, as shown in Table SI.4.1 of Supporting Information. The divergence observed between a_{E1} and a_{E2} suggests the presence of GS pyrene aggregates. Indeed, when the monomer and excimer decays were fitted using Equations 4.1, 4.2, and 4.16, assuming that $[Py^*_{free}]_{(t=0)} = 0$, $[ES^*]_{(t=0)} = 0$ and $[E0^*]_{(t=0)} \neq 0$, a_{E1} could be set equal to $-a_{E2}$ in the analysis. The values obtained from the analysis for τ_{E0} and k_{-1} were reasonable and $k_1[Py]$ increased linearly

with pyrene concentration (see Table SI.4.2a). Thus, for the remainder of this report, all analyses will include the assumption that $[E0^*]_{(t=0)} \neq 0$ and the excimer decays will be fitted with Equation 4.16.

The parameters $k_1[Py]$, k_{-1}, and τ_{E0} retrieved from the fits of the decays to Equations 4.1, 4.2, and 4.16 are given in Table SI.4.2a of Supporting Information. The product $k_1[Py]$ was seen to increase linearly with pyrene concentration with a slope equal to k_1. Within experimental error, k_{-1} and τ_{E0} were found to be independent of the pyrene concentration and hence were averaged over all concentrations. The values determined for k_1, k_{-1}, and τ_{E0} along with the values obtained by Birks for pyrene in cyclohexane are listed in Table 4.2. The study of pyrene in cyclohexane is used as a benchmark since the kinetic parameters given in Table 4.2 can be compared to those obtained by Birks. Within experimental error, the lifetime of the pyrene excimer τ_{E0} (64 ± 9 ns), the rate constant of dissociation of pyrene excimers, k_{-1} ($6 \pm 2 \times 10^6$ s^{-1}), and the diffusional rate constant for excimer formation by diffusion k_1 ($6.6 \pm 0.3 \times 10^9$ $M^{-1}s^{-1}$) agreed very well with the τ_{E0}, k_{-1}, and k_1 values obtained by Birks which were found to equal 65 ns, 6.5×10^6 s^{-1}, and 6.65×10^9 $M^{-1}s^{-1}$, respectively. The excellent agreement found between the set of parameters determined by Birks and this study suggest that our experimental protocol is appropriate and can be applied to study more complex excimer forming systems.

Table 4.2**:** Parameters retrieved from Birks' scheme analysis of pyrene in cyclohexane from current study and previously obtained by Birks.

	τ_M ns	τ_{E0} ns	k_{-1} $\times 10^6$ s^{-1}	k_1 $\times 10^9$ $M^{-1}s^{-1}$
Current Study	422	64 ± 9	6 ± 2	6.6 ± 0.3
J.B. Birks	450	65	6.5	6.65

Although there is excellent agreement between the parameters for pyrene in cyclohexane obtained by this study and that of Birks, it is noticeable that the a_{E0}/a_{E2} ratio increases continuously with decreasing pyrene concentration. At first glance, this trend suggests that more pyrene aggregates are present at low pyrene concentration, which is contrary to expectation. Upon closer examination, the conclusions based on the relative changes of the a_{E0}/a_{E2} ratio are misleading since a_{E0} is directly proportional to $[E0^*]_{(t=0)}$ according to Equation 4.16 whereas a_{E2} is related to $[Py^*_{diff}]_{(t=0)}$ times $k_1[Py]/\left(\tau_2^{-1}-\tau_1^{-1}\right)$ according to Equation 4.2. Accounting for this, the molar fraction of GS aggregate $f^f_{agg}=[E0^*]_{(t=0)}/\left([E0^*]_{(t=0)}+[Py^*_{diff}]_{(t=0)}\right)$ can be determined according to Equation 4.27 and is given in Table SI.4.2. f^f_{agg} is found to be small and decreases continuously with decreasing pyrene concentrations, as expected.

$$f^f_{agg}=\frac{[E0^*]_{(t=0)}}{[E0^*]_{(t=0)}+[Py^*_{diff}]_{(t=0)}}=\frac{\dfrac{a_{E0}}{a_{E2}}}{\dfrac{a_{E0}}{a_{E2}}-\dfrac{\left(\tau_2^{-1}-\tau_1^{-1}\right)}{k_1[Py]}} \qquad (4.27)$$

Excimer formation was also studied for pyrene in *N*,*N*-dimethylformamide (DMF) and acetonitrile as well as for 1-pyrenemethanol in acetonitrile. Each pair of monomer and excimer decays was analyzed globally according to Birks' scheme based on Equations 4.1, 4.2, and 4.16 with the parameters obtained from the fit given in Table SI.4.2. For all solutions of pyrene and 1-pyrenemethanol, $k_1[Py]$ increased linearly with increasing pyrene concentration as shown in Figure 4.2. From the slopes of the linear regressions, values of k_1 were obtained and are listed along with the averaged values of k_{-1} and τ_{E0} for each pair of solvent and pyrene derivative in Table 4.3. The values

of k_1 were determined to be 1.86 ± 0.03, 11.1 ± 0.1, and 10.9 ± 0.1 × 10^9 $M^{-1}s^{-1}$ for solutions of pyrene in DMF, pyrene in acetonitrile, and 1-pyrenemethanol in acetonitrile, respectively.

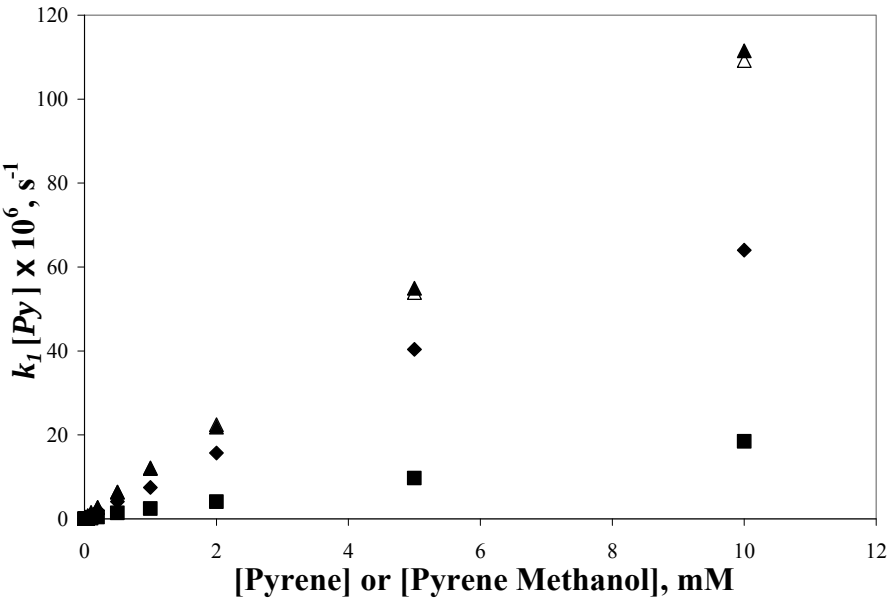

Figure 4.2: Diffusional quenching according to the Birks' scheme for pyrene in cyclohexane (◆), DMF (■), and acetonitrile (▲), and 1-pyrenemethanol in acetonitrile (△).

There appears to be little difference in the rate of excimer formation between pyrene and 1-pyrenemethanol in acetonitrile and DMF.[43] The averaged excimer lifetime τ_{E0} determined for pyrene in DMF and acetonitrile equalled 55 ± 10 and 49 ± 6 ns, respectively. These lifetimes are comparable to the τ_{E0} values obtained by Birks for pyrene in polar organic solvents like ethanol (53 ns) and acetone (43.5 ns). Values of the rate constant for pyrene excimer dissociation k_{-1} were determined to be 7 ± 4 and 8 ± 3 × 10^6 s^{-1} for pyrene in DMF and acetonitrile, respectively. Again, these k_{-1} values are comparable to those found by Birks for pyrene excimer dissociation in ethanol (7 × 10^6 s^{-1}) and

acetone (12×10^6 s^{-1}). Thus, the values for k_{-1} appear to be independent of the solvent type used. The values determined for k_1 do not appear to depend on the inverse of the solvent viscosity, which at first appears counterintuitive since k_1 represents a process that is diffusion controlled. Indeed, k_1 for pyrene in DMF is six times smaller than in acetonitrile although the viscosity of DMF is little over double that of acetonitrile. This discrepancy will be further discussed in the Discussion section.

Table 4.3: Averaged parameters retrieved from Birks' scheme analysis of pyrene in cyclohexane, DMF, and acetonitrile and 1-pyrenemethanol in acetonitrile and DMF (obtained from Ingratta and Duhamel)[41].

Fluorophore	Solvent	τ_{E0} ns	k_{-1} $\times 10^6$ s^{-1}	k_1 $\times 10^9$ $M^{-1}s^{-1}$
Pyrene	cyclohexane	64 ± 9	6 ± 2	6.6 ± 0.3
	DMF	55 ± 10	7 ± 4	1.86 ± 0.03
	acetonitrile	49 ± 6	8 ± 3	11.1 ± 0.1
1-pyrenemethanol	acetonitrile	58 ± 9	3 ± 2	10.9 ± 0.1
	DMF	49 ± 3	2 ± 1	1.96 ± 0.01

In addition to the Birks' scheme, the monomer and excimer fluorescence decays for the solutions of pyrene in cyclohexane, DMF, and acetonitrile and 1-pyrenemethanol in acetonitrile were also fitted according to the model free global analysis based on a sum of exponentials (Equations 4.11, 4.12 and 4.16). The parameters retrieved from these fits are listed in Table SI.4.3. From Table SI.4.3, the lifetime of the aggregated pyrene species τ_{E0} for each solvent/pyrene derivative pair was found to be independent of pyrene concentration. Averaging the τ_{E0} values over all concentrations, τ_{E0} was determined to be 52 ± 7, 45 ± 8, 48 ± 6, and 49 ± 1 ns, for pyrene in cyclohexane, DMF, and acetonitrile and 1-pyrenemethanol in acetonitrile, respectively. These values are listed in Table 4.4.

The τ_{E0} values are within the same range as the values obtained from the analysis of the decays according to the Birks scheme. The average rate constant for excimer formation by diffusion $<k_1>$, calculated using Equation 4.8 or 4.9, was plotted against pyrene concentration in Figures 4.3a and 4.3b, respectively. The slope obtained by linear regression analysis of the data shown in Figure 4.3a yields $<k_1>$ values of 6.6 ± 0.2, 1.89 ± 0.03, 11.3 ± 0.1, and 11.0 ± 0.1 × 10^9 $M^{-1}s^{-1}$, for pyrene in cyclohexane, pyrene in DMF, pyrene in acetonitrile, and 1-pyrenemethanol in acetonitrile, respectively. When compared to the k_1 values retrieved from the Birks' scheme analysis listed in Table 4.3, one can immediately see that the rate constants $<k_1>$ calculated with Equation 4.8 and k_1 are equivalent. Thus, the use of the sum of exponentials based on the global model free analysis of the monomer and excimer decays yield results which are equivalent to those obtained with the well-established Birks' scheme.

Table 4.4**:** Averaged parameters retrieved from model free analysis of pyrene in cyclohexane, DMF, and acetonitrile and 1-pyrenemethanol in acetonitrile.

Fluorophore	Solvent	τ_{E0} ns	$<k_1>$ (Eq. 8) × 10^9 $M^{-1}s^{-1}$	$<k_1>$ (Eq. 9) × 10^9 $M^{-1}s^{-1}$
Pyrene	cyclohexane	52 ± 7	6.6 ± 0.2	5.3 ± 0.1
	DMF	45 ± 8	1.89 ± 0.03	1.48 ± 0.00
	acetonitrile	48 ± 6	11.3 ± 0.1	8.2 ± 0.0
1-Pyrenemethanol	acetonitrile	49 ± 1	11.0 ± 0.1	10.5 ± 0.1

As mentioned in the Theory section, Equations 4.8 or 4.9 represent two expressions of $<k_1>$ which are found in the literature.[33,39] The difference between the two expressions is that Equations 4.8 and 4.9 are based on the averaged rate constants of excimer formation $\left(<\tau^{-1}> - \frac{1}{\tau_M}\right)$ and the

average lifetime of the monomer $\left(\frac{1}{<\tau>}-\frac{1}{\tau_M}\right)$, respectively. In Figure 4.3b, $<k_1>$ has been calculated according to Equation 4.9 and plotted as a function of pyrene concentration. While $<k_1>$ increases linearly with increasing pyrene concentration in Figure 4.3b, the $<k_1>$ values obtained using $<\tau>^{-1}$ are not equivalent to those obtained using $<\tau^{-1}>$. Since the $<k_1>$ values using $<\tau^{-1}>$ are identical to the $k_1[Py]$ values obtained with the Birks' scheme, the former procedure was adopted to determine $<k_1>$ in all following experiments. The MF analysis was applied to determine the contributions of the pyrene species to the fluorescence decays of the pyrene monomer and excimer. As would be expected for pyrene and 1-pyrenemethanol in organic solvents, f_{agg}^{f} was determined (using Equations 4.17 – 4.21) to be 5% or less for all solutions studied, confirming that no pyrene aggregation takes place. The change in f_{agg}^{f} as a function of pyrene concentration is shown in Figure SI.4.2 in Supporting Information. It increases with increasing pyrene concentration.

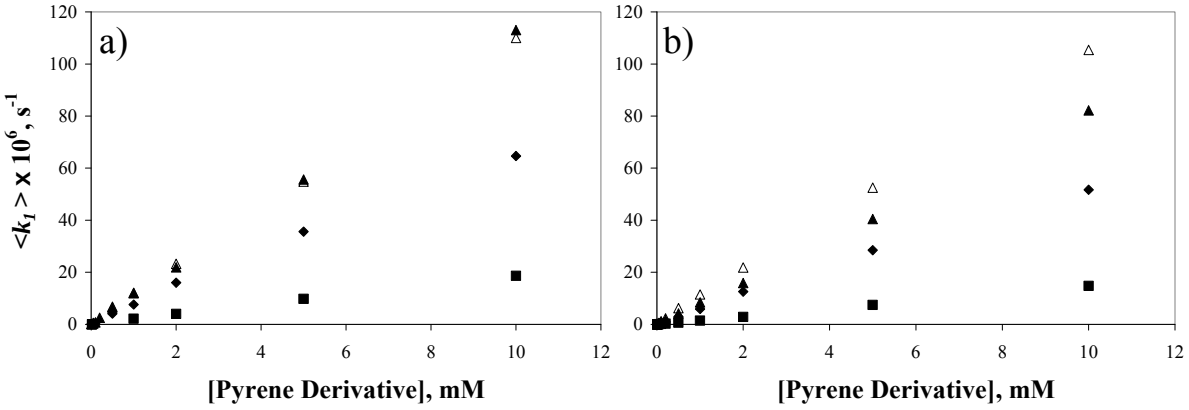

Figure 4.3: Diffusional quenching according to the model free approach for pyrene in cyclohexane (◆), DMF (■), and acetonitrile (▲), and 1-pyrenemethanol in acetonitrile (△) calculated using a) Equation 8 and b) Equation 9.

Having established that the model free approach yields a set of kinetic parameters that describe satisfyingly excimer formation for pyrene and 1-pyrenemethanol in various organic solvents, this analysis was applied to a poly(ethylene oxide) chain having a number-averaged molecular weight of 2,500 g/mol labelled at one end with pyrene (PyPEO). As acetonitrile is considered a good solvent for both pyrene and poly(ethylene oxide),[44] the monomer and excimer fluorescence decays for PyPEO in acetonitrile for concentrations ranging from 2 μM to 7 mM were acquired and analyzed according to the model free approach. This was done in order to determine whether the model free analysis could describe the dynamics of unassociated pyrenes attached to a long non-fluorescent polymer chain in a good solvent. It is important to note that the model free analysis yielded good fits for PyPEO in acetonitrile only when assuming that $[ES^*]_{(t=0)} \neq 0$. Thus the analysis of the excimer decays assumed the presence of short-lived pyrene aggregates *ES** having a lifetime τ_{ES} fixed to a value of 3.5 ns. This lifetime of 3.5 ns was taken as the averaged values of the short decay time obtained from the fit of the excimer decays of the PyPEO solutions in acetonitrile with a sum of exponentials. A lifetime of 3.5 ns for *ES** is close to the τ_{ES} values obtained for other pyrene-labelled macromolecules forming short-lived GS pyrene aggregates.[25–27] The parameters obtained from the fits are listed in Table SI.4.4. The contribution of *ES** to the fluorescence decays given by f_{ES}^f was small. Together, $f_{ES}^f + f_{E0}^f$ amounted to less than 10% for all PyPEO concentrations so that PyPEO can be considered to be unaggregated in acetonitrile up to a concentration of 7 mM (Figure 4.4). The rate constant of excimer formation by diffusion $\langle k_1 \rangle$ does not increase linearly with PyPEO concentration, as shown in Figure 4.5. Since the addition of PyPEO at concentrations as high as 5 – 10 mM has a significant effect on the solution viscosity η, the parameter $\langle k_1 \rangle$ might be affected by the viscosity increase. Thus the viscosity of the solutions was determined by taking viscometry measurements of a range of PyPEO concentrations and interpolating the viscosities of the individual PyPEO concentrations which are

presented in Table SI.4.5 of Supporting Information. Upon multiplying $\langle k_1 \rangle$ by the ratio η/η_0 where η and η_0 are respectively the viscosities of the solution and solvent, a linear trend was obtained yielding a $\langle k_1 \rangle \eta/\eta_0$ value of $5.0 \pm 0.2 \times 10^9$ $M^{-1}s^{-1}$. This value is half that found for pyrene and 1-pyrenemethanol in acetonitrile. This result is reasonable since the smaller $\langle k_1 \rangle \eta/\eta_0$ value reflects the slower kinetics of excimer formation experienced by the bulkier PyPEO in acetonitrile.

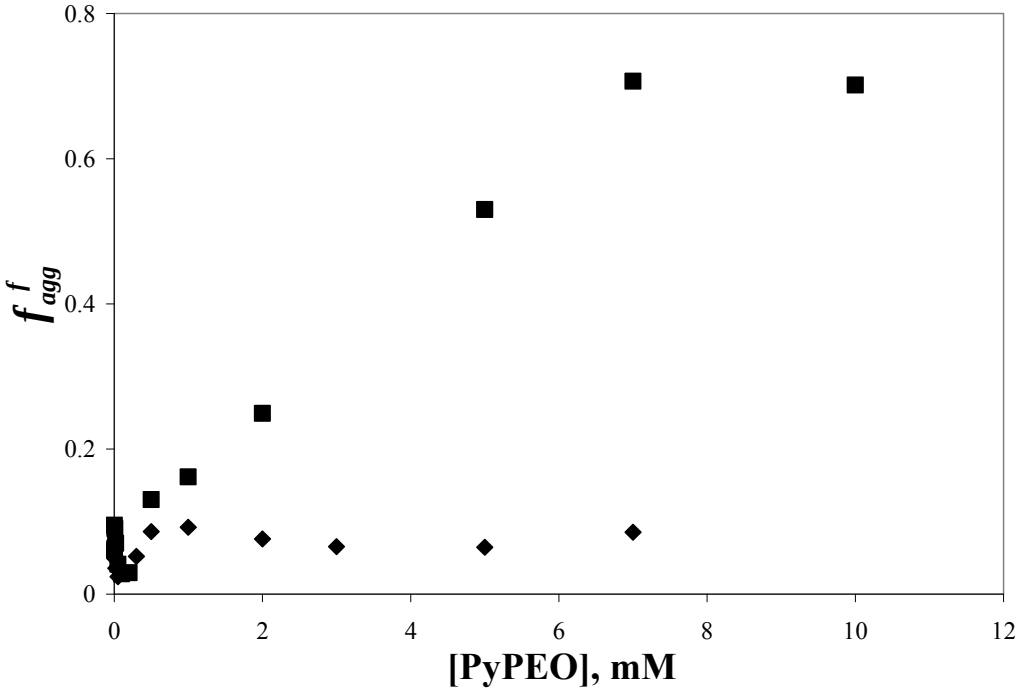

Figure 4.4: Fluorescence contribution to the monomer and excimer by the aggregated pyrene fraction for PyPEO in acetonitrile (◆), and water (■).

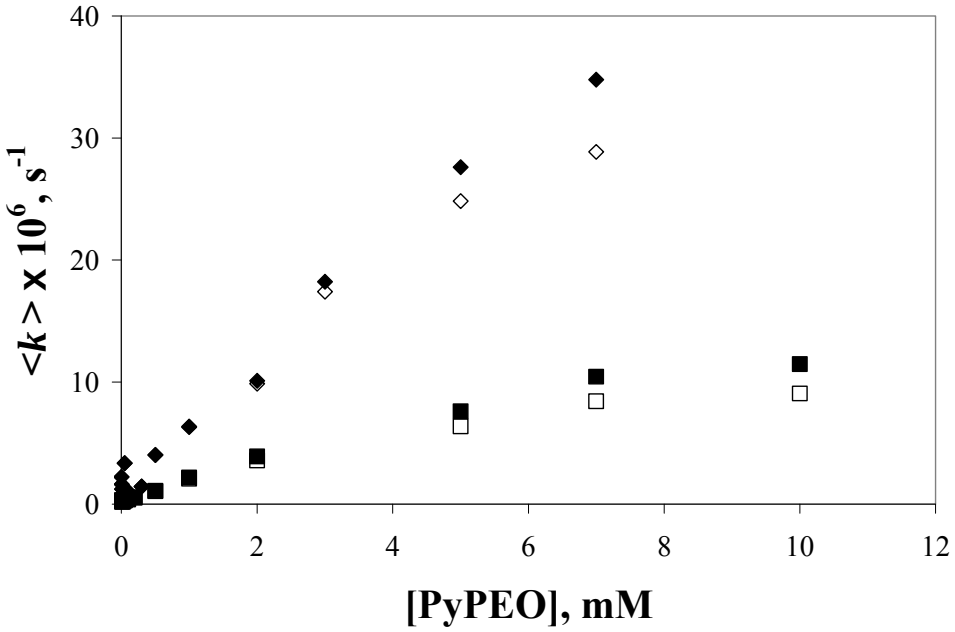

Figure 4.5: Viscosity uncorrected (hollow) and corrected (filled) excimer formation rate constants for PyPEO in acetonitrile (◆, ◇), and water (■, □).

Finally, the model free analysis was applied to the monomer and excimer fluorescence decays acquired for aqueous solutions of PyPEO in order to determine the fluorescence fractions of the pyrene species present in solution. As was the case for PyPEO in acetonitrile, it was necessary to include a short-lived species having a lifetime of 3.5 ns to fit the excimer decays. Its contribution was found to be important at PyPEO concentrations greater than 1 mM. The parameters obtained from the model free analysis of the monomer and excimer decays acquired for PyPEO solutions in water are listed in Table SI.4.6. Significant differences were found between the trends obtained with the parameters $<k_1>$ and f_{agg}^{f} in solutions of PyPEO in water and acetonitrile. While f_{agg}^{f} was less than 10% and essentially independent of PyPEO concentration in acetonitrile, f_{agg}^{f} in water increased to

values as high as 0.70 within the same PyPEO concentration range (Figure 4.4). Furthermore, whereas multiplying $\langle k_1 \rangle$ by η/η_0 resulted in a linear increase with increasing PyPEO concentration, the same is not observed in water as shown in Figure 4.5 where $\langle k_1 \rangle \eta/\eta_0$ deviates from linearity for PyPEO concentrations greater than 1 mM. Incidentally, f_{agg}^{f} takes values greater than 0.15 in the same PyPEO range. This coincidence suggests that the aggregation of PyPEO is likely the cause of the deviation. Thus, the pyrene concentration [*Py*] which assumes that the pyrenes are homogeneously distributed in solution is not equivalent to [*PyPEO*] for PyPEO in water. Although the plot of $\langle k_1 \rangle \eta/\eta_0$ against [*PyPEO*] in water shows a substantial degree of curvature, the ratio I_E/I_M of the intensities of the excimer (I_E), integrated from the fluorescence emission spectra between 500 to 530 nm, to that of the monomer (I_M), integrated from the fluorescence emission spectra between 372 to 378 nm, exhibits a linear relationship with PyPEO concentration in water as is shown in Figure SI.4.3 in Supporting Information. The linearity of I_E/I_M with [*PyPEO*] has also been reported previously for aqueous solutions of PyPEO having the same molecular weight.[45] The I_E/I_M ratio, being referred to as the "coiling index",[15] is a common approach to the characterization of pyrene-labelled polymers in solution. This coiling index is often considered to represent the same effect as $\langle k_1 \rangle$. For PyHMWSPs such as PyPEO however, this does not appear to be true with $\langle k_1 \rangle \eta/\eta_0$ which was observed to plateau in Figure 4.4 whereas I_E/I_M exhibits a linear dependence with PyPEO concentration in Figure SI.4.2. Since $\langle k_1 \rangle \eta/\eta_0$ accounts only for diffusionally formed excimers while I_E/I_M includes both excimers generated by the direct excitation of GS pyrene aggregates and by diffusive encounters of pyrene monomers, differences in the trends of $\langle k_1 \rangle \eta/\eta_0$ and I_E/I_M are expected.

The results presented earlier for pyrene excimer formation suggests that the model free analysis can be used to characterize the kinetics of excimer formation by diffusion. Furthermore, the MF analysis seems to respond to the presence of GS pyrene aggregation as was formed by PyPEO in

water, where f_{agg} increases with [PyPEO] in Figure 4.4. Consequently, the MF analysis appears to be an alternate analytical tool to the FBM to describe the kinetics of excimer formation of a pyrene-labelled polymer and its level of pyrene association f_{agg}^{f}. These considerations led to the conclusion that the MF analysis could be applied to determine the molar absorbance coefficient of the pyrene aggregates formed by PyPEO in water.

To this end, the monomer and excimer fluorescence decays of 5, 10, and 13 mM solutions of PyPEO in water were acquired using excitation wavelengths ranging from 325 to 347 nm with one nanometer increments. These three PyPEO concentrations were selected since they displayed sufficient broadening of their absorption spectra compared to the 2 μM solution of unassociated PyPEO in water (Figure SI.4.4 of Supporting Information). Indeed, their P_A values, defined as the ratio of the maximum absorption in Figure SI.4.4 to that of the nearest trough, for 5, 10, and 13 mM PyPEO solutions were found to equal 2.1, 1.8, and 1.7, respectively. These P_A values indicate considerable broadening in their absorption spectra compared to the 2 μM PyPEO solution which has a P_A value of 2.6. Since the level of aggregation of a pyrene-labelled macromolecule is reflected by a P_A value much smaller than 3.0, the 2 μM PyPEO solution in water is substantially less aggregated than the three other solutions. The monomer and excimer decays at each excitation wavelength were fitted globally with the model free approach and the obtained parameters are listed in Table SI.4.7. As was seen previously,[23] the fluorescence fractions exhibit substantial excitation wavelength dependency in Figure 4.6. The calculated molar fraction of aggregated pyrenes f_{agg} exhibits a smaller excitation wavelength dependency compared to f_{agg}^{f} as the undulations in Figure 4.6 are less pronounced and less patterned for f_{agg}. Based on the trends shown in Figure 4.6, f_{agg} increases with increasing PyPEO concentration, being equal to 0.51 ± 0.04, 0.74 ± 0.04, and 0.78 ± 0.04 for aqueous PyPEO solutions of 5, 10, and 13 mM, respectively.

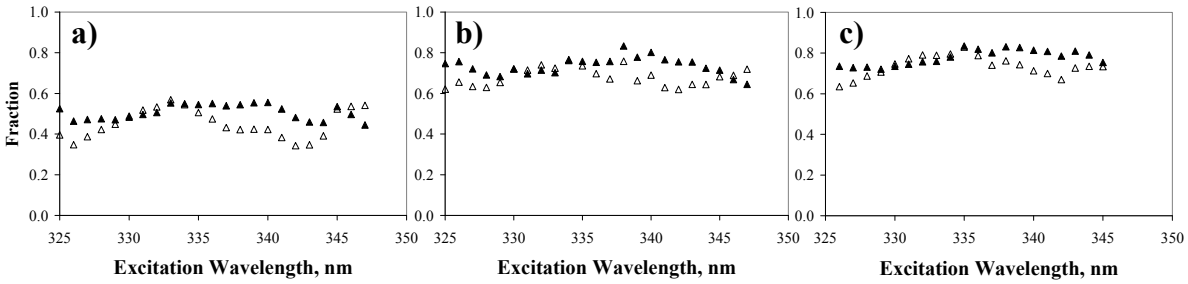

Figure 4.6: Actual (filled) and fluorescence (hollow) fractions of aggregated pyrenes for aqueous solutions of PyPEO having concentrations of a) 5, b) 10 and c) 13 mM.

In addition to f_{agg}, the molar absorbance coefficient of the pyrene aggregates ε_{E0} was also calculated for each of the three PyPEO concentrations. The three sets of molar absorbance coefficients are shown in Figure 4.7 along with the molar absorbance coefficient of unassociated PyPEO. The molar absorbance coefficient spectra of the aggregated species, with an average P_A value equal to 1.8 ± 0.1, exhibit much broader peaks compared to the unassociated species. Despite the differences in f_{agg} between the three concentrations, there is easonable agreement between the ε_{E0} values determined for the three PyPEO concentrations. The molar absorbance coefficients for the pyrene aggregates obtained for the three PyPEO concentrations between 325 and 347 nm were averaged and the average value $<\varepsilon_{E0}>$ is listed in Table 4.5 as a function of wavelength. Compared to the $<\varepsilon_{E0}>$ spectrum obtained from the PyPDMA experiments[23] shown in Figure 4.8, the $<\varepsilon_{E0}>$ spectrum of PyPEO is relatively similar to that of PyPDMA, the $<\varepsilon_{E0}>$ spectrum of PyPDMA in water being broader and red-shifted compared to that of PyPEO. This is not entirely unexpected since the aggregates of PyPDMA (*E0* and *EL*) and PyPEO (*E0* and *ES*) are composed of different pyrene species.

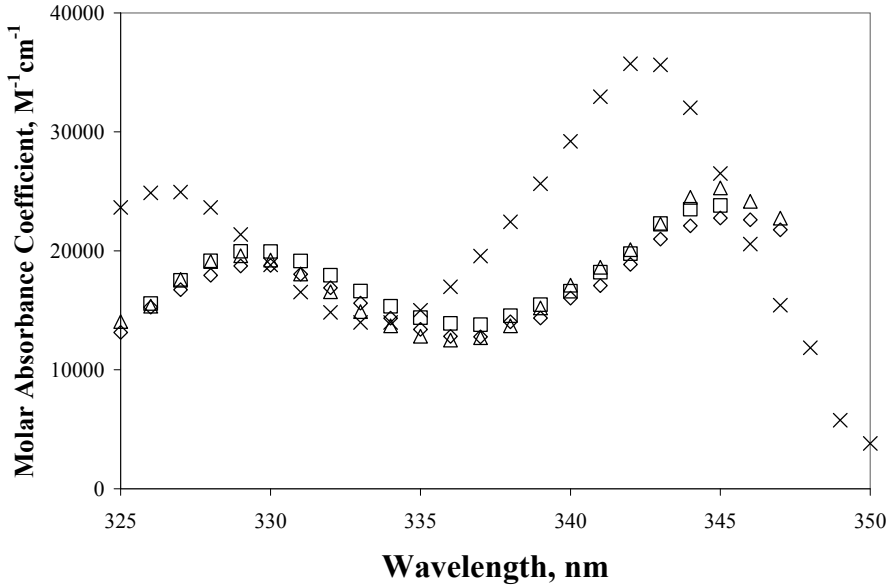

Figure 4.7: Molar absorbance coefficients of unassociated PyPEO in water (×) and pyrene aggregates determined for PyPEO solutions in water of 5 (△), 10 (◇), and 13 (□) mM.

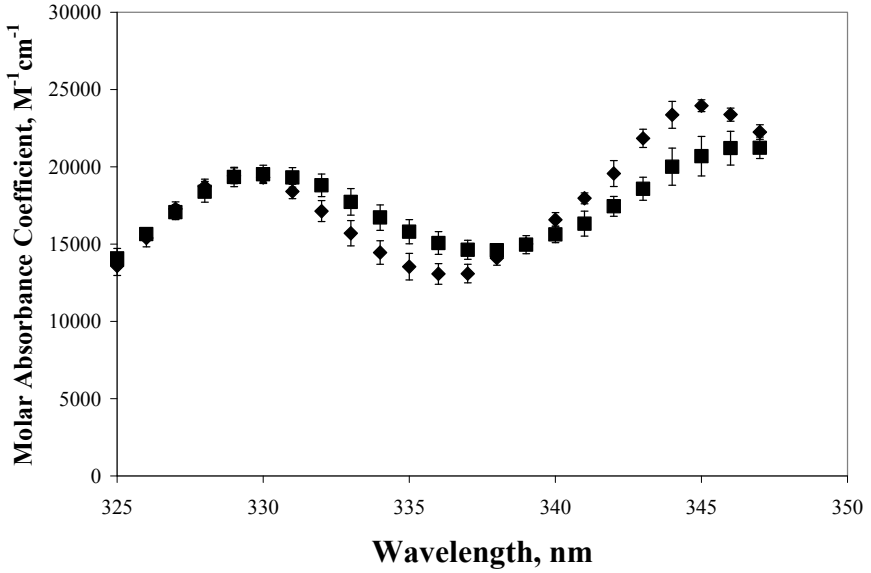

Figure 4.8: Averaged molar absorbance coefficients of pyrenes that are aggregated, $<\varepsilon_{E0}>$, determined for PyPEO (◆) and PyPDMA (■) in water.

Table 4.5: Averaged extinction coefficient of the pyrene aggregates ε_{E0} for PyPEO in water.

Wavelength nm	$<\varepsilon_{E0}>$ $L \cdot mol^{-1} \cdot cm^{-1}$	$\pm <\varepsilon_{E0}>$ $L \cdot mol^{-1} \cdot cm^{-1}$	Wavelength nm	$<\varepsilon_{E0}>$ $L \cdot mol^{-1} \cdot cm^{-1}$	$\pm <\varepsilon_{E0}>$ $L \cdot mol^{-1} \cdot cm^{-1}$
325	13600	600	338	14100	400
326	15400	200	339	15000	600
327	17300	500	340	16600	500
328	18700	700	341	18000	800
329	19400	600	342	19600	600
330	19300	600	343	21800	700
331	18400	600	344	23400	1200
332	17100	700	345	24000	1300
333	15700	900	346	23400	1100
334	14500	800	347	22300	700
335	13500	800			
336	13100	700			
337	13100	600			

4.6 Discussion

To effectively understand and model the network formed by HMWSPs in solution, it is critical to determine f_{agg}, i.e. the molar fraction of hydrophobic pendants which are aggregated. For many years, pyrene has been used as the replacement of the hydrophobic pendant of HMWSPs to characterize polymeric networks by fluorescence. Despite the intensive use of this approach, an

effective procedure for the quantitative determination of f_{agg} was developed only recently. This was accomplished by applying the FBM to analyze the fluorescence decays of poly(*N*,*N*-dimethylacrylamide) randomly labelled with pyrene (PyPDMA).[23] The current study aimed at determining f_{agg} for poly(ethylene oxide) labelled at one end with pyrene (PyPEO). PyPEO is a key component found in pyrene labelled analogs of the commercially available HASE and HEUR polymers.[20,21,46] The level of association of PyPEO in water can be controlled by adjusting the polymer concentration. Since excimer formation by the diffusive encounter between two pyrenes attached at a single end of a PEO chain and randomly along a PDMA chain is bound to be described by different models, the study of aqueous solutions of PyPEO required the development of an alternative procedure to model excimer formation by diffusion between two PyPEO chains. To this end, the model free analysis based on a sum of exponentials[38] was applied after gauging its validity by probing the process of excimer formation for pyrene derivatives in organic solvents.

First, the monomer and excimer fluorescence decays of pyrene in cyclohexane were analyzed globally according to the Birks' scheme using Equations 4.1, 4.2, and 4.16. The analysis yielded values for $k_1[Py]$, τ_{E0}, and k_{-1} which were in close agreement with the values obtained by Birks.[31] The same procedure was further applied to study the kinetics of excimer formation for pyrene dissolved in *N*,*N*-dimethylformamide (DMF) and acetonitrile and 1-pyrenemethanol in acetonitrile. Values for $k_1[Py]$, k_{-1}, and τ_{E0} were obtained for these solutions. The diffusional rate constant k_1 obtained from the analysis ranked according to the following sequence: $(k_1)^{pyrene}_{acetonitrile} \cong (k_1)^{pyrene\,methanol}_{acetonitrile} > (k_1)^{pyrene}_{cyclohexane} > (k_1)^{pyrene}_{DMF}$. This sequence does not agree with the relationship expected between k_1 and the inverse of solvent viscosity. Since the viscosity of DMF (0.794 mPa.s at 25 °C)[47] is 2.2 times greater than the viscosity of acetonitrile (0.369 mPa.s at 25 °C),[47] k_1 in acetonitrile would be expected to be 2.2 fold greater than in DMF. Instead k_1 was experimentally found to be 6.0 times greater in acetonitrile than in DMF. Similarly, the viscosity of cyclohexane

(0.894 mPa.s at 25 °C)[47] suggests that k_1 should be 13% greater in DMF than in cyclohexane. Instead k_1 in cyclohexane was found to be 3.5 fold greater than in DMF. It is worth pointing out that the k_1 values obtained for pyrene in acetone and ethanol by Birks do not obey the correlation expected to exist between k_1 and $1/\eta$.[31] Such discrepancies have been observed by other researchers and have been rationalized by evoking the effect of solvent polarity and the solvent sphere formed on the efficiency of excimer formation.[40] The much lower polarity of cyclohexane (dielectric constant $\varepsilon = 2.02$)[47] seems to favour excimer formation, apparently by decreasing the primary solvent sphere of the solvated chromophore.

The absence of relationship existing between k_1 and sovent viscosity for small pyrene derivatives in organic solvent contrasts starkly with the use of excimer formation between pyrene derivatives covalently attached onto macromolecules to probe the internal dynamics of macromolecules in solution. Indeed numerous studies have established that the rate of excimer formation for pyrene-labelled polymers is inversely proportional to solvent viscosity.[28,30] The correct relationship found between k_1 and $1/\eta$ for pyrene-labelled polymers is rationalized by considering that excimer formation occurs in a sequential manner.[30] First, slow long range diffusive motion of the polymer backbone brings the two monomers bearing pyrene pendants close to each other. Second, the pyrenes rearrange rapidly to form the excimer. The first step in this sequential model is the rate limiting step. It is controlled by solvent viscosity and is unaffected by the solvation sphere effect found for molecular pyrene.

The parameters obtained with the Birks' scheme were compared to the $\langle k_1 \rangle[Py]$ and τ_{E0} values obtained by the model free global analysis. The nearly identical values found for k_1 and $\langle k_1 \rangle$ and the close agreement found for the τ_{E0} values obtained from the Birks' scheme and the model free analysis indicate that the two analyses yield similar and consistent information on the kinetics of excimer formation. Thus, the model free global analysis appears to be an effective tool to probe the

diffusional encounters of small molecules in solution and was therefore applied to study the process of excimer formation for PyPEO. The organic solvent acetonitrile is considered to be a good solvent for both pyrene and poly(ethylene oxide) and thus is a good solvent for PyPEO. This was confirmed by the finding that f_{agg}^{f} was always smaller than 10% regardless of PyPEO concentration.

Light scattering and surface tension measurements have shown that PyPEO begins to form aggregates in water at concentrations larger than 2 μM.[45] These aggregates consisted of a hydrophobic core of pyrenes surrounded by a corona of PEO chains. From the global MF analysis of the monomer and excimer fluorescene decays, it was determined that only at PyPEO concentrations greater than 0.2 mM PyPEO does the level of aggregation of the pyrenes become significant ($f_{agg}^{f} > 0.1$). This is not surprising since according to their fluorescence emission spectra (Figure SI.4.1), the intensity of the excimer is negligible, probably due to the poor fluorescence quantum yield of pyrene aggregates.[48] As the PyPEO concentration increases beyond 0.2 mM, the concentration of aggregated PyPEO increases at the expense of the concentration of unassociated PyPEO. This was demonstrated clearly by the increase of f_{agg}^{f}, increasing from less than 0.10 for PyPEO concentrations smaller than 0.2 mM up to 0.70 for a 10 mM PyPEO solution. It is important to point out that these values of f_{agg}^{f} were obtained for PyPEO in water despite the lack of an obvious rise time present in the excimer fluorescence decay even at the lowest concentrations of PyPEO studied. Although some species may contribute to a rise time in the excimer decay, we suspect that the rise time is hidden underneath more prominent decay features thus preventing an accurate estimation of its contribution. In order to effectively estimate the contribution from the hidden rise time, it is necessary to jointly analyze the excimer decay with the monomer since the decay times characterizing the rise time in the excimer is more easily resolved in the monomer and could be used to restrict the optimisation of the decay times in the excimer decay. Thus, the accurate determination of the parameters describing the diffusional excimer formation

processes of PyPEO in water required the global analysis of the monomer and excimer fluorescence decays.

Although informative, f_{agg}^{f} is a relative representation of the level of aggregation of the pyrene pendants. An absolute measure of the molar fraction of aggregated pyrenes is given by f_{agg}. f_{agg} can be determined from the combined knowledge of f_{agg}^{f} and ε_{E0}. ε_{E0} was determined as a function of wavelength by applying the model free analysis to a set of monomer and excimer decays acquired with 1 nm excitation wavelength increments with PyPEO aqueous solutions of 5, 10, and 13 mM. The wavelength dependency of f_{agg} determined for the 5, 10, and 13 mM PyPEO solutions was strongly reduced when compared to that of the fluorescence fraction f_{agg}^{f}. These experiments provide an absolute measure of f_{agg} for these PyPEO solutions. The averaged molar absorbance coefficient $<\varepsilon_{E0}>$ obtained for PyPEO was compared to that obtained for PyPDMA in Figure 4.8. The two spectra were similar with the $<\varepsilon_{E0}>$ spectrum for PyPDMA being broader and red-shifted compared to that of PyPEO. To verify that this discrepancy between $<\varepsilon_{E0}>$ values obtained for PyPEO and PyPDMA was not due to the model used, the monomer and excimer fluorescence decays of three aqueous PyPDMA solutions used in Chapter 3 were analyzed using the global model free analysis and the ε_{E0} values resulting from this analysis are shown in Figure SI.4.5 of Supporting Information. It is important to note that since PyPMDA is a polymer randomly labelled with pyrene, the MF analysis of PyPDMA required modification of Equation 4.11 according to Equation 4.15 in order to account for the pyrene species Py_{free}^{*}. The perfect agreement found between the ε_{E0} values calculated using the model free and FBM global analysis for the three PyPDMA solutions implies that the difference in $<\varepsilon_{E0}>$ determined for PyPEO and PyPDMA is not due to differences in the model used to describe the diffusional encounters of pyrene. This difference in $<\varepsilon_{E0}>$ is not entirely surprising as the size and

composition of the pyrene aggregates formed by PyPDMA and PyPEO are different. In addition to the pyrene aggregates formed by PyPDMA (3.1 pyrenes per aggregate)[23] being smaller than PyPEO (20 pyrenes per aggregate),[45] PyPDMA aggregates are composed of the pyrene species *E0* and the long-lived pyrene dimer species *EL* while PyPEO aggregates are constituted of the *E0* and *ES* species. The different composition of the pyrene aggregates might alter the approximation made earlier that all aggregated pyrene species absorb with the same molar absorbance coefficient ε_{E0}. For instance, the molar absorbance coefficient of *ES* might be closer to ε_M than ε_{E0}. However, if the molar absorbance coefficient of the pyrene species *ES* is approximated to ε_M, the calculated pyrene fractions f_{diff} and f_{agg} maintain the wavelength dependency found for f_{diff}^{f} and f_{agg}^{f} as shown in Figure SI.4.6 of Supporting Information. This indicates that while the approximation of the molar absorbance coefficient for *ES* being equal to ε_{E0} might not be entirely accurate, it is a much better approximation than assuming that *ES* absorbs with the molar absorbance coefficient ε_M. The pyrene aggregates formed by PyPEO in water exhibit a broadening and red-shifting of their absorbance peaks similar to that found for PyPDMA in water although there are observable differences between the absorbance spectra of the pyrene-labelled polymers in water. This difference in their absorbance spectra is likely due to differences in pyrene aggregate composition.

4.7 Conclusions

The networking ability of the commercially available HASE and HEUR associative polymers is based in both cases on the aggregation of poly(ethylene oxide) chains end-capped with a hydrophobic moiety. To gain information on the level of association of these polymers, a model poly(ethylene oxide) chain capped at one end with a pyrene moiety (PyPEO) was studied using a model free global analysis. The model free (MF) global analysis was first applied to study excimer formation of molecular pyrene in organic solvents and the kinetic parameters retrieved from their

analysis were compared to those obtained with the well-established Birks' scheme. By defining $< k_1 >=< \tau^{-1} > - \frac{1}{\tau_M}$ rather than $< k_1 >= \frac{1}{< \tau >} - \frac{1}{\tau_M}$, good agreement was reached between the values of $<k_1>$ obtained from the MF analysis and those of k_1 obtained from the Birks' scheme for all pyrene solutions in organic solvent studied. The fact that analysis of the fluorescence decays with the MF approach or the well-established Birks' scheme yielded comparable kinetic parameters was taken as a validation of the MF analysis. The MF approach was also used to determine the fluorescence fractions f_{agg}^{f} and f_{diff}^{f} of PyPEO in solvents where the PyPEO was unassociated (acetonitrile) and associated into micelles (water). The MF global analysis was found to effectively characterize the fractions of each pyrene species to the decays, even for the difficult case of PyPEO in water whose lack of rise time in the excimer decays could have prevented successful analysis of the decays. With the fluorescence fractions determined for PyPEO in water, the true level of association f_{agg} was characterized for three concentrations of PyPEO in water and resulted also in the determination of the averaged molar absorbance coefficient of the aggregated pyrenes $<\varepsilon_{E0}>$. The $<\varepsilon_{E0}>$ spectrum obtained for PyPDMA was broader and red-shifted compared to the $<\varepsilon_{E0}>$ spectrum obtained for PyPEO. Since $[Py_{agg}]_{PyPEO} = [E0] + [ES]$ while $[Py_{agg}]_{PyPDMA} = [E0] + [EL]$, the difference observed in the $<\varepsilon_{E0}>$ spectra might indicate that the assumption of *ES* and *E0* absorbing similarly might not be entirely accurate, although it is a much better approximation than assuming that *ES* absorbs as the pyrene monomer or that it does not absorb.

Chapter 5
Determination of the Level of Association of Hydrophobically-Modified Alkali-Swellable Emulsion Polymers Randomly Labelled with Pyrene

5.1 Overview

The protocol used to determine the molar fractions of the pyrene species in solution was applied to aqueous solutions of pyrene-labelled hydrophobically-modified alkali-swellable emulsion (PyHASE) polymers. The results from applying the protocol did not yield wavelength independent molar fractions of the different pyrene species present in solution. The inability to obtain wavelength independent molar fractions is likely due to the complexity of the excimer kinetics involved for PyHASE solutions. Thus the level of association of the pyrene pendants in solution cannot be quantitatively determined using the protocol introduced in Chapters 3 and 4 for the PyHASE solution.

5.2 Introduction

Hydrophobically-modified alkali-swellable emulsion (HASE) polymers are hydrophobically-modified water-soluble polymers (HMWSPs) used as viscosity modifier additives in paint and coating formulations.[1,2] The peculiar viscoelastic properties of aqueous HASE solutions are due to the amphiphilic structure of HASEs which enables the polymer at concentrations above its overlap concentration to self-assemble into reversible crosslinked networks held together by hydrophobic aggregates. The interesting rheological properties that this reversible network imparts on the solution have led to the implementation of models that attempt to predict these viscoelastic properties.[3—10] Among the several parameters used by the models, the molar fraction of the hydrophobic pendants which are aggregated in solution, f_{agg}, is critical to describe the structure of the reversible network.[5,6]

The f_{agg} value of a HMWSP has been obtained by conducting a combination of fluorescence and absorbance measurements on a modified HMWSP where the typically alkyl-based hydrophobic pendants have been substituted by the chromophore pyrene (PyHMWSP).[11,12] The substitution of the typical hydrophobe with pyrene to yield PyHMWSP results in a polymer possessing rheological properties similar to that of its non-pyrene labelled equivalents.[13,14] Pyrene is an ideal choice for studying the level of association due to its ability to form excimers whose emission is separate from that of the monomer and signals pyrene association.[15,16] Pyrene excimers may be formed by either the diffusive encounter of an excited pyrene monomer with a ground-state (GS) pyrene or the direct excitation of pre-associated GS pyrene aggregates. The kinetics of excimer formation are described by the modified Birks' scheme shown in Scheme 5.1.[17]

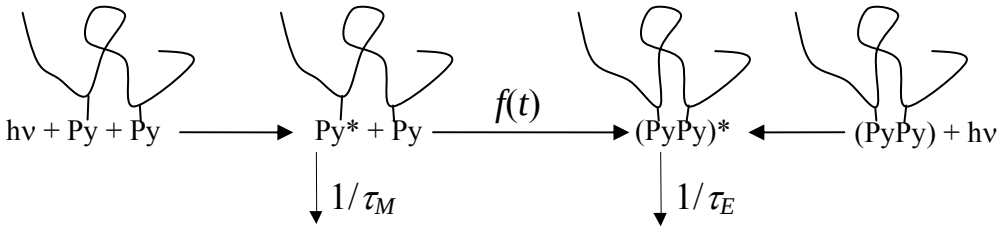

Scheme 5.1: Birks' scheme modified to include direct excitation of GS pyrene aggregates.

Excimers formed by both direct excitation of GS pyrene aggregates or diffusive encounters between an excited and a GS pyrene possess similar fluorescence emission spectra. In order to distinguish between the two types of excimers, time-resolved fluorescence measurements can be performed where their different rates of excimer formation enable their differentiation.[15] In addition, GS pyrene aggregates also bear a different absorbance profile having an absorption spectrum that is relatively broader and red-shifted compared to that of unaggregated or monomeric pyrenes.[16] Therefore, the pyrene pendants of a PyHMWSP in solution can be classified as either aggregated or

unaggregated. These two classifications can be further divided according to their fluorescence characteristics. Within the time that an excited pyrene remains excited, unaggregated pyrenes may be separated into isolated pyrenes that do not form excimer (Py_{free}) and those that form excimer via diffusive encounter with GS pyrenes (Py_{diff}). Aggregated pyrenes (Py_{agg}) consist of up to three species being well-stacked pyrene dimers (*E0*), long-lived pyrene dimers (*EL*), and short-lived pyrene aggregates (*ES*).

To date f_{agg} has been determined quantitatively for two different PyHMWSPs, namely poly(*N*,*N*-dimethylacrylamide) randomly labelled with pyrene (PyPDMA)[11] and poly(ethylene oxide) terminated at one end with a pyrene unit (PyPEO).[12] This was accomplished by determining the contributions of all pyrene species defined above to the monomer and excimer fluorescence decays and comparing them to the absorption spectrum of the solution. These contributions referred to as the fluorescence fractions are listed in Table 5.1. In addition to yielding the level of association f_{agg} of the PyHMWSPs, these studies also yielded the molar absorbance coefficient of their pyrene aggregates ε_{E0} over a range of wavelengths. It was observed that the aggregates of PyPDMA which are composed of the pyrene species *E0* and *EL*, have an ε_{E0} spectrum that is broader and red-shifted compared to that of the PyPEO aggregates which are composed of the pyrene species *E0* and *ES*.

The purpose of this study is to apply the protocol established in the PyPDMA and PyPEO studies in order to determine f_{agg} for aqueous solutions of pyrene-labelled HASE polymers (PyHASE) and the molar absorbance coefficients of their aggregates, ε_{E0}. The monomer and excimer fluorescence decays of alkaline sodium carbonate solutions containing PyHASE having pyrene contents of 12 and 65 μmol pyrene/g of polymer (PyHASE12 and PyHASE65, respectively) were acquired using a range of excitation wavelengths from 325 to 347 nm with one nanometer intervals. The kinetics of excimer formation via the diffusive encounters of pyrenes described by the time-dependent rate constant $f(t)$ in Scheme 5.1 was handled using the fluorescence blob model (FBM) and

was described in greater detail previously.[11,12,18] Using global analysis, the monomer and excimer fluorescence decays were fitted simultaneously to Equations 5.1 and 5.2, respectively.

$$[M^*] = [Py^*_{diff}]_{(t=0)} \exp\left(-\left(A_2 + \frac{1}{\tau_M}\right)t - A_3\left(1-\exp(-A_4 t)\right)\right) + [Py^*_{free}]_{(t=0)} \exp\left(-\frac{t}{\tau_M}\right) \tag{5.1}$$

$$[E^*] = -[Py^*_{diff}]_{(t=0)}\, e^{-A_3} \sum_{i=0}^{\infty} \frac{A_3{}^i}{i!} \frac{A_2 + i\,A_4}{\frac{1}{\tau_M} - \frac{1}{\tau_{E0}} + A_2 + i\,A_4} \exp\left(-\left(\frac{1}{\tau_M} + A_2 + i\,A_4\right)t\right) + \left([E0^*]_{(t=0)} + [Py^*_{diff}]_{(t=0)}\, e^{-A_3} \sum_{i=0}^{\infty} \frac{A_3{}^i}{i!} \frac{A_2 + i\,A_4}{\frac{1}{\tau_M} - \frac{1}{\tau_{E0}} + A_2 + i\,A_4}\right) e^{-t/\tau_{E0}} + [ES^*]_{(t=0)}\, e^{-t/\tau_{ES}} + [EL^*]_{(t=0)}\, e^{-t/\tau_{EL}} \tag{5.2}$$

In Equations 5.1 and 5.2, the parameters A_2, A_3, and A_4 are functions of the FBM parameters k_{blob}, $\langle n \rangle$, and $k_{ex}[blob]$ which are the quenching rate constant inside a blob containing one excited and one ground-state pyrene, the average number of pyrenes per blob, and the rate constant of pyrene exchange between blobs, respectively. The expressions of A_2, A_3, and A_4 are given in Equation 5.3.

$$A_2 = \langle n \rangle \frac{k_{blob} k_{ex}[blob]}{k_{blob} + k_{ex}[blob]} \qquad A_3 = \langle n \rangle \frac{k_{blob}^2}{\left(k_{blob} + k_{ex}[blob]\right)^2}$$

$$A_4 = k_{blob} + k_{ex}[blob] \tag{5.3}$$

Table 5.1: Notation used for the molar absorbance coefficients, fluorescence fractions and molar fractions of the pyrene species.

Excited Pyrene Species	Molar Absorbance Coefficient	Fluorescence Fraction	Molar Fraction
Py^*_{diff}	ε_M	f^f_{diff}	f_{diff}
Py^*_{free}	ε_M	f^f_{free}	f_{free}
$E0^*$	ε_{E0}	f^f_{E0}	f_{E0}
EL^*	$\varepsilon_{EL} \approx \varepsilon_{E0}$	f^f_{EL}	f_{EL}
ES^*	$\varepsilon_{ES} \approx \varepsilon_{E0}$	f^f_{ES}	f_{ES}
Py^*_{agg}	ε_{E0}	f^f_{agg}	f_{agg}

5.3 Results and Discussion

The global analysis of the measured monomer and excimer fluorescence decays with Equations 5.1 and 5.2 yielded "good fits" having χ^2 values of 1.3 or less with the residuals and autocorrelation function of the residuals randomly distributed around zero. The fluorescence fractions obtained from the global FBM analysis are given in Table SI.5.1 of Supporting Information. The fluorescence fraction of aggregated pyrenes f^f_{agg} is shown as a function of wavelength in Figure 5.1. As was observed for PyPEO and PyPDMA, f^f_{agg} exhibits a strong wavelength dependency for PyHASE highlighting the difference in absorbance between aggregated and unaggregated pyrenes. According to Figure 5.1, PyHASE12 and PyHASE65 display similar levels of aggregation.

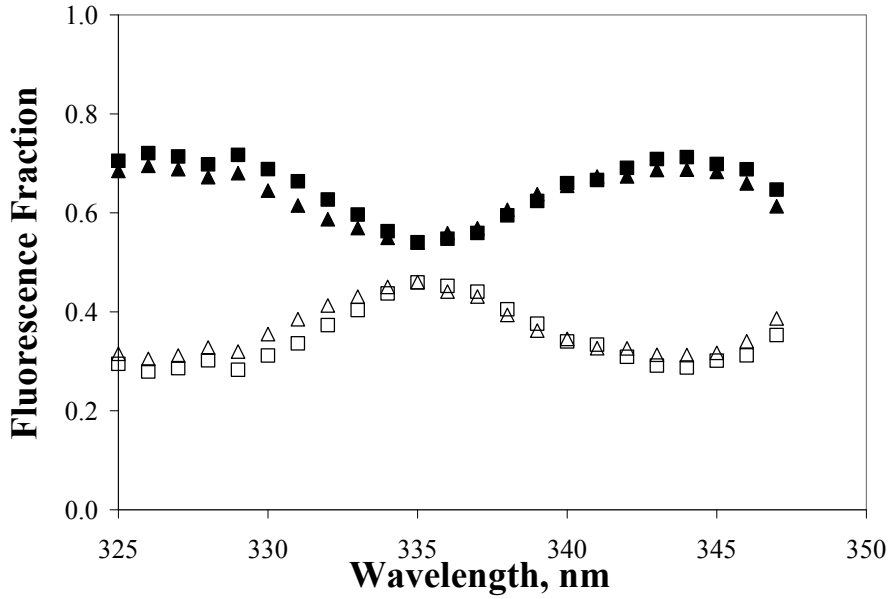

Figure 5.1: Fluorescence fractions of aggregated (hollow) and unaggregated (filled) pyrenes for PyHASE12 (■,□) and PyHASE65 (▲,△) in 0.01 M Na_2CO_3, pH 9 solution.

The fluorescence fractions obtained from the global FBM analysis of the monomer and excimer fluorescence decays and the solution absorbance were used to determine the molar fractions of the pyrene species using the expressions given in Equations 5.4 – 5.6.

$$f_{diff} = \frac{f_{diff}^{f} \times Abs}{\varepsilon_M \times [Py]_T} \tag{5.4}$$

$$f_{free} = \frac{f_{free}^{f} \times Abs}{\varepsilon_M \times [Py]_T} \tag{5.5}$$

$$f_{agg} = \frac{\left(f_{E0}^{f} + f_{EL}^{f} + f_{ES}^{f}\right) \times Abs}{\varepsilon_{E0} \times [Py]_T} = 1 - f_{diff} - f_{free} \tag{5.6}$$

In Equations 5.4 – 5.6, $[Py]_T$ is defined as the total molar pyrene concentration in solution. In order to calculate the molar fractions, the molar absorbance coefficient of the unassociated pyrenes ε_M needed to be determined. ε_M was obtained from the absorbance of a 2 μM aqueous solution of PyPEO dilute enough to ensure that the pyrenes were essentially unaggregated.

Processing the fluorescence fractions $f_{diff}^{f} + f_{free}^{f}$ and f_{agg}^{f} shown in Figure 5.1 through Equaions 4 – 5 yielded f_{agg} which is plotted as a function of wavelength in Figure 5.2. The values of f_{agg} display a strong wavelength dependency in Figure 5.2. One critical criterion defining the successful application of the protocol used to determine f_{agg} requires that the values of f_{agg} obtained from the protocol be wavelength independent. This was observed for both PyPEO and PyPDMA solutions where f_{agg} showed little to no dependency on wavelength compared to f_{agg}^{f}. The trends shown in Figure 5.2 demonstrate that this is not the case for the PyHASE samples.

In Figure 5.3a, the absorption spectra of PyHASE12 and PyHASE65 normalized at the 0-0 transition peak are red-shifted compared to the absorption spectrum of a 2 mM solution of PyPEO. However, the spectra show little difference in terms of peak broadness, yielding P_A values of 2.4, 2.6, and 2.6 for the PyHASE12, PyHASE65, and PyPEO samples, respectively. Contrasting the minimal peak broadening observed for PyHASE, the absorption spectra of PyPDMA exhibit considerable broadening as observed in Figure 5.3b where the PA value equals 2.5, 1.7, 1.6, and 1.4 for the PyPDMA6, PyPDMA263, PyPDMA479, and PyPDMA645 samples, respectively. The lack of broadening in the absorption spectra of the PyHASE solutions is striking considering that the PyHASE solutions are expected to show substantial pyrene aggregation as implied by their excimer decay profiles having little to no rise time present at the early times (Figure 5.4).

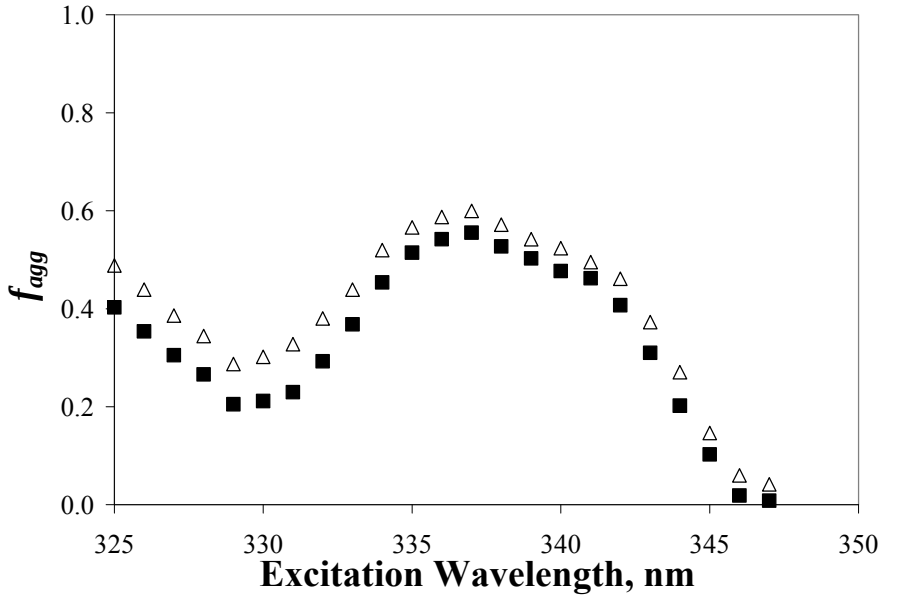

Figure 5.2: Molar fraction of aggregated pyrenes for PyHASE12 (■), PyHASE35 (◆), and PyHASE65 (△) in 0.01 M Na_2CO_3, pH 9 solution using $\varepsilon_M = \varepsilon_M^{PyPEO}$.

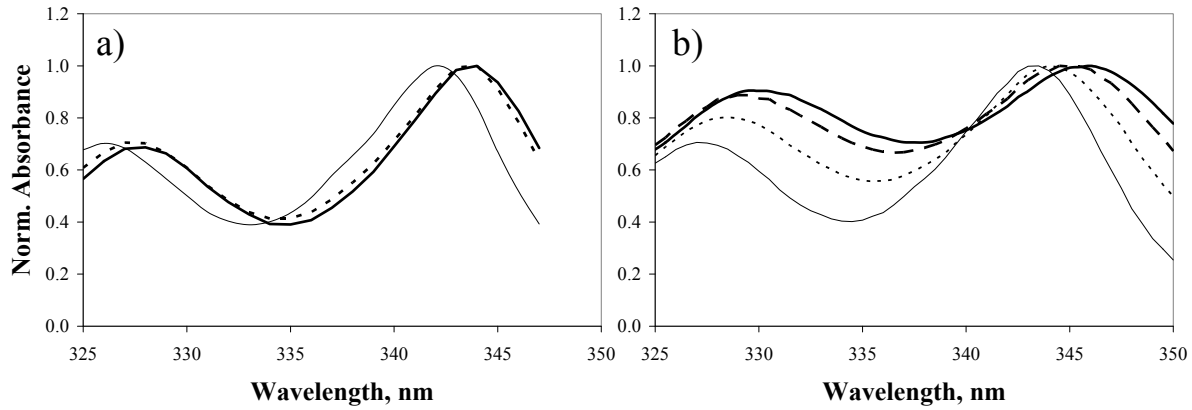

Figure 5.3: Absorption spectra normalized at the 0-0 transition peak for a) PyHASE12 (▪▪▪), PyHASE 65 (▬▬), and 2 mM PyPEO (—) solutions; b) PyPDMA solutions having pyrene contents of 6 (—), 263 (▪▪▪), 479 (▬ ▬ ▬) , and 645 (▬▬) mM pyrene/g polymer.

Indeed, the fluorescence decay of the PyHASE65 excimer overlaps perfectly that of the PyPDMA645 excimer and the pyrene pendants of the PyPDMA645 sample were found to be strongly aggregated.[11] As the excimer decays of PyHASE and PyPDMA bear striking similarity in profile, the scheme used to model the excimer kinetics of PyPDMA solutions was applied to PyHASE solutions. The scheme used to describe excimer formation in PyPDMA solutions is shown in Scheme 5.2. In Scheme 5.2 there exists an intermediate aggregated pyrene species Py_{k2} that absorbs and emits as a monomer but can quickly rearrange, described by a rate constant k_2, to form *E0*. For pyrene solutions where k_2 is considerably larger than the diffusional time-dependent rate constant $f(t)$, Scheme 5.2 can be approximated by Scheme 5.1 and the expressions describing the monomer and excimer fluorescence can be simplified back to Equations 5.1 and 5.2.

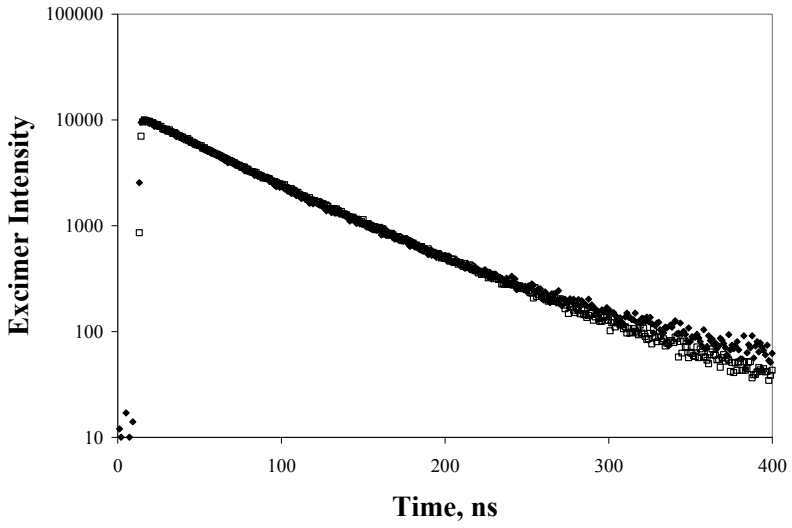

Figure 5.4: Excimer fluorescence decays of a solution of PyHASE65 (◆) and PyPDMA (□) having a pyrene content of 645 μM/g, λ_{ex} = 332 nm.

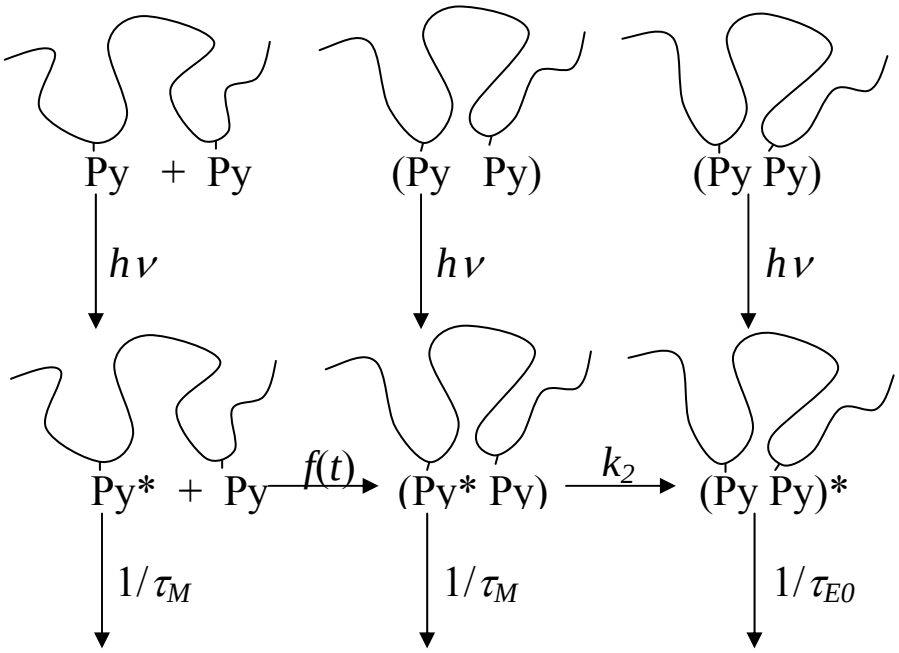

Scheme 5.2: Birks' scheme modified to include the aggregated pyrene intermediate Py^{*}_{k2} and GS pyrene aggregates.

Suprisingly though, the analysis of the PyHASE decays using the set of equations derived for PyPDMA according to Scheme 5.2 was unsuccessful, yielding residuals that were not randomly distributed around zero. The source of the pattern found in the residuals was due to the presence of the pyrene species *ES** which contributed a short decay time of 3.5 ns to the fluorescence excimer which were not accounted for in the equations derived for the PyPDMA samples in Chapter 3. Modification of the equations derived for PyPDMA to account for the pyrene species *ES** yielded good fits having residuals randomly distributed around zero. However the f_{agg} values were found to be wavelength dependent and both the FBM parameters and the rate constant of excimer formation k_2 exhibited significant scatter. The scatter was attributed to the similar values taken by τ_{ES} (3.5 ns) and $1/k_2$ (4.5 ns) which complicates their resolution through the FBM analysis. Our efforts to improve the resolution of the analysis program by fixing various parameters were not successful resulting in

wavelength-dependent f_{agg} trends. These failed attempts led to the conclusion that the fluorescence decays acquired with the PyHASE samples constituted a data set that was not suited to resolve the numerous kinetic processes handled by the equations derived in Chapter 3. Thus, only global analysis using Equations 5.1 and 5.2, which do not account for Py_{k2}, was applied to the analysis of the PyHASE fluorescence decays. Fitting the monomer and excimer fluorescence decays with Equations 5.1 and 5.2 also yielded good fits with the residuals randomly distributed around zero but also gave tighter values for the FBM parameters as a function of wavelength.

5.4 Conclusions

The protocol established in the previous chapters was applied to the fluorescence decays of PyHASE in an attempt to characterize the level of aggregation of pyrenyl pendants in solution. While global analysis of the monomer and excimer fluorescence decays of PyHASE successfully yielded the fluorescence fractions f_{diff}^{f}, f_{free}^{f}, and f_{agg}^{f}, the molar fraction f_{agg} obtained exhibited wavelength dependent characteristics. The inability to satisfactorily determine wavelength independent f_{agg} values prevents the quantitative determination of the level of pyrene aggregation in solution. However, qualitative information retrieved from the fluorescence fraction f_{agg}^{f} may still yield valuable insight on changes in the level of association. This will be particularly useful to monitor changes in the level of association of reversible networks generated in PyHASE aqueous solutions when shear is applied to the solution as done in Chapter 6.

Chapter 6
Simultaneous Probing of Hydrophobic Interactions of an Associative Thickener under Sheared Conditions Using Fluorescence

6.1 Overview

A rheometer was interfaced with both a steady-state and a time-resolved fluorometer to enable simultaneous rheological and fluorescence measurements. Simultaneous fluorescence and rheological measurements were performed on solutions of a model associative thickener, pyrene-labelled hydrophobically-modified alkali-swellable emulsion (PyHASE) polymer, to investigate the changes in the level of association of the hydrophobic pendants when a shearing force is applied. The level of association of PyHASE concentrations between the overlap concentration of 0.5 w/w% to 5 w/w% was measured for shear rates of 0, 0.1 and 100 s^{-1}. Over the range of shear rates studied, the viscosity decreased by over four orders of magnitude, indicating considerable shear thinning. Despite the drop in viscosity observed for sheared solutions of PyHASE, the level of association remained constant for all shear rates studied. The lack of change in the level of association of PyHASE solutions upon shear implies that the hydrophobes rearrange themselves from inter- to intramolecular associations. Latex particles were added to track this switching from inter- to intramolecular aggregation. However, no change in the level of association was observed as a function of shear rate. Although the nature of the hydrophobic rearrangement with shear could not be determined conclusively, these experiments demonstrate quantitatively that the level of association for a PyHASE solution does not change even with considerable shear thinning occurring. These results provide valuable insight on the mechanisms governing the deterioration of a reversible polymeric network of an associative polymer held together by hydrophobic interactions.

6.2 Introduction

Hydrophobically-modified water-soluble polymers (HMWSPs) are water-soluble polymers onto which hydrophobic pendants have been attached. HMWSPs have been used as rheological modifiers in aqueous solution by taking advantage of their ability to form reversible networks.[1] As the pendants of the HMWSPs form intermolecular hydrophobic aggregates, the extended network so created greatly increases the macroscopic viscosity of the aqueous HMWSP solution. This network, held together by the hydrophobic aggregates, is easily disrupted by the application of a shear force. The rearrangement of the aggregates induced by the disruption of the network results in a decrease in viscosity, a phenomenon termed shear thinning. Due to their important industrial role as rheological modifiers, several studies have attempted to model the viscoelastic properties of these peculiar polymeric systems.[2–10] By considering a single HMWSP as a water-soluble chain bearing several "stickers" capable of binding reversibly to other stickers, the diffusion of that chain through the network requires the coordinated detachment and reattachment of many stickers, a concept called "sticky reptation".[2,3] Three parameters can be used to characterize sticky reptation. These parameters are the average number of hydrophobic pendants per aggregate (N_{agg}),[4,9,11,12] the overall fraction of hydrophobic pendants that are associated in solution (f_{agg}) which describes the static network at equilibrium,[2,3,13] and the residence time of a hydrophobic pendant in an aggregate (τ_{res}), which is the inverse of the rate of sticker detachment.[2–5,9]

The importance placed in defining the network of HMWSPs according to these parameters led to an intensive research effort made in the experimental determination of these three parameters for a variety of HMWSP systems. The typical method to determine N_{agg} consists in incorporating a hydrophobic fluorophore and quencher into the hydrophobic aggregates and monitoring the quenching of the excited fluorophore according to models that were established to determine the size of a surfactant micelle.[14–16] The residence time, τ_{res}, has been equated to the relaxation time of the network

generated by simple HMWSP such as monodispersed telechelic hydrophobically-modified ethoxylated urethane (HEUR) polymers where solutions behave like Maxwell fluids.[4] However, τ_{res} cannot be directly determined by this method for more complicated HMWSP systems such as hydrophobically-modified alkali-swellable emulsion (HASE) polymers, as τ_{res} becomes hidden within the distribution of relaxation times of the HASE network.[17] The fraction of hydrophobic pendants which are aggregated, f_{agg}, or the level of association has been determined by a combination of time-resolved fluorescence and absorbance measurements for model systems where the fluorophore pyrene replaced the more typically used alkyl hydrophobic pendants.[18,19]

The ability of pyrene to form excimer has led to its use as a fluorescent label for polymers to study a variety of polymer properties in solution such as coil-to-globule transitions, chain dynamics, and polymer self-association.[20–24] Earlier studies aiming at describing the interactions between the pyrene labels used to probe HMWSPs were limited to monitoring the changes in the spectral features of pyrene, such as the degree of peak broadening in its absorbance spectrum or the magnitude of red-shift between the monomer and excimer excitation spectra, to get qualitative information on the degree of pyrene aggregation.[25] Qualitative information on the level of pyrene aggregation can also be obtained from the analysis of the pyrene excimer fluorescence decays. Since a pyrene aggregate forms an excimer quasi-instantaneously upon excitation by UV-light, a pyrene aggregate forms excimer without delay and hence no rise time can be detected in the excimer decay. If the excimer is formed via the diffusive encounter between two pyrene pendants, excimer formation is delayed and a rise time is observed in the excimer decay. Information on the level of pyrene aggregation is obtained from the magnitude of the ratio A_{E-}/A_{E+} where A_{E-} and A_{E+} represent the sums of, respectively, the negative and positive pre-exponential factors retrieved from the analysis of the excimer decays with a sum of exponentials.[26]

More recently the difference between the excimer formed by diffusion or direct excitation of a pyrene aggregate has been used most effectively to determine the fraction of aggregated pyrenes contributing to the fluorescence decays f_{agg}^{f}.[27–29] Assuming that a pyrene molecule in a pyrene aggregate has the same molar absorbance coefficient as the pyrene monomer, f_{agg}^{f} equals the molar fraction of aggregated pyrenes f_{agg}. The same procedure has been used to determine the molar absorbance coefficient of a pyrene aggregate which can be used in conjunction with f_{agg}^{f} to find the molar fraction of aggregated pyrenes f_{agg}.[18,19]

The peculiar rheological properties of HMWSPs are believed to result from a rearrangement of the polymeric network taking place at the molecular level. Consequently, changes in the parameters that describe the rheological properties of HMWSP solutions at the molecular level are expected to reflect the changes in macroscopic viscoelastic properties of the solution. For instance, as a shearing force is applied, the perturbations to the network induce a strain on the network, particularly at the junction points, which causes the hydrophobic aggregates to rearrange. The observation that the extent of network rearrangement is related to the applied shear rate[30] suggests that this perturbation affects individual polymer coils and might be significant enough to shift the equilibrium between associated and unassociated hydrophobic pendants towards a polymer conformation that favours unassociated hydrophobes, thus changing the overall level of association. This study attempts to answer this question by monitoring the changes in the level of association of a pyrene-labelled HASE (PyHASE) while a shear force is applied to the solution.

The simultaneous coupling of rheology with other techniques such as small-angle light scattering[31–34] and fluorescence microscopy[35] has been successfully performed for several polymeric systems. However, to the best of our knowledge, a single example exists in the literature where fluorescence and rheological measurements were simultaneously performed on a pyrene labelled

HEUR (PyHEUR) by coupling a steady-state fluorometer to a rheometer having a cone-and-plate geometry.[36] Surprisingly, when considering the massive change in the rheological response of the HMWSP solution, this study reported no change in the fluorescence spectra of the PyHEUR sample upon application of shear. Only when the PyHEUR sample contained 25 wt% of acrylic latex particles did the fluorescence spectra show a slight decrease in excimer formation. We hypothesized that the weak response of the fluorescence signal to the massive drop in viscosity observed upon shearing the PyHEUR solution could be due to an inherent deficiency of the experimental set up used. Indeed, since excimers generated by diffusive encounters between pyrene pendants or direct excitation of a pyrene aggregate emit in a similar fashion, differences between the two processes accounting for excimer formation cannot be easily distinguished in a steady-state fluorescence spectrum. As discussed earlier, these differences are readily assessed by acquiring a time-resolved fluorescence decay. With this in mind, an experimental set up was developed for the acquisition of the steady-state fluorescence spectrum and time-resolved fluorescence decays of a fluorescently labelled HMWSP solution as it is sheared with a parallel plate or couette flow geometry. This report presents the fluorescence spectra and decays obtained with a PyHASE solution subjected to no shear and shears of 0.1 and 100 s^{-1}. Within experimental error, the fluorescence spectra and decays of the PyHASE solutions do not show any changes even if shears as high as 100 s^{-1} are applied, implying that association of the hydrophobic pyrenes is unaffected even when the solution viscosity decreases by four orders of magnitude.

6.3 Experimental

Materials: Hexanes (HPLC grade, Fisher), THF (distilled in glass, Caledon), sodium chloride (GR ACS, EMD), hydrogen peroxide (30% certified ACS, Fisher), sulfuric acid (reagent ACS Pur, Fisher), 1,1,1,3,3,3-hexamethyldisilizane (97%, Aldrich), and sodium carbonate (anhydrous, EMD) were used

as received. All aqueous solutions were prepared with Milli-Q water with a resistivity of over 18 MΩ•cm. The polystyrene latex particles were synthesized by Abdul Munam of the Gauthier group and had average diameters of 480 and 420 nm from SEM[37] and dynamic light scattering measurements (Figure SI.6.1 in Supporting Information), respectively.

Pyrene-Labelled HASE Polymer: The pyrene-labelled HASE (PyHASE) polymer was synthesized at DOW Chemical (Union Carbide division) via emulsion polymerization, the details of which are described elsewhere.[38,39] The water of the latex dispersion was removed under vacuum and the polymer was then dissolved in THF. The PyHASE was then purified of residual reactants by precipitation in hexanes three times and then centrifuged to separate any crosslinked polymer. The polymer contained 65 μmol of pyrene per gram of polymer (PyHASE65), as determined by UV-Vis absorbance measurements in THF using the molar absorption coefficient of 1-pyrenemethanol at 344 nm (42,700 $M^{-1}cm^{-1}$) as a standard. Finally, the THF solvent was removed under vacuum and the polymer was dissolved in a 0.01 M Na_2CO_3 solution maintained at pH 9. The overlap concentration of PyHASE65 in the sodium carbonate solution was determined to be 0.5 w/w% by viscometry measurements.

Steady-State Fluorescence Measurements: The steady–state fluorescence spectra were obtained using a Photon Technology International LS–100 steady–state fluorometer with a continuous Ushio UXL-75Xe xenon arc lamp and a PTI 814 photomultiplier detection system. The emission spectra were acquired by exciting the samples at 344 nm. The fluorescence intensities were calculated by integrating the intensities from 372 to 378 nm for the pyrene monomer, I_M, and from 500 to 530 nm for the pyrene excimer, I_E. All solutions were left aerated.

Time-Resolved Fluorescence Measurements: The fluorescence decay profiles were acquired with an IBH Ltd. time-resolved fluorometer equipped with an IBH 340 nm NanoLED. All solutions were excited at 344 nm. The emission wavelength was set at 375 and 510 nm during acquisition of the

pyrene monomer and excimer fluorescence decays, respectively. To reduce the noise stemming from stray scattered light, cutoff filters of 370 and 495 nm were used to acquire the monomer and excimer decays, respectively. All samples were left aerated. All decays were collected over 1,024 channels with a minimum of 10,000 counts taken at the maximum of the monomer and excimer decays to ensure a high signal–to–noise ratio. A Ludox solution was used to obtain the instrument response function. All measured decays were deconvoluted from the lamp profile and fitted to the desired function using a least–squares analysis.[40] The resulting fits were characterized as "good" when the χ^2 parameter was smaller than 1.3 and the residuals and the autocorrelation function of the residuals were randomly distributed around zero.

Analysis of the Fluorescence Decays: In aqueous solution, the pyrene pendants of PyHASE can be classified into two categories: unassociated and associated. The excited unassociated pyrene species consist of isolated excited pyrenes, referred to as Py^*_{free}, that do not form excimer and hence fluoresce with their natural lifetime τ_M, and excited pyrenes that form excimer via diffusional encounters with ground-state pyrenes, Py^*_{diff}. The excited pyrene species that are aggregated can be further classified as well-stacked pyrene dimers that behave as excimers, $E0^*$, long-lived pyrene dimers, EL^*, and short-lived ground-state pyrene aggregates, ES^*. The three aggregated pyrene species represent all excited aggregated pyrene species which are referred to as Py^*_{agg}. To retrieve information on the diffusional formation of excimer, the monomer and excimer decays were fitted with the fluorescence blob model (FBM).[20,41] Accounting for the five pyrene species defined earlier, the monomer and excimer fluorescence decays were fitted with Equations 6.1 and 6.2.

$$[M^*]=[Py^*_{diff}]_{(t=0)}\exp\left[-\left(A_2+\frac{1}{\tau_M}\right)t-A_3\left(1-\exp\left(-A_4\,t\right)\right)\right]+[Py^*_{free}]_{(t=0)}\ \exp\left(-t/\tau_M\right) \quad (6.1)$$

$$\begin{aligned}[E^*]=&-[Py^*_{diff}]_{(t=0)}\,e^{-A_3}\sum_{i=0}^{\infty}\frac{A_3{}^i}{i!}\frac{A_2+i\,A_4}{\frac{1}{\tau_M}-\frac{1}{\tau_{E0}}+A_2+i\,A_4}\exp\left(-\left(\frac{1}{\tau_M}+A_2+i\,A_4\right)t\right)\\&+\left([E0^*]_{(t=0)}+[Py^*_{diff}]_{(t=0)}\,e^{-A_3}\sum_{i=0}^{\infty}\frac{A_3{}^i}{i!}\frac{A_2+i\,A_4}{\frac{1}{\tau_M}-\frac{1}{\tau_{E0}}+A_2+i\,A_4}\right)e^{-t/\tau_{E0}}\\&+[ES^*]_{(t=0)}\,e^{-t/\tau_{ES}}+[EL^*]_{(t=0)}\,e^{-t/\tau_{EL}}\end{aligned} \quad (6.2)$$

The parameters A_2, A_3, and A_4 used in Equations 6.1 and 6.2 are functions of the parameters k_{blob}, $\langle n\rangle$, and $k_{ex}[blob]$ which are the rate constant of quenching by one ground-state pyrene in a blob, the average number of pyrenes per blob, and the product of the rate constant describing pyrenes exchanging between blobs time the local blob concentration, respectively. The parameters of A_2, A_3, and A_4 used in Equations 6.1 and 6.2 are expressed as a function of k_{blob}, $\langle n\rangle$, and $k_{ex}[blob]$ in Equation 6.3.

$$A_2=\langle n\rangle\frac{k_{blob}k_{ex}[blob]}{k_{blob}+k_{ex}[blob]} \qquad A_3=\langle n\rangle\frac{k^2_{blob}}{\left(k_{blob}+k_{ex}[blob]\right)^2}$$

$$A_4=k_{blob}+k_{ex}[blob] \quad (6.3)$$

As previously shown, the parameters obtained from the fits of the monomer and excimer decays to Equations 6.1 and 6.2 can be used to calculate the contributions to the fluorescence decays by the pyrenes that are aggregated f^f_{agg}, form excimers via diffusion f^f_{diff}, or are isolated f^f_{free}.[29]

The natural lifetime of pyrene τ_M was found to increase with PyHASE65 concentration. This increase in τ_M is due to the increase in viscosity experienced by the PyHASE65 solution as the polymer concentration is increased. The value of τ_M used for analysis was obtained by fitting the monomer decay acquired for the PyHASE65 solutions in a triangular cell with a sum of exponentials and taking the largest decay time as τ_M. Thus, τ_M was determined to be 190 ns for 0.5 and 1 w/w%, 200 ns for 2 w/w%, and 210 ns for 3, 4 and 5 w/w% PyHASE65 concentrations.

Error Analysis of the Fluorescence Fractions: The joint rheometer/fluorometer apparatus generates a substantial amount of background noise in all monomer and excimer decays. The effect of the background on the accuracy of the fluorescence fractions retrieved from the global analysis of the pyrene monomer and excimer fluorescence decays with Equations 6.1 and 6.2 was estimated by fitting 10 pairs of simulated monomer and excimer decays having varying levels of background noise and with different patterns of Poisson noise added. These decay pairs were fitted globally using Equations 6.1 and 6.2 and the averaged fluorescence fractions retrieved from the fits given in Table SI.6.1 of Supporting Information. As is shown in Table SI.6.1a, as the background noise increased, some parameters were recovered with wide error bars, particularly τ_{EL}. Upon fixing the values of both τ_{E0} and τ_{ES} in the analysis, the error associated with the fluorescence fractions became independent of background noise levels as shown in Table SI.6.1b. The values of the fluorescence fractions of the simulated decays (0.20 ± 0.00, 0.20 ± 0.00, and 0.60 ± 0.02 for f_{diff}^{f}, f_{free}^{f}, and f_{agg}^{f}, respectively) were in excellent agreement with the initial values (0.20, 0.20, and 0.60 for f_{diff}^{f}, f_{free}^{f}, and f_{agg}^{f}, respectively), suggesting that fixing the value of some of the parameters improves the robustness of the fitting software used. The global analysis of all decays obtained by the rheometer/fluorometer apparatus were fitted with fixed values of τ_{ES} and τ_{E0}. The value for τ_{ES} was fixed to 3.5 ns as found in earlier reports,[42] while τ_{E0} was fixed to the value obtained from fitting the decays acquired for the

solution in the triangular cell. The error estimated for the fluorescence fraction f_{agg}^{f} of 0.60 was approximately 3%. Since the fluorescence fractions values obtained for all PyHASE65 solutions were determined to be relatively insensitive to the range of PyHASE65 concentrations studied, it was assumed that the error on the f_{agg}^{f} values was equal to 3%.

Rheology Measurements: Rheology measurements were carried out on a stress-controlled Paar Physica DSR 4000 rheometer interfaced with a UDS 200 tower. For PyHASE65 concentrations of 2 w/w% and greater, a parallel plate geometry with a custom-made measuring device having a 50 mm diameter fused silica plate was used with a gap width of 1 mm for all samples. For PyHASE65 concentrations of less than 2 w/w%, a bob and cup geometry was used. The bob consisted of a stainless steel cylinder 45 mm in diameter with a 24^{o} cone-shaped bottom and the fused silica cup had an inner diameter of 49 mm. All data points were taken within the sensitivity range of the instrument according to the specifications provided by the manufacturer. Steady-shear viscosity (flow) measurements were performed at room temperature (23 ± 1 ^{o}C) to probe the shear thinning effect over shear rates intervals ranging from 0.001 to 1000 s^{-1}.

Joint Rheometer/Fluorometer Measurements: A schematic of the joint rheometer/fluorometer apparatus is described in Figure 6.1. The simultaneous fluorescence probing of the level of pyrene association for PyHASE65 solutions under shear was performed at the rheometer site. Fluorescence measurements of both the steady-state and time-resolved fluorescence were performed remotely on the PyHASE65 solution sheared in the rheometer with the fluorescence signals being delivered via fibre optic cables to the fluorometers. The excitation light is focused onto the end of the Superguide G high OH UV-Vis nylon jacketed optical fibres purchased from Fiberguide Industries situated inside the fluorometer sample chambers as shown in Figure 6.2. Irradiation of one end of the fibre results in light emerging at the other end that is collimated by the 12 mm × 18 mm collimator fused silica lenses also obtained from Fiberguides Industries. Depending on the measurement device used for the

rheological studies, the collimated excitation light is used to irradiate the sample either from above through the measurement device (parallel plate) or from the side through a window in the outside wall of the sample chamber (Couette flow) as shown in Figure 6.3. The entire rheometer including the collimators is encased in a light shielding box to prevent stray light from interfering with the fluorescence measurements (Figure 6.4).

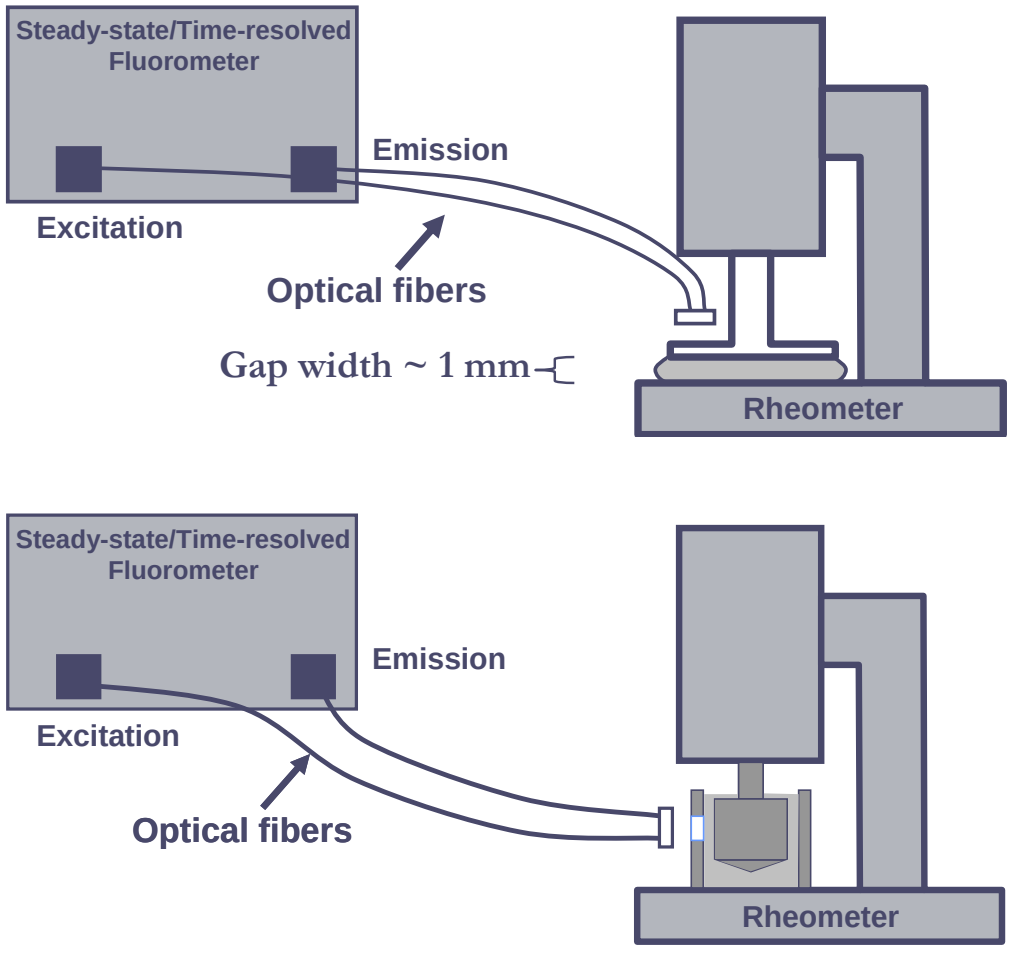

Figure 6.1: Joint rheometer/fluorometer setup with A) parallel plate and B) bob and cup (Couette flow) geometries.

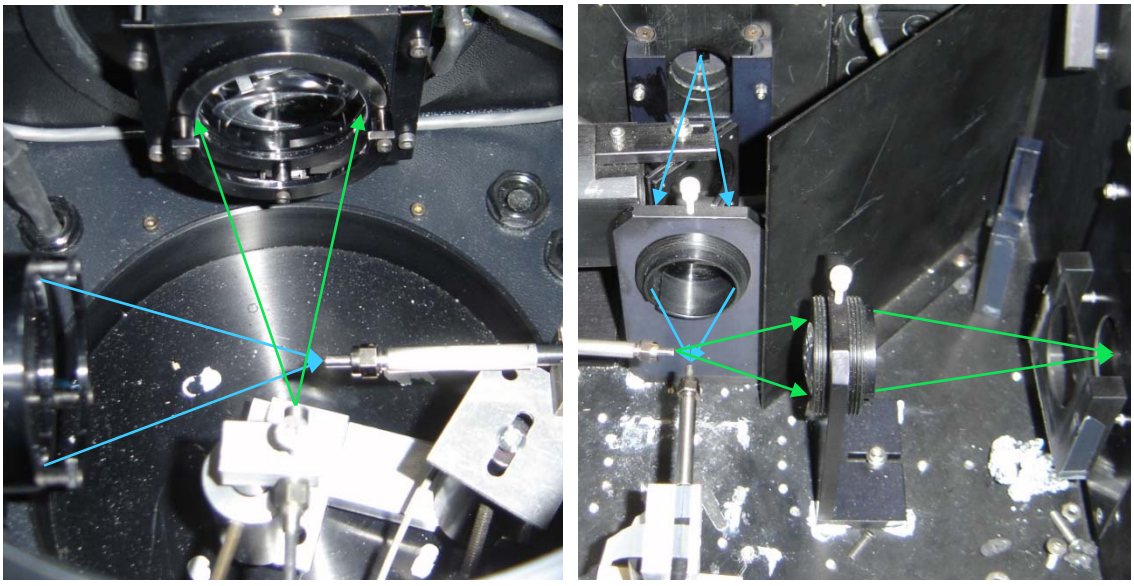

Figure 6.2: Fibre optic set up inside the sample chambers of the single photon counter (left) and the steady-state flurometer (right).

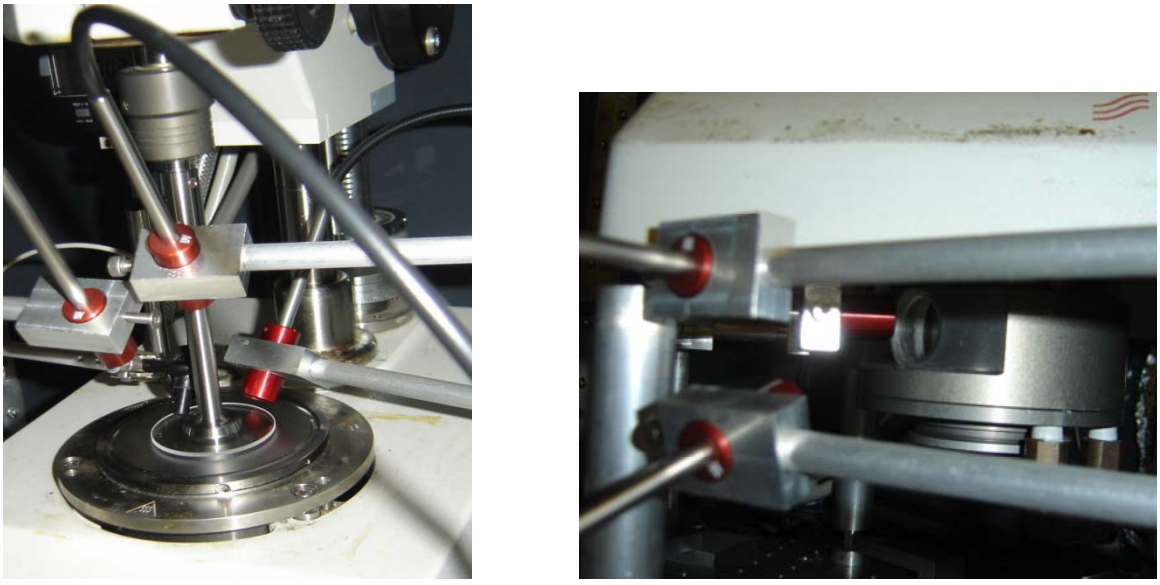

Figure 6.3: Fibre optic configuration at the rheometer site for the parallel plate (left) and the Couette flow (right) geometries.

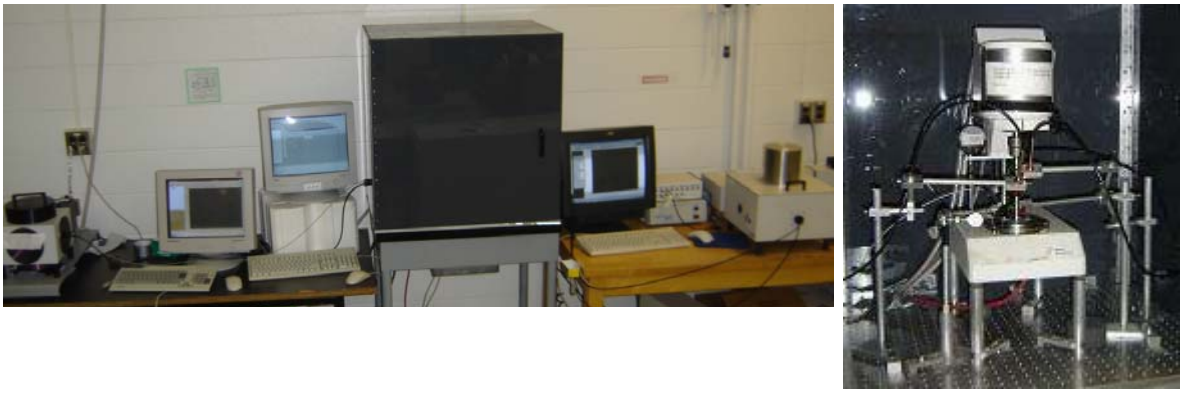

Figure 6.4: The light shielding poly(vinyl chloride) box encasing the rheometer (left) and the rheometer inside the box (right).

Assuming non-slip conditions, the shear rates experienced by a sample in both the parallel plate and bob and cup geometries are not dependent on the depth between the measuring device and the plate or cup.[43] Regardless, a range of depths were probed by varying the concentration of PyHASE65. By increasing the concentration of PyHASE65 from 0.5 to 5 w/w%, the depth where 90% of the photons are absorbed by the PyHASE65 solution decreases from 1 to 0.1 mm.

6.4 Results and Discussion

Shear thinning experiments were carried out using the bob and cup (Couette flow) and parallel plate geometries with PyHASE65 solutions having polymer concentrations of 0.5 and 1 w/w% and 2, 3, 4 and 5 w/w%, respectively. Plots of viscosity versus shear rate were acquired and are referred to as shear thinning profiles. The shear rate and viscosity obtained in all shear thinning profiles acquired for this study are listed in Table SI.6.2. In addition, the shear thinning profiles of the PyHASE solutions acquired with the parallel plate and bob and cup geometries are shown in Figures 6.5 and 6.6, respectively. While shear thinning is occurring, no definitive newtonian plateau was observed for the 2 to 5 w/w% solutions within the shear rates studied between 0.001 to 1000 s^{-1}. This result is not

surprising since previous work with PyHASE indicated that such a plateau would only be observed at shear rates lower than 0.001 s^{-1}.[44] A Newtonian plateau was observed for the 0.5 w/w% PyHASE solution in Figure 6.6. While there was shear thinning occurring for the 0.5 and 1 w/w% solutions, the overall viscosity of these solutions becomes close to that of water (0.89 mPa·s).

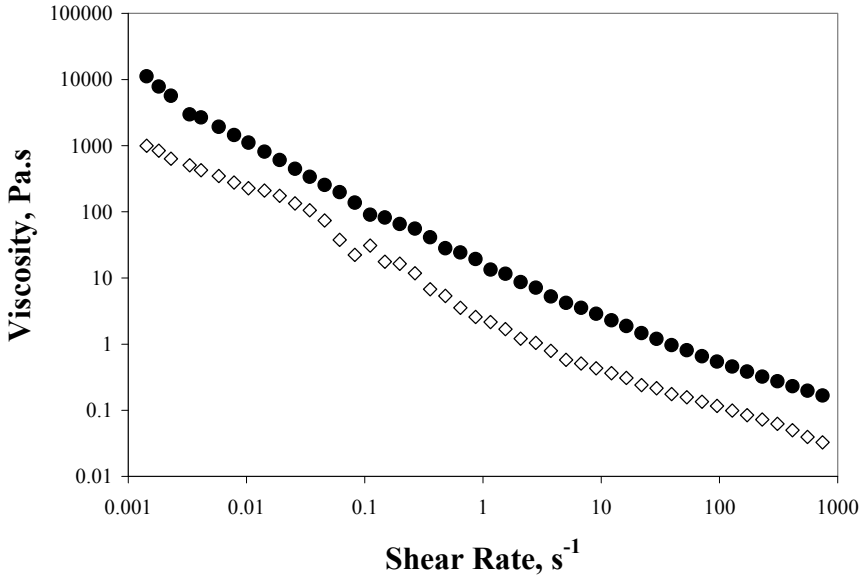

Figure 6.5: Shear thinning profiles of 2 (◇) and 5 (●) w/w% PyHASE65 in 0.01 M Na_2CO_3, pH 9 aqueous solution using the parallel plate geometry.

The steady-state emission spectra of the PyHASE65 solutions were acquired for all concentrations using the remote rheometer/fluorometer apparatus at three shear rates: 0, 0.1 and 100 s^{-1}. According to the shear thinning profiles recorded in Figure 6.5, the viscosities of the 2 and 5 w/w% PyHASE65 solutions varies by at least two orders of magnitude between each shear rate. In addition, the fluorescence spectrum of these PyHASE65 solutions was acquired in the

spectrofluorometer using the front face geometry with a triangular cell to compare it with the fluorescence spectrum of the PyHASE65 solution acquired in the rheometer without shear, i.e. with a 0 s^{-1} shear rate. When normalized at the 375 nm peak of the monomer, the emission fluorescence spectra acquired at all shear rates for a specific concentration exhibited no significant change in their profile as demonstrated in Figure 6.7 for the 5 w/w% PyHASE65 solution. Even when the emission spectrum of the 5 w/w% solution obtained in the triangular cuvette was overlapped with the spectra acquired remotely in the rheometer, no substantial difference could be found between the spectra. This lack of change in the fluorescence spectra was surprising, considering that it occurred despite a change in the macroscopic viscosity by over four orders of magnitude.

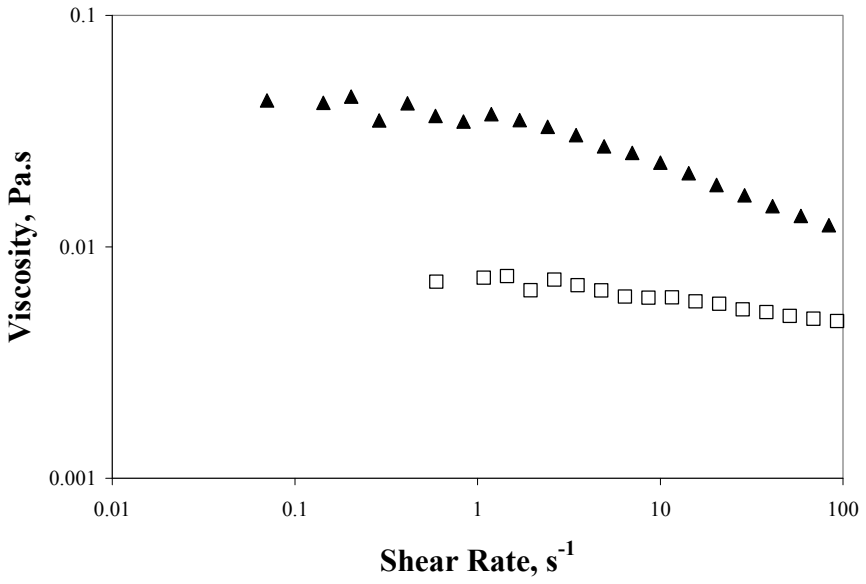

Figure 6.6: Shear thinning profiles of 0.5 (□) and 1 (▲) w/w% PyHASE65 in 0.01 M Na_2CO_3, pH 9 aqueous solution using the bob and cup geometry.

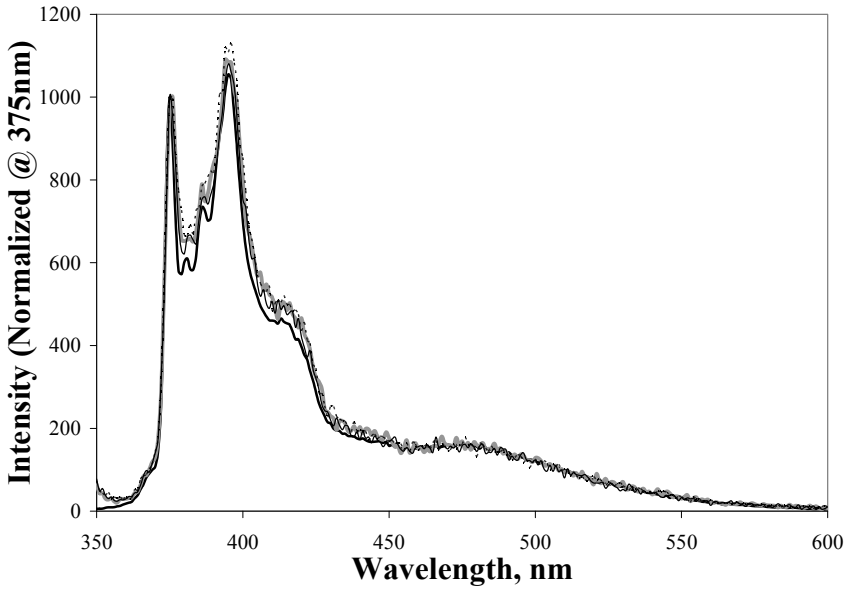

Figure 6.7: Overlapped fluorescence emission spectra normalized at 375 nm of 5 w/w% PyHASE65 solution in 0.01 M Na_2CO_3, pH 9 aqueous solutions acquired with steady-shear rates of 0 (—), 0.1 (—), and 100 (…) s^{-1} and also in a triangular cuvette (—).

To summarize the information obtained with the fluorescence spectra in Figure 6.7, the ratio I_E/I_M was determined for each spectrum. The efficiency of pyrene excimer formation can be characterized by taking the ratio of the fluorescence intensity of the excimer I_E, integrated from 500 to 530 nm, over that of the monomer I_M, integrated from 372 to 378 nm. The I_E/I_M ratio can be considered as a measure of the strength of pyrene-pyrene association, since strong pyrene aggregation will result in more excimer and a larger I_E/I_M ratio. As shown in Figure 6.8, the pyrene associative strength characterized by the I_E/I_M ratio does not depend on shear rate. This result suggests that the level of pyrene association remains constant despite the large changes expected to take place in the arrangement of the polymeric network when shear is applied to the solution.

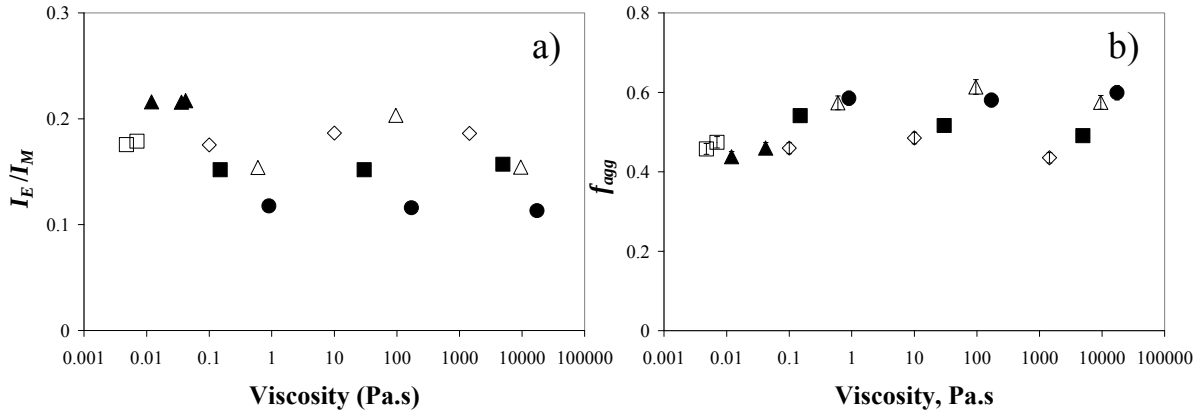

Figure 6.8: a) I_E/I_M ratio and b) f_{agg} of 0.5 (□), 1 (▲), 2 (◇), 3 (■), 4 (△), and 5 (●) w/w% PyHASE65 solutions as a function of the measured shear viscosity.

However, since the information contained in a steady-state fluorescence spectrum does not enable one to differentiate between an excimer formed via the diffuse encounter of two pyrenes or the direct excitation of a pyrene aggregate, the insensitivity of the pyrene fluorescence spectra to shear may not necessarily mean that the fraction of aggregated ground-state pyrenes does not change with shear. Time-resolved fluorescence measurements of the monomer and excimer decays provide information on the time-scale over which an excimer is formed, either quasi-instantaneously via direct excitation of a pyrene aggregate or more slowly via diffusive encounters. In particular, this laboratory has developed a procedure based on the global analysis of the monomer and excimer fluorescence decays that yields the fractional contributions to the solution fluorescence of all the pyrene species present in solution. These fractions referred to as f_{diff}^{f}, f_{free}^{f}, and f_{agg}^{f} enables the quantitative characterization of the level of association of the pyrene-labelled HMWSP in solution. To this end, the monomer and excimer fluorescence decays were acquired for the PyHASE65 solutions

simultaneously with their emission spectra. As with the emission spectra of the 5 w/w% PyHASE65 solutions, the monomer and excimer fluorescence decays acquired at the three different shear rates all overlapped as shown in Figure 6.9.

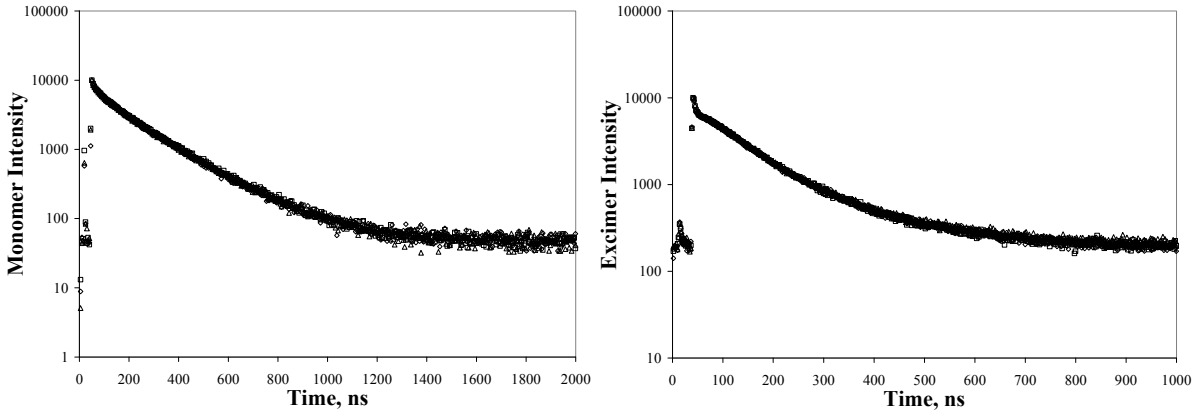

Figure 6.9: Overlapped fluorescence decays of the monomer (left) and excimer (right) of 5 w/w% PyHASE65 solution in 0.01 M Na_2CO_3, pH 9 aqueous solution acquired at steady-shear rates of 0 (◇), 0.1 (□), and 100 (△) s^{-1}.

The global analysis of the monomer and excimer decays was carried out with Equations 6.1 and 6.2, respectively, with the parameters obtained from the fits listed in Table SI.6.3 of Supporting Information. It should be noted that the increased background noise levels of the acquired fluorescence decays yielded greater errors on the values obtained for the fluorescence fractions. To account for this, the monomer and excimer fluorescence decays of the solutions of PyHASE65 were acquired using the triangular cell. These decays had hardly any noise and were used to estimate the values of the lifetimes τ_{E0} and τ_{ES}. These values are given in Table 6.1. The lifetimes were then fixed in the global analysis of the monomer and excimer decays of the PyHASE65 solutions acquired with

the joint rheometer/fluorometer apparatus. The fits yielded the fluorescence fractions f_{agg}^{f}, f_{diff}^{f}, and f_{free}^{f} which are listed in Table 6.1 with their corresponding measured viscosities. Examination of the fractions shows that they remained constant with shear rate despite the large changes in solution viscosity. However, f_{agg}^{f} was found to increase slightly from 0.46 ± 0.01 at 0.5 w/w% to about 0.60 ± 0.02 at 5 w/w% suggesting some enhanced pyrene aggregation as the PyHASE concentration increases.

The phenomenon of shear thinning observed for a reversible HMWSP network in aqueous solution has found great industrial interest due to its commercial applications. Thus, it would be useful to study the state of the network at the molecular level while it is being disturbed by shearing forces. The component of a HMWSP that plays a key role in thickening the solution is the hydrophobe. Being aggregated intermolecularly at rest, they are displaced by the strain induced by the external shear. This effect was investigated with PyHASE65. Analysis of the steady-state fluorescence spectra and the pyrene monomer and excimer fluorescence decays obtained for the sheared PyHASE65 solutions indicate that the relative amount of the hydrophobic pyrene pendants that were aggregated remained unchanged, despite a four orders of magnitude drop in the overall solution viscosity. This result implies that the equilibrium between the associated and unassociated pyrenes under zero shear conditions is unaffected by the application of shear. Thus the application of shear to the solution induces the hydrophobic pendants of HMWSPs to rearrange in a manner that merely reduces the number of intermolecular bridges in favour of intramolecular associations rather than increasing the number of dangling ends.[1,10,36,45,46]

Table 6.1: Pyrene fluorescence fractions of PyHASE65 in 0.01 M Na_2CO_3, pH 9 aqueous solutions obtained by the FBM global analysis of the monomer and excimer decays with τ_{E0} and τ_{ES} fixed. Note: samples marked with * were analyzed using decays obtained for solutions in a triangular cell.

[PyHASE65] w/w%	$Depth_{@90\%Abs}$ mm	Shear Rate s^{-1}	Viscosity Pa.s	τ_M ns	τ_{E0} ns	f^f_{diff}	f^f_{free}	f^f_{agg}
0.5	1.0	0*	0.0071	190	56	0.27	0.26	0.46
		0	0.0071	190	56	0.31	0.21	0.47
		100	0.0048	190	56	0.32	0.22	0.46
1	0.50	0*	0.042	190	56	0.33	0.25	0.42
		0	0.042	190	56	0.30	0.24	0.46
		100	0.012	190	56	0.34	0.23	0.44
2	0.25	0*	1440	200	60	0.34	0.19	0.47
		0	1440	200	60	0.29	0.27	0.44
		0.1	10	200	60	0.34	0.18	0.49
		100	0.11	200	60	0.33	0.21	0.46
3	0.17	0*	4950	210	62	0.31	0.17	0.52
		0	4950	210	62	0.29	0.22	0.49
		0.1	30	210	62	0.29	0.19	0.52
		100	0.15	210	62	0.28	0.18	0.54
4	0.13	0*	9520	210	64	0.23	0.19	0.58
		0	9520	210	64	0.23	0.20	0.57
		0.1	96	210	64	0.20	0.19	0.61
		100	0.60	210	64	0.21	0.21	0.57
5	0.10	0*	17300	210	68	0.19	0.19	0.63
		0	17300	210	68	0.19	0.21	0.60
		0.1	170	210	68	0.22	0.20	0.58
		100	0.9	210	68	0.20	0.21	0.59

The fluorescence results demonstrate that as the pyrene labelled PyHASE65 solution is being sheared, the fraction of aggregated hydrophobes remains unchanged. In other words, while the

hydrophobes rearrange themselves to favour the formation of intra- versus intermolecular aggregates as the solution is sheared, this rearrangement occurs without affecting the balance between the associated and unassociated hydrophobes. To investigate this concept further, latex polystyrene particles having an average diameter of 480 nm were added to the solution. Experiments conducted by Richey et al.[36] indicated that the addition of large amounts of latex particles induced a small reduction in the excimer intensity as the sample was sheared. The explanation for this effect was that the pyrene pendants involved in the formation of intermolecular bridges generating excimer would rearrange themselves by binding onto the latex particle surface, thus reducing the fluorescence excimer intensity as illustrated in Scheme 6.1. It is important to note that the maximum latex content of 2 w/w% attempted in this study was far less than that of 25 w/w% prepared by Richey et al., as higher latex contents did not yield homogeneous solutions with PyHASE65. The dispersions exhibited shear thinning behaviour as shown in Table SI.6.4 of Supporting Information and Figure 6.10. Once again though, the fluorescence data suggest that the application of shear to the solutions induces no change in the level of pyrene association as observed by the lack of change in the I_E/I_M ratio and the fraction f_{agg}^{f} as is shown in Figure 6.11 and Table 6.2, respectively. The lack of change in I_E/I_M and f_{agg}^{f} with shear rate suggests that the influence of the latex is too subtle to have any significant effect on the fluorescence character of the PyHASE65 solutions even when investigated with the more sensitive time-resolved fluorescence measurements. Another reason for this lack of sensitivity is that the PyHASE65 used in these experiments is considered to have a high pyrene content compared to the PyHASE samples studied by Prazeres et al.[44] PyHASE samples having a larger pyrene content are expected to generate more intramolecular pyrene aggregates due to their more hydrophobic character. As shear thinning occurs, the few intermolecular junctions required to disrupt the entire network and alleviate the strain caused by the shear force may not significantly affect the ratio of inter- to intramolecular associations. Thus even in the presence of latex the fluorescence

of the PyHASE65 solutions may not be affected appreciably by shear. An experiment that might clearly probe the switch taking place between inter- and intramolecular polymeric aggregates more may require the spiking of non-fluorescent commercial HASE solutions with a small percentage of a low labelling level PyHASE like PyHASE12, which has been shown to generate more intermolecular associations.

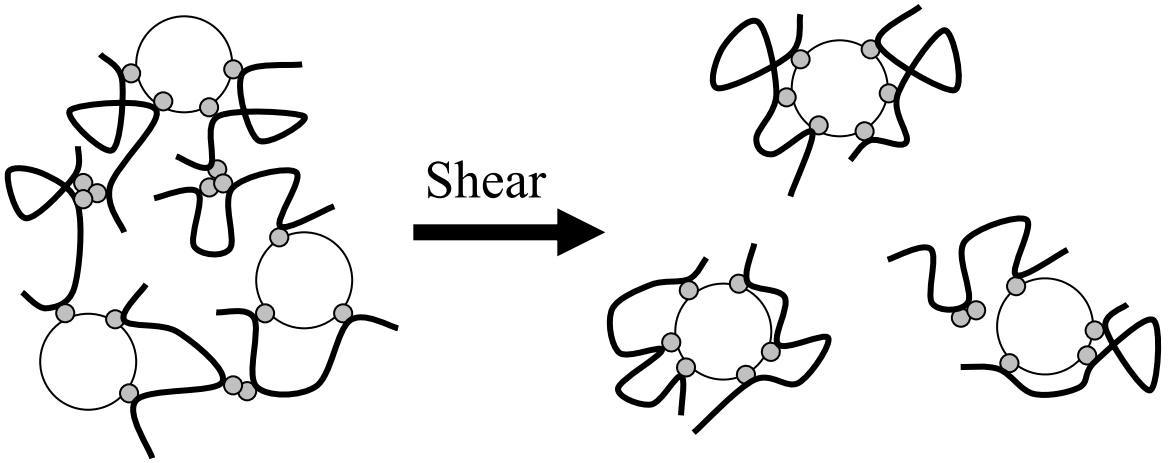

Scheme 6.1: Proposed effect of an external shearing force on the equilibrium between associated and unassociated hydrophobic pendants of an HMWSP network in the presence of latex particles.

The results presented so far were analyzed assuming that the fluorescence experiments probe the bulk of the solution. However, the fluorescence results might actually reflect the behaviour of the thin layer of PyHASE adsorbed onto the surface of the quartz plate and not that of the bulk. The pyrene pendants found in this layer would be expected to behave differently from those found in the bulk. Depending on the thickness of this layer with respect to the solution depth probed by

fluorescence, the fluorescence contribution from the adsorbed layer might significantly influence the fluorescence data. Typically, only a monolayer of the polymer is expected to adsorb onto the surface of fused silica where, depending on the surface density of adsorbed polymer, the polymers can be in either a flatten or extended conformation.[47,48] A study of the adsorption of amphiphilic PEO-polytetrahydrofuran-PEO tri-block copolymers onto fused silica surfaces at water interfaces saw increased adsorption of the polymer in order to minimize contact between the hydrophobic components of the copolymer and water.[48] The increased adsorption results in a thicker layer of adsorbed polymer which is weakly held together by hydrophobic interactions much like the aggregates of the copolymers in the bulk.

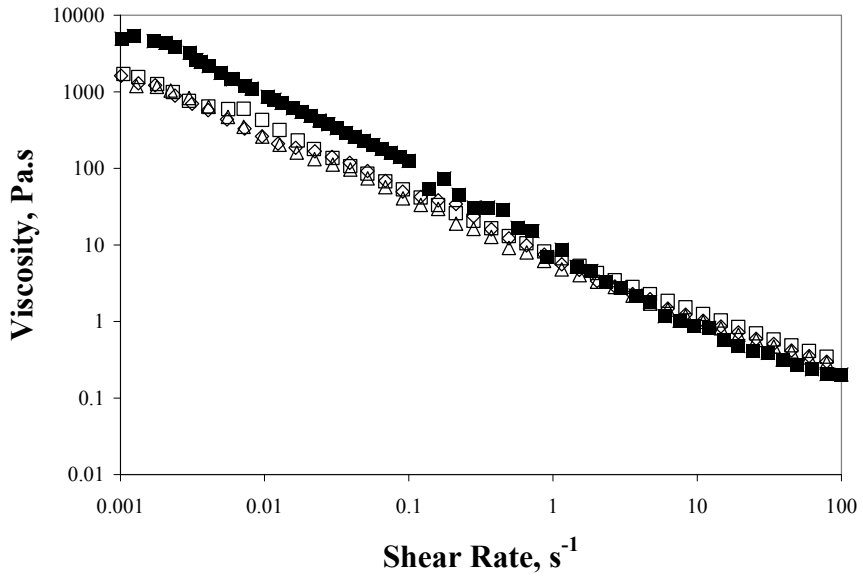

Figure 6.10: Shear thinning profiles of 3 w/w% PyHASE65 in 0.01 M Na_2CO_3, pH 9 aqueous solution with 0 (■), 0.5 (◇), 1 (□), and 2 (△) w/w% 480 nm diameter polystyrene latex particles.

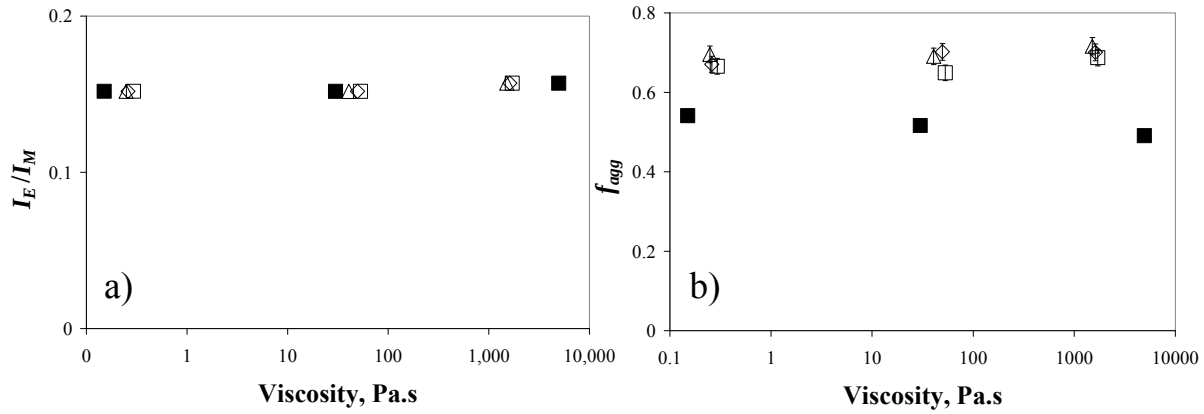

Figure 6.11: I_E/I_M ratio of 3 w/w% PyHASE65solution in the presence of 0 (■), 0.5 (◇), 1 (□), and 2 (△) w/w% 480 nm diameter polystyrene latex particles as a function of the measured shear viscosity.

Table 6.2: Pyrene fluorescence fractions of 3 w/w% PyHASE65 solutions with 480 nm polystyrene latex particles obtained by global FBM analysis of the monomer and excimer decays with τ_{E0} = 62 ns and τ_{ES} = 3.5 ns.

Latex content w/w%	Shear Rate s^{-1}	Viscosity Pa.s	f^{f}_{diff}	f^{f}_{free}	f^{f}_{agg}
0	0	4950	0.29	0.22	0.49
	0.1	30	0.29	0.19	0.52
	100	0.15	0.28	0.18	0.54
0.5	0	1620	0.16	0.14	0.70
	0.1	50	0.16	0.13	0.70
	100	0.26	0.18	0.15	0.67
1	0	1710	0.16	0.16	0.69
	0.1	53	0.20	0.16	0.65
	100	0.29	0.18	0.16	0.67
2	0	1510	0.14	0.15	0.72
	0.1	41	0.17	0.14	0.69
	100	0.25	0.17	0.14	0.70

To draw comparisons to the immobilized layer of PyHASE on the fused silica measuring device, the thickness of the adsorbed polymer layer should be at most three times the radius of gyration of the polymer. According to the study by Wang et al.,[49] the radius of gyration of HASE polymers at pH 9 is less than 100 nm. Thus the thickness of the adsorbed layer is expected to be less than 300 nm. An estimate of the light absorbed by such a layer at even the highest concentration studied of 5 w/w% PyHASE65 in this report would be less than 0.7% of the total light absorbed. This calculation suggests that the overall contribution of the PyHASE65 adsorbed onto the surface of the fused silica contributes a negligible amount to the overall fluorescence of the solution.

Regardless, an attempt to verify this claim experimentally was made by acquiring the monomer and excimer fluorescence decays of PyHASE65 solutions adsorbed onto pre-treated fused silica cuvettes. The fused silica surface was made both hydrophilic using a heated piranha solution[50] and hydrophobic by treating the surface with liquid hexamethyldisilizane (HMDS).[51,52] A 3 w/w% PyHASE65 solution was allowed to settle in the treated cuvette for five minutes to enable adsorption of PyHASE65 onto the surface. The PyHASE solution was then pipetted out of the cell and five successive rinses of the cell with 0.01 M Na_2CO_3 solution removed any excess PyHASE65 that was not adsorbed onto the surface of the cuvette. Afterwards, the monomer and excimer fluorescence decays of the PyHASE adsorbed onto the surface of the cuvette were acquired using the front face geometry and were fitted using a sum of exponentials. The parameters retrieved from the analysis of the monomer and excimer decays are listed in Table 6.3. According to the fits, both hydrophilic and hydrophobic treatments of the fused silica yielded identical monomer and excimer fluorescence decays. The excimer decays of PyHASE65 adsorbed onto the cuvette walls treated by either the piranha solution or HMDS showed no apparent rise time indicating that the pyrenes are immobilized. Overall, these decays bear little resemblance to the decays of the concentrated PyHASE65 solutions obtained with the joint rheometer/fluorometer system as they have a shorter but heavier weighted long

monomer decay time and lack a rise time in the excimer. Since the monomer and excimer decays of PyHASE65 adsorbed on the cuvette walls are considerably different from those acquired with the PyHASE65 solutions, it can be concluded that regardless of the thickness of the PyHASE65 layer adsorbed onto the quartz surface, this layer does not affect our fluorescence experiments.

Table 6.3: Fitted parameters using a sum of exponentials for the fluorescence monomer (top) and excimer (bottom) decays for 3 w/w% solutions of PyHASE65 in the bulk using an untreated triangular cell, adsorbed onto a piranha treated (hydrophilic), and 1,1,1,3,3,3-hexamethyldisilizane (hydrophobic) treated surface of fused silica.

Treatment	τ_{M1} ns	a_{M1}	τ_{M2} ns	a_{M2}	τ_{M3} ns	a_{M3}	χ^2
Bulk/ Untreated	16.9	0.247	98.5	0.284	209.3	0.469	1.04
Piranha	9.0	0.233	70.8	0.230	149.2	0.537	0.99
HMDS	10.4	0.175	64.0	0.270	150.7	0.555	1.08

Treatment	τ_{E1} ns	a_{E1}	τ_{E2} ns	a_{E2}	τ_{E3} ns	a_{E3}	τ_{E4} ns	a_{E4}	χ^2
Bulk/ Untreated	3.1	0.530	39.3	-0.198	68.6	0.531	178.1	0.137	1.01
Piranha	53.8	0.894	131.2	0.106					1.03
HMDS	56.3	0.911	143.3	0.089					1.13

In this study, steady-shear rate experiments were performed at a shear rate of 0, 0.1 and 100 s^{-1} while the fluorescence spectrum and monomer and excimer decays of the PyHASE65 solutions

were acquired. Since the shear rate was held constant for each fluorescence measurement, one can assume that the association of the hydrophobic pendants had reached equilibrium during acquisition. Thus, deformation of the network which could momentarily shift the balance of aggregated to unaggregated hydrophobes had already occurred prior to the initiation of the fluorescence data acquisition. To investigate whether shear withdrawal would induce an instantaneous shift in the level of association, the fluorescence intensity of the solution was monitored at 375 nm over time as the shear rate was brought from 100 to 0 s^{-1}. Since there is a trade off between the signal-to-noise ratio and time resolution, this experiment was performed at varying data acquisition rates (Figure 6.12). As the resolution of the instrument increased from 0.001 to 1 second per data point, the signal-to-noise ratio (S/N) dropped from 25% (Figure 6.12d) to 0.4% (Figure 6.12a). However at all resolutions monitored even with S/N of less than 5% (measured time intervals of 10 ms or greater), no fluorescence change was detected at the transition. This indicates that any effect to the balance of aggregated to unaggregated hydrophobes caused by the sudden withdrawal of shear exists on a time scale smaller than 10 ms.

6.5 Conclusions

The level of association of a pyrene labelled HASE polymer was monitored while the solutions were subjected to shear thinning. This was accomplished by performing simultaneous fluorescence, transmitted to the fluorometer via fibre optic cables, and rheological measurements. The analysis of the obtained monomer and excimer fluorescence decays by the FBM global analysis gave the pyrene fluorescence fractions which are related to the actual pyrene fractions in the solution. For all concentrations studied between the overlap concentration of 0.5 to 5 w/w%, no changes in the level of association, f_{agg}^{f}, were observed (Figure 6.8b) despite large changes in the solution viscosity due to considerable shear thinning (Figure 6.5). This lack of change in f_{agg}^{f} implied that the hydrophobic

pendants that were displaced from the aggregates when the network was sheared quickly formed new aggregates.

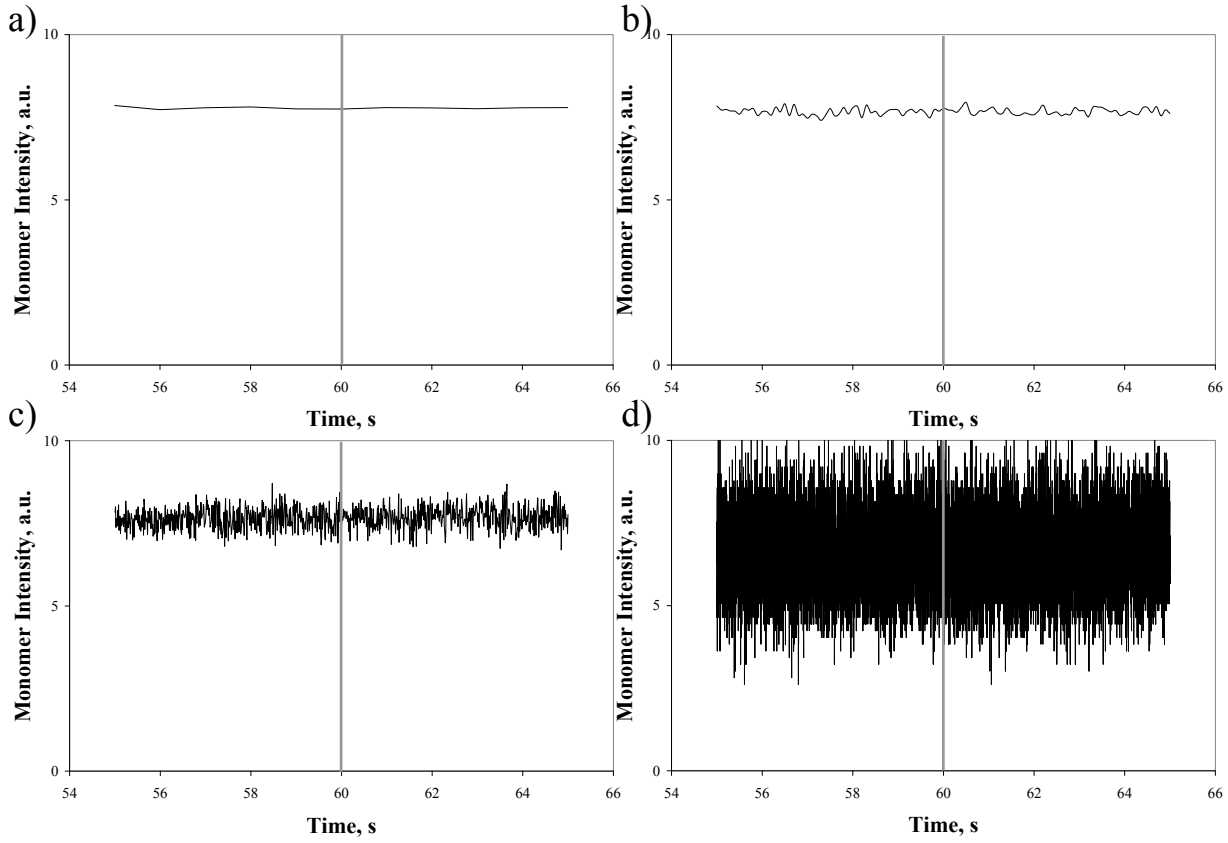

Figure 6.12: Fluorescence intensity at 375 nm of 3 w/w% PyHASE65 sheared at a rate of 100 s^{-1} withdrawing the shear after 60 s at resolutions of a) 1; b) 10; c) 100; d) 999 points per second.

According to the trends shown in Figure 6.12, the rearrangement of the displaced hydrophobic pendants occurs on a time scale smaller than 10 milliseconds. These results indicate that the new aggregates are likelier to form intramolecularly in order to explain the drop in the overall solution

viscosity. In an attempt to probe the switch occurring between intermolecular bridging to intramolecular associations, latex particles were added to the PyHASE65 solution. Unfortunately, at the latex contents that this study was able to achieve, no changes in the level of association were observed (Figure 6.11b).

The static reversible network can be defined by three parameters, N_{agg}, f_{agg}, and the ratio of inter- to intramolecular associations. The lack of change in the fluorescence character of PyHASE65 solutions upon being sheared indicates that the parameters N_{agg} and f_{agg} are unaffected by shear. Thus, the decrease in macroscopic viscosity must be due to a shift in the ratio of inter- to intramolecular association. Future experiments will aim to probe this phenomenon.

Chapter 7
Summary

The purpose of this thesis was to characterize the self-assembly of pyrene-labelled amphiphilic molecules in aqueous solution. The amphiphilic molecules considered were pyrene-labelled phospholipids (PLLs) forming liposomes, and three pyrene-labelled water-soluble polymers, namely pyrene-labelled poly(*N*,*N*-dimethylacrylamide) (PyPDMA), pyrene-labelled poly(ethylene oxide) (PyPEO), and pyrene-labelled hydrophobically-modified alkali-swellable emulsion (PyHASE) polymers forming reversible networks. The labelling of the macromolecules with the chromophore pyrene enabled us to take advantage of the excimer forming capability of pyrene to monitor hydrophobic aggregation of the amphiphilic molecules by fluorescence. The use of pyrene as a fluorescent label to monitor self-assembly at the molecular level is well documented.[1,2] Despite its extensive use, the fluorescence and absorbance properties of pyrene in its aggregated form are poorly characterized, making it impossible to quantitatively determine the molar fraction of pyrenes that are aggregated in solution (f_{agg}). This thesis attempted to characterize the absorbance properties of a series of pyrene aggregates thereby enabling the quantitative determination of f_{agg} for model pyrene-labelled hydrophobically modified water-soluble polymers (PyHMWSPs).

In Chapter 2, time-resolved fluorescence measurements on liposomes prepared with 1 mol% of pyrene-labelled lipids (PLLs) with a head group bearing either an alcohol (PSOH) or an imido diacetic acid (PSIDA) and 99 mol% of 1-palmitoyl-2-oleyl-3-*sn*-phosphatidylcholines (POPC) or 99 mol% of distearylphosphatidylcholine (DSPC) yielded information on the organization of the lipids within the membrane bilayer. The monomer and excimer fluorescence decays were fitted globally using the fluorescence blob model (FBM) to describe the kinetics of excimer formation.[3] The results from the global analysis led to the conclusion that the PLLs were homogeneously distributed on the

surface of the POPC vesicles while the PLLs phase-separated in the DSPC vesicles, partitioning into the amorphous channels separating the semi-crystalline regions of DSPC.[4] Large f_{agg}^{f} values found for PSIDA suggested that the imido diacetic acid head group of PSIDA induces self-aggregation and phase separation in both POPC and DSPC membranes. The addition of external cations such as Cu^{2+} and La^{3+} was shown to hinder diffusional encounters between isolated PSIDA lipids but was also found to not significantly affect the aggregated clusters. This counterintuitive result led to the conclusion that the cations target preferentially unassociated PSIDAs rather than aggregated PSIDA clusters which was rationalized by proposing that electrostatic repulsion prevents successive binding of metal ions to an aggregate. Another development of the liposome work was the realization that quenching of the pyrenyl pendant of PSIDA by Cu^{2+} could be used to determine the microviscosity of the lipid membrane in which PSIDA was embedded. PSIDA in the DSPC membrane is believed to locate itself into the amorphous channels of DSPC. This environment probed by PSIDA was found to be 5.4 times more viscous than the environment probed by PSIDA in the POPC membrane. From these fluorescence measurements, information on the organization of the membranes of two different liposomes was obtained in addition to gaining further insight on the mechanism of binding of multivalent ions with functionalized polar head groups.

In Chapters 3, 4, and 5, the pyrene aggregates of three PyHMWSPs were characterized using fluorescence and absorbance measurements. Chapter 3 determined the molar absorption coefficient of pyrene aggregates, ε_{E0}, for a series of pyrene-labelled poly(*N*,*N*-dimethylacrylamide)s (PyPDMA) having pyrene contents ranging from 263 to 645 μmol of pyrene per gram of polymer. The global analysis of the monomer and excimer fluorescence decays yielded the fractions of the various pyrene species present in solution weighed by their molar absorbance coefficient and radiative rate contants. Combining the fractions obtained from the global analysis of the fluorescence decays with the absorption of the PyPDMA solution enabled the determination of the level of association f_{agg} for

PyPDMA and the molar absorbance coefficient of pyrene aggregates ε_{E0}. For all pyrene contents studied, similar ε_{E0} values over the range of wavelengths from 325 to 350 nm were obtained. The averaged ε_{E0} was found to be red-shifted relative to the molar absorbance coefficient of unassociated pyrenes by 3 nm in addition to having a value at the 0-0 peak of 21,000 $M^{-1}cm^{-1}$ compared to a value of 34,700 $M^{-1}cm^{-1}$ for unassociated pyrenes. The broader and red-shifted ε_{E0} spectrum obtained for the aggregated pyrenes of aqueous solutions of PyPDMA agrees with previous observations made about the absorption spectra of other pyrene-labelled polymers thought to generate pyrene aggregation.[1] The protocol established in Chapter 3 was then applied to other PyHMWSPs such as those studied in Chapters 4 and 5.

Chapter 4 applied the protocol developed in Chapter 3 to the aggregates made from aqueous solutions of short chains of poly(ethylene oxide) terminated at one end with a pyrenyl pendant (PyPEO). Monomer and excimer fluorescence decays of a PyPEO polymer in water were fitted to a model free global analysis to determine the fraction of pyrenes that were aggregated in solution f_{agg} and also the molar absorbance coefficient of the pyrene aggregates, ε_{E0}. Prior to the application of the procedure, a model free (MF) analysis had to be developed which made no assumptions on the kinetics of excimer formation. This was necessary as the kinetics of excimer formation of PyPEO are different from those of randomly-labelled polymers such as PyPDMA which can be described by the FBM. To test the validity of the MF approach, it was first applied to the monomer and excimer fluorescence decays of solutions of molecular pyrene dissolved in cyclohexane, acetonitrile and *N*,*N*-dimethylformamide (DMF) and 1-pyrenemethanol dissolved in acetonitrile. The diffusional rate constant of excimer formation defined as $< k_1 >=< \tau^{-1} > -\frac{1}{\tau_M}$ obtained from the MF analysis matched exactly the rate constant k_1 obtained from the Birks' scheme.[5] Thus it was concluded that the MF analysis was capable of yielding kinetic information on excimer formation that is similar to that

obtained with the well-established Birks' scheme. With the validity of the MF analysis verified, the protocol was applied to the analysis of the fluorescence decays of PyPEO. This study yielded the level of association f_{agg} of PyPEO in water and the molar absorbance coefficient of their aggregates ε_{E0} for a range of wavelengths from 325 to 347 nm. The overall features of the ε_{E0} spectrum obtained for PyPEO in water were similar to those observed for the ε_{E0} spectrum obtained for aqueous solutions of PyPDMA. The small differences found in the ε_{E0} spectra were attributed to differences in the nature of the pyrene aggregates, being composed of *E0* and *EL* species for PyPDMA and *ES* and *E0* species for PyPEO.

The protocol was applied to PyHASE solutions as described in Chapter 5. Unlike the results seen in Chapter 3 and 4, the level of association f_{agg} obtained for PyHASE were not wavelength independent. The absorption spectra of PyHASE was observed to have minimal peak broadening suggesting low pyrene aggregation even though the excimer decays showed little rise time. It was concluded that the monomer and excimer decays of PyHASE solutions were too complex to quantitatively determine the level of pyrene aggregation although qualitative changes in the level of association could still be monitored using the fluorescence fraction f_{agg}^{f}.

Chapter 6 focused on the simultaneous fluorescence and rheological measurements of PyHASE solutions, in order to investigate the changes in the level of association of the hydrophobic pendants for a reversible network when a shearing force is applied. To accomplish this task, a rheometer was interfaced with both a steady-state and time-resolved fluorometer to enable simultaneous rheological and fluorescence measurements. The level of association of PyHASE concentrations between the overlap concentration of 0.5 w/w% to 5 w/w% was measured for shear rates of 0, 0.1 and 100 s^{-1}. Over the range of shear rates studied, considerable shear thinning occurred as the viscosity was observed to decrease significantly, by four orders of magnitude for the higher concentrations studied. Despite the drop in viscosity observed for the sheared solutions of PyHASE,

the level of association remained constant for all shear rates studied. The lack of change in the level of association for PyHASE solutions upon application of shear implies that shear does not alter the equilibrium between aggregated and isolated pyrene pendants but rather induces the hydrophobes to rearrange themselves from inter- to intramolecular associations.[6–8] The addition of latex polystyrene particles was attempted in an effort to trap the pyrene pendants onto the surface of the latex particle as the switching takes place. Unfortunately this experiment was unsuccessful as no change to the level of association was observed as a function of shear rate. Although the switching from inter- to intramolecular associations with shear could not be determined conclusively, these experiments demonstrate quantitatively that the level of pyrene association of PyHASE solutions remains constant while the solution undergoes shear-thinning. These results provide valuable insight on the mechanisms governing the deterioration of a reversible polymeric network of hydrophobically-modified water-soluble polymers by shear.

The use of pyrene to characterize the self-assembly of pyrene-labelled macromolecules has already been well-established.[1,2] Standard steady-state and time-resolved fluorescence measurements are known to provide extensive insight about the nature of self-assembled macromolecules. However, this information retrieved from these types of experiments is mostly qualitative in nature resulting from suggested explanations that rationalize the observed effects qualitatively. For instance, the broadening of an absorption spectrum of a pyrene-labeled macromolecule in water is rationalized by saying that pyrene aggregates have a broader absorption spectrum, although the absorption spectrum of a pyrene aggregate has never been reported in the literature. The absence of a risetime in an excimer decay suggests that excimer are formed instantaneously from the direct excitation of a pyrene aggregate. Although sensible from a qualitative point of view, these explanations are almost never put to the ultimate test via a quantitative analysis of the fluorescence and absorption data. One major contribution of this thesis is to have attempted, and in many cases succeeded, in deriving a set of

sensible equations that describe quantitatively the phenomena at hand and developed improved analysis programs that can retrieve reliable kinetic parameters from complex fluorescence decays.

These enhanced analytical tools were applied to determine for the first time a spectrum of the molar absorbance coefficient as a function of wavelength for two types of pyrene aggregates generated by aqueous solutions of poly(*N*,*N*-dimethylacrylamide) randomly labeled with pyrene (Py-PDMA) and poly(ethylene oxide) terminated at one end with a pyrenyl pendant (PyPEO). These analysis programs were also applied to determine the apparent level of pyrene aggregation f_{agg} for two pyrene-labeled lipids, PyPDMA, PyPEO, and PyHASE, a pyrene-labeled hydrophobically modified alkali swellable copolymer.

Finally, this thesis demonstrated for the first time that both steady-state and time-resolved fluorescence measurements can be conducted on a solution of a pyrene-labeled associative thickener, namely PyHASE, while it is being sheared in a rheometer. Again, the analytical tools developed for the global analysis of the monomer and excimer fluorescence decays were applied to the decays acquired with PyHASE solutions sheared in the rheometer. These coupled experiments are important because information about the nature of the pyrene excimer, whether formed by diffusion or direct excitation of a pyrene aggregate, can only be inferred from the analysis of fluorescence decays. Consequently, the experiments conducted in Chapter 6 constitute the only evidence in the literature suggesting that the level of association between the hydropbic pendants of an associative thickener (AT) does not change while the AT solution is being sheared.

Appendix

Chapter 2 Supporting Information

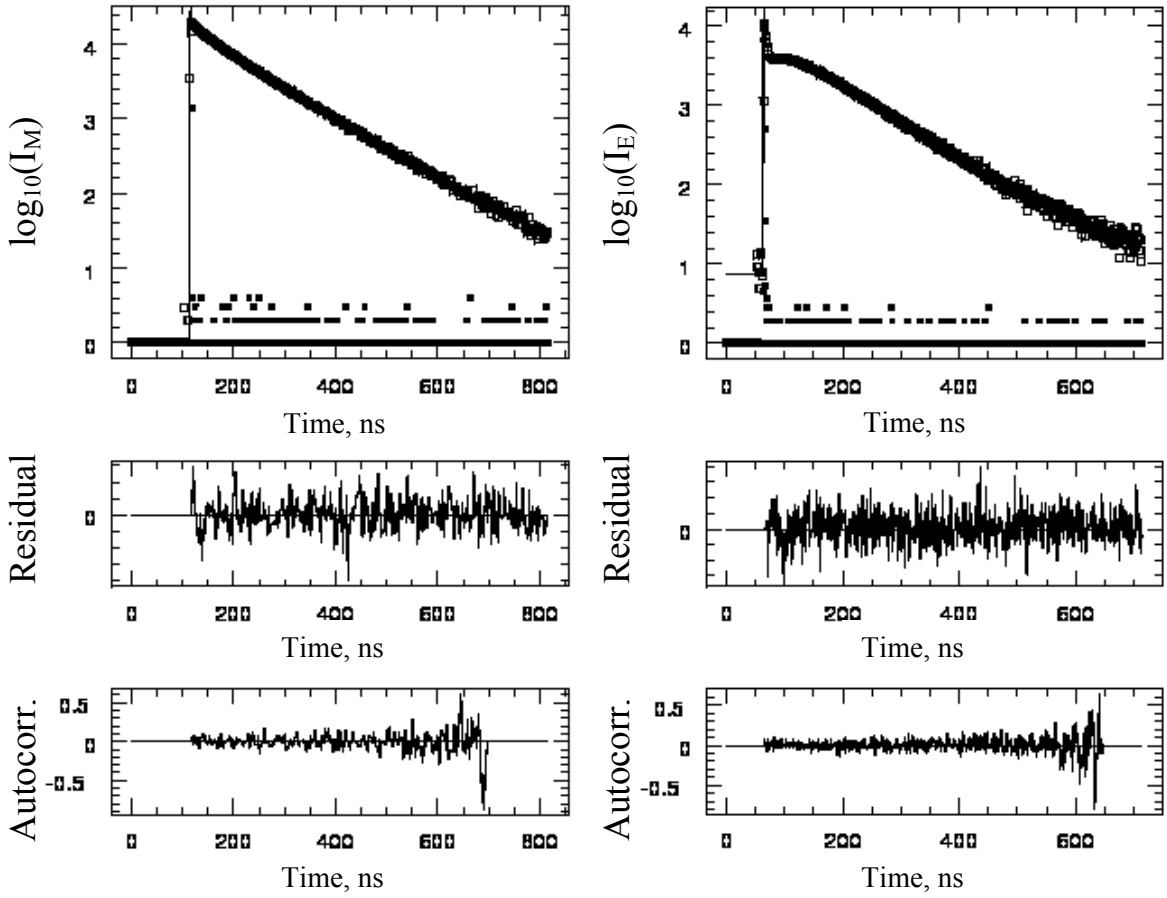

Figure SI.2.1: Global analysis of the monomer (left) and excimer (right) fluorescence decays of a solution of DSPC with 1 mol% of PSIDA and 100 μM Ca^{2+}.

Table SI.2.1a: Pre-exponential factors and decay times retrieved from fitting the monomer and excimer decays of POPC solutions containing 1 mol% PSOH with Equation 2.1.

$[Cu^{2+}]$ μM	$[Ca^{2+}]$ μM	$[La^{3+}]$ μM	τ_{M1} ns	a_{M1}	τ_{M2} ns	a_{M2}	χ^2	τ_{E1} ns	a_{E1}	τ_{E2} ns	a_{E2}	χ^2
0	0	0	47.1	0.199	106.0	0.801	1.18	31.4	-7.817	100.8	8.817	1.19
0.1	0	0	44.5	0.197	103.0	0.803	0.97	30.0	-6.894	96.2	7.894	1.16
1	0	0	42.9	0.188	103.8	0.812	1.15	30.9	-6.770	96.6	7.770	1.19
10	0	0	37.7	0.177	101.6	0.823	1.13	30.7	-6.245	95.3	7.245	1.17
100	0	0	43.9	0.210	104.7	0.790	1.03	30.6	-6.040	97.4	7.040	1.17
1000	0	0	42.6	0.215	106.8	0.785	1.02	29.8	-6.698	101.5	7.698	1.04
0	0.1	0	44.2	0.215	104.4	0.785	1.14	31.1	-7.215	96.7	8.215	1.28
0	1	0	38.9	0.171	101.9	0.829	1.06	30.7	-7.201	95.5	8.201	1.13
0	10	0	39.0	0.183	104.7	0.817	1.02	30.9	-7.495	97.5	8.495	1.07
0	100	0	37.4	0.182	102.4	0.818	1.08	30.6	-7.369	96.3	8.369	1.12
0	1000	0	40.9	0.178	104.5	0.822	1.03	31.1	-6.899	97.6	7.899	1.23
0	10000	0	39.3	0.180	101.4	0.820	0.97	30.9	-6.994	94.4	7.994	1.18
0	0	0.1	46.2	0.205	104.0	0.795	1.03	30.6	7.457	96.8	8.457	1.19
0	0	1	31.4	0.170	101.2	0.830	1.01	30.7	-7.360	85.2	8.360	1.14
0	0	10	37.0	0.159	103.7	0.841	0.99	31.0	-7.385	98.2	8.385	1.19
0	0	100	38.8	0.200	102.6	0.800	1.19	30.5	-6.849	95.6	7.849	1.19
0	0	1000	33.9	0.187	105.2	0.813	1.02	30.2	-6.797	99.1	7.797	1.00
0	0	10000	45.3	0.252	104.8	0.748	1.09	30.4	-6.317	95.2	7.317	1.12

Table SI.2.1b: Pre-exponential factors and decay times retrieved from fitting the monomer and excimer decays of DSPC solutions containing 1 mol% PSOH with Equation 2.1.

$[Cu^{2+}]$ μM	$[Ca^{2+}]$ μM	$[La^{3+}]$ μM	τ_{M1} ns	a_{M1}	τ_{M2} ns	a_{M2}	τ_{M3} ns	a_{M3}	χ^2	τ_{E1} ns	a_{E1}	τ_{E2} ns	a_{E2}	τ_{E3} ns	a_{E3}	χ^2
0	0	0	16.6	0.170	75.7	0.398	163.2	0.43	1.07	21.6	-3.055	98.8	3.965	236.7	0.090	0.98
0.1	0	0	16.2	0.171	74.4	0.387	163.4	0.44	1.10	21.7	-3.222	97.2	4.081	207.7	0.141	1.06
1	0	0	21.1	0.182	79.2	0.389	164.6	0.43	1.17	22.1	-3.088	95.7	3.702	162.4	0.386	1.30
10	0	0	18.9	0.164	75.8	0.389	163.4	0.45	1.00	20.9	-3.281	99.2	4.188	233.6	0.094	1.28
100	0	0	21.8	0.176	80.5	0.406	164.8	0.418	1.02	21.3	-3.174	97.6	3.992	197.2	0.181	1.10
1000	0	0	20.3	0.165	89.2	0.392	173.0	0.44	0.92	21.6	-3.014	97.8	3.804	196.8	0.210	1.16
0	0.1	0	16.4	0.165	76.5	0.414	164.2	0.42	1.13	21.4	-3.476	92.4	3.875	147.0	0.601	1.19
0	1	0	16.5	0.170	71.9	0.384	160.7	0.45	1.10	21.6	-3.226	97.0	3.986	178.7	0.240	1.10
0	10	0	22.5	0.187	80.4	0.378	164.0	0.44	1.02	22.2	-3.132	94.7	3.832	169.1	0.300	1.24
0	100	0	23.6	0.189	83.6	0.399	165.7	0.41	1.02	21.2	-3.280	101.7	4.226	286.2	0.054	1.21
0	1000	0	15.5	0.148	68.1	0.370	159.1	0.48	1.12	21.3	-3.164	95.5	3.830	164.0	0.334	1.07
0	10000	0	21.9	0.211	88.9	0.429	170.7	0.36	1.16	20.9	-3.035	100.7	3.975	279.4	0.060	0.99
0	0	0.1	18.1	0.172	77.7	0.403	164.9	0.42	0.97	21.0	-3.420	97.3	4.219	179.7	0.201	1.18
0	0	1	17.0	0.152	69.5	0.382	159.1	0.47	1.12	21.7	-3.274	98.5	4.144	219.4	0.130	1.02
0	0	10	21.0	0.181	83.5	0.426	168.8	0.39	0.99	21.3	-3.210	99.0	4.140	257.3	0.070	1.23
0	0	100	20.1	0.172	77.4	0.400	165.1	0.43	0.97	21.3	-3.324	100.1	4.257	270.2	0.067	1.15
0	0	1000	15.6	0.150	74.0	0.396	164.1	0.45	1.04	21.8	-2.925	96.5	3.756	194.4	0.170	1.17
0	0	10000	19.7	0.190	79.0	0.417	163.8	0.39	0.91	21.2	-3.071	97.3	3.949	212.0	0.121	1.01

Table SI.2.1c: Pre-exponential factors and decay times retrieved from fitting the monomer and excimer decays of POPC solutions containing 1 mol% PSIDA with Equation 2.1.

$[Cu^{2+}]$ μM	$[Ca^{2+}]$ μM	$[La^{3+}]$ μM	τ_{M1} ns	a_{M1}	τ_{M2} ns	a_{M2}	τ_{M3} ns	a_{M3}	χ^2	τ_{E1} ns	a_{E1}	τ_{E2} ns	a_{E2}	τ_{E3} ns	a_{E3}	τ_{E4} ns	a_{E4}	χ^2
0	0	0	10.4	0.124	50.4	0.327	94.7	0.548	1.04	3.1	0.808	32.3	-0.579	82.9	0.771			1.11
0.1	0	0	7.8	0.116	40.4	0.284	89.0	0.601	1.04	2.9	0.799	32.4	-0.514	80.1	0.714			1.07
1	0	0	5.7	0.123	34.3	0.352	87.0	0.525	1.03	3.0	0.805	11.5	-0.233	72.9	0.428			1.03
10	0	0	9.0	0.200	36.6	0.658	77.2	0.142	0.95	2.9	0.839	11.5	-0.150	52.1	0.311			1.15
100	0	0	7.5	0.214	35.4	0.627	74.0	0.159	1.06	2.8	0.831	12.6	-0.122	51.8	0.290			1.10
1000	0	0	7.8	0.276	35.7	0.592	80.8	0.132	1.17	2.3	0.746	16.5	-0.093	39.0	0.276	69.6	0.070	1.17
0	0.1	0	12.7	0.124	46.2	0.260	90.0	0.616	0.97	2.8	0.816	32.6	-0.527	80.4	0.711			0.95
0	1	0	11.6	0.130	50.1	0.295	90.4	0.575	1.03	3.1	0.808	31.7	-0.565	80.9	0.757			1.09
0	10	0	8.8	0.136	41.7	0.236	87.8	0.628	1.19	3.0	0.807	32.8	-0.588	79.0	0.781			0.88
0	100	0	9.1	0.132	51.0	0.329	92.6	0.539	1.21	3.1	0.812	32.8	-0.574	80.6	0.762			1.07
0	1000	0	12.7	0.160	61.2	0.417	100.1	0.423	0.98	3.0	0.812	31.5	-0.518	82.5	0.706			1.06
0	10000	0	10.4	0.131	46.9	0.255	96.7	0.614	0.97	3.2	0.820	31.2	-0.482	85.0	0.663			1.04
0	0	0.1	4.5	0.140	39.2	0.260	89.2	0.600	1.04	3.1	0.808	32.3	-0.549	80.7	0.741			1.12
0	0	1	8.0	0.122	48.8	0.307	93.7	0.572	0.97	2.9	0.817	32.1	-0.500	82.3	0.683			1.05
0	0	10	13.7	0.121	56.2	0.292	104.6	0.587	1.03	3.1	0.821	31.1	-0.444	89.3	0.622			0.93
0	0	100	7.7	0.136	50.6	0.258	107.1	0.607	1.06	3.1	0.805	29.6	-0.401	91.5	0.596			0.96
0	0	1000	3.7	0.182	41.8	0.225	107.3	0.593	1.08	3.1	0.784	29.1	-0.420	90.4	0.636			1.02
0	0	10000	7.8	0.126	48.6	0.261	109.9	0.612	0.97	3.1	0.796	31.6	-0.335	90.6	0.539			1.09

Table SI.2.1d: Pre-exponential factors and decay times retrieved from fitting the monomer and excimer decays of DSPC solutions containing 1 mol% PSIDA with Equation 1.

$[Cu^{2+}]$ μM	$[Ca^{2+}]$ μM	$[La^{3+}]$ μM	τ_{M1} ns	a_{M1}	τ_{M2} ns	a_{M2}	τ_{M3} ns	a_{M3}	χ^2	τ_{E1} ns	a_{E1}	τ_{E2} ns	a_{E2}	τ_{E3} ns	a_{E3}	τ_{E4} ns	a_{E4}	χ^2
0	0	0	15.5	0.370	62.1	0.440	149.7	0.191	1.09	3.7	0.518	23.4	-0.475	73.2	0.870	129.0	0.087	0.94
0.1	0	0	13.4	0.347	57.2	0.436	142.2	0.217	1.15	3.2	0.537	24.7	-0.472	70.8	0.849	124.7	0.086	0.96
1	0	0	11.3	0.401	56.1	0.408	149.0	0.191	1.03	2.7	0.582	35.3	-0.731	49.6	0.832	96.1	0.317	1.19
10	0	0	9.9	0.499	53.2	0.335	163.1	0.166	1.19	4.0	0.584			50.4	0.322	102.7	0.094	1.11
100	0	0	9.3	0.509	51.7	0.334	164.8	0.157	1.19	4.4	0.561			45.6	0.284	91.7	0.155	1.18
1000	0	0	10.6	0.500	55.0	0.336	164.2	0.164	1.18	4.4	0.552			47.9	0.340	99.1	0.108	1.26
0	0.1	0	12.7	0.325	55.2	0.448	142.7	0.226	1.30	2.9	0.540	24.0	-0.456	72.7	0.833	122.1	0.082	1.16
0	1	0	13.2	0.347	56.3	0.437	141.8	0.216	1.26	3.3	0.533	24.0	-0.521	69.1	0.834	112.1	0.155	1.16
0	10	0	12.1	0.334	54.0	0.442	141.6	0.224	1.05	3.4	0.565	23.5	-0.495	69.9	0.785	113.0	0.145	1.16
0	100	0	12.1	0.325	54.9	0.444	140.9	0.231	1.16	3.6	0.517	24.9	-0.536	68.0	0.793	107.4	0.226	0.82
0	1000	0	14.0	0.354	60.2	0.439	146.5	0.207	1.23	3.2	0.552	24.4	-0.499	66.1	0.662	99.9	0.285	1.07
0	10000	0	13.1	0.365	58.6	0.443	149.8	0.192	1.06	3.3	0.532	25.5	-0.482	57.0	0.565	95.4	0.385	0.94
0	0	0.1	12.7	0.341	56.7	0.445	143.4	0.214	1.14	3.5	0.494	25.0	-0.609	60.0	0.670	94.5	0.445	1.16
0	0	1	16.7	0.379	69.6	0.450	163.6	0.171	1.04	2.9	0.525	25.2	-0.453	71.8	0.790	116.0	0.139	1.16
0	0	10	14.9	0.325	70.1	0.448	173.1	0.227	1.23	3.4	0.536	27.1	-0.478	66.4	0.620	107.3	0.322	1.09
0	0	100	13.1	0.324	71.3	0.433	180.2	0.243	1.16	3.5	0.556	25.5	-0.413	72.5	0.662	118.7	0.195	1.13
0	0	1000	11.2	0.276	67.0	0.409	180.7	0.315	1.14	3.5	0.555	27.3	-0.341	75.7	0.637	131.6	0.150	1.18
0	0	10000	15.1	0.303	80.1	0.415	192.0	0.283	1.02	3.3	0.584	28.3	-0.264	77.0	0.559	135.3	0.122	0.95

Table SI.2.1e: Pre-exponential factors and decay times retrieved from fitting the monomer decay of POPC and DSPC solutions containing 0.1 mol% of PSOH and PSIDA with Equation 1.

Lipid	τ_{M1} ns	a_{M1}	τ_{M2} ns	a_{M2}	τ_{M3} ns	a_{M3}	$<\tau_M>$ ns	χ^2
0.1 % PSOH/POPC			33.8	0.078	114.7	0.922	108.4	1.08
0.1 % PSOH/DSPC			70.9	0.156	185.6	0.844	167.7	1.07
0.1 % PSIDA/POPC			42.5	0.354	111.2	0.646	86.9	1.07
0.1 % PSIDA/DSPC	19.7	0.173	79.6	0.276	176.2	0.551	122.5	1.19

Table SI.2.2a: FBM parameters obtained from globally fitting the monomer and excimer decays of POPC solutions containing 1 mol% of PSOH with Cu^{2+} or Ca^{2+} ions added.

$[Cu^{2+}]$ μM	$[Ca^{2+}]$ μM	$k_{ex}[blob]$ $\times 10^7\ s^{-1}$	k_{blob} $\times 10^7\ s^{-1}$	$<n>$	a_{Mdiff}	a_M	a_{Ediff}	τ_{E0} ns	a_{E0}	τ_{EL} ns	a_{EL}	χ^2
0	0	1.0 ± 0.1	1.6 ± 0.0	0.47 ± 0.01	0.575 ± 0.008	0.425 ± 0.008	0.966 ± 0.001	63.6 ± 0.7	0.003 ± 0.002	134 ± 3	0.030 ± 0.002	1.15
0.1	0	0.9 ± 0.1	1.4 ± 0.0	0.68 ± 0.01	0.496 ± 0.008	0.504 ± 0.008	0.940 ± 0.001	65.3 ± 0.7	0.007 ± 0.002	142 ± 3	0.052 ± 0.002	1.15
1	0	1.6 ± 0.1	1.6 ± 0.0	0.52 ± 0.01	0.522 ± 0.008	0.478 ± 0.008	0.947 ± 0.001	56.3 ± 0.7	0.010 ± 0.002	142 ± 3	0.043 ± 0.002	1.24
10	0	1.7 ± 0.1	1.8 ± 0.0	0.43 ± 0.01	0.596 ± 0.008	0.404 ± 0.008	0.959 ± 0.001	55.2 ± 0.7	0.025 ± 0.002	161 ± 3	0.016 ± 0.002	1.13
100	0	1.4 ± 0.1	1.3 ± 0.0	0.48 ± 0.01	0.582 ± 0.008	0.418 ± 0.008	0.959 ± 0.001	55.2 ± 0.7	0.025 ± 0.002	156 ± 3	0.016 ± 0.002	1.20
1000	0	1.1 ± 0.1	1.4 ± 0.0	0.49 ± 0.01	0.631 ± 0.008	0.369 ± 0.008	0.960 ± 0.001	57.1 ± 0.7	0.023 ± 0.002	143 ± 3	0.018 ± 0.002	1.07
0	0.1	1.0 ± 0.1	1.3 ± 0.0	0.54 ± 0.01	0.655 ± 0.008	0.345 ± 0.008	0.955 ± 0.001	59.4 ± 0.7	0.039 ± 0.002	176 ± 3	0.006 ± 0.002	1.14
0	1	1.7 ± 0.1	1.6 ± 0.0	0.49 ± 0.01	0.504 ± 0.008	0.496 ± 0.008	0.957 ± 0.001	54.7 ± 0.7	0.007 ± 0.002	146 ± 3	0.036 ± 0.002	1.06
0	10	1.4 ± 0.1	1.6 ± 0.0	0.48 ± 0.01	0.578 ± 0.008	0.422 ± 0.008	0.962 ± 0.001	56.2 ± 0.7	0.014 ± 0.002	146 ± 3	0.024 ± 0.002	1.03
0	100	1.2 ± 0.1	1.1 ± 0.0	0.71 ± 0.01	0.490 ± 0.008	0.510 ± 0.008	0.943 ± 0.001	58.8 ± 0.7	0.012 ± 0.002	141 ± 3	0.045 ± 0.002	1.27
0	1000	1.7 ± 0.1	1.5 ± 0.0	0.47 ± 0.01	0.582 ± 0.008	0.418 ± 0.008	0.960 ± 0.001	52.7 ± 0.7	0.009 ± 0.002	137 ± 3	0.031 ± 0.002	1.06
0	10000	1.1 ± 0.1	1.5 ± 0.0	0.59 ± 0.01	0.553 ± 0.008	0.447 ± 0.008	0.955 ± 0.001	59.6 ± 0.7	0.000 ± 0.000	133 ± 3	0.045 ± 0.002	1.23

Table SI.2.2b: FBM parameters obtained from globally fitting the monomer and excimer decays of POPC solutions containing 1 mol% of PSOH with La^{3+} ions added.

$[La^{3+}]$ μM	$k_{ex}[blob]$ $\times 10^7\ s^{-1}$	k_{blob} $\times 10^7\ s^{-1}$	$<n>$	a_{Mdiff}	a_M	a_{Ediff}	τ_{E0} ns	a_{E0}	τ_{EL} ns	a_{EL}	χ^2
0.1	1.3 ± 0.1	1.5 ± 0.0	0.59 ± 0.01	0.568 ± 0.008	0.432 ± 0.008	0.951 ± 0.001	57.3 ± 0.7	0.014 ± 0.002	142 ± 3	0.035 ± 0.002	1.09
1	1.3 ± 0.1	1.7 ± 0.0	0.45 ± 0.01	0.535 ± 0.008	0.465 ± 0.008	0.963 ± 0.001	57.7 ± 0.7	0.012 ± 0.002	152 ± 3	0.024 ± 0.002	1.06
10	1.3 ± 0.1	1.4 ± 0.0	0.55 ± 0.01	0.590 ± 0.008	0.410 ± 0.008	0.955 ± 0.001	55.6 ± 0.7	0.004 ± 0.002	131 ± 3	0.041 ± 0.002	1.09
100	1.3 ± 0.1	1.5 ± 0.0	0.44 ± 0.01	0.573 ± 0.008	0.427 ± 0.008	0.968 ± 0.001	54.8 ± 0.7	0.010 ± 0.002	144 ± 3	0.022 ± 0.002	1.10
1000	1.6 ± 0.1	2.0 ± 0.0	0.39 ± 0.01	0.594 ± 0.008	0.406 ± 0.008	0.975 ± 0.001	54.7 ± 0.7	0.008 ± 0.002	146 ± 3	0.017 ± 0.002	1.18
10000	1.0 ± 0.1	1.4 ± 0.0	0.52 ± 0.01	0.611 ± 0.008	0.389 ± 0.008	0.962 ± 0.001	59.1 ± 0.7	0.021 ± 0.002	151 ± 3	0.017 ± 0.002	1.12

Table SI.2.2c: FBM parameters obtained from globally fitting the monomer and excimer decays of DSPC solutions containing 1 mol% of PSOH with Cu^{2+} or Ca^{2+} ions added.

$[Cu^{2+}]$ μM	$[Ca^{2+}]$ μM	$k_{ex}[blob]$ $\times 10^7\ s^{-1}$	k_{blob} $\times 10^7\ s^{-1}$	$<n>$	a_{Mdiff}	a_M	a_{Ediff}	τ_{E0} ns	a_{E0}	τ_{EL} ns	a_{EL}	χ^2
0	0	0.9 ± 0.0	2.3 ± 0.0	0.73 ± 0.01	0.744 ± 0.003	0.256 ± 0.003	0.900 ± 0.002	57.6 ± 0.8	0.057 ± 0.004	155 ± 6	0.043 ± 0.003	1.12
0.1	0	0.8 ± 0.0	1.9 ± 0.0	0.79 ± 0.01	0.732 ± 0.003	0.268 ± 0.003	0.878 ± 0.002	59.8 ± 0.8	0.103 ± 0.004	193 ± 6	0.018 ± 0.003	1.19
1	0	0.7 ± 0.0	1.6 ± 0.0	0.84 ± 0.01	0.746 ± 0.003	0.254 ± 0.003	0.862 ± 0.002	59.0 ± 0.8	0.093 ± 0.004	155 ± 6	0.046 ± 0.003	1.25
10	0	0.8 ± 0.0	2.2 ± 0.0	0.75 ± 0.01	0.740 ± 0.003	0.260 ± 0.003	0.896 ± 0.002	59.2 ± 0.8	0.076 ± 0.004	174 ± 6	0.028 ± 0.003	1.24
100	0	0.8 ± 0.0	1.6 ± 0.0	0.83 ± 0.01	0.750 ± 0.003	0.250 ± 0.003	0.867 ± 0.002	56.8 ± 0.8	0.100 ± 0.004	168 ± 6	0.033 ± 0.003	1.18
1000	0	0.8 ± 0.0	1.9 ± 0.0	0.71 ± 0.01	0.672 ± 0.003	0.328 ± 0.003	0.876 ± 0.002	59.4 ± 0.8	0.109 ± 0.004	209 ± 6	0.015 ± 0.003	1.00
0	0.1	0.8 ± 0.0	2.1 ± 0.0	0.75 ± 0.01	0.756 ± 0.003	0.244 ± 0.003	0.884 ± 0.002	61.6 ± 0.8	0.106 ± 0.004	218 ± 6	0.009 ± 0.003	1.20
0	1	0.8 ± 0.0	2.0 ± 0.0	0.79 ± 0.01	0.754 ± 0.003	0.246 ± 0.003	0.866 ± 0.002	63.4 ± 0.8	0.117 ± 0.004	197 ± 6	0.017 ± 0.003	1.26
0	10	0.7 ± 0.0	1.9 ± 0.0	0.78 ± 0.01	0.756 ± 0.003	0.244 ± 0.003	0.870 ± 0.002	63.4 ± 0.8	0.119 ± 0.004	197 ± 6	0.011 ± 0.003	1.26
0	100	0.8 ± 0.0	1.9 ± 0.0	0.78 ± 0.01	0.749 ± 0.003	0.251 ± 0.003	0.890 ± 0.002	60.0 ± 0.8	0.079 ± 0.004	169 ± 6	0.031 ± 0.003	1.24
0	1000	0.7 ± 0.0	1.8 ± 0.0	0.80 ± 0.01	0.744 ± 0.003	0.256 ± 0.003	0.876 ± 0.002	59.0 ± 0.8	0.090 ± 0.004	160 ± 6	0.035 ± 0.003	1.21
0	10000	0.8 ± 0.0	2.0 ± 0.0	0.78 ± 0.01	0.753 ± 0.003	0.247 ± 0.003	0.866 ± 0.002	61.2 ± 0.8	0.107 ± 0.004	174 ± 6	0.027 ± 0.003	1.25

Table SI.2.2d: FBM parameters obtained from globally fitting the monomer and excimer decays of DSPC solutions containing 1 mol% of PSOH with La^{3+} ions added.

$[La^{3+}]$ μM	$k_{ex}[blob]$ $\times 10^7\ s^{-1}$	k_{blob} $\times 10^7\ s^{-1}$	$<n>$	a_{Mdiff}	a_M	a_{Ediff}	τ_{E0} ns	a_{E0}	τ_{EL} ns	a_{EL}	χ^2
0.1	0.8 ± 0.0	1.9 ± 0.0	0.77 ± 0.01	0.741 ± 0.003	0.259 ± 0.003	0.875 ± 0.002	60.2 ± 0.8	0.110 ± 0.004	193 ± 6	0.016 ± 0.003	1.10
1	0.8 ± 0.0	1.7 ± 0.0	0.83 ± 0.01	0.750 ± 0.003	0.250 ± 0.003	0.873 ± 0.002	58.4 ± 0.8	0.094 ± 0.004	168 ± 6	0.033 ± 0.003	1.18
10	0.8 ± 0.0	1.8 ± 0.0	0.79 ± 0.01	0.739 ± 0.003	0.261 ± 0.003	0.873 ± 0.002	59.6 ± 0.8	0.109 ± 0.004	190 ± 6	0.018 ± 0.003	1.08
100	0.8 ± 0.0	1.8 ± 0.0	0.81 ± 0.01	0.733 ± 0.003	0.267 ± 0.003	0.860 ± 0.002	60.9 ± 0.8	0.119 ± 0.004	193 ± 6	0.021 ± 0.003	1.22
1000	0.9 ± 0.0	1.9 ± 0.0	0.76 ± 0.01	0.720 ± 0.003	0.280 ± 0.003	0.873 ± 0.002	57.9 ± 0.8	0.106 ± 0.004	189 ± 6	0.020 ± 0.003	1.17
10000	0.7 ± 0.0	1.7 ± 0.0	0.83 ± 0.01	0.772 ± 0.003	0.228 ± 0.003	0.861 ± 0.002	59.9 ± 0.8	0.118 ± 0.004	186 ± 6	0.021 ± 0.003	1.01

Table SI.2.2e: FBM parameters obtained from globally fitting the monomer and excimer decays of POPC solutions containing 1 mol% of PSIDA with Ca^{2+} ions added.

$[Ca^{2+}]$ μM	$k_{ex}[blob]$ $\times 10^7\ s^{-1}$	k_{blob} $\times 10^7\ s^{-1}$	$\langle n \rangle$	a_{Mdiff}	a_M	a_{Ediff}	τ_{E0} ns	a_{E0}	τ_{EL} ns	a_{EL}	τ_{ES} ns	a_{ES}	χ^2
0	1.5 ± 0.1	2.1 ± 0.2	0.61 ± 0.02	0.801 ± 0.005	0.199 ± 0.005	0.593 ± 0.006	53.6 ± 1.5	0.021 ± 0.009	112 ± 16	0.353 ± 0.007	3.6 ± 0.1	0.353 ± 0.004	1.21
0.1	1.3 ± 0.1	2.7 ± 0.2	0.54 ± 0.02	0.757 ± 0.005	0.243 ± 0.005	0.587 ± 0.006	58.5 ± 1.5	0.029 ± 0.009	157 ± 16	0.007 ± 0.007	4.0 ± 0.1	0.377 ± 0.004	1.21
1	1.4 ± 0.1	2.5 ± 0.2	0.56 ± 0.02	0.741 ± 0.005	0.260 ± 0.005	0.560 ± 0.006	56.2 ± 1.5	0.021 ± 0.009	117 ± 16	0.029 ± 0.007	3.7 ± 0.1	0.390 ± 0.004	1.14
10	1.7 ± 0.1	3.1 ± 0.2	0.50 ± 0.02	0.792 ± 0.005	0.208 ± 0.005	0.591 ± 0.006	54.4 ± 1.5	0.023 ± 0.009	134 ± 16	0.013 ± 0.007	3.8 ± 0.1	0.373 ± 0.004	1.13
100	1.8 ± 0.1	3.0 ± 0.2	0.49 ± 0.02	0.824 ± 0.005	0.176 ± 0.005	0.619 ± 0.006	53.4 ± 1.5	0.028 ± 0.009	182 ± 16	0.004 ± 0.004	3.9 ± 0.1	0.350 ± 0.004	1.17
1000	1.6 ± 0.1	2.7 ± 0.2	0.52 ± 0.02	0.849 ± 0.005	0.151 ± 0.005	0.615 ± 0.006	53.9 ± 1.5	0.033 ± 0.009	133 ± 16	0.006 ± 0.006	3.9 ± 0.1	0.346 ± 0.004	1.11
10000	1.3 ± 0.1	2.7 ± 0.2	0.54 ± 0.02	0.757 ± 0.005	0.243 ± 0.005	0.587 ± 0.006	58.5 ± 1.5	0.029 ± 0.009	157 ± 16	0.007 ± 0.007	4.0 ± 0.1	0.377 ± 0.004	1.21

Table SI.2.2f: FBM parameters obtained from globally fitting the monomer and excimer decays of POPC solutions containing 1 mol% of PSIDA with La^{3+} ions added.

$[La^{3+}]$ μM	$k_{ex}[blob]$ $\times 10^7\ s^{-1}$	k_{blob} $\times 10^7\ s^{-1}$	$<n>$	a_{Mdiff}	a_M	a_{Ediff}	τ_{E0} ns	a_{E0}	τ_{El} ns	a_{El}	τ_{ES} ns	a_{ES}	χ^2
0.1	1.1 ± 0.1	1.7 ± 0.2	0.66 ± 0.02	0.862 ± 0.005	0.138 ± 0.005	0.585 ± 0.006	56.3 ± 1.5	0.049 ± 0.009	101 ± 16	0.012 ± 0.007	3.6 ± 0.1	0.354 ± 0.004	1.15
1	1.4 ± 0.1	2.1 ± 0.2	0.59 ± 0.02	0.817 ± 0.005	0.183 ± 0.005	0.577 ± 0.006	56.4 ± 1.6	0.051 ± 0.009	128 ± 16	0.006 ± 0.007	3.5 ± 0.1	0.365 ± 0.004	1.19
10	1.4 ± 0.1	2.4 ± 0.2	0.60 ± 0.02	0.624 ± 0.005	0.376 ± 0.005	0.527 ± 0.005	58.1 ± 1.6	0.006 ± 0.006	115 ± 16	0.052 ± 0.015	3.6 ± 0.1	0.416 ± 0.004	1.16
100	1.3 ± 0.1	2.8 ± 0.1	0.61 ± 0.02	0.551 ± 0.005	0.449 ± 0.005	0.512 ± 0.006	64.7 ± 1.8	0.043 ± 0.010	156 ± 13	0.018 ± 0.007	3.7 ± 0.1	0.426 ± 0.005	1.14
1000	1.4 ± 0.1	2.4 ± 0.1	0.75 ± 0.02	0.479 ± 0.003	0.521 ± 0.003	0.478 ± 0.005	61.4 ± 1.8	0.033 ± 0.0018	132 ± 13	0.053 ± 0.015	3.6 ± 0.1	0.437 ± 0.004	1.12
10000	1.5 ± 0.1	2.4 ± 0.1	0.79 ± 0.03	0.464 ± 0.003	0.536 ± 0.003	0.405 ± 0.005	62.1 ± 2.3	0.028 ± 0.018	129 ± 7	0.066 ± 0.015	3.5 ± 0.1	0.501 ± 0.004	1.12

Table SI.2.2g: FBM parameters obtained from globally fitting the monomer and excimer decays of DSPC solutions containing 1 mol% of PSIDA with Ca^{2+} ions added.

$[Ca^{2+}]$ μM	$k_{ex}[blob]$ $\times 10^7\ s^{-1}$	k_{blob} $\times 10^7\ s^{-1}$	$\langle n \rangle$	a_{Mdiff}	a_M	a_{Ediff}	τ_{E0} ns	a_{E0}	τ_{EL} ns	a_{EL}	τ_{ES} ns	a_{ES}	χ^2
0	0.6 ± 0.0	1.9 ± 0.0	1.35 ± 0.01	0.916 ± 0.002	0.084 ± 0.002	0.423 ± 0.006	61.9 ± 1.3	0.226 ± 0.018	127 ± 17	0.031 ± 0.018	3.9 ± 0.1	0.320 ± 0.005	1.09
0.1	0.5 ± 0.0	1.5 ± 0.0	1.46 ± 0.01	0.918 ± 0.002	0.082 ± 0.002	0.406 ± 0.006	61.3 ± 1.3	0.243 ± 0.018	118 ± 17	0.026 ± 0.018	2.9 ± 0.1	0.325 ± 0.005	1.18
1	0.5 ± 0.0	1.6 ± 0.0	1.43 ± 0.01	0.922 ± 0.002	0.078 ± 0.002	0.434 ± 0.006	59.9 ± 1.3	0.227 ± 0.018	122 ± 17	0.031 ± 0.018	3.4 ± 0.1	0.308 ± 0.005	1.22
10	0.5 ± 0.0	1.6 ± 0.0	1.44 ± 0.01	0.917 ± 0.002	0.083 ± 0.002	0.439 ± 0.006	59.6 ± 1.3	0.220 ± 0.018	128 ± 17	0.028 ± 0.018	3.7 ± 0.1	0.313 ± 0.005	1.22
100	0.5 ± 0.0	1.6 ± 0.0	1.40 ± 0.01	0.920 ± 0.002	0.080 ± 0.002	0.439 ± 0.006	61.1 ± 1.3	0.232 ± 0.018	124 ± 17	0.031 ± 0.018	3.7 ± 0.1	0.298 ± 0.005	1.02
1000	0.6 ± 0.0	1.8 ± 0.0	1.33 ± 0.01	0.908 ± 0.002	0.092 ± 0.002	0.433 ± 0.006	59.8 ± 1.3	0.206 ± 0.018	114 ± 17	0.037 ± 0.018	3.5 ± 0.1	0.324 ± 0.005	1.19
10000	0.6 ± 0.0	1.9 ± 0.0	1.37 ± 0.01	0.906 ± 0.002	0.094 ± 0.002	0.393 ± 0.006	57.0 ± 1.3	0.188 ± 0.018	107 ± 17	0.081 ± 0.018	3.7 ± 0.1	0.337 ± 0.005	1.03

Table SI.2.2h: FBM parameters obtained from globally fitting the monomer and excimer decays of DSPC solutions containing 1 mol% of PSIDA with La^{3+} ions added.

$[La^{3+}]$ μM	$k_{ex}[blob]$ $\times 10^7\ s^{-1}$	k_{blob} $\times 10^7\ s^{-1}$	$<n>$	a_{Mdiff}	a_M	a_{Ediff}	τ_{E0} ns	a_{E0}	τ_{EL} ns	a_{EL}	τ_{ES} ns	a_{ES}	χ^2
0.1	0.6 ± 0.0	1.9 ± 0.0	1.34 ± 0.01	0.913 ± 0.002	0.087 ± 0.002	0.461 ± 0.006	60.1 ± 1.3	0.225 ± 0.018	122 ± 17	0.027 ± 0.018	4.0 ± 0.1	0.287 ± 0.005	1.28
1	0.6 ± 0.0	1.6 ± 0.1	1.37 ± 0.02	0.893 ± 0.002	0.107 ± 0.002	0.411 ± 0.006	62.1 ± 1.2	0.236 ± 0.018	121 ± 11	0.036 ± 0.009	3.2 ± 0.1	0.317 ± 0.005	1.01
10	0.8 ± 0.0	2.0 ± 0.1	1.20 ± 0.02	0.814 ± 0.002	0.186 ± 0.002	0.435 ± 0.006	62.3 ± 1.2	0.204 ± 0.009	138 ± 11	0.039 ± 0.009	4.0 ± 0.1	0.321 ± 0.005	1.12
100	1.0 ± 0.0	2.6 ± 0.1	1.06 ± 0.01	0.765 ± 0.001	0.235 ± 0.001	0.456 ± 0.008	59.7 ± 1.0	0.153 ± 0.011	138 ± 7	0.049 ± 0.007	4.6 ± 0.1	0.342 ± 0.004	1.10
1000	1.1 ± 0.0	2.7 ± 0.1	1.02 ± 0.01	0.689 ± 0.002	0.311 ± 0.002	0.407 ± 0.008	61.1 ± 1.0	0.162 ± 0.010	144 ± 7	0.062 ± 0.007	4.5 ± 0.1	0.370 ± 0.005	1.16
10000	0.9 ± 0.0	2.3 ± 0.1	1.09 ± 0.02	0.678 ± 0.002	0.322 ± 0.002	0.336 ± 0.008	66.3 ± 0.9	0.207 ± 0.010	152 ± 7	0.049 ± 0.007	4.1 ± 0.1	0.408 ± 0.005	0.93

Table SI.2.3a: Selected FBM parameters obtained from globally fitting the monomer and excimer decays of POPC solutions containing 1 mol% of PSOH.

$[Cu^{2+}]$ μM	$[Ca^{2+}]$ μM	$[La^{3+}]$ μM	f_{agg}	f_{diff}	f_{free}	$k_{blob} \times \langle n \rangle \times 10^7\ s^{-1}$
0	0	0	0.02 ± 0.00	0.56 ± 0.01	0.42 ± 0.01	0.76 ± 0.03
0.1	0	0	0.03 ± 0.00	0.48 ± 0.01	0.49 ± 0.01	0.93 ± 0.03
1	0	0	0.03 ± 0.00	0.51 ± 0.01	0.46 ± 0.01	0.85 ± 0.03
10	0	0	0.02 ± 0.00	0.58 ± 0.01	0.39 ± 0.01	0.78 ± 0.03
100	0	0	0.02 ± 0.00	0.57 ± 0.01	0.41 ± 0.01	0.65 ± 0.03
1000	0	0	0.03 ± 0.00	0.61 ± 0.01	0.36 ± 0.01	0.70 ± 0.03
0	0.1	0	0.03 ± 0.00	0.63 ± 0.01	0.34 ± 0.01	0.68 ± 0.03
0	1	0	0.02 ± 0.00	0.49 ± 0.01	0.48 ± 0.01	0.76 ± 0.03
0	10	0	0.02 ± 0.00	0.56 ± 0.01	0.41 ± 0.01	0.77 ± 0.03
0	100	0	0.03 ± 0.00	0.48 ± 0.01	0.50 ± 0.01	0.80 ± 0.03
0	1000	0	0.02 ± 0.00	0.57 ± 0.01	0.41 ± 0.01	0.71 ± 0.03
0	10000	0	0.03 ± 0.00	0.54 ± 0.01	0.44 ± 0.01	0.86 ± 0.03
0	0	0.1	0.03 ± 0.00	0.55 ± 0.01	0.42 ± 0.01	0.89 ± 0.03
0	0	1	0.02 ± 0.00	0.52 ± 0.01	0.46 ± 0.01	0.76 ± 0.03
0	0	10	0.03 ± 0.00	0.57 ± 0.01	0.40 ± 0.01	0.78 ± 0.03
0	0	100	0.02 ± 0.00	0.56 ± 0.01	0.42 ± 0.01	0.64 ± 0.03
0	0	1000	0.02 ± 0.00	0.59 ± 0.01	0.40 ± 0.01	0.78 ± 0.03
0	0	10000	0.02 ± 0.00	0.60 ± 0.01	0.38 ± 0.01	0.72 ± 0.03

Table SI.2.3b: Selected FBM parameters obtained from globally fitting the monomer and excimer decays of DSPC solutions containing 1 mol% of PSOH.

$[Cu^{2+}]$ μM	$[Ca^{2+}]$ μM	$[La^{3+}]$ μM	f_{agg}	f_{diff}	f_{free}	$k_{blob} \times \langle n \rangle \times 10^7\ s^{-1}$
0	0	0	0.08 ± 0.00	0.69 ± 0.00	0.24 ± 0.00	1.70 ± 0.02
0.1	0	0	0.09 ± 0.00	0.66 ± 0.00	0.24 ± 0.00	1.48 ± 0.02
1	0	0	0.11 ± 0.00	0.67 ± 0.00	0.23 ± 0.00	1.38 ± 0.02
10	0	0	0.08 ± 0.00	0.68 ± 0.00	0.24 ± 0.00	1.64 ± 0.02
100	0	0	0.10 ± 0.00	0.67 ± 0.00	0.22 ± 0.00	1.31 ± 0.02
1000	0	0	0.09 ± 0.00	0.61 ± 0.00	0.30 ± 0.00	1.33 ± 0.02
0	0.1	0	0.09 ± 0.00	0.69 ± 0.00	0.22 ± 0.00	1.56 ± 0.02
0	1	0	0.10 ± 0.00	0.68 ± 0.00	0.22 ± 0.00	1.60 ± 0.02
0	10	0	0.10 ± 0.00	0.68 ± 0.00	0.22 ± 0.00	1.50 ± 0.02
0	100	0	0.08 ± 0.00	0.69 ± 0.00	0.23 ± 0.00	1.49 ± 0.02
0	1000	0	0.10 ± 0.00	0.67 ± 0.00	0.23 ± 0.00	1.47 ± 0.02
0	10000	0	0.10 ± 0.00	0.67 ± 0.00	0.22 ± 0.00	1.53 ± 0.02
0	0	0.1	0.10 ± 0.00	0.67 ± 0.00	0.23 ± 0.00	1.48 ± 0.02
0	0	1	0.10 ± 0.00	0.68 ± 0.00	0.22 ± 0.00	1.40 ± 0.02
0	0	10	0.10 ± 0.00	0.67 ± 0.00	0.24 ± 0.00	1.44 ± 0.02
0	0	100	0.11 ± 0.00	0.66 ± 0.00	0.24 ± 0.00	1.47 ± 0.02
0	0	1000	0.09 ± 0.00	0.65 ± 0.00	0.25 ± 0.00	1.43 ± 0.02
0	0	10000	0.11 ± 0.00	0.69 ± 0.00	0.20 ± 0.00	1.43 ± 0.02

Table SI.2.3c: Selected FBM parameters obtained from globally fitting the monomer and excimer decays of POPC solutions containing 1 mol% of PSIDA.

$[Ca^{2+}]$ μM	$[La^{3+}]$ μM	f_{agg}	f_{diff}	f_{free}	$k_{blob} \times \langle n \rangle \times 10^7\ s^{-1}$
0	0	0.50 ± 0.01	0.40 ± 0.00	0.10 ± 0.00	1.27 ± 0.12
0.1	0	0.35 ± 0.01	0.49 ± 0.00	0.16 ± 0.00	1.48 ± 0.12
1	0	0.37 ± 0.01	0.47 ± 0.00	0.16 ± 0.00	1.42 ± 0.12
10	0	0.35 ± 0.01	0.51 ± 0.00	0.13 ± 0.00	1.58 ± 0.12
100	0	0.34 ± 0.01	0.55 ± 0.00	0.12 ± 0.00	1.46 ± 0.12
1000	0	0.35 ± 0.01	0.55 ± 0.00	0.10 ± 0.00	1.39 ± 0.12
10000	0	0.35 ± 0.01	0.49 ± 0.00	0.16 ± 0.00	1.48 ± 0.12
0	0.1	0.38 ± 0.01	0.53 ± 0.00	0.09 ± 0.01	1.16 ± 0.12
0	1	0.37 ± 0.01	0.51 ± 0.00	0.11 ± 0.01	1.21 ± 0.12
0	10	0.36 ± 0.01	0.40 ± 0.00	0.24 ± 0.01	1.46 ± 0.16
0	100	0.34 ± 0.01	0.36 ± 0.00	0.29 ± 0.01	1.74 ± 0.10
0	1000	0.34 ± 0.01	0.31 ± 0.00	0.34 ± 0.01	1.83 ± 0.10
0	10000	0.41 ± 0.01	0.28 ± 0.00	0.32 ± 0.01	1.90 ± 0.14

Table SI.2.3d: Selected FBM parameters obtained from globally fitting the monomer and excimer decays of DSPC solutions containing 1 mol% of PSIDA.

$[Ca^{2+}]$ μM	$[La^{3+}]$ μM	f_{agg}	f_{diff}	f_{free}	$k_{blob} \times \langle n \rangle \times 10^7\ s^{-1}$
0	0	0.56 ± 0.02	0.41 ± 0.01	0.04 ± 0.00	2.58 ± 0.06
0.1	0	0.57 ± 0.02	0.39 ± 0.01	0.04 ± 0.00	2.17 ± 0.06
1	0	0.55 ± 0.02	0.42 ± 0.01	0.04 ± 0.00	2.29 ± 0.06
10	0	0.54 ± 0.02	0.42 ± 0.01	0.04 ± 0.00	2.27 ± 0.06
100	0	0.54 ± 0.02	0.42 ± 0.01	0.04 ± 0.00	2.20 ± 0.06
1000	0	0.54 ± 0.02	0.41 ± 0.01	0.04 ± 0.00	2.39 ± 0.06
10000	0	0.58 ± 0.02	0.38 ± 0.01	0.04 ± 0.00	2.58 ± 0.06
0	0.1	0.52 ± 0.01	0.44 ± 0.01	0.04 ± 0.00	2.50 ± 0.06
0	1	0.56 ± 0.01	0.39 ± 0.01	0.05 ± 0.00	2.25 ± 0.08
0	10	0.51 ± 0.01	0.40 ± 0.01	0.09 ± 0.00	2.33 ± 0.08
0	100	0.48 ± 0.01	0.40 ± 0.01	0.12 ± 0.00	2.75 ± 0.10
0	1000	0.50 ± 0.01	0.34 ± 0.01	0.16 ± 0.00	2.72 ± 0.10
0	10000	0.57 ± 0.01	0.29 ± 0.01	0.14 ± 0.00	2.53 ± 0.11

Chapter 3 Supporting Information

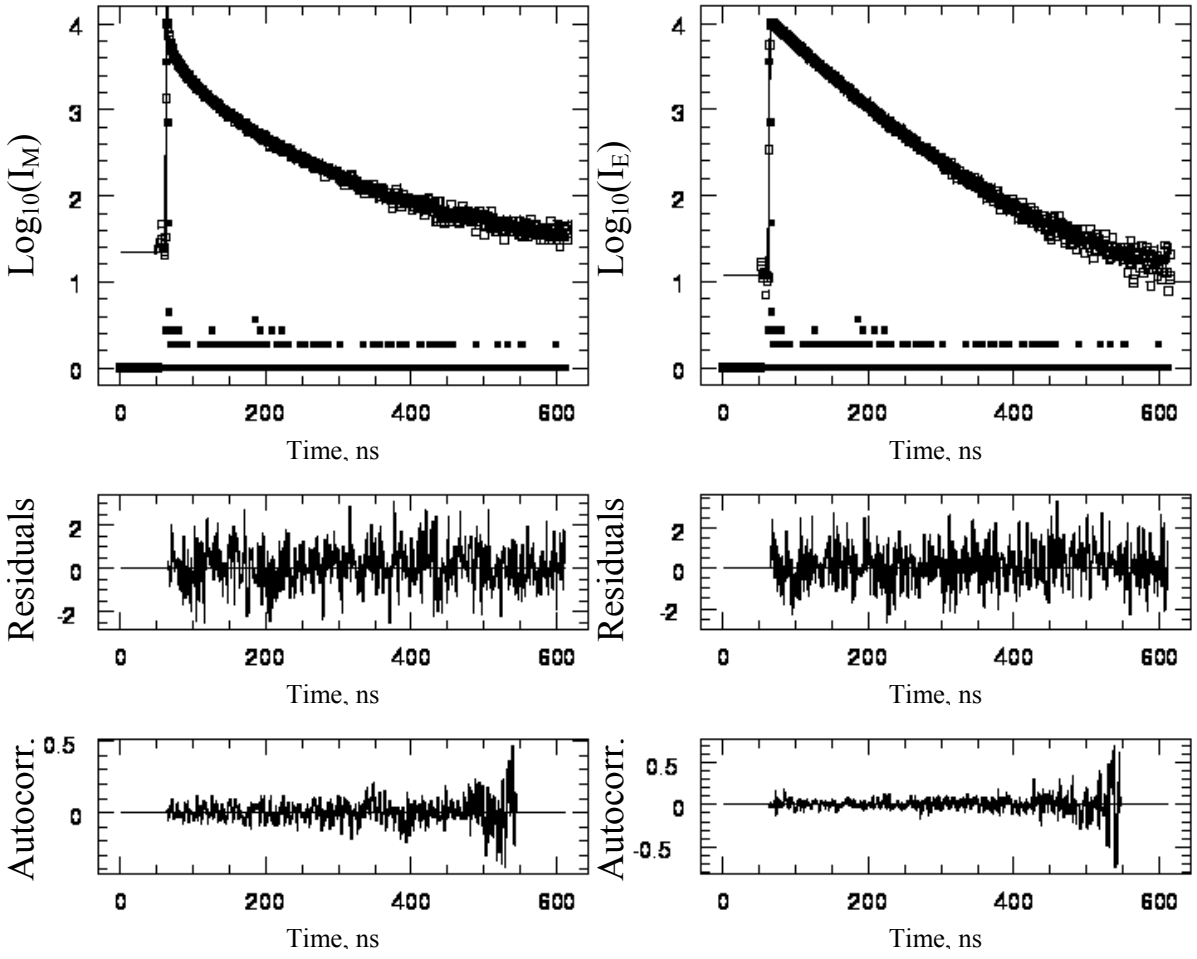

Figure SI.3.1: Global analysis of the monomer (left) and excimer (right) fluorescence decays acquired with 0.09 g/L (OD = 1) PyPDMA645 in water; λ_{ex} = 334 nm. The quasi-absence of risetime in the excimer decay is noticeable.

Equations used for the monomer species:

$$[Py^{*}_{diff}]=[Py^{*}_{diff}]_o \exp\left(-\left(A_2+\frac{1}{\tau_M}\right)t-A_3\left(1-\exp(-A_4 t)\right)\right) \quad \text{(SI.3.1)}$$

$$[Py^{*}_{k2}]=\left([Py^{*}_{k2}]_o+[Py^{*}_{diff}]_o e^{-A_3}\sum_{i=0}^{\infty}\frac{A_3^i}{i!}\frac{A_2+iA_4}{A_2+iA_4-k_2}\right)\exp\left(-\left(k_2+\frac{1}{\tau_M}\right)t\right)$$

$$-[Py^{*}_{diff}]_o e^{-A_3}\sum_{i=0}^{\infty}\frac{A_3^i}{i!}\frac{A_2+iA_4}{A_2+iA_4-k_2}\exp\left(-\left(A_2+iA_4+\frac{1}{\tau_M}\right)t\right) \quad \text{(SI.3.2)}$$

$$[Py^{*}_{free}]=[Py^{*}_{free}]_o \exp\left(-\frac{t}{\tau_M}\right) \quad \text{(SI.3.3)}$$

Equations used for the excimer:

$$[E0^*] = k_2 \left(\left([Py^*_{k2}]_o + [Py^*_{diff}]_o e^{-A_3} \sum_{i=0}^{\infty} \frac{A_3^i}{i!} \frac{A_2 + iA_4}{A_2 + iA_4 - k_2} \right) \times \frac{\exp\left(-\frac{t}{\tau_{E0}}\right) - \exp\left(-\left(k_2 + \frac{1}{\tau_M}\right)t\right)}{k_2 + \frac{1}{\tau_M} - \frac{1}{\tau_{E0}}} + \right.$$

$$\left. [Py^*_{diff}]_o e^{-A_3} \sum_{i=0}^{\infty} \frac{A_3^i}{i!} \frac{A_2 + iA_4}{A_2 + iA_4 - k_2} \frac{\exp\left(-\left(A_2 + iA_4 + \frac{1}{\tau_M}\right)t\right) - \exp\left(-\frac{t}{\tau_{E0}}\right)}{A_2 + iA_4 + \frac{1}{\tau_M} - \frac{1}{\tau_{E0}}} \right)$$

$$+ [E0^*]_o \times \exp\left(-\frac{t}{\tau_{E0}}\right) \qquad \text{(SI.3.4)}$$

$$[El] = [El^*]_o \times \exp\left(-\frac{t}{\tau_{El}}\right) \qquad \text{(SI.3.5)}$$

Table SI.3.1: Comparison of the FBM parameters obtained by global analysis of the monomer (λ_{em} = 375 nm with 370 nm cutoff filter) and excimer (λ_{em} = 510 nm with 370 and 495 nm cutoff filters) decays for a 0.3 g/L (OD = 2.5) PyPDMA479 solution acquired using an instrument response function obtained by either a latex scattering solution or the MIMIC analysis of the decays of fluorescence standards. λ_{ex} = 340 nm, excitation slit width = 6 nm, emission slit width = 32 nm.

Excitation	<n>	k_{blob} $\times 10^7$ s^{-1}	k_e[blob] $\times 10^7$ s^{-1}	τ_{E0} ns	τ_D ns	χ^2
Scattering solution	1.21 (±0.03)	1.4 (±0.1)	0.4 (±0.0)	36.9 (±2.0)	73.0 (±1.5)	1.17 (±0.02)
Fluorescence standards	1.19 (±0.03)	1.4 (±0.1)	0.4 (±0.0)	37.0 (±2.2)	72.6 (±1.5)	1.19 (±0.04)

Excitation	f_{diff}	f_{k2}	f_{free}	f_{E0}	f_{El}	f_{agg}
Scattering solution	0.22 (±0.02)	0.13 (±0.02)	0.01 (±0.00)	0.27 (±0.04)	0.37 (±0.04)	0.64 (0.03)
Fluorescence standards	0.21 (±0.02)	0.10 (±0.02)	0.01 (±0.00)	0.29 (±0.06)	0.39 (±0.03)	0.68 (±0.04)

Table SI.3.2a: Blob model parameters obtained by global analysis of the monomer and excimer decays for PyPDMA645 having a concentration of 0.09 g/L (OD = 1).

Excitation Wavelength Nm	<n>	$k_{blob} \times 10^7$ s^{-1}	$k_e[blob] \times 10^7$ s^{-1}	τ_{E0} ns	τ_D ns	χ^2
325	1.5	2.1	0.9	36.9	72.6	1.1
326	1.6	1.8	0.9	44.4	81.8	1.0
327	1.8	1.4	0.4	42.5	77.4	1.1
328	1.7	1.6	0.6	41.8	78.5	1.0
329	1.7	1.8	0.6	48.3	86.5	1.1
330	1.6	1.8	0.7	43.2	79.5	1.1
331	1.7	1.7	0.6	44.2	79.2	1.0
332	1.8	1.6	0.5	46.3	85.0	1.3
333	1.7	1.9	0.8	47.5	84.7	1.1
334	1.7	1.8	0.7	44.7	78.4	1.1
335	1.8	1.6	0.6	44.6	79.0	1.0
336	1.8	1.7	0.6	42.2	78.0	1.0
337	1.8	1.7	0.5	42.2	78.1	1.2
338	1.7	1.7	0.7	45.4	82.8	1.1
339	2.0	1.2	0.4	44.7	82.6	1.0
340	1.8	1.4	0.5	41.7	79.2	1.0
341	1.8	1.4	0.5	44.4	81.7	1.1
342	1.7	1.7	0.6	37.3	75.5	1.1
343	1.6	1.7	0.7	45.3	83.2	1.2
344	1.6	1.7	0.6	36.4	73.4	1.0
345	1.6	1.8	0.6	43.0	79.2	1.2
346	1.6	1.9	0.6	41.5	77.5	1.1

Table SI.3.2b: Fluorescence contribution fractions obtained for PyPDMA645 having a concentration of 0.09 g/L (OD = 1).

Excitation Wavelength nm	f_{diff}^{f}	f_{free}^{f}	f_{E0}^{f}	f_{D}^{f}	f_{k2}^{f}
325	0.13	0.01	0.33	0.44	0.09
326	0.10	0.01	0.53	0.29	0.07
327	0.09	0.00	0.46	0.37	0.08
328	0.11	0.01	0.46	0.34	0.08
329	0.06	0.00	0.66	0.24	0.04
330	0.08	0.00	0.52	0.33	0.07
331	0.07	0.00	0.53	0.34	0.06
332	0.06	0.00	0.62	0.25	0.06
333	0.04	0.00	0.67	0.24	0.04
334	0.05	0.00	0.57	0.33	0.04
335	0.05	0.00	0.58	0.32	0.04
336	0.08	0.00	0.51	0.34	0.07
337	0.07	0.00	0.52	0.35	0.06
338	0.07	0.00	0.59	0.30	0.05
339	0.09	0.00	0.55	0.28	0.07
340	0.12	0.00	0.47	0.33	0.08
341	0.11	0.01	0.52	0.29	0.07
342	0.16	0.01	0.34	0.40	0.10
343	0.12	0.01	0.53	0.26	0.09
344	0.15	0.01	0.30	0.45	0.09
345	0.11	0.00	0.46	0.33	0.09
346	0.10	0.01	0.46	0.36	0.08

Table SI.3.3a: Blob model parameters obtained by global analysis of the monomer and excimer decays for PyPDMA645 having a concentration of 2.2 g/L (OD = 30).

Excitation Wavelength nm	<n>	$k_{blob} \times 10^7$ s^{-1}	$k_e[blob] \times 10^7$ s^{-1}	τ_{E0} ns	τ_D ns	χ^2
325	1.6	1.6	0.5	42.2	76.9	1.2
326	1.6	1.6	0.5	42.6	78.9	1.1
327	1.6	1.7	0.5	46.1	80.0	1.0
328	1.6	1.6	0.5	46.2	80.9	1.1
329	1.6	1.7	0.6	43.8	78.5	1.1
330	1.7	1.5	0.4	45.4	80.8	1.2
331	1.6	1.6	0.5	44.4	79.9	1.2
332	1.6	1.8	0.6	48.7	86.9	1.2
333	1.6	1.7	0.6	44.6	80.8	1.2
334	1.7	1.5	0.5	44.3	78.6	1.1
335	1.7	1.6	0.5	43.1	77.8	1.2
336	1.7	1.7	0.5	44.0	78.4	1.2
337	1.7	1.5	0.5	44.1	78.8	1.2
338	1.7	1.4	0.5	44.7	79.8	1.2
339	1.7	1.4	0.5	47.0	82.7	1.1
340	1.7	1.5	0.5	47.1	82.1	1.1
341	1.5	1.6	0.5	45.4	81.4	1.1
342	1.7	1.4	0.5	45.5	81.2	1.2
343	1.6	1.4	0.5	46.2	83.0	1.2
344	1.4	1.9	0.7	44.4	80.0	1.1
345	1.6	1.6	0.6	41.6	77.4	1.1
346	1.5	1.8	0.5	44.3	80.0	1.1
347	1.5	1.9	0.6	41.1	75.8	1.2
348	1.5	2.0	0.6	45.0	79.1	1.1
349	1.5	1.9	0.6	45.9	79.8	1.1
350	1.5	2.6	0.8	41.3	74.0	1.0

Table SI.3.3b: Fluorescence contribution fractions obtained for PyPDMA645 having a concentration of 2.2 g/L (OD = 30).

Excitation Wavelength nm	f_{diff}^{f}	f_{free}^{f}	f_{E0}^{f}	f_{D}^{f}	f_{k2}^{f}
325	0.10	0.00	0.42	0.38	0.10
326	0.11	0.00	0.43	0.34	0.11
327	0.06	0.00	0.55	0.33	0.06
328	0.06	0.00	0.56	0.32	0.06
329	0.08	0.00	0.49	0.34	0.08
330	0.06	0.00	0.55	0.31	0.07
331	0.06	0.00	0.53	0.32	0.08
332	0.04	0.00	0.69	0.22	0.04
333	0.06	0.00	0.56	0.31	0.07
334	0.04	0.00	0.55	0.35	0.06
335	0.07	0.00	0.51	0.36	0.06
336	0.05	0.00	0.53	0.36	0.05
337	0.07	0.00	0.52	0.34	0.07
338	0.06	0.00	0.54	0.34	0.06
339	0.05	0.00	0.60	0.29	0.06
340	0.06	0.00	0.58	0.30	0.07
341	0.09	0.00	0.53	0.32	0.06
342	0.09	0.00	0.51	0.31	0.08
343	0.09	0.00	0.53	0.29	0.09
344	0.10	0.00	0.48	0.34	0.09
345	0.11	0.00	0.40	0.37	0.11
346	0.09	0.00	0.50	0.33	0.08
347	0.08	0.00	0.42	0.41	0.09
348	0.05	0.00	0.56	0.34	0.05
349	0.03	0.00	0.59	0.34	0.04
350	0.05	0.00	0.44	0.45	0.06

Table SI.3.4a: Blob model parameters obtained by global analysis of the monomer and excimer decays for PyPDMA479 having a concentration of 1.8 g/L (OD = 15).

Excitation Wavelength nm	<n>	$k_{blob} \times 10^7$ s^{-1}	$k_e[blob] \times 10^7$ s^{-1}	τ_{E0} ns	τ_D ns	χ^2
325	1.1	1.5	0.6	44.8	83.6	1.1
326	1.1	1.5	0.6	39.9	78.1	1.1
327	1.1	1.5	0.6	45.2	82.7	1.1
328	1.2	1.4	0.5	42.1	77.8	1.1
329	1.1	1.5	0.6	42.7	78.5	1.1
330	1.1	1.7	0.6	44.5	81.8	1.1
331	1.1	1.8	0.6	39.9	73.3	1.2
332	1.1	1.7	0.6	42.3	75.9	1.1
333	1.2	1.6	0.5	46.5	84.2	1.1
334	1.1	1.8	0.5	40.1	73.2	1.1
335	1.2	1.5	0.5	43.4	79.1	1.1
336	1.2	1.6	0.6	44.0	78.8	1.2
337	1.2	1.4	0.5	40.4	75.9	1.2
338	1.2	1.4	0.6	42.5	79.5	1.1
339	1.2	1.4	0.5	41.1	77.8	1.2
340	1.1	1.6	0.6	45.7	81.7	1.2
341	1.2	1.3	0.5	42.3	78.7	1.1
342	1.2	1.4	0.6	39.7	76.4	1.1
343	1.1	1.6	0.6	44.5	83.2	1.1
344	1.1	1.5	0.6	38.5	75.7	1.1
345	1.1	0.2	0.6	42.0	79.3	1.2
346	1.1	1.6	0.7	44.8	81.3	1.1
347	1.2	1.5	0.5	45.0	82.4	1.1
348	1.2	1.4	0.4	44.5	80.1	1.1
349	1.1	2.1	0.7	46.0	80.9	1.2
350	1.1	2.3	0.7	46.2	79.5	1.2

Table SI.3.4b: Fluorescence contribution fractions obtained for PyPDMA479 having a concentration of 1.8 g/L (OD = 15).

Excitation Wavelength nm	f_{diff}^{f}	f_{free}^{f}	f_{E0}^{f}	f_{D}^{f}	f_{k2}^{f}
325	0.22	0.02	0.40	0.21	0.15
326	0.24	0.02	0.29	0.30	0.14
327	0.21	0.02	0.43	0.22	0.13
328	0.20	0.02	0.33	0.29	0.16
329	0.19	0.02	0.37	0.27	0.15
330	0.19	0.02	0.44	0.21	0.13
331	0.17	0.02	0.32	0.37	0.12
332	0.15	0.01	0.40	0.32	0.12
333	0.13	0.01	0.54	0.20	0.12
334	0.14	0.01	0.36	0.38	0.11
335	0.15	0.01	0.47	0.26	0.11
336	0.15	0.01	0.47	0.26	0.11
337	0.18	0.01	0.37	0.32	0.12
338	0.19	0.02	0.40	0.26	0.13
339	0.22	0.02	0.35	0.28	0.13
340	0.18	0.02	0.44	0.24	0.12
341	0.23	0.02	0.34	0.27	0.15
342	0.26	0.02	0.28	0.30	0.14
343	0.24	0.02	0.39	0.21	0.13
344	0.27	0.02	0.23	0.32	0.15
345	0.24	0.02	0.33	0.27	0.14
346	0.20	0.02	0.41	0.23	0.14
347	0.18	0.01	0.44	0.22	0.14
348	0.16	0.01	0.43	0.24	0.15
349	0.11	0.01	0.53	0.25	0.10
350	0.09	0.01	0.55	0.25	0.09

Table SI.3.5a: Blob model parameters obtained by global analysis of the monomer and excimer decays for PyPDMA479 having a concentration of 0.08 g/L (OD = 0.7).

Excitation Wavelength nm	<n>	$k_{blob} \times 10^7$ s^{-1}	$k_e[blob] \times 10^7$ s^{-1}	τ_{E0} ns	τ_D ns	χ^2
325	1.0	1.9	0.7	47.5	83.7	1.1
326	1.2	1.4	0.5	40.6	77.9	1.1
327	1.1	1.7	0.7	45.2	79.8	1.1
328	1.2	1.5	0.5	43.7	78.3	1.2
329	1.2	1.4	0.5	47.7	85.8	1.1
330	1.2	1.5	0.5	79.5	92.1	1.2
331	1.2	1.5	0.6	45.0	80.2	1.1
332	1.2	1.4	0.5	45.6	81.5	1.1
333	1.2	1.5	0.5	44.5	79.4	1.1
334	1.2	1.5	0.5	42.7	78.2	1.0
335	1.1	1.7	0.6	42.2	76.9	1.1
336	1.2	1.5	0.5	42.0	74.9	1.0
337	1.1	1.6	0.6	42.9	79.3	1.1
338	1.1	1.6	0.6	40.8	75.8	1.2
339	1.1	1.6	0.6	47.4	92.3	1.1
340	1.1	1.6	0.6	43.6	82.2	1.1
341	1.1	1.5	0.6	42.5	79.6	1.1
342	1.1	1.5	0.6	44.2	83.8	1.0
343	1.1	1.5	0.6	43.6	81.5	1.1
344	1.1	1.7	0.6	45.1	82.3	1.1
345	1.1	1.7	0.6	44.8	82.0	1.1
346	1.1	1.7	0.6	44.6	81.6	1.1
347	1.1	1.7	0.6	46.2	82.6	1.1
348	1.2	1.7	0.6	42.3	77.3	1.0
349	1.1	2.1	0.6	43.9	75.9	1.1
350	1.1	2.3	0.7	41.9	75.1	1.1

Table SI.3.5b: Fluorescence contribution fractions obtained for having a concentration of 0.08 g/L (OD = 0.7).

Excitation Wavelength nm	f_{diff}^{f}	f_{free}^{f}	f_{E0}^{f}	f_{D}^{f}	f_{k2}^{f}
325	0.22	0.02	0.40	0.21	0.15
326	0.24	0.02	0.29	0.30	0.14
327	0.21	0.02	0.43	0.22	0.13
328	0.20	0.02	0.33	0.29	0.16
329	0.19	0.02	0.37	0.27	0.15
330	0.19	0.02	0.44	0.21	0.13
331	0.17	0.02	0.32	0.37	0.12
332	0.15	0.01	0.40	0.32	0.12
333	0.13	0.01	0.54	0.20	0.12
334	0.14	0.01	0.36	0.38	0.11
335	0.15	0.01	0.47	0.26	0.11
336	0.15	0.01	0.47	0.26	0.11
337	0.18	0.01	0.37	0.32	0.12
338	0.19	0.02	0.40	0.26	0.13
339	0.22	0.02	0.35	0.28	0.13
340	0.18	0.02	0.44	0.24	0.12
341	0.23	0.02	0.34	0.27	0.15
342	0.26	0.02	0.28	0.30	0.14
343	0.24	0.02	0.39	0.21	0.13
344	0.27	0.02	0.23	0.32	0.15
345	0.24	0.02	0.33	0.27	0.14
346	0.20	0.02	0.41	0.23	0.14
347	0.18	0.01	0.44	0.22	0.14
348	0.16	0.01	0.43	0.24	0.15
349	0.11	0.01	0.53	0.25	0.10
350	0.09	0.01	0.55	0.25	0.09

Table SI.3.6a: Blob model parameters obtained by global analysis of the monomer and excimer decays for PyPDMA479 having a concentration of 0.01 g/L (OD = 0.1).

Excitation Wavelength nm	<n>	$k_{blob} \times 10^7$ s^{-1}	$k_e[blob] \times 10^7$ s^{-1}	τ_{E0} ns	τ_D ns	χ^2
326	1.1	1.7	0.7	37.0	72.2	1.0
328	1.2	1.5	0.6	38.1	74.0	1.1
330	1.2	1.5	0.5	34.6	70.3	1.1
332	1.2	1.5	0.5	39.1	73.3	1.0
334	1.1	1.9	0.6	41.6	77.5	1.0
336	1.2	1.6	0.5	44.0	79.1	1.0
338	1.2	1.5	0.5	40.8	76.6	1.1
340	1.2	1.4	0.5	36.2	73.4	1.0
342	1.3	1.4	0.6	40.7	78.9	1.0
344	1.1	1.8	0.6	37.3	73.4	1.1

Table SI.3.6b: Fluorescence contribution fractions obtained for PyPDMA479 having a concentration of 0.01 g/L (OD = 0.1).

Excitation Wavelength nm	f_{diff}^{f}	f_{free}^{f}	f_{E0}^{f}	f_{D}^{f}	f_{k2}^{f}
326	0.26	0.03	0.20	0.36	0.14
328	0.24	0.03	0.29	0.31	0.12
330	0.24	0.02	0.22	0.37	0.14
332	0.17	0.02	0.34	0.35	0.12
334	0.17	0.02	0.40	0.30	0.12
336	0.15	0.01	0.45	0.28	0.10
338	0.21	0.02	0.33	0.30	0.14
340	0.25	0.03	0.22	0.36	0.14
342	0.26	0.03	0.33	0.25	0.13
344	0.24	0.03	0.18	0.39	0.16

Table SI.3.7a: Blob model parameters obtained by global analysis of the monomer and excimer decays for PyPDMA263 having a concentration of 4.8 g/L (OD = 30).

Excitation Wavelength nm	<n>	$k_{blob} \times 10^7$ s^{-1}	$k_e[blob] \times 10^7$ s^{-1}	τ_{E0} ns	τ_D ns	χ^2
325	0.7	1.8	0.7	37.1	79.6	1.1
326	0.8	1.2	0.4	40.5	85.9	1.1
327	0.8	1.2	0.5	44.1	93.3	1.0
328	0.8	1.6	0.7	44.6	89.8	1.1
329	0.8	1.6	0.6	41.4	81.8	1.1
330	0.8	1.4	0.6	43.2	85.4	1.1
331	0.8	1.4	0.5	41.4	82.3	1.0
332	0.8	1.4	0.5	45.2	93.2	1.1
333	0.8	1.6	0.5	43.5	86.8	1.1
334	0.8	1.6	0.6	41.1	79.6	1.0
335	0.8	1.4	0.5	43.9	88.5	1.1
336	0.9	1.1	0.4	44.6	90.8	1.1
337	0.8	1.3	0.5	38.8	78.4	1.1
338	0.8	1.3	0.5	39.6	82.6	1.1
339	0.9	1.0	0.4	45.5	97.2	1.1
340	0.8	1.3	0.5	42.9	90.1	1.1
341	0.9	1.2	0.5	43.4	95.3	1.1
342	0.8	1.5	0.6	44.2	94.5	1.0
343	0.8	1.2	0.5	41.7	93.6	1.1
344	0.8	1.4	0.6	40.7	88.7	1.1
345	0.8	1.4	0.6	47.3	105.6	1.1
346	0.8	1.5	0.6	48.4	103.5	1.1
347	0.8	1.4	0.5	45.2	92.9	1.1
348	0.8	1.8	0.6	41.9	80.2	1.0
349	0.8	1.6	0.6	44.4	87.2	1.1
350	0.9	1.7	0.5	40.2	76.0	1.1

Table SI.3.7b: Fluorescence contribution fractions obtained for PyPDMA263 having a concentration of 4.8 g/L (OD = 30).

Excitation Wavelength nm	f_{diff}^{f}	f_{free}^{f}	f_{E0}^{f}	f_{D}^{f}	f_{k2}^{f}
325	0.38	0.11	0.22	0.18	0.11
326	0.35	0.07	0.26	0.16	0.16
327	0.33	0.07	0.34	0.11	0.15
328	0.27	0.08	0.38	0.14	0.13
329	0.29	0.07	0.30	0.20	0.14
330	0.28	0.07	0.36	0.16	0.14
331	0.27	0.06	0.35	0.18	0.13
332	0.24	0.05	0.47	0.11	0.12
333	0.23	0.05	0.46	0.15	0.11
334	0.22	0.06	0.40	0.22	0.11
335	0.22	0.05	0.48	0.14	0.12
336	0.22	0.04	0.48	0.14	0.12
337	0.27	0.05	0.31	0.24	0.13
338	0.31	0.06	0.33	0.18	0.11
339	0.29	0.05	0.40	0.11	0.15
340	0.33	0.08	0.30	0.15	0.14
341	0.34	0.08	0.30	0.12	0.16
342	0.35	0.09	0.31	0.12	0.13
343	0.38	0.09	0.25	0.12	0.16
344	0.38	0.09	0.25	0.15	0.13
345	0.32	0.09	0.38	0.08	0.14
346	0.26	0.07	0.43	0.10	0.14
347	0.26	0.06	0.41	0.15	0.12
348	0.26	0.07	0.36	0.19	0.12
349	0.20	0.05	0.47	0.14	0.13
350	0.18	0.05	0.40	0.25	0.11

Chapter 4 Supporting Information

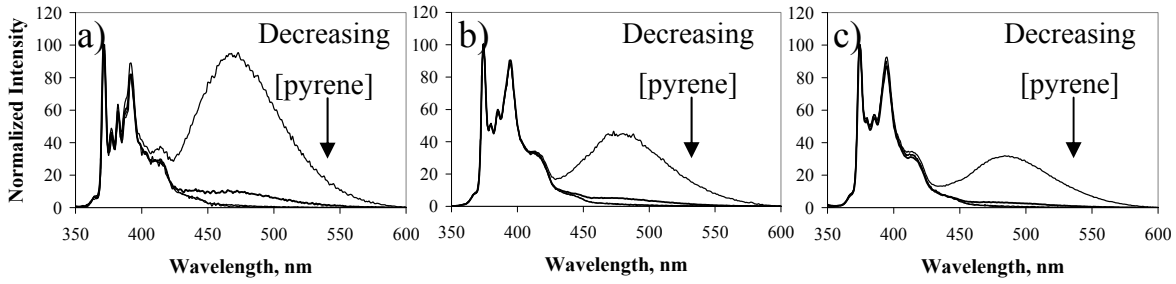

Figure SI.4.1: Fluorescence emission spectra normalized at the 0-0 transition peak for solutions of a) pyrene in acetonitrile, b) PyPEO in acetonitrile, and c) PyPEO in water having concentrations of 2 mM, 0.2 mM, 0.02 mM, and 0.002 mM.

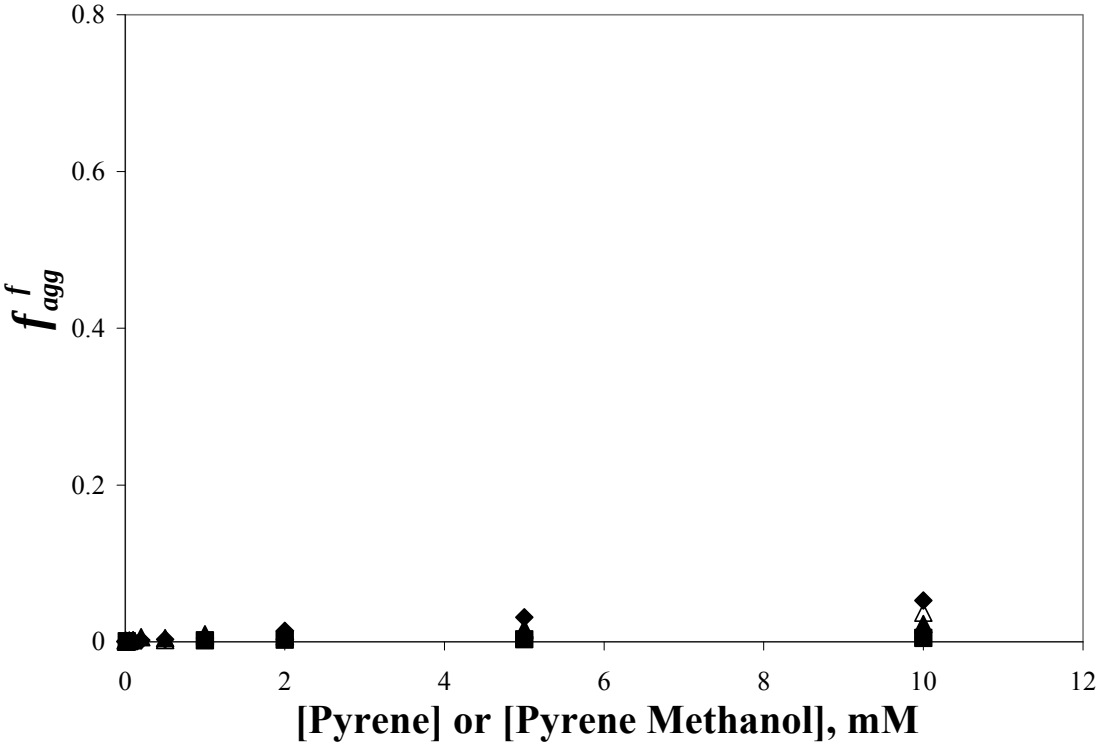

Figure SI.4.2: Fluorescence contribution to the monomer and excimer decays by the aggregated pyrene fraction for pyrene in cyclohexane (◆), DMF (■), and acetonitrile (▲), and 1-pyrenemethanol in acetonitrile (△).

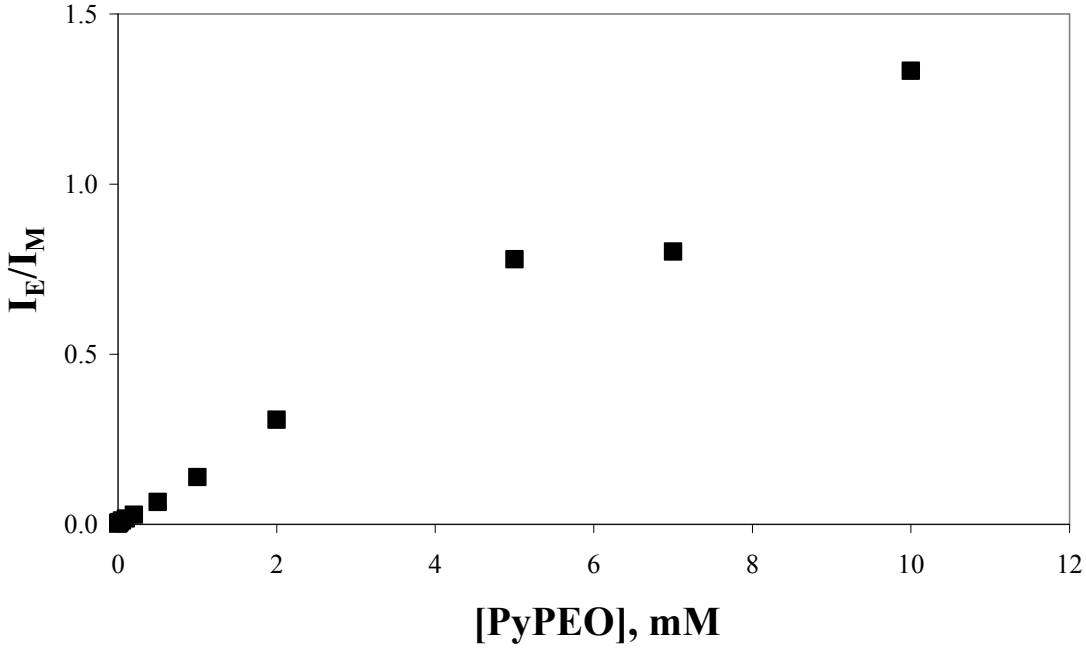

Figure SI.4.3: I_E/I_M ratio for PyPEO solutions in water.

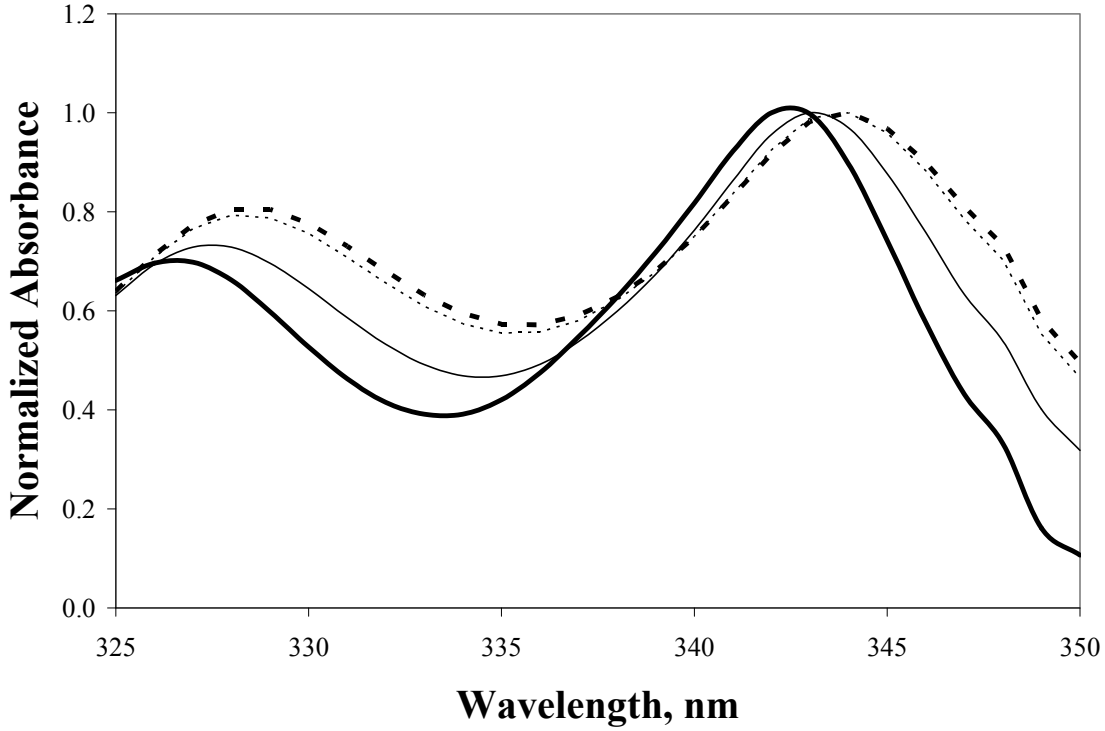

Figure SI.4.4: Absorbance spectra normalized at the 0-0 transition peak for aqueous PyPEO solutions of 2 μM (▬), 5 mM (—), 10 mM (····), and 13 mM (▪▪▪).

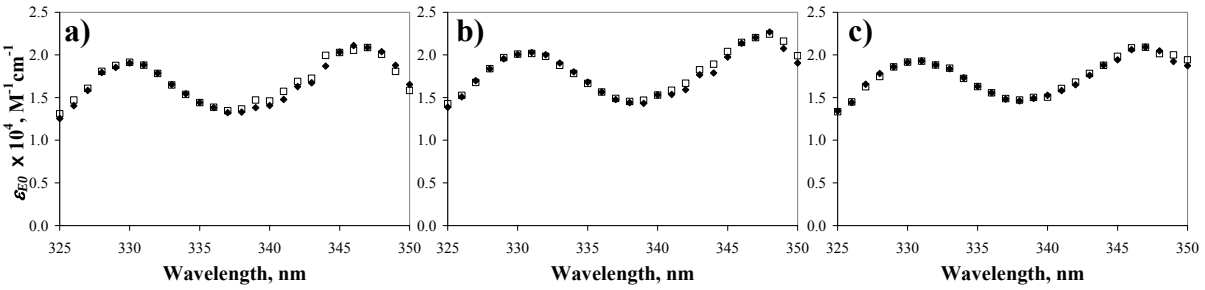

Figure SI.4.5: Molar absorbance coefficients of the pyrene aggregate obtained using model free (hollow) and FBM (filled) analyses for aqueous solutions of PyPDMA with labeling levels of a) 263, b) 479, and c) 645 μmol pyrene/g polymer having 4.8, 1.8, and 2.2 g/L concentrations, respectively.

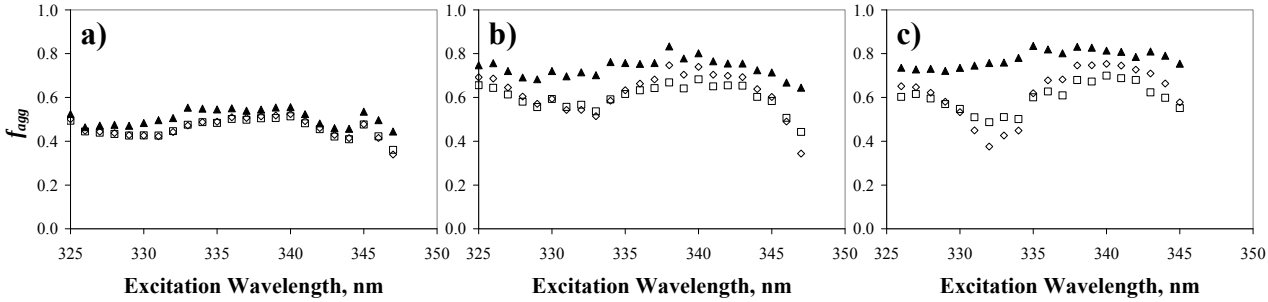

Figure SI.4.6: Fractions of pyrenes aggregated in solution for aqueous solutions of PyPEO having concentrations of a) 5 mM, b) 10 mM, and c) 13 mM assuming pyrene species *ES* absorbs as ε_M (◇), ε_{E0} (▲), and does not absorb (□).

Table SI.4.1: Birks' scheme parameters retrieved for degassed solutions of pyrene in cyclohexane using Equations 1 and 2 assuming $a_{E1} \neq a_{E2}$ to fit the monomer and excimer fluorescence decays, respectively.

[Pyrene] μM	τ_1 ns	τ_2 ns	a_1 ns	a_2 ns	a_{E1} ns	a_{E2} ns	τ_{E0} ns	$k_1[Py]$ $\times 10^6$ s^{-1}	k_{-1} $\times 10^6$ s^{-1}	χ^2
10	46.4	414	0.01	0.99	-0.10	0.13	185	0.3	15.9	0.99
20	46.5	408	0.02	0.98	-0.14	0.17	152	0.4	4.7	1.03
50	44.5	378	0.01	0.99	-0.26	0.28	80.6	0.6	9.8	1.05
100	44.6	345	0.02	0.98	-0.27	0.29	65.9	0.8	7.0	1.06
200	44.7	286	0.04	0.96	-0.30	0.31	72.5	2.0	7.7	1.06
500	42.9	201	0.08	0.92	-0.48	0.49	64.3	4.1	6.2	1.05
1000	40.8	134	0.14	0.86	-0.60	0.61	57.6	7.5	4.7	1.03
2000	35.5	88.5	0.40	0.60	-2.28	2.32	58.7	15.7	4.3	1.21
5000	22.8	66.2	0.77	0.23	-1.67	1.73	57.2	34.9	4.1	1.25
10000	13.8	57.9	0.89	0.11	-1.01	1.06	53.6	64.0	4.6	1.19

Table SI.4.2a: Birks' scheme parameters retrieved for degassed solutions of pyrene in cyclohexane taking into account GS pyrene aggregates of *E0*.

[Pyrene] μM	τ_1 ns	τ_2 ns	a_1	a_2	a_{E1}	a_{E2}	τ_{E0} ns	a_{E0}	$\frac{a_{E0}}{a_{E2}}$	$k_1[Py]$ $\times 10^6$ s^{-1}	k_{-1} $\times 10^6$ s^{-1}	$\frac{[E0^*]_{(t=0)}}{[E0^*]_{(t=0)}+[Py^*_{diff}]_{(t=0)}}$	χ^2
10	49.6	414	0.00	1.00	-0.13	0.13	58.9	0.03	0.23	0.06	3.2	0.001	1.20
20	49.4	408	0.00	1.00	-0.17	0.17	67.0	0.03	0.18	0.11	5.3	0.001	1.08
50	45.8	379	0.01	0.99	-0.28	0.28	69.5	0.02	0.07	0.44	7.3	0.002	1.05
100	46.0	346	0.03	0.97	-0.29	0.29	81.6	0.02	0.07	1.0	9.0	0.003	1.06
200	45.5	287	0.05	0.95	-0.31	0.31	73.6	0.01	0.03	2.0	7.6	0.004	1.05
500	43.1	202	0.08	0.92	-0.49	0.49	64.5	0.01	0.02	4.1	6.2	0.003	1.05
1000	41.0	134	0.14	0.86	-0.61	0.61	57.8	0.01	0.02	7.5	4.7	0.006	1.06
2000	35.7	88.6	0.40	0.60	-2.30	2.30	59.0	0.04	0.02	16	4.3	0.017	1.03
5000	20.6	64.6	0.83	0.17	-0.85	0.85	57.7	0.03	0.04	40	3.9	0.047	1.21
10000	13.8	58.1	0.89	0.11	-1.01	1.01	53.8	0.05	0.05	64	4.6	0.056	1.19

Table SI.4.2b: Birks' scheme parameters retrieved for degassed solutions of pyrene in DMF taking into account GS pyrene aggregates of *E0*.

[Pyrene] μM	τ_1 ns	τ_2 ns	a_1	a_2	a_{E1}	a_{E2}	τ_{E0} ns	a_{E0}	$\frac{a_{E0}}{a_{E2}}$	$k_1[Py]$ $\times 10^6$ s^{-1}	k_{-1} $\times 10^6$ s^{-1}	$\frac{[E0^*]_{(t=0)}}{[E0^*]_{(t=0)}+[Py^*_{diff}]_{(t=0)}}$	χ^2
2	46.9	279	0.00	1.00	-0.05	0.05	61.7	0.06	1.20	0.11	5.1	0.001	1.11
5	51.0	285	0.00	1.00	-0.05	0.05	56.2	0.05	1.00	0.00	1.8	0.000	1.16
10	49.8	285	0.00	1.00	-0.09	0.09	56.7	0.06	0.67	0.01	2.4	0.000	1.15
20	38.6	284	0.00	1.00	-0.10	0.10	52.1	0.05	0.50	0.02	6.7	0.000	1.05
50	36.0	283	0.00	1.00	-0.16	0.16	37.3	0.04	0.25	0.03	1.0	0.000	0.98
100	37.8	277	0.00	1.00	-0.14	0.14	49.0	0.02	0.14	0.14	6.0	0.001	1.02
200	36.6	269	0.01	0.99	-0.36	0.36	64.4	0.03	0.08	0.43	12	0.001	1.06
500	36.3	244	0.04	0.96	-0.39	0.39	74.0	0.01	0.03	1.4	13	0.002	1.05
1000	35.8	210	0.05	0.95	-0.41	0.41	62.8	0.01	0.02	2.5	11	0.002	1.02
2000	35.0	167	0.07	0.93	-0.46	0.46	53.2	0.01	0.02	4.1	8.2	0.003	1.01
5000	32.7	104	0.17	0.83	-1.20	1.20	48.7	0.01	0.01	9.7	6.4	0.003	1.01
10000	28.7	71	0.38	0.62	-2.25	2.25	46.6	0.02	0.01	18	5.5	0.006	1.14

Table SI.4.2c: Birks' scheme parameters retrieved for degassed solutions of pyrene in acetonitrile taking into account GS pyrene aggregates of *E0*.

[Pyrene] μM	τ_1 ns	τ_2 ns	a_1	a_2	a_{E1}	a_{E2}	τ_{E0} ns	a_{E0}	$\frac{a_{E0}}{a_{E2}}$	$k_1[Py]$ $\times 10^6$ s^{-1}	k_{-1} $\times 10^6$ s^{-1}	$\frac{[E0^*]_{(t=0)}}{[E0^*]_{(t=0)}+[Py^*_{diff}]_{(t=0)}}$	χ^2
5	39.0	311	0.00	1.00	-0.26	0.26	46.2	0.09	0.35	0.11	4.0	0.000	1.23
10	37.1	320	0.00	1.00	-0.27	0.27	47.3	0.04	0.15	0.01	5.8	0.000	1.07
20	35.8	314	0.00	1.00	-0.27	0.27	37.4	0.04	0.15	0.06	1.2	0.000	1.07
50	35.2	291	0.01	0.99	-0.28	0.28	53.0	0.02	0.07	0.50	9.4	0.000	1.10
100	34.8	265	0.02	0.98	-0.29	0.29	55.3	0.02	0.07	1.1	10	0.001	1.06
200	33.8	220	0.05	0.95	-0.30	0.30	59.6	0.01	0.03	2.7	12	0.001	1.03
500	31.7	151	0.12	0.88	-0.52	0.52	53.7	0.01	0.02	6.4	10	0.002	1.25
1000	29.3	102	0.22	0.78	-0.63	0.63	49.1	0.01	0.02	12	8.5	0.002	1.18
2000	24.7	73.0	0.42	0.58	-0.69	0.69	47.2	0.01	0.01	22	8.0	0.003	1.12
5000	14.5	53.7	0.78	0.22	-1.53	1.53	46.0	0.03	0.02	55	7.9	0.003	1.22
10000	8.0	48.8	0.91	0.09	-1.08	1.08	45.4	0.03	0.03	110	8.2	0.006	1.17

Table SI.4.2d: Birks' scheme parameters retrieved for degassed solutions of 1-pyrenemethanol in acetonitrile taking into account GS pyrene aggregates of *E0*.

[PyMeOH] μM	τ_1 ns	τ_2 ns	a_1	a_2	a_{E1}	a_{E2}	τ_{E0} ns	a_{E0}	$\frac{a_{E0}}{a_{E2}}$	$k_1[Py]$ $\times 10^6$ s^{-1}	$\frac{k_{-1}}{1}$ $\times 10^6$ s^{-1}	$\frac{[E0^*]_{(t=0)}}{[E0^*]_{(t=0)}+[Py^*_{diff}]_{(t=0)}}$	χ^2
2	58.6	255	0.00	1.00	-0.28	0.28	65.7	0.14	0.50	0.00	1.9	0.000	1.09
5	52.5	252	0.00	1.00	-0.14	0.14	61.7	0.04	0.29	0.05	2.8	0.001	1.05
10	51.9	248	0.00	1.00	-0.21	0.21	66.5	0.03	0.14	0.15	4.3	0.002	1.19
20	49.7	241	0.01	0.99	-0.22	0.22	78.5	0.02	0.09	0.41	7.2	0.002	1.05
50	47.7	223	0.01	0.99	-0.46	0.46	61.8	0.02	0.04	0.77	4.6	0.002	1.07
100	46.9	196	0.02	0.98	-0.48	0.48	57.9	0.01	0.02	1.6	3.7	0.002	1.07
200	46.3	161	0.03	0.97	-0.57	0.57	53.0	0.01	0.02	2.7	2.3	0.002	1.09
500	45.8	102	0.04	0.96	-0.87	0.87	48.8	0.00	0.00	6.4	0.87	0.003	1.11
1000	43.2	71.4	0.22	0.78	-4.01	4.01	50.3	0.02	0.00	12	1.2	0.008	1.12
2000	34.7	53.3	0.76	0.24	-5.25	5.25	49.1	0.03	0.01	22	0.82	0.014	1.29
5000	17.0	50.1	0.97	0.03	-1.94	1.94	49.3	0.03	0.02	54	0.77	0.023	1.30
10000	8.8	49.5	0.99	0.01	-1.23	1.23	49.2	0.05	0.04	110	0.88	0.046	1.24

Table SI.4.3a: Model free global analysis parameters retrieved for degassed solutions of pyrene in cyclohexane.

[Pyrene] μM	τ_1 ns	τ_2 ns	a_1	a_2	a_{Ediff}	τ_{E0} ns	a_{E0}	$k_1[Py]$ $\times 10^6$ s^{-1}	χ^2
2	418		1.00		1.00	48.9	0.00	0.02	1.28
5	417	241	0.99	0.01	1.00	45.4	0.00	0.04	1.07
10	414		1.00		1.00	47.5	0.00	0.05	1.10
20	408	50.2	1.00	0.00	1.00	56.4	0.00	0.08	1.06
50	378		1.00		1.00	44.9	0.00	0.27	1.07
100	347	182	0.99	0.01	1.00	46.0	0.00	0.52	1.05
200	286		1.00		1.00	45.0	0.00	1.1	1.17
500	202	43.0	0.92	0.08	1.00	64.9	0.00	4.1	1.06
1000	134	38.3	0.87	0.13	1.00	57.7	0.00	7.6	0.98
2000	86.2	33.0	0.64	0.36	0.99	58.8	0.01	16	1.12
5000	62.1	21.8	0.26	0.74	0.97	57.3	0.03	36	1.22
10000	55.8	13.6	0.12	0.88	0.95	53.8	0.05	65	1.17

Table SI.4.3b: Model free global analysis retrieved for degassed solutions of pyrene in DMF.

[Pyrene] μM	τ_1 ns	τ_2 ns	a_1	a_2	a_{Ediff}	τ_{E0} ns	a_{E0}	$k_1[Py]$ $\times 10^6$ s^{-1}	χ^2
5	283		1.000		1.00	54.8	0.00	0.03	1.24
10	283		1.000		1.00	47.5	0.00	0.03	1.29
20	283	47.8	1.000	0.00	1.00	39.7	0.00	0.02	1.01
50	279		1.000		1.00	38.4	0.00	0.08	1.22
100	275		1.000		1.00	37.0	0.00	0.13	1.17
200	265		1.000		1.00	34.8	0.00	0.27	1.06
500	240		1.000		1.00	35.4	0.00	0.66	1.12
1000	208	36.0	0.96	0.04	1.00	54.4	0.00	2.2	1.01
2000	166	35.0	0.93	0.07	1.00	52.7	0.00	4.1	0.97
5000	104	31.8	0.83	0.17	1.00	48.9	0.00	9.8	1.05
10000	70.4	28.0	0.63	0.37	1.00	46.6	0.00	19	1.15

Table SI.4.3c: Model free global analysis retrieved for degassed solutions of pyrene in acetonitrile.

[Pyrene] μM	τ_1 ns	τ_2 ns	a_1	a_2	a_{Ediff}	τ_{E0} ns	a_{E0}	$k_1[Py]$ $\times 10^6$ s^{-1}	χ^2
5	311	39.5	1.00	0.00	1.00	46.3	0.00	0.11	1.20
10	318	32.5	1.00	0.00	1.00	56.5	0.00	0.03	1.18
20	313	32.6	1.00	0.00	1.00	50.7	0.00	0.10	1.07
50	292	30.7	1.00	0.00	1.00	37.0	0.00	0.34	1.11
100	265	37.4	1.00	0.01	1.00	40.0	0.00	0.77	1.13
200	221	35.5	0.95	0.05	0.99	57.9	0.01	2.6	1.07
500	151	31.1	0.89	0.12	1.00	53.6	0.00	6.4	1.22
1000	102	29.0	0.79	0.22	0.99	49.0	0.01	12	1.16
2000	72.4	24.3	0.59	0.41	0.99	46.9	0.01	22	1.08
5000	52.3	14.2	0.23	0.77	0.99	46.0	0.01	56	1.07
10000	47.7	7.9	0.10	0.91	0.98	45.5	0.02	110	1.17

Table SI.4.3d: Model free global analysis retrieved for degassed solutions of 1-pyrenemethanol in acetonitrile.

[Pyrene] μM	τ_1 ns	τ_2 ns	a_1	a_2	a_{Ediff}	τ_{E0} ns	a_{E0}	$k_1[Py]$ $\times 10^6$ s^{-1}	χ^2
2	253		1.00		1.00	49.4	0.00	0.04	1.29
5	252		1.00		1.00	49.7	0.00	0.05	1.05
10	248		1.00		1.00	49.0	0.00	0.11	1.18
20	241		1.00		1.00	47.8	0.00	0.23	1.07
50	223	41.0	1.00	0.00	1.00	49.9	0.00	0.61	1.10
100	195		1.00		1.00	46.3	0.00	1.2	1.16
200	161		1.00		1.00	46.6	0.00	2.3	1.22
500	102	38.0	0.94	0.06	1.00	50.7	0.00	6.8	1.18
1000	73.7	47.7	0.66	0.34	0.99	50.5	0.01	12	1.21
2000	43.9	26.3	0.71	0.29	0.99	49.3	0.01	23	1.21
5000	38.0	16.5	0.06	0.94	0.98	49.4	0.02	55	1.23
10000	44.3	8.7	0.01	0.99	0.96	49.1	0.04	110	1.23

Table SI.4.4: Model free global analysis retrieved for degassed solutions of PyPEO in acetonitrile.

[Pyrene] μM	τ_1 ns	τ_2 ns	a_1	a_2	a_{Ediff}	τ_{E0} ns	a_{E0}	τ_{ES} ns	a_{ES}	$k_1[Py]$ $\times 10^6$ s^{-1}	χ^2
2	279	60.0	0.96	0.04	0.91	52.9	0.03	3.5	0.06	2.2	1.06
5	271	12.9	0.98	0.02	0.93	53.9	0.02	3.5	0.05	1.6	1.07
10	270	13.4	0.98	0.02	0.95	54.7	0.02	3.5	0.03	1.2	1.04
20	267	18.3	0.99	0.01	0.97	52.2	0.02	3.5	0.01	0.84	1.18
50	258	11.6	0.96	0.04	0.98	54.1	0.00	3.5	0.02	3.4	1.09
100	247	21.5	0.99	0.01	0.97	55.8	0.03	3.5	0.00	1.0	1.17
200	223	24.7	0.98	0.02	0.95	47.0	0.02	3.5	0.03	1.4	1.22
500	175	33.0	0.92	0.08	0.92	68.5	0.04	3.5	0.04	4.0	0.98
1000	131	34.1	0.89	0.11	0.90	58.3	0.04	3.5	0.06	6.3	1.07
2000	90.2	31.0	0.89	0.11	0.92	51.6	0.04	3.5	0.04	9.9	1.06
3000	57.4	28.6	0.79	0.21	0.93	50.3	0.05	3.5	0.02	17	1.04
5000	44.5	29.1	0.49	0.51	0.94	46.8	0.06	3.5	0.00	25	1.07
7000	40.5	26.0	0.43	0.57	0.91	47.5	0.07	3.5	0.02	29	1.14

Table SI.4.5a: Measured viscosities for solutions of PyPEO in acetonitrile.

[PyPEO] mM	η mPa•s
0	0.369
2.4	0.381
3.2	0.388
4.0	0.397
8.0	0.465

Table SI.4.5b: Measured viscosities for solutions of PyPEO in water.

[PyPEO] mM	η mPa•s
0	0.890
1.2	0.913
2.4	0.987
3.6	1.078
7.0	1.052
10.0	1.141

Table SI.4.6: Model free global analysis retrieved for aqueous solutions of PyPEO.

[Pyrene] μM	τ_1 ns	τ_2 ns	a_1	a_2	a_{Ediff}	τ_{E0} ns	a_{E0}	τ_{ES} ns	a_{ES}	$k_1[Py]$ $\times 10^6$ s^{-1}	χ^2
2	155	51	0.95	0.05	0.90	38.5	0.10	3.5	0.00	0.22	1.15
5	151	110	0.96	0.04	0.94	38.5	0.06	3.5	0.00	0.27	1.28
10	149	118	0.97	0.03	0.91	41.2	0.09	3.5	0.00	0.31	1.28
20	152	143	0.89	0.11	0.93	42.5	0.07	3.5	0.00	0.19	1.29
50	148		1.00		0.96	41.1	0.04	3.5	0.00	0.30	1.20
100	146		1.00		0.97	40.9	0.03	3.5	0.00	0.38	1.13
200	143		1.00		0.97	41.9	0.03	3.5	0.00	0.54	1.10
500	136	43.8	0.99	0.01	0.87	39.2	0.13	3.5	0.00	1.1	1.16
1000	126	42.2	0.96	0.04	0.84	35.8	0.16	3.5	0.00	2.1	1.15
2000	111	39.5	0.94	0.06	0.75	34.9	0.22	3.5	0.03	3.6	1.06
5000	90.9	36.8	0.89	0.11	0.47	39.8	0.38	3.5	0.15	6.4	1.15
7000	78.7	40.0	0.82	0.18	0.29	39.7	0.35	3.5	0.36	8.4	1.30
10000	79.6	28.0	0.87	0.13	0.30	43.2	0.42	3.5	0.28	9.1	1.18

Table SI.4.7a: Model free global analysis retrieved for a 5×10^{-3} M PyPEO solution in water excited with a range of wavelengths.

[PyPEO] μM	τ_1 ns	τ_2 ns	a_1	a_2	a_{Ediff}	τ_{E0} ns	a_{E0}	τ_{ES} ns	a_{ES}	χ^2
325	91.9	32.9	0.92	0.08	0.60	37.7	0.34	3.5	0.06	1.01
326	92.8	43.4	0.84	0.16	0.65	34.3	0.31	3.5	0.03	1.03
327	91.4	37.5	0.88	0.12	0.61	35.7	0.33	3.5	0.06	1.01
328	91.0	33.5	0.89	0.12	0.58	37.2	0.35	3.5	0.07	1.14
329	90.9	34.0	0.88	0.12	0.55	37.6	0.37	3.5	0.08	1.07
330	90.7	31.9	0.89	0.11	0.51	38.9	0.39	3.5	0.10	1.22
331	91.1	38.1	0.86	0.14	0.48	38.6	0.40	3.5	0.12	1.13
332	91.7	39.0	0.86	0.15	0.47	38.5	0.43	3.5	0.11	1.11
333	89.6	32.9	0.87	0.13	0.43	39.1	0.42	3.5	0.15	1.15
334	90.7	38.8	0.85	0.15	0.46	38.4	0.42	3.5	0.12	1.07
335	92.5	42.7	0.83	0.17	0.49	37.3	0.39	3.5	0.12	1.12
336	93.1	47.7	0.81	0.19	0.53	36.9	0.38	3.5	0.10	1.11
337	91.6	41.6	0.85	0.15	0.57	36.8	0.35	3.5	0.08	1.06
338	91.0	39.3	0.87	0.13	0.58	38.0	0.34	3.5	0.08	1.13
339	89.5	31.3	0.91	0.09	0.58	38.9	0.33	3.5	0.10	1.02
340	89.5	27.5	0.91	0.09	0.58	40.4	0.34	3.5	0.09	1.09
341	89.5	35.7	0.89	0.11	0.62	37.0	0.30	3.5	0.08	1.00
342	88.3	32.4	0.92	0.09	0.66	35.4	0.29	3.5	0.05	1.00
343	89.1	35.5	0.90	0.10	0.65	35.1	0.28	3.5	0.07	1.11
344	87.4	37.7	0.88	0.12	0.61	35.1	0.31	3.5	0.08	1.01
345	89.0	40.5	0.86	0.14	0.48	38.9	0.41	3.5	0.11	1.11
346	88.2	30.7	0.89	0.11	0.46	39.0	0.41	3.5	0.13	1.13
347	88.7	35.8	0.88	0.12	0.46	39.2	0.41	3.5	0.13	1.06

Table SI.4.7b: Model free global analysis retrieved for a 1×10^{-2} M PyPEO solution in water excited with a range of wavelengths.

[PyPEO] μM	τ_1 ns	τ_2 ns	a_1	a_2	a_{Ediff}	τ_{E0} ns	a_{E0}	τ_{ES} ns	a_{ES}	χ^2
325	73.8	12.1	0.85	0.15	0.38	41.3	0.36	3.5	0.26	1.28
326	74.3	11.5	0.83	0.18	0.34	41.8	0.34	3.5	0.32	1.28
327	75.7	23.2	0.84	0.17	0.37	39.2	0.36	3.5	0.28	1.20
328	75.8	29.6	0.83	0.17	0.37	37.6	0.37	3.5	0.26	1.13
329	76.6	31.2	0.82	0.18	0.35	37.9	0.37	3.5	0.29	1.20
330	75.5	30.2	0.84	0.17	0.28	40.4	0.41	3.5	0.31	1.10
331	76.6	35.0	0.79	0.21	0.29	39.1	0.40	3.5	0.32	1.12
332	76.0	31.4	0.83	0.18	0.26	39.9	0.40	3.5	0.34	1.09
333	73.5	13.0	0.80	0.20	0.28	40.2	0.37	3.5	0.36	1.23
334	74.9	22.1	0.81	0.19	0.23	40.5	0.35	3.5	0.42	1.19
335	75.0	26.5	0.80	0.20	0.26	39.9	0.37	3.5	0.37	1.13
336	74.1	22.1	0.83	0.17	0.30	39.6	0.37	3.5	0.33	1.27
337	74.0	25.5	0.85	0.15	0.33	38.6	0.35	3.5	0.32	1.14
338	77.9	34.0	0.81	0.19	0.24	39.4	0.26	3.5	0.50	1.30
339	77.2	36.9	0.81	0.19	0.34	36.2	0.28	3.5	0.38	1.26
340	74.9	17.5	0.85	0.15	0.31	41.7	0.31	3.5	0.38	1.25
341	76.1	13.2	0.83	0.17	0.37	41.6	0.30	3.5	0.33	1.18
342	75.8	13.6	0.84	0.16	0.38	42.0	0.33	3.5	0.29	1.19
343	74.4	12.2	0.83	0.17	0.36	43.8	0.35	3.5	0.29	1.23
344	74.1	11.4	0.83	0.17	0.36	42.1	0.34	3.5	0.31	1.08
345	74.1	10.8	0.81	0.19	0.32	43.4	0.37	3.5	0.31	1.14
346	78.6	22.4	0.83	0.17	0.31	41.1	0.36	3.5	0.33	1.24
347	77.0	25.7	0.82	0.18	0.28	39.5	0.36	3.5	0.36	1.11

Table SI.4.7c: Model free global analysis retrieved for a 1.3×10^{-2} M PyPEO solution in water excited with a range of wavelengths.

[PyPEO] μM	τ_1 ns	τ_2 ns	a_1	a_2	a_{Ediff}	τ_{E0} ns	a_{E0}	τ_{ES} ns	a_{ES}	χ^2
326	72.2	13.9	0.83	0.17	0.36	38.0	0.30	3.5	0.33	1.17
327	73.3	19.8	0.85	0.15	0.35	39.8	0.36	3.5	0.29	1.15
328	72.5	18.6	0.84	0.16	0.31	39.6	0.35	3.5	0.34	1.18
329	72.6	17.5	0.83	0.17	0.29	39.9	0.35	3.5	0.35	1.14
330	74.9	34.3	0.77	0.23	0.25	38.9	0.33	3.5	0.42	1.28
331	71.4	12.5	0.81	0.19	0.23	40.4	0.29	3.5	0.48	1.29
332	72.8	20.5	0.79	0.21	0.21	38.6	0.26	3.5	0.53	1.25
333	73.0	22.9	0.79	0.21	0.21	38.6	0.28	3.5	0.51	1.16
334	75.5	30.3	0.77	0.23	0.20	37.0	0.24	3.5	0.56	1.27
335	73.8	19.5	0.78	0.22	0.17	40.8	0.24	3.5	0.59	1.10
336	75.1	30.2	0.77	0.23	0.21	39.5	0.27	3.5	0.52	1.23
337	74.3	25.6	0.80	0.20	0.26	37.5	0.25	3.5	0.49	1.15
338	73.4	18.4	0.81	0.19	0.24	42.0	0.29	3.5	0.47	1.22
339	73.7	22.3	0.83	0.17	0.26	40.7	0.27	3.5	0.47	1.23
340	73.0	18.6	0.84	0.16	0.29	42.8	0.33	3.5	0.38	1.18
341	72.9	20.4	0.82	0.18	0.30	42.2	0.31	3.5	0.38	1.17
342	72.3	19.0	0.85	0.15	0.33	41.8	0.34	3.5	0.33	1.16
343	76.6	27.4	0.84	0.16	0.27	39.5	0.23	3.5	0.49	1.26
344	73.7	20.0	0.83	0.17	0.26	41.2	0.26	3.5	0.48	1.11
345	72.8	16.6	0.83	0.17	0.27	40.8	0.28	3.5	0.45	1.09

Chapter 5 Supporting Information

Table SI.5.1a: Parameters retrieved from the global FBM analysis of the monomer and excimer fluorescence decays of a 95 g/L PyHASE12 in 0.01 M Na_2CO_3, pH 9 solution.

λ_{exc} nm	$k_{ex}[blob]$ $\times 10^7\ s^{-1}$	a_{Mblob}	k_{blob} $\times 10^7\ s^{-1}$	<n>	τ_M ns	a_{Mfree}	a_{Ediff}	τ_{E0} ns	a_{EE0}	τ_{EEL} ns	a_{EEL}	τ_{ES} ns	a_{EES}	χ^2
325	1.0	0.563	8.2	1.54	165	0.437	0.574	50.0	0.029	170.9	0.048	3.5	0.348	1.10
326	1.0	0.568	8.6	1.51	165	0.432	0.595	50.0	0.028	184.5	0.041	3.5	0.337	1.00
327	1.1	0.574	9.0	1.55	165	0.426	0.589	50.0	0.028	171.6	0.045	3.5	0.338	1.19
328	1.0	0.589	8.8	1.59	165	0.411	0.577	50.0	0.029	173.6	0.041	3.5	0.353	0.93
329	1.1	0.542	8.4	1.55	165	0.458	0.578	50.0	0.029	183.6	0.042	3.5	0.350	0.97
330	1.0	0.589	8.7	1.59	165	0.411	0.565	50.0	0.031	175.9	0.038	3.5	0.366	1.05
331	0.8	0.630	9.0	1.64	165	0.370	0.554	50.0	0.031	169.9	0.037	3.5	0.377	1.01
332	0.8	0.649	8.5	1.71	165	0.351	0.522	50.0	0.034	178.3	0.030	3.5	0.414	0.99
333	0.8	0.658	8.3	1.77	165	0.342	0.493	50.0	0.036	173.6	0.033	3.5	0.437	1.07
334	0.7	0.705	8.6	1.84	165	0.295	0.476	50.0	0.037	146.6	0.042	3.5	0.445	1.13
335	0.7	0.709	8.1	1.87	165	0.291	0.455	50.0	0.039	141.2	0.043	3.5	0.464	1.07
336	0.7	0.701	8.1	1.86	165	0.299	0.459	50.0	0.038	144.4	0.046	3.5	0.457	1.14
337	0.7	0.681	7.9	1.83	165	0.319	0.464	50.0	0.036	125.4	0.064	3.5	0.435	1.00
338	0.8	0.649	7.8	1.72	165	0.351	0.488	50.0	0.035	144.4	0.054	3.5	0.422	1.02
339	1.0	0.598	7.2	1.76	165	0.402	0.498	50.0	0.032	129.2	0.092	3.5	0.379	1.11
340	1.1	0.586	7.8	1.63	165	0.414	0.532	50.0	0.031	149.9	0.069	3.5	0.368	0.99
341	1.0	0.576	7.2	1.69	165	0.424	0.535	50.0	0.030	145.0	0.073	3.5	0.362	1.11
342	1.1	0.553	7.3	1.62	165	0.447	0.553	50.0	0.028	136.9	0.078	3.5	0.341	1.11
343	1.1	0.548	7.9	1.54	165	0.452	0.572	50.0	0.028	156.0	0.062	3.5	0.338	1.09
344	1.0	0.555	7.8	1.58	165	0.445	0.579	50.0	0.028	153.0	0.060	3.5	0.333	1.14
345	1.0	0.567	7.4	1.64	165	0.433	0.568	50.0	0.029	160.4	0.053	3.5	0.350	1.05
346	1.0	0.585	8.2	1.60	165	0.415	0.563	50.0	0.030	159.5	0.046	3.5	0.360	1.11
347	0.9	0.633	8.1	1.79	165	0.367	0.537	50.0	0.032	145.1	0.052	3.5	0.379	1.14

Table SI.5.1b: Parameters retrieved from the global FBM analysis of the monomer and excimer fluorescence decays of a 1.3 g/L PyHASE35 in 0.01 M Na_2CO_3, pH 9 solution.

λ_{exc} nm	$k_{ex}[blob]$ $\times 10^7\ s^{-1}$	a_{Mblob}	k_{blob} $\times 10^7\ s^{-1}$	<n>	τ_M ns	a_{Mfree}	a_{Ediff}	τ_{E0} ns	a_{EE0}	τ_{EEL} ns	a_{EEL}	τ_{ES} ns	a_{EES}	χ^2
325	0.8	0.376	7.5	0.60	165	0.624	0.444	50.0	0.425	132.6	0.079	3.5	0.051	1.07
326	0.8	0.380	8.6	0.61	165	0.620	0.428	50.0	0.452	141.5	0.066	3.5	0.055	1.14
327	0.8	0.395	8.2	0.61	165	0.605	0.410	50.0	0.475	147.3	0.058	3.5	0.057	1.27
328	0.8	0.405	10.4	0.63	165	0.595	0.417	50.0	0.479	156.7	0.046	3.5	0.058	1.09
329	0.8	0.407	8.4	0.66	165	0.593	0.319	50.0	0.563	164.8	0.050	3.5	0.068	1.08
330	0.7	0.440	10.3	0.71	165	0.560	0.278	50.0	0.593	153.2	0.057	3.5	0.072	1.11
331	0.8	0.431	6.7	0.66	165	0.569	0.213	50.0	0.641	148.4	0.069	3.5	0.078	0.97
332	0.7	0.444	4.2	0.71	165	0.556	0.137	50.0	0.693	136.0	0.086	3.5	0.084	1.10
333	0.6	0.474	4.3	0.69	165	0.526	0.100	50.0	0.714	134.5	0.099	3.5	0.086	1.03
334	0.7	0.471	4.7	0.69	165	0.529	0.091	50.0	0.718	135.6	0.104	3.5	0.087	1.02
335	0.7	0.448	3.6	0.68	165	0.552	0.112	50.0	0.684	130.5	0.120	3.5	0.083	1.07
336	0.7	0.452	3.9	0.66	165	0.548	0.125	50.0	0.653	126.9	0.143	3.5	0.079	1.06
337	0.6	0.438	3.6	0.68	165	0.562	0.191	50.0	0.601	130.9	0.135	3.5	0.073	1.09
338	0.7	0.422	4.6	0.59	165	0.578	0.275	50.0	0.534	126.5	0.126	3.5	0.065	1.06
339	0.7	0.427	4.1	0.62	165	0.573	0.305	50.0	0.515	132.3	0.117	3.5	0.062	1.08
340	0.8	0.414	5.2	0.55	165	0.586	0.362	50.0	0.473	128.5	0.109	3.5	0.057	1.06
341	0.8	0.392	5.3	0.55	165	0.608	0.404	50.0	0.450	134.2	0.092	3.5	0.054	1.05
342	0.8	0.390	5.6	0.55	165	0.610	0.441	50.0	0.435	148.4	0.072	3.5	0.053	1.08
343	0.8	0.380	6.6	0.59	165	0.620	0.422	50.0	0.449	143.9	0.075	3.5	0.054	1.10
344	0.8	0.380	8.4	0.60	165	0.620	0.432	50.0	0.459	152.0	0.053	3.5	0.056	1.09
345	0.8	0.394	8.4	0.66	165	0.606	0.407	50.0	0.488	162.8	0.046	3.5	0.059	1.16
346	0.7	0.427	9.0	0.74	165	0.573	0.287	50.0	0.584	152.2	0.058	3.5	0.071	1.12
347	0.7	0.452	7.0	0.76	165	0.548	0.176	50.0	0.686	157.3	0.055	3.5	0.083	1.16

Table SI.5.1c: Parameters retrieved from the global FBM analysis of the monomer and excimer fluorescence decays of a 10 g/L PyHASE65 in 0.01 M Na_2CO_3, pH 9 solution.

λ_{exc} nm	$k_{ex}[blob]$ $\times 10^7\ s^{-1}$	a_{Mblob}	k_{blob} $\times 10^7\ s^{-1}$	<n>	τ_M ns	a_{Mfree}	a_{Ediff}	τ_{E0} ns	a_{EE0}	τ_{EEL} ns	a_{EEL}	τ_{ES} ns	a_{EES}	χ^2
325	0.8	0.549	5.1	1.17	165	0.451	0.544	50.0	0.251	179.9	0.029	3.5	0.176	1.01
326	1.0	0.536	5.8	1.09	165	0.464	0.550	50.0	0.252	188.1	0.022	3.5	0.176	0.99
327	0.9	0.548	5.8	1.09	165	0.452	0.548	50.0	0.253	178.5	0.022	3.5	0.177	1.12
328	0.9	0.561	5.7	1.12	165	0.439	0.535	50.0	0.261	182.4	0.022	3.5	0.182	1.12
329	0.9	0.532	5.9	1.10	165	0.468	0.531	50.0	0.265	211.9	0.018	3.5	0.186	1.04
330	0.9	0.569	6.1	1.17	165	0.431	0.508	50.0	0.275	179.8	0.025	3.5	0.192	1.02
331	0.9	0.578	5.7	1.21	165	0.422	0.480	50.0	0.293	185.4	0.022	3.5	0.205	1.10
332	0.8	0.596	5.9	1.21	165	0.404	0.459	50.0	0.304	159.1	0.025	3.5	0.213	1.07
333	0.7	0.600	5.4	1.21	165	0.400	0.442	50.0	0.314	159.5	0.023	3.5	0.220	0.97
334	0.7	0.597	5.2	1.23	165	0.403	0.422	50.0	0.325	164.0	0.025	3.5	0.228	1.05
335	0.7	0.597	5.2	1.19	165	0.403	0.412	50.0	0.328	150.9	0.030	3.5	0.230	1.07
336	0.8	0.584	5.7	1.11	165	0.416	0.425	50.0	0.324	171.8	0.024	3.5	0.227	1.13
337	0.7	0.582	5.0	1.12	165	0.418	0.435	50.0	0.314	143.8	0.032	3.5	0.220	1.08
338	0.8	0.564	5.3	1.08	165	0.436	0.465	50.0	0.299	166.6	0.027	3.5	0.210	1.16
339	0.8	0.560	5.2	1.08	165	0.440	0.497	50.0	0.282	172.3	0.024	3.5	0.197	1.15
340	0.8	0.555	5.3	1.05	165	0.445	0.513	50.0	0.270	158.6	0.028	3.5	0.189	1.03
341	0.8	0.551	5.4	1.07	165	0.449	0.532	50.0	0.260	171.9	0.027	3.5	0.182	1.13
342	0.8	0.554	5.3	1.08	165	0.446	0.534	50.0	0.260	177.5	0.025	3.5	0.182	1.25
343	0.8	0.550	5.5	1.04	165	0.450	0.546	50.0	0.253	168.8	0.024	3.5	0.177	1.09
344	0.8	0.549	5.3	1.06	165	0.451	0.547	50.0	0.254	177.9	0.022	3.5	0.178	1.15
345	0.6	0.591	7.0	1.04	165	0.409	0.560	50.0	0.253	259.4	0.009	3.5	0.177	1.16
346	0.7	0.598	7.4	1.07	165	0.402	0.537	50.0	0.269	277.5	0.006	3.5	0.188	1.07
347	0.6	0.617	6.9	1.15	165	0.383	0.495	50.0	0.292	290.3	0.009	3.5	0.204	1.14

Chapter 6 Supporting Information

Table SI.6.1a: Parameters retrieved by fitting the simulated monomer and excimer fluorescence decays to Equations 1 and 2, respectively, with τ_{E0} and τ_{ES} unfixed.

Background	τ_{E0} ns	τ_{EL} ns	τ_{ES} ns	f_{diff}^{f}	f_{free}^{f}	f_{agg}^{f}
$Back_{monomer}$ = 10 $Back_{excimer}$ = 30	69 ± 2	183 ± 5	3.4 ± 0.2	0.20 ± 0.01	0.20 ± 0.01	0.60 ± 0.03
$Back_{monomer}$ = 30 $Back_{excimer}$ = 100	69 ± 2	182 ± 8	3.4 ± 0.2	0.20 ± 0.01	0.20 ± 0.01	0.60 ± 0.04
$Back_{monomer}$ = 100 $Back_{excimer}$ = 300	69 ± 3	182 ± 11	3.4 ± 0.2	0.20 ± 0.01	0.20 ± 0.01	0.60 ± 0.04
$Back_{monomer}$ = 300 $Back_{excimer}$ = 1000	68 ± 4	183 ± 18	3.4 ± 0.2	0.20 ± 0.01	0.20 ± 0.01	0.61 ± 0.05
Inputted values	68	180	3.5	0.20	0.20	0.60

Table SI.6.1b: Parameters retrieved by fitting the simulated monomer and excimer fluorescence decays to Equations 1 and 2, respectively, with τ_{E0} and τ_{ES} fixed to the inputted value.

Background	τ_{E0} ns	τ_{EL} ns	τ_{ES} ns	f_{diff}^{f}	f_{free}^{f}	f_{agg}^{f}
$Back_{monomer}$ = 10 $Back_{excimer}$ = 30	68	181 ± 3	3.5	0.20 ± 0.00	0.20 ± 0.00	0.60 ± 0.02
$Back_{monomer}$ = 30 $Back_{excimer}$ = 100	68	181 ± 4	3.5	0.20 ± 0.00	0.20 ± 0.01	0.60 ± 0.02
$Back_{monomer}$ = 100 $Back_{excimer}$ = 300	68	179 ± 3	3.5	0.20 ± 0.00	0.20 ± 0.00	0.60 ± 0.02
$Back_{monomer}$ = 300 $Back_{excimer}$ = 1000	68	180 ± 5	3.5	0.20 ± 0.00	0.20 ± 0.01	0.60 ± 0.02
Inputted values	68	180	3.5	0.20	0.20	0.60

Table SI.6.2a: Viscosity profiles of PyHASE in 0.01 M Na_2CO_3, pH 9 solutions under steady shear using the parallel plate geometry.

[PyHASE] 2.0 w/w%		[PyHASE] 3.0 w/w%		[PyHASE] 4.0 w/w%		[PyHASE] 5.0 w/w%	
Shear Rate s^{-1}	Viscosity Pa.s	Shear Rate s^{-1}	Viscosity Pa.s	Shear Rate s^{-1}	Viscosity Pa.s	Shear Rate s^{-1}	Viscosity Pa.s
0.001	1,440	0.00102	4,950	0.00104	9,520	0.000959	17,300
0.0014	997	0.00124	5,360	0.00127	8,250	0.00143	11,200
0.00173	842	0.0017	4,580	0.00143	7,550	0.00181	7,850
0.00249	634	0.00205	4,360	0.00201	5,420	0.0023	5,690
0.00327	505	0.00239	3,880	0.00273	3,990	0.0033	2,970
0.00432	427	0.00302	3,240	0.00328	3,250	0.00413	2,670
0.00579	348	0.00336	2,610	0.00408	2,560	0.00583	1,930
0.00784	277	0.00361	2460	0.00515	2,000	0.00785	1,450
0.0106	227	0.0041	2160	0.00645	1,570	0.0104	1,110
0.0139	209	0.00496	1770	0.00772	1,300	0.0142	812
0.019	175	0.00587	1470	0.0105	954	0.0191	606
0.0252	134	0.00602	1460	0.013	768	0.0257	449
0.0342	106	0.00734	1200	0.0169	585	0.0343	339
0.046	74	0.00812	1100	0.0213	460	0.0458	255
0.0613	37.8	0.0105	859	0.0271	360	0.0613	198
0.0822	22.3	0.0117	789	0.0337	290	0.0825	138
0.11	31	0.0131	714	0.0428	227	0.111	90.7
0.148	17.6	0.0157	611	0.0542	181	0.148	82
0.199	16.4	0.018	544	0.0687	146	0.198	65.3
0.266	11.8	0.0208	483	0.0865	119	0.266	55.8
0.358	6.75	0.024	424	0.11	101	0.357	41.1
0.481	5.36	0.0277	375	0.139	89.8	0.48	28.1
0.643	3.54	0.0316	334	0.175	78.1	0.644	24.3
0.863	2.58	0.0368	290	0.222	63.4	0.865	19.4
1.16	2.16	0.0421	260	0.281	48.7	1.16	13.4
1.56	1.68	0.0487	229	0.356	37.6	1.55	11.6
2.08	1.21	0.0567	202	0.45	28.8	2.08	8.65
2.8	1.04	0.0649	180	0.569	22.4	2.8	7.14
3.75	0.792	0.0749	160	0.72	18.4	3.75	5.24
5.04	0.577	0.0868	140	0.911	16.1	5.04	4.2
6.76	0.508	0.0998	125	1.15	14.3	6.76	3.54
9.06	0.431	0.138	53.4	1.46	10.9	9.06	2.87
12.2	0.363	0.176	73.7	1.84	8.42	12.2	2.29
16.3	0.308	0.222	45.2	2.33	6.59	16.3	1.88
21.9	0.241	0.282	30.8	2.95	5.73	21.9	1.47
29.4	0.215	0.355	30.9	3.73	5.35	29.4	1.2

39.4	0.176	0.449	28.7	4.72	4.12	39.4	0.966
52.9	0.157	0.568	16.8	5.96	3.16	52.9	0.807
71	0.135	0.72	15.1	7.54	2.77	71	0.658
95.2	0.116	0.913	6.97	9.55	2.48	95.2	0.545
128	0.0993	1.15	8.64	12.1	1.89	128	0.458
171	0.0843	1.46	5.18	15.3	1.62	171	0.385
230	0.0724	1.84	4.57	19.3	1.45	230	0.323
309	0.0622	2.33	3.31	24.4	1.12	309	0.274
414	0.05	2.95	2.76	30.9	1.04	414	0.232
556	0.0394	3.73	2.18	39.1	0.822	555	0.197
745	0.0327	4.71	1.8	49.4	0.731	745	0.167
		5.96	1.17	62.5	0.607		
		7.55	1.02	79	0.54		
		9.55	0.869	100	0.473		
		12.1	0.826				
		15.3	0.574				
		19.3	0.478				
		24.4	0.411				
		30.9	0.387				
		39.1	0.317				
		49.4	0.271				
		62.5	0.237				
		79.1	0.206				
		100	0.203				

Table SI.6.2b: Viscosity profiles of PyHASE in 0.01 M Na_2CO_3, pH 9 solutions under steady shear using the couette flow geometry.

[PyHASE] 0.5 w/w%		[PyHASE] 1.0 w/w%	
Shear Rate s^{-1}	Viscosity Pa.s	Shear Rate s^{-1}	Viscosity Pa.s
0.594	0.00707	0.0703	0.0429
0.8	0.00508	0.1	0.0185
1.08	0.00735	0.143	0.0419
1.45	0.00747	0.203	0.0446
1.95	0.0065	0.289	0.0352
2.63	0.00722	0.413	0.0417
3.53	0.00683	0.588	0.0368
4.76	0.00648	0.838	0.0348
6.4	0.0061	1.19	0.0374
8.62	0.00603	1.7	0.0353
11.6	0.00605	2.42	0.033
15.6	0.00582	3.46	0.0304
21	0.00568	4.92	0.0272
28.3	0.00537	7.02	0.0255
38.1	0.00523	10	0.0231
51.2	0.00503	14.3	0.0208
69	0.00489	20.3	0.0185
92.8	0.00478	28.9	0.0167
125	0.00471	41.2	0.015
168	0.00466	58.8	0.0136
226	0.00489	83.8	0.0124
305	0.00657	119	0.0115
410	0.00777	170	0.0108
		242	0.0103
		346	0.01

Table SI.6.3: FBM parameters obtained from the global analysis parameters of the monomer and excimer decays for PyHASE65 in 0.01 M Na_2CO_3, pH 9 aqueous solutions with τ_M and τ_{E0} fixed to the values given in Table 1 and τ_{ES} was fixed to 3.5 ns in the analysis. Note: samples marked with * were analyzed using decays obtained for solutions in a triangular cell.

[PyHASE65] w/w%	Shear Rate s^{-1}	$k_{ex}[blob]$ $\times 10^7$ s^{-1}	<n>	k_{blob} $\times 10^7$ s^{-1}	a_{Mblob}	a_{Mfree}	a_{Eblob}	a_{EE0}	a_{EEL}	a_{EES}
0.5	0*	0.8	1.04	2.4	0.51	0.49	0.37	0.28	0.05	0.30
	0	0.7	1.09	2.5	0.59	0.41	0.40	0.36	0.05	0.19
	100	0.7	1.09	2.7	0.59	0.41	0.41	0.35	0.06	0.17
1	0*	0.6	1.05	2.5	0.58	0.42	0.45	0.30	0.04	0.21
	0	0.4	1.80	1.7	0.55	0.45	0.39	0.30	0.11	0.20
	100	0.6	1.30	2.0	0.60	0.40	0.43	0.31	0.09	0.17
2	0*	0.5	0.89	2.6	0.64	0.36	0.42	0.28	0.03	0.27
	0	0.7	1.06	2.4	0.52	0.48	0.40	0.27	0.06	0.27
	0.1	0.6	1.04	2.7	0.65	0.35	0.41	0.25	0.07	0.28
	100	0.6	1.00	2.8	0.61	0.39	0.42	0.27	0.06	0.26
3	0*	0.5	0.85	2.2	0.65	0.35	0.38	0.27	0.05	0.31
	0	0.5	1.05	1.8	0.57	0.43	0.37	0.23	0.06	0.33
	0.1	0.7	0.97	2.9	0.60	0.40	0.36	0.28	0.05	0.31
	100	0.6	0.97	2.7	0.60	0.40	0.34	0.28	0.06	0.32
4	0*	0.6	0.95	2.0	0.54	0.46	0.28	0.27	0.07	0.38
	0	0.7	1.00	2.8	0.54	0.46	0.28	0.23	0.07	0.42
	0.1	0.4	1.25	1.6	0.51	0.49	0.24	0.25	0.10	0.41
	100	0.7	0.95	2.4	0.50	0.50	0.27	0.24	0.08	0.41
5	0*	0.5	1.10	2.0	0.50	0.50	0.23	0.27	0.09	0.42
	0	0.7	1.00	2.3	0.47	0.53	0.24	0.25	0.08	0.43
	0.1	0.8	0.94	3.2	0.52	0.48	0.27	0.23	0.06	0.44
	100	0.7	0.99	2.5	0.49	0.51	0.26	0.26	0.07	0.41

Table SI.6.4: Viscosity profiles of 3 w/w% PyHASE in 0.01 M Na_2CO_3, pH 9 solutions under steady shear with 480 nm PS latex particles added.

PS Latex Content 0 w/w%		PS Latex Content 0.5 w/w%		PS Latex Content 1.0 w/w%		PS Latex Content 2.0 w/w%	
Shear Rate s^{-1}	Viscosity Pa.s	Shear Rate s^{-1}	Viscosity Pa.s	Shear Rate s^{-1}	Viscosity Pa.s	Shear Rate s^{-1}	Viscosity Pa.s
0.00102	4,950	0.00101	1,620	0.00105	1,710	0.000933	1,510
0.00124	5,360	0.00133	1,290	0.00133	1,560	0.00129	1,190
0.0017	4,580	0.00174	1,220	0.0018	1,260	0.00179	1,160
0.00205	4,360	0.00239	890	0.00231	992	0.00223	1,040
0.00239	3,880	0.00314	698	0.00299	759	0.00299	830
0.00302	3,240	0.00406	577	0.00408	643	0.00409	639
0.00382	2,550	0.00548	436	0.00559	593	0.00556	469
0.00524	1,710	0.00727	331	0.00717	599	0.00716	349
0.00658	1,150	0.00959	262	0.00962	429	0.00964	261
0.00835	674	0.0124	210	0.0127	316	0.0127	203
0.0105	349	0.0164	186	0.017	231	0.0167	161
0.0133	328	0.0223	167	0.022	179	0.0222	132
0.0168	375	0.0293	141	0.0296	136	0.0297	112
0.0215	409	0.0389	118	0.0393	107	0.0393	96.6
0.0265	354	0.0517	92.2	0.0517	85.1	0.0518	74.2
0.0338	261	0.0687	68.6	0.0687	67.7	0.0687	56.8
0.0428	138	0.0907	49.6	0.0911	53.1	0.0912	40.6
0.0542	147	0.121	42.4	0.121	41.7	0.121	33.3
0.0687	143	0.16	38.3	0.16	33.1	0.16	29.5
0.0872	139	0.212	34.3	0.212	26	0.213	19
0.11	78.2	0.281	23.6	0.281	20.6	0.281	16.2
0.138	53.4	0.373	16	0.373	16.5	0.373	12.7
0.176	73.7	0.495	12.2	0.495	13	0.494	9.13
0.222	45.2	0.655	9.89	0.655	10.5	0.657	7.97
0.282	30.8	0.869	7.46	0.869	8.22	0.868	6.18
0.355	30.9	1.15	5.58	1.15	6.68	1.15	4.78
0.449	28.7	1.52	4.73	1.53	5.33	1.53	4.04
0.568	16.8	2.02	3.39	2.02	4.3	2.02	3.3
0.72	15.1	2.68	2.87	2.68	3.45	2.68	2.83
0.913	6.97	3.56	2.28	3.56	2.82	3.56	2.17
1.15	8.64	4.71	1.96	4.71	2.27	4.72	1.71
1.46	5.18	6.25	1.47	6.25	1.86	6.25	1.43
1.84	4.57	8.29	1.23	8.29	1.53	8.29	1.18
2.33	3.31	11	1.02	11	1.25	11	0.986
2.95	2.76	14.6	0.858	14.6	1.03	14.6	0.816
3.73	2.18	19.3	0.721	19.3	0.847	19.3	0.669

4.71	1.8	25.6	0.592	25.6	0.699	25.6	0.574
5.96	1.17	33.9	0.508	33.9	0.581	33.9	0.472
7.55	1.02	45	0.417	45	0.487	45	0.404
9.55	0.869	59.6	0.352	59.6	0.41	59.6	0.339
12.1	0.826	79.1	0.299	79.1	0.346	79.1	0.29
15.3	0.574	105	0.259	105	0.294	105	0.248
19.3	0.478	139	0.217	139	0.251	139	0.214
24.4	0.411	184	0.185	184	0.215	184	0.186
30.9	0.387	244	0.157	244	0.186	244	0.162
39.1	0.317	324	0.132	324	0.161	324	0.142
49.4	0.271	429	0.114	429	0.14	429	0.124
62.5	0.237	569	0.0965	569	0.121	569	0.108
79.1	0.206	754	0.0816	754	0.105	754	0.095
100	0.203						

Table SI.6.5: FBM parameters obtained from the global analysis parameters of the monomer and excimer decays with τ_{E0} = 62 ns and τ_{ES} = 3.5 ns for 3 w/w% solutions of PyHASE65 with 480 nm polystyrene latex particles.

Latex Content w/w%	Shear Rate s^{-1}	$k_{ex}[blob]$ $\times 10^7$ s^{-1}	$<n>$	k_{blob} $\times 10^7$ s^{-1}	a_{Mblob}	a_{Mfree}	a_{Eblob}	a_{EE0}	a_{EEL}	a_{EES}
0	0	0.5	1.05	1.8	0.57	0.43	0.37	0.23	0.06	0.33
	0.1	0.7	0.97	2.9	0.60	0.40	0.36	0.28	0.05	0.31
	100	0.6	0.97	2.7	0.60	0.40	0.34	0.28	0.06	0.32
0.5	0	0.4	1.00	2.6	0.45	0.55	0.19	0.21	0.13	0.47
	0.1	0.4	1.02	2.5	0.45	0.55	0.19	0.20	0.15	0.46
	100	0.5	1.15	2.3	0.46	0.54	0.21	0.21	0.13	0.44
1	0	0.6	1.10	2.4	0.50	0.50	0.19	0.22	0.14	0.46
	0.1	0.6	1.03	2.9	0.44	0.56	0.23	0.22	0.10	0.45
	100	0.7	1.03	3.4	0.48	0.52	0.21	0.22	0.11	0.46
2	0	0.6	1.12	2.7	0.52	0.48	0.16	0.18	0.15	0.51
	0.1	0.9	0.99	3.8	0.47	0.53	0.19	0.20	0.10	0.51
	100	0.8	1.02	3.9	0.45	0.55	0.19	0.19	0.10	0.52

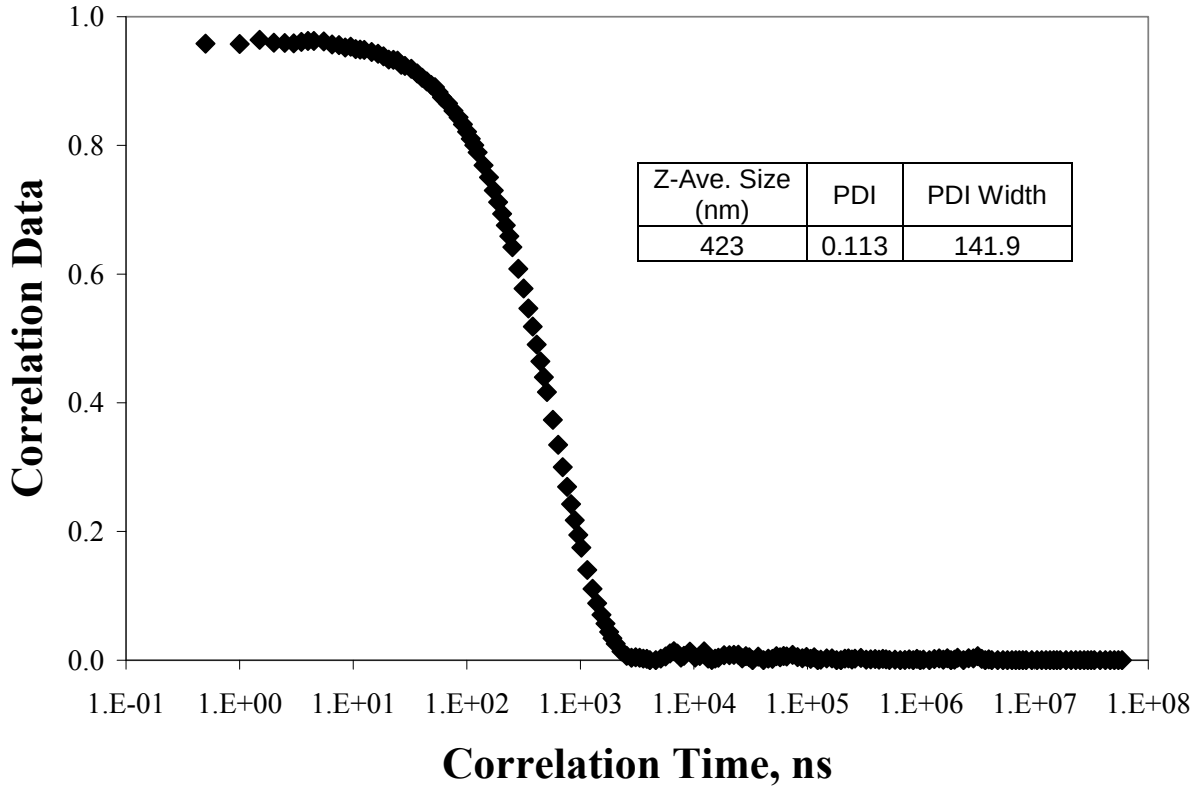

Figure SI.6.1: Small-angle light scattering of the polystyrene latex particle with the Z-averaged particle size of 423 nm given in the inset table.

References

Chapter 1

1. Cantor, C.R.; and Schimmel, P.R. *Biophysical Chemistry Part I The Conformation of Biological Macromolecule*; W.H. Freeman and Company: New York, 1980, pp 279–288.
2. Jonsson, B.; Lindman, B.; Holmberg, K.; Kronberg, B. *Surfactants and Polymers in Aqueous Solution*; John Wiley & Sons: Toronto, 1998.
3. Myers, D. *Surfactant Science and Technology, 2nd Ed.*; VCH: New York, 1992.
4. Cantor, C.R.; and Schimmel, P.R. *Biophysical Chemistry Part III The Behavior of Biological Macromolecule*; W.H. Freeman and Company: New York, 1980, pp 1340–1348.
5. Disher, D.E.; Eisenberg, A. *Science* **2002**, *297*, 967–973.
6. Lasic, D.D.; Papahadjopoulos, D. *Science* **1995**, *267*, 1275–1276.
7. Papahadjopoulos, D.; Allen, T.M.; Gabizon, A.; Mayhew, E.; Matthay, K.; Huang, S.K.; Lee, K.D.; Woodle, M.C.; Lasic, D.D.; Redemann, C.; Martin, F.J. *Proc. Natl. Acad. Sci. USA* **1991**, *88*, 11460–11464.
8. Zhu, H.; McShane, M.J. *J. Am. Chem. Soc.* **2005**, *127*, 13448–13449.
9. Huang, S.K.; Mayhew, E.; Gilani, S.; Lasic, D.D.; Martin, F.J.; Papahadjopoulos, D. *Cancer Res.* **1992**, *52*, 6774–6781.
10. *Polymers as Rheology Modifiers*, Schulz, D.N.; Glass, J.E., Ed. ACS Symposium Series 462; American Chemical Society: Washington, DC, 1991.
11. *Hydrophilic Polymers. Performance with Environmental Acceptability*, Glass, J.E., Ed.; Advances in Chemistry 248; American Chemical Society: Washington, DC, 1996.
12. Arnold, A.; Cloutier, I.; Ritcey, A.M.; Auger, M. *Chem. Phys. Lipids* **2005**, *133*, 165–179.
13. Michonova-Alexova, E.I.; Sugar, I.P. *J. Phys. Chem. B* **2001**, *105*, 10076–10083.

14. Kaasgaard, T.; Leidy, C.; Crowe, J.H.; Mouritsen, O.G.; Jorgensen, K. *Biophys. J.* **2003**, *85*, 350–360.

15. Sasaki, D.Y. *Cell Biochem. Biophys.* **2003**, *39*, 145–161.

16. Schultz, Z.D.; Pazos, I.M.; McNeil-Watson, F.K.; Lewis, E.N.; Levin, I.W. *J. Phys. Chem. B* **2009**, *113*, 9932–9941.

17. Singh, A.; Markowitz, M.; Gaber, B.P. *Langmuir* **1992**, *8*, 1570–1577.

18. Hauser, H.; Shipley, G.G. *Biochemistry* **1984**, *23*, 34–41.

19. Ohnishi, S.; Ito, T. *Biochemistry* **1974**, *13*, 881–887.

20. Alberts, B.; Bray, J.; Lewis, J.; Raff, M.; Roberts, K.; Watson, J.D. *Molecular Biology of the Cell 3rd Edition*, Garland Publishers: New York, 1994, Chapter 15.

21. Binder, W.H.; Barragan, V.; Menger, F.M. *Angew. Chem. Int. Ed.* **2003**, *42*, 5802–5827.

22. Laude, A.J.; Prior, I.A. *Mol. Membr. Biol.* **2004**, *21*, 193–205.

23. Simons, K.; Ikonen, E. *Nature* **1997**, *387*, 569–572.

24. Rajendran, L.; Simons, K. *J. Cell Sci.* **2005**, *118*, 1099–1102.

25. Pincus, J.L.; Jin, C.; Huang, W.; Jacobs, H.K.; Gopalan, A.S.; Song, Y.; Shelnutt, J.A.; Sasaki, D.Y. *J. Mater. Chem.* **2005**, *15*, 2938–2945.

26. Sasaki, D.Y.; Waggoner, T.A.; Last, J.A.; Alam, T.M. *Langmuir* **2002**, *18*, 3714–3721.

27. Last, J.A.; Waggoner, T.A.; Sasaki, D.Y. *Biophys. J.* **2001**, *81*, 2737–2742.

28. Reichert, A.; Nagy, J.O.; Spevak, W.; Charych, D. *J. Am. Chem. Soc.* **1995**, *117*, 829–830.

29. Pan, J.J.; Charych, D. *Langmuir* **1997**, *13*, 1365–1367.

30. Song, X.; Nolan, J.; Swanson, B.I. *J. Am. Chem. Soc.* **1998**, *120*, 11514–11515.

31. Bondurant, B.; Last, J.A.; Waggoner, T.A.; Slade, A.; Sasaki, D.Y. *Langmuir* **2003**, *19*, 1829–1837.

32. Winnik, M.A.; Yekta, A. *Curr. Opin. Colloid Interface Sci.* **1997**, *2*, 424–436.

33. Witten, T.A.; Cohen, M.H. *Macromolecules* **1985**, *18*, 1915–1918.

34. Richey, B.; Kirk, A.B.; Eisenhart, E.K.; Fitzwater, S.; Hook, J. *J. Coatings Technol.* **1991**, *63*, 31–40.

35. Tirtaatmadja, V.; Tam, K.C.; Jenkins, R.D. *Macromolecules* **1997**, *30*, 1426–1433.

36. Biggs, S.; Selb, J.; Candau, F. *Langmuir* **1992**, *8*, 838–847.

37. Annable, T.; Buscall, R.; Ettelaie, R. *Colloids Surf. A, Physicochem. Eng Aspects* **1996**, *112*, 97–116.

38. Annable, T.; Buscall, R.; Ettelaie, R.; Whittlestone, D. *J. Rheol.* **1993**, *37*, 695–726.

39. Rubinstein, M.; Semenov, A.N. *Macromolecules* **2001**, *34*, 1058–1068.

40. Leibler, L.; Rubinstein, M.; Colby, R.H. *Macromolecules* **1991**, *24*, 4701–4707.

41. Tanaka, F.; Edwards, S.F. *J. Non-Newtonian Fluid Mech.* **1992**, *43*, 247–271.

42. Baxandall, L.G. *Macromolecules* **1989**, *22*, 1982–1988.

43. Semenov, A.N.; Rubinstein, M. *Macromolecules* **1998**, *31*, 1373–1385.

44. Semenov, A.N.; Rubinstein, M. *Macromolecules* **1998**, *31*, 1386–1397.

45. Tripathi, A.; Tam, K.C.; McKinley, G.H. *Macromolecules* **2006**, *39*, 1981–1999.

46. Duhamel, J. *Molecular Interfacial Phenomena of Polymers and Biopolymers*, Chen, P. Ed. Woodhead Publishing Ltd.: Cambridge, 2005, p214–248.

47. Winnik, F.M. *Chem. Rev.* **1993**, *93*, 587–614.

48. Winnik, F.M.; Regismond, S.T.A.; Anghel, D.F. *Associative Polymers in Aqueous Media*, Glass, J.E., Ed.; ACS Symposium Series 765; American Chemical Society: Washington, DC, 2000, pp286–302.

49. Morawetz, H. *J. Lumin.* **1989**, *43*, 59–71.

50. Birks, J.B. *Photophysics of Aromatic Molecules*; Wiley: New York, 1970, pp 301–371.

51. Cuniberti, C.; Perico, A. *Euro. Poly. J.* **1980**, *16*, 887–893.

52. Duhamel, J.; Kanagalingam, S.; O'Brien, T.J.; Ingratta, M.W. *J. Am. Chem. Soc.* **2003**, *125*, 12810–12822.

53. Picarra, S.; Duhamel, J.; Fedorov, A.; Martinho, J.M.G. *J. Phys. Chem. B* **2004**, *108*, 12009–12015.

54. Picarra, S.; Gomes, P.T.; Martinho, J.M.G. *Macromolecules* **2003**, *33*, 3947–3950.

55. Farinha, J.P.S.; Picarra, S.; Miesel, K.; Martinho, J.M.G. *J. Phys. Chem. B* **2001**, *105*, 10536–10545.

56. Winnik, M.A. *Acc. Chem. Res.* **1985**, *18*, 73–79.

57. Duhamel, J. *Acc. Chem. Res.* **2006**, *39*, 953–960.

58. Mathew, A.K.; Duhamel, J.; Gao, J. *Macromolecules* **2001**, *34*, 1454–1469.

59. Prazeres, T.J.V.; Beingessner, R.; Duhamel, J.; Olesen, K.; Shay, G.; Bassett, D.R. *Macromolecules* **2001**, *34*, 7876–7884.

60. Siu, H.; Duhamel, J. *Macromolecules* **2004**, *37*, 9287–9289.

61. Lacowicz, J.R. *Principles of Fluorescence Spectroscopy*; Plenum Press: New York, 1983.

62. Lentz, B.R.; Barenholz, Y.; Thompson, T.E. *Biochemistry* **1976**, *15*, 4521–4528.

63. Prazeres, T.J.V.; Duhamel, J.; Olesen, K.; Shay, G. *J. Phys. Chem. B* **2005**, *109*, 17406–17416.

64. Siu, H.; Duhamel, J. *J. Phys. Chem. B* **2005**, *109*, 1770–1780.

65. Siu, H.; Duhamel, J. *J. Phys. Chem. B* **2008**, *112*, 15301–15312.

Chapter 2

1. Simon, K; Ehehalt, R. *J.Clin. Invest.* **2002**, *110*, 597–603.
2. Manco, M.; Calvani, M.; Mingrone, G. *Diabetes, Obesity and Metabolism* **2004**, *6*, 402–413.
3. Chauhan, N.B. *J. Lipid Research* **2003**, *44*, 2019–2029.
4. Vigh, L.; Escriba, P.V.; Sonnleitner, A.; Sonnleitner, M.; Piotto, S.; Maresca, B.; Horvath, I.; Harwood, J.L. *Prog. Lipid Res.* **2005**, *44*, 303–344.
5. Laude, A.J.; Prior, I.A. *Molec. Membr. Biol.* **2004**, *21*, 193–205.
6. Binder, W.H.; Barragan, V.; Menger, F.M. *Angew. Chem. Int. Ed.* **2003**, *42*, 5802–5827.
7. Veatch, S.L.; Keller, S.L. *Biochim. Biophys. Acta* **2005**, *1746*, 172–185.
8. Welti, R.; Glaser, M. *Chem. Phys. Lipids* **1994**, *73*, 121–137.
9. Papahadjopoulos, D. *J. Coll. Interf. Sci.* **1977**, *58*, 459–470.
10. Veatch, S.L.; Keller, S.L. *Phys. Rev. Lett.* **2005**, *94*, 148101(1)–148101(4).
11. Sasaki, D.Y. *Cell Biochem. Biophys.* **2003**, *39*, 145–161.
12. Roy, B.C.; Peterson, R.; Mallik, S.; Campiglia, A.D. *J. Org. Chem.* **2000**, *65*, 3644–3651.
13. Noble, G.T.; Fitsch, S.L.; Liem, K.P.; Webb, S.J. *Org. Biomol. Chem.* **2009**, *7*, 5245–5254.
14. Jelinek, R.; Kolusheva, S. *Top. Curr. Chem.* **2007**, *277*, 155–180.
15. Sasaki, D.Y.; Waggoner, T.A.; Last, J.A.; Alam, T.M. *Langmuir* **2002**, *18*, 3714–3721.
16. Pincus, J.L.; Jin, C.; Huang, W.; Jacobs, H.K.; Gopalan, A.S.; Song, Y.; Shelnutt, J.A.; Sasaki, D.Y. *J. Mater. Chem.* **2005**, *15*, 2938–2945.
17. Sasaki, D.Y.; Shnek, D.R.; Pack, D.W.; Arnold, F.H. *Angew. Chem. Int. Ed. Engl.* **1995**, *34*, 905–907.
18. Last, J.A.; Waggoner, T.A.; Sasaki, D.Y. *Biophys. J.* **2001**, *81*, 2737–2742.
19. Birks, J.B. *Photophysics of Aromatic Molecules*; Wiley: New York, 1970, pp 301–371.
20. Mathew, A.K.; Duhamel, J.; Gao, J. *Macromolecules* **2001**, *34*, 1454–1469.

21. Prazeres, T.J.V.; Beingessner, R.; Duhamel, J.; Olesen, K.; Shay, G.; Bassett, D.R. *Macromolecules* **2001**, *34*, 7876–7884.
22. Duhamel, J. *Acc. Chem. Res.* **2006**, *39*, 953–960.
23. Siu, H.; Duhamel, J. *Macromolecules* **2004**, *37*, 9287–9289.
24. Ng, K.; Pack, D.W.; Sasaki, D.Y.; Arnold, F.H. *Langmuir* **1995**, *11*, 4048–4055.
25. James, D.R.; Demmer, D.R.M.; Verrall, R.E.; Steer, R.P. *Rev. Sci. Instrum.* **1983**, *54*, 1121–1130.
26. Tachiya, M. *Chem. Phys. Lett.* **1975**, *33*, 289–292.
27. Tachiya, M. *J. Chem. Phys.* **1982**, *76*, 340–348.
28. Costa, T.; Seixas de Melo, J.; Burrows, H.D. *J. Phys. Chem. B.* **2009**, *113*, 618–626.
29. Press, W.H.; Flannery, B.P.; Teukolsky, S.A.; Vetterling, W.T. *Numerical Recipes. The Art of Scientific Computing (Fortran Version)*; Cambridge University Press: Cambridge, 1992, pp 523–528.
30. Lentz, B. R.; Barenholz, Y.; Thompson, T. E. *Biochemistry* **1976**, *15*, 4521-4528.
31. Ingratta, M.; Duhamel, J. *J. Phys. Chem. B* **2009**, *113*, 2284–2292.
32. Kanagalingam, S.; Spartalis, J.; Cao, T.M.; Duhamel, J. *Macromolecules* **2002**, *35*, 8571–8577.
33. Ingratta, M.; Duhamel, J. *Macromolecules* **2009**, *42*, 1244–1251.
34. Bales, B.L.; Almgren, M. *J. Phys. Chem.* **1995**, *99*, 15153–15162.
35. Duhamel, J.; Yekta, A.; Hu, Y.; Winnik, M. A. *Macromolecules* **1992**, *25*, 7024-7030.
36. Arnold, A.; Cloutier, I.; Ritcey, A.M.; Auger, M. *Chem. Phys. Lipids* **2005**, *133*, 165–179.
37. Hartmann, W.; Galla, H.J. *Biochim. Biophys. Acta* **1978**, *509*, 474–490.
38. Galla, H.J.; Sackmann, E. *Biochim. Biophys. Acta* **1974**, *339*, 103–115.
39. Mandel, M. *Euro. Poly. J.* **1970**, *6*, 807–822.
40. Lentz, B. R.; Barenholz, Y.; Thompson, T. E. *Biochemistry* **1976**, *15*, 4529-4537.

Chapter 3

1. Cantor, C. R.; Schimmel, P. R. *Biophysical Chemistry Part I*: *The Conformation of Biological Macromolecules* W. H. Freeman and Co., San Francisco, 1980.
2. Eisenberg, A.; Kim, J.-S. *Introduction to Ionomers* John Wiley & Sons, Toronto, 1998.
3. Stryer, L. *Biochemistry* W. H. Freeman and Co., New York, 1993.
4. Schultz, D. N.; Glass, J. E., Eds. *Polymer as Rheology Modifiers*, ACS Symposium Series 462; American Chemical Society, Washington, DC, 1991.
5. J. E. Glass Ed. *Hydrophilic Polymers. Performance with Environmental Acceptability. Adv. Chem. Ser*. 248; Am. Chem. Soc. Washington, 1996.
6. Glass, J. E. Ed. *Associative Polymers in Aqueous Media*. *Adv. Chem. Ser*. 248; Am. Chem. Soc. Washington, 2000.
7. Karplus, M.; Weaver, D. L. *Nature* **1976**, *260*, 404-406.
8. Cantor, C. R.; Schimmel, P. R. *Biophysical Chemistry Part II*: *Techniques for the Study of Biological Structure and Function*. W. H. Freeman and Co., San Francisco, 1980.
9. Lakowicz, J. R. *Principles of Fluorescence Spectroscopy*; Kluwer Academic/Plenum Publishers: New York, 1999.
10. Winnik, F. M. *Chem. Rev.* **1993**, *93*, 587-614.
11. Duhamel, J. *Pyrene Fluorescence to Study Polymeric Systems*. *Molecular Interfacial Phenomena of Polymers and Biopolymers.* Chen, P. Editor, Woodhead Publishing Company, **2005**, p214-248.
12. Duhamel, J. *Acc. Chem. Res.* **2006**, *39*, 953-960.
13. Vangani, V. ; Duhamel, J.; Nemeth, S.; Jao, T.-C. *Macromolecules* **1999**, *32*, 2845-2854.
14. Vangani, V.; Drage, J.; Mehta, J.; Mathew, A. K.; Duhamel, J. *J. Phys. Chem. B* **2001**, *105*, 4827-4839.
15. Siu, H.; Duhamel, J. *J. Phys. Chem. B* **2005**, *109*, 1770-1780.

16. Prazeres, T. J. V.; Beingessner, R.; Duhamel, J.; Olesen, K.; Shay, G.; Bassett, D. R. *Macromolecules* **2001**, *34*, 7876-7884.
17. Mathew, A. K.; Siu, H.; Duhamel, J. *Macromolecules* **1999**, *32*, 7100-7108.
18. Strickler, S. J.; Berg, R. A. *J. Chem. Phys.* **1962**, *37*, 814-822.
19. Kanagalingam, S.; Ngan, C. F.; Duhamel, J. *Macromolecules* **2002**, *35*, 8560-8570.
20. O'Connor, D. V.; Phillips, D. *Time-Correlated Single Photon Counting* Academic Press, 1984.
21. Press, W. H.; Flannery, B. P.; Teukolsky, S. A.; Vetterling, W. T. *Numerical Recipes. The Art of Scientific Computing (Fortran Version)*; Cambridge University Press: Cambridge, 1992.
22. Demas, J. N. *Excited State Lifetime Measurements*; Academic Press: New York, 1983.
23. Birks, J. B. in *Photophysics of Aromatic Molecules*. Wiley: New York, 1970.
24. Slewyn, J. E.; Steinfeld, J. I. *J. Phys. Chem.* **1972**, *76*, 762-774.
25. Anghel, D. F.; Alderson, V.; Winnik, F. M.; Mizusaki, M.; Morishima, Y. *Polymer* **1998**, *39*, 3035-3044.
26. Anghel, D. F.; Toca-Herrera, J. L.; Winnik, F. M.; Rettig, W.; v. Kliting, R. *Langmuir* **2002**, *18*, 5600-5606.
27. Winnik, F. M.; Regismond, S. T. A.; Goddard, E. D. *Langmuir* **1997**, *13*, 111-114.
28. Siu, H.; Duhamel, J. *Macromolecules* **2005**, *38*, 7184-7186.
29. Siu, H.; Duhamel, J. *Macromolecules* **2004**, *37*, 9287-9289.
30. Siu, H.; Prazeres, T. J. V.; Duhamel, J.; Olesen, K.; Shay, G. *Macromolecules* **2005**, *38*, 2865-2875.
31. Dai, S.; Tam, K. C.; Jenkins, R. D.; Bassett, D. R. *Macromolecules* **2000**, *33*, 7021-7028.
32. Zachariasse, K. A.; Duveneck, G.; Busse, R. *J. Am. Chem. Soc.* **1984**, *106*, 1045-1051.
33. Zachariasse, K. A.; Striker, G. *Chem. Phys. Lett.* **1988**, *145*, 251-254.
34. Reynders, P.; Kühnle, W.; Zachariasse, K. A. *J. Am. Chem. Soc.* **1990**, *112*, 3929-3939.

35. Reynders, P.; Kühnle, W.; Zachariasse, K. A. *J. Phys. Chem.* **1990**, *94*, 4073-4082.

36. Zachariasse, K. A.; Duveneck, G.; Kühnle, W.; Leinhos, U.; Reynders, P. *In Photochemical Processes in Organized Molecular Systems* Ed. Honda, K. North-Holland Delta Series, NY, 1991, pp 83-101.

37. Zachariasse, K. A.; Maçanita, A. L.; Kühnle, W. *J. Phys. Chem. B* **1999**, *103*, 9356-9365.

38. Farinha, J. P. S.; Martinho, J. M. G.; Xu, H.; Winnik, M. A.; Quirk, R. P. *J. Polym. Sci.*: *Part B*: *Polym. Phys.* **1994**, *32*, 1635-1642.

39. Farinha, J. P. S.; Piçarra, S.; Miesel, K.; Martinho, J. M. G. *J. Phys. Chem. B* **2001**, *105*, 10536-10545.

40. Picarra, S.; Relogio, P.; Afonso, C. A. M.; Martinho, J. M. G.; Farinha, J. P. S. *Macromolecules* **2003**, *36*, 8119-8129.

41. Picarra, S.; Relogio, P.; Afonso, C. A. M.; Martinho, J. M. G.; Farinha, J. P. S. *Macromolecules*, **2004**, *37*, 1670-1670.

42. Picarra, S.; Duhamel, J.; Fedorov, A.; Martinho, J. M. G. *J. Phys. Chem. B.* **2004**, *108*, 12009-12015.

43. Brown, R.; Lacombe, S.; Cardy, H. *Micropor. Mesopor. Mater.* **2003**, *59*, 93-103.

44. Chakarova, S. D.; Schröder, E. *J. Chem. Phys.* **2005**, *122*, 054102.

45. Podeszwa, R.; Szalewicz, K. *Phys. Chem. Chem. Phys.* **2008**, *10*, 2735-2746.

46. Stepanek, M.; Krijtova, K.; Prochazka, K.; Teng, Y.; Webber, S. E.; Munk, P. *Acta Polym.* **1998**, *49*, 96-102.

47. Yekta, A.; Xu, B.; Duhamel, J.; Adiwidjaja, H.; Winnik, M. A. *Macromolecules* **1995**, *28*, 956-966.

48. Char, K.; Frank, C. W.; Gast, A. P. *Macromolecules* **1989**, *22*, 3177-3180.

49. Duhamel, J.; Yekta, A.; Hu, Y.; Winnik, M. A. *Macromolecules* **1992**, *25*, 7024-7030.

50. Seixas, de Melo, J.; Costa, T.; da G. Miguel, M.; Lindman, B.; Schillen, K. *J. Phys. Chem. B* **2003**, *107*, 12605-12621.

51. Seixas de Melo, J.; Costa, T.; Francisco, A.; Maçanita, A. L.; Gago, S.; Gonçalves, I. S. *Phys. Chem. Chem. Phys.* **2007**, *9*, 1370-1385.

52. Lee, S.; Duhamel, J. *Macromolecules* **1998**, 93-9200.

53. Siu, H.; Duhamel, J. *Macromolecules* **2006**, *39*, 1144-1155.

Chapter 4

1. Winnik, M.A.; Yekta, A. *Curr. Opin. Colloid Interface Sci.* **1997**, *2*, 424–436.
2. *Polymers as Rheology Modifiers*, Schulz, D.N.; Glass, J.E., Ed. ACS Symposium Series 462; American Chemical Society: Washington, DC, 1991.
3. *Hydrophobic Polymers. Performance with Environmental Acceptability*, Glass, J.E., Ed.; Advances in Chemistry 248; American Chemical Society: Washington, DC, 1996.
4. *Water-Soluble Polymers. Beauty with Performance*, Glass, J.E., Ed.; Advances in Chemistry 213; American Chemical Society: Washington, DC, 1986.
5. Rubinstein, M.; Semenov, A.N. *Macromolecules* **2001**, *34*, 1058–1068.
6. Leibler, L.; Rubinstein, M.; Colby, R.H. *Macromolecules* **1991**, *24*, 4701–4707.
7. Annable, T.; Buscall, R.; Ettelaie, R.; Whittlestone, D. *J. Rheol.* **1993**, *37*, 695–726.
8. Tanaka, F.; Edwards, S.F. *J. Non-Newtonian Fluid Mech.* **1992**, *43*, 247–271.
9. Baxandall, L.G. *Macromolecules* **1989**, *22*, 1982–1988.
10. Semenov, A.N.; Rubinstein, M. *Macromolecules* **1998**, *31*, 1373–1385.
11. Semenov, A.N.; Rubinstein, M. *Macromolecules* **1998**, *31*, 1386–1397.
12. Tripathi, A.; Tam, K.C.; McKinley, G.H. *Macromolecules* **2006**, *39*, 1981–1999.
13. Witten, T.A.; Cohen, M.H. *Macromolecules* **1985**, *18*, 1915–1918.
14. Semenov, A.N.; *Europhys. Lett.* **2006**, *76*, 1116–1122.
15. Duhamel, J. *Molecular Interfacial Phenomena of Polymers and Biopolymers*, Chen, P., Ed.; Woodhead Publishing Limited: Cambridge, 2005, pp214–248.
16. Duhamel, J. *Acc. Chem. Res.* **2006**, *39*, 953–960.
17. Farinha, J.P.S.; Picarra, S.; Miesel, K.; Martinho, J.M.G. *J. Phys. Chem. B* **2001**, *105*, 10536–10545.
18. Winnik, F.M. *Chem. Rev.* **1993**, *93*, 587–614.

19. Winnik, F.M.; Regismond, S.T.A.; Anghel, D.F. *Associative Polymers in Aqueous Media*, Glass, J.E., Ed.; ACS Symposium Series 765; American Chemical Society: Washington, DC, 2000, pp286–302.
20. Siu, H.; Duhamel, J. *Macromolecules* **2004**, *37*, 9287–9289.
21. Prazeres, T.J.V.; Beingessner, R.; Duhamel, J.; Olesen, K.; Shay, G.; Bassett, D.R. *Macromolecules* **2001**, *34*, 7876–7884.
22. Kanagalingam, S.; Ngan, C.F.; Duhamel, J. *Macromolecules* **2002**, *35*, 8560–8570.
23. Chapter 3 or Siu, H.; Duhamel, J. *J. Chem. Phys. B* **2008**, *112*, 15301–15312.
24. Martinho, J.M.G.; Campos, M.; Tencer, M.; Winnik, M.A. *Macromolecules* **1987**, *20*, 1582–1587.
25. Chapter 2 or *manuscript in preparation.*
26. Chapter 5 or *manuscript in preparation.*
27. Costa, T.; Seixas de Melo, J.; Burrows, H.D. *J. Phys. Chem. B* **2009**, *113*, 618–626.
28. Cheung, S.T.; Winnik, M.A.; Redpath, A.E.C. *Makromol. Chem.* **1982**, *183*, 1815–1824.
29. Cuniberti, C.; Perico, A. *Euro. Poly. J.* **1977**, *13*, 369–374.
30. Ingratta, M.; Hollinger, J.; Duhamel, J. *J. Am. Chem. Soc.* **2008**, *130*, 9420–9428.
31. Birks, J.B. *Photophysics of Aromatic Molecules*; Wiley: New York, 1970, pp 301–371.
32. Birks, J.B.; Dyson, D.J.; Munro, I.H. *Proc. Roy. Soc. A* **1963**, *275*, 575–588.
33. Winnik, M.A.; Egan, L.S.; Tencer, M.; Croucher, M.D. *Polymer* **1987**, *28*, 1553–1560.
34. Mathew, A.K.; Duhamel, J.; Gao, J. *Macromolecules* **2001**, *34*, 1454–1469.
35. Vangani, V.; Duhamel, J.; Nemeth, S.; Jao, T.C. *Macromolecules* **1999**, *32*, 2845–2854.
36. Mathew, A.K.; Siu, H.; Duhamel, J. *Macromolecules* **1999**, *32*, 7100–7108.
37. Picarra, S.; Relogio, P.; Afonso, C.A.M.; Martinho, J.M.G.; Farinha, J.P.S. *Macromolecules* **2003**, *36*, 8119–8129.

38. Siu, H.; Duhamel, J. *J. Phys. Chem. B* **2005**, *109*, 1770–1780.

39. Winnik, M.A.; Redpath, A.E.C.; Paton, K.; Danhelka, J. *Polymer* **1984**, *25*, 91–99.

40. Nosowitz, M.; Halpern, A.M. *J. Phys. Chem.* **1986**, *90*, 906–911.

41. Press, W.H.; Flannery, B.P.; Teukolsky, S.A.; Vetterling, W.T. *Numerical Recipes. The Art of Scientific Computing (Fortran Version)*; Cambridge University Press: Cambridge, 1992, pp 523 – 528.

42. Hara, K.; Ware, W.R. *Chem. Phys.* **1980**, *51*, 61–68.

43. Ingratta, M.; Duhamel, J. *J. Phys. Chem. B* **2008**, *112*, 9209–9218.

44. *Polymer Handbook*, Brandup, J.; Immergut, E.H.; Grulke, E.A., Ed.; John Wiley & Sons, Inc.: New York, 1999, Section VII, pg 571.

45. Siu, H.; Prazeres, T.J.V.; Duhamel, J.; Olesen, K.; Shay, G. *Macromolecules* **2005**, *38*, 2865–2875.

46. Richey, B.; Kirk, A.B.; Eisenhart, E.K.; Fitzwater, S.; Hook, J. *J. Coatings Technol.* **1991**, *63*, 31–40.

47. *CRC Handbook of Chemistry and Physics 89th Edition 2008 – 2009 (online)*, Lide, D.R., Ed.; Section 6, http://www.hbcpnetbase.com (10-09-2009).

48. Siu, H.; Duhamel, J. *Macromolecules* **2005**, *38*, 7184–7186.

Chapter 5

1. *Polymers as Rheology Modifiers*, Schulz, D.N.; Glass, J.E., Ed. ACS Symposium Series 462; American Chemical Society: Washington, DC, 1991.
2. *Hydrophilic Polymers. Performance with Environmental Acceptability*, Glass, J.E., Ed.; Advances in Chemistry 248; American Chemical Society: Washington, DC, 1996.
3. Witten, T.A.; Cohen, M.H. *Macromolecules* **1985**, *18*, 1915–1918.
4. Annable, T.; Buscall, R.; Ettelaie, R.; Whittlestone, D. *J. Rheol.* **1993**, *37*, 695–726.
5. Rubinstein, M.; Semenov, A.N. *Macromolecules* **2001**, *34*, 1058–1068.
6. Leibler, L.; Rubinstein, M.; Colby, R.H. *Macromolecules* **1991**, *24*, 4701–4707.
7. Tanaka, F.; Edwards, S.F. *J. Non-Newtonian Fluid Mech.* **1992**, *43*, 247–271.
8. Semenov, A.N.; Rubinstein, M. *Macromolecules* **1998**, *31*, 1373–1385.
9. Semenov, A.N.; Rubinstein, M. *Macromolecules* **1998**, *31*, 1386–1397.
10. Tripathi, A.; Tam, K.C.; McKinley, G.H. *Macromolecules* **2006**, *39*, 1981–1999.
11. Chapter 3 or Siu, H.; Duhamel, J. *J. Phys. Chem. B* **2008**, *112*, 15301–15312.
12. Chapter 4 or *manuscript in preparation*.
13. Prazeres, T.J.V.; Duhamel, J.; Olesen, K.; Shay, G. *J. Phys. Chem. B* **2005**, *109*, 17406–17416.
14. Richey, B.; Kirk, A.B.; Eisenhart, E.K.; Fitzwater, S.; Hook, J. *J. Coatings Technol.* **1991**, *63*, 31–40.
15. Duhamel, J. *Molecular Interfacial Phenomena of Polymers and Biopolymers*, Chen, P. Ed. Woodhead Publishing Ltd.: Cambridge, 2005, p214–248.
16. Winnik, F.M. *Chem. Rev.* **1993**, *93*, 587–614.
17. Birks, J.B. *Photophysics of Aromatic Molecules*; Wiley: New York, 1970, pp 301–371.
18. Mathew, A.K.; Siu, H.; Duhamel, J. *Macromolecules* **1999**, *32*, 7100–7108.

Chapter 6

1. Winnik, M.A.; Yekta, A. *Curr. Opin. Colloid Interface Sci.* **1997**, *2*, 424–436.
2. Rubinstein, M.; Semenov, A.N. *Macromolecules* **2001**, *34*, 1058–1068.
3. Leibler, L.; Rubinstein, M.; Colby, R.H. *Macromolecules* **1991**, *24*, 4701–4707.
4. Annable, T.; Buscall, R.; Ettelaie, R.; Whittlestone, D. *J. Rheol.* **1993**, *37*, 695–726.
5. Tanaka, F.; Edwards, S.F. *J. Non-Newtonian Fluid Mech.* **1992**, *43*, 247–271.
6. Baxandall, L.G. *Macromolecules* **1989**, *22*, 1982–1988.
7. Semenov, A.N.; Rubinstein, M. *Macromolecules* **1998**, *31*, 1373–1385.
8. Semenov, A.N.; Rubinstein, M. *Macromolecules* **1998**, *31*, 1386–1397.
9. Tripathi, A.; Tam, K.C.; McKinley, G.H. *Macromolecules* **2006**, *39*, 1981–1999.
10. Witten, T.A.; Cohen, M.H. *Macromolecules* **1985**, *18*, 1915–1918.
11. Annable, T.; Buscall, R.; Ettelaie; R.; Shepherd, P.; Whittlestone, D. *Langmuir* **1994**, *10*, 1060–1070.
12. Annable, T.; Buscall, R.; Ettelaie, R. *Colloids Surf. A, Physicochem. Eng Aspects* **1996**, *112*, 97–116.
13. Jimenez-Regalado, E.; Selb, J.; Candau, F. *Langmuir* **2000**, *16*, 8611–8621.
14. Yekta, A.; Xu, B.; Duhamel, J.; Adiwidjaja, H.; Winnik, M.A. *Macromolecules* **1995**, *28*, 956–966.
15. Yekta, A.; Duhamel, J.; Adiwidjaja, H.; Brochard, P.; Winnik, M.A. *Langmuir* **1993**, *9*, 881–883.
16. Araujo, E.; Rharbi, Y.; Huang, X.; Winnik, M.A.; Bassett, D.R.; Jenkins, R.D. *Langmuir* **2000**, *16*, 8664–8671.
17. Jimenez-Regalado, E.; Selb, J.; Candau, F. *Macromolecules* **1999**, *32*, 8580–8588.
18. Chapter 3 or Siu, H.; Duhamel, J. *J. Phys. Chem. B* **2008**, *112*, 15301–15312.
19. Chapter 4 or *manuscript in preparation*.

20. Duhamel, J. *Acc. Chem. Res.* **2006**, *39*, 953–960.

21. Morawetz, H. *J. Lumin.* **1989**, *43*, 59–71.

22. Piccara, S.; Duhamel, J.; Fedorov, A.; Martinho, J.M.G. *J. Phys. Chem. B* **2004**, *108*, 12009–12015.

23. Winnik, F.M. *Macromolecules* **1990**, *23*, 1647–1649.

24. Duhamel, J. *Molecular Interfacial Phenomena of Polymers and Biopolymers*, Chen, P. Ed. Woodhead Publishing Ltd.: Cambridge, 2005, p214–248.

25. Winnik, F.M. *Chem. Rev.* **1993**, *93*, 587–614.

26. Mathew, A.K.; Duhamel, J.; Gao, J. *Macromolecules* **2001**, *34*, 1454–1469.

27. Siu, H.; Duhamel, J. *Macromolecules* **2004**, *37*, 9287–9289.

28. Siu, H.; Duhamel, J. *J. Phys. Chem. B* **2005**, *109*, 1770–1780.

29. Prazeres, T.J.V., Beingessner, R.; Duhamel, J.; Olesen, K.; Shay, G.; Bassett, D.R. *Macromolecules* **2001**, *34*, 7876–7884.

30. *Polymers as Rheology Modifiers*, Schulz, D.N.; Glass, J.E., Ed. ACS Symposium Series 462; American Chemical Society: Washington, DC, 1991.

31. Matsuzuka, K.; Hashimoto, T. *Rev. Sci. Instrum.* **1999**, *70*, 2387–2397.

32. Paulin, S.E.; Ackerson, B.J.; Wolfe, M.S. *Phys. Rev. E* **1997**, *55*, 5812.

33. Lauger, J.; Gronski, W. *Rheol. Acta* **1995**, *34*, 70–79.

34. Tsunashima, Y. *J. Chem. Phys.* **1995**, *102*, 4673–4682.

35. Hur, J.S.; Shaqfeh, E.S.G.; Babcock, H.P.; Smith, D.E.; Chu, S. *J. Rheol.* **2001**, *45*, 421–450.

36. Richey, B.; Kirk, A.B.; Eisenhart, E.K.; Fitzwater, S.; Hook, J. *J. Coatings Technol.* **1991**, *63*, 31–40.

37. Munam, A. *Graft Polymers: From Dendrimer Hybrids to Latex Particles* Ph.D. Thesis, University of Waterloo, **2007**, Chapter 6.

38. Jenkins, R.D.; DeLong, L.M.; Bassett, D.R. *Hydrophilic Polymers. Performance with Environmental Acceptability*, Glass, J.E., Ed.; Advances in Chemistry 248; American Chemical Society: Washington, DC, 1996, pp 425–447.
39. Shay, G.D.; Kravitz, F.K.; Brizgys, P.V. *Polymers as Rheology Modifiers*, Schulz, D.N.; Glass, J.E., Ed. ACS Symposium Series 462; American Chemical Society: Washington, DC, 1991 pp 121–141.
40. Press, W.H.; Flannery, B.P.; Teukolsky, S.A.; Vetterling, W.T. *Numerical Recipes. The Art of Scientific Computing (Fortran Version)*; Cambridge University Press: Cambridge, 1992, pp 523–528.
41. Mathew, A.K.; Siu, H.; Duhamel, J. *Macromolecules* **1999**, *32*, 7100–7108.
42. Costa, T.; Seixas de Melo, J.; Burrows, H.D. *J. Phys. Chem. B* **2009**, *113*, 618–626.
43. Walters, K. *Rheometry* Chapman and Hall: London, 1975, Chapter 4.
44. Prazeres, T.J.V.; Duhamel, J.; Olesen, K.; Shay, G. *J. Phys. Chem. B* **2005**, *109*, 17406–17416.
45. Tirtaatmadja, V.; Tam, K.C.; Jenkins, R.D. *Macromolecules* **1997**, *30*, 1426–1433.
46. Biggs, S.; Selb, J.; Candau, F. *Langmuir* **1992**, *8*, 838–847.
47. Trens, P.; Denoyel, R. *Langmuir* **1993**, *9*, 519–522.
48. Eskilsson, K.; Ninham, B.W.; Tiberg, F.; Yaminsky, V.V. *Langmuir* **1998**, *14*, 7287–7291.
49. Wang, C.; Tam, K.C.; Jenkins, R.D. *J. Phys. Chem. B* **2002**, *106*, 1195–1204.
50. Jorgensen, A.M.; Mogensen, K.B. *Microsystem Engineering of Lab-on-a-Chip Devices*; Wiley-VCH: Weinheim, 2004, pp159.
51. Gun'ko, V.M.; Turov, V.V.; Bogatyrev, V.M.; Charmas, B.; Skubiszewska-Zieba, J.; Leboda, R.; Pakhovchishin, S.V.; Zarko, V.I.; Petrus, L.V.; Stebelska, O.V.; Tsapko, M.D. *Langmuir* **2003**, *19*, 10816–10828.
52. Hertl, W.; Hair, M.L. *J. Phys. Chem.* **1971**, *75*, 2181–2185.

Chapter 7

1. Winnik, F.M. *Chem. Rev.* **1993**, *93*, 587–614.
2. Duhamel, J. *Molecular Interfacial Phenomena of Polymers and Biopolymers*, Chen, P. Ed. Woodhead Publishing Ltd.: Cambridge, 2005, p214–248.
3. Duhamel, J. *Acc. Chem. Res.* **2006**, *39*, 953–960.
4. Galla, H.J.; Sackmann, E. *Biochim. Biophys. Acta* **1974**, *339*, 103–115.
5. Birks, J.B. *Photophysics of Aromatic Molecules*; Wiley: New York, 1970, pp 301–371.
6. Winnik, M.A.; Yekta, A. *Curr. Opin. Colloid Interface Sci.* **1997**, *2*, 424–436.
7. Tirtaatmadja, V.; Tam, K.C.; Jenkins, R.D. *Macromolecules* **1997**, *30*, 1426–1433.
8. Biggs, S.; Selb, J.; Candau, F. *Langmuir* **1992**, *8*, 838–847.